

DEVELOPMENT AND SUBSEQUENT DEMISE OF AN  
OCEANIC SPREADING CENTER: THE  
TROODOS OPHIOLITE, CYPRUS

CENTRE FOR NEWFOUNDLAND STUDIES

**TOTAL OF 10 PAGES ONLY  
MAY BE XEROXED**

(Without Author's Permission)

CHRISTOPHER H. ASH, B.Sc.





National Library  
of Canada

Bibliothèque nationale  
du Canada

Canadian Theses Service

Service des thèses canadiennes

Ottawa, Canada  
K1A 0N4

## NOTICE

The quality of this microform is heavily dependent upon the quality of the original thesis submitted for microfilming. Every effort has been made to ensure the highest quality of reproduction possible.

If pages are missing, contact the university which granted the degree.

Some pages may have indistinct print especially if the original pages were typed with a poor typewriter ribbon or if the university sent us an inferior photocopy.

Reproduction in full or in part of this microform is governed by the Canadian Copyright Act, R.S.C. 1970, c. C-30, and subsequent amendments.

## AVIS

La qualité de cette microforme dépend grandement de la qualité de la thèse soumise au microfilmage. Nous avons tout fait pour assurer une qualité supérieure de reproduction.

S'il manque des pages, veuillez communiquer avec l'université qui a conféré le grade.

La qualité d'impression de certaines pages peut laisser à désirer, surtout si les pages originales ont été dactylographiées à l'aide d'un ruban usé ou si l'université nous a fait parvenir une photocopie de qualité inférieure.

La reproduction, même partielle, de cette microforme est soumise à la Loi canadienne sur le droit d'auteur, SRC 1970, c. C-30, et ses amendements subséquents.

**Development and Subsequent Demise  
of an Oceanic Spreading Center:  
the Troodos Ophiolite, Cyprus**

By

**Christopher H. Ash, B.Sc.**

A thesis submitted to the School of Graduate  
Studies in partial fulfillment of the  
requirements for the degree of  
Master of Science

Department of Earth Sciences  
Memorial University of Newfoundland  
September, 1990

St. John's

Newfoundland



National Library  
of Canada

Bibliothèque nationale  
du Canada

Canadian Theses Service    Service des thèses canadiennes

Ottawa, Canada  
K1A 0N4

The author has granted an irrevocable non-exclusive licence allowing the National Library of Canada to reproduce, loan, distribute or sell copies of his/her thesis by any means and in any form or format, making this thesis available to interested persons.

The author retains ownership of the copyright in his/her thesis. Neither the thesis nor substantial extracts from it may be printed or otherwise reproduced without his/her permission.

L'auteur a accordé une licence irrévocable et non exclusive permettant à la Bibliothèque nationale du Canada de reproduire, prêter, distribuer ou vendre des copies de sa thèse de quelque manière et sous quelque forme que ce soit pour mettre des exemplaires de cette thèse à la disposition des personnes intéressées.

L'auteur conserve la propriété du droit d'auteur qui protège sa thèse. Ni la thèse ni des extraits substantiels de celle-ci ne doivent être imprimés ou autrement reproduits sans son autorisation.

ISBN 0-315-65302-7



MEMORIAL UNIVERSITY OF NEWFOUNDLAND

This is to authorize the Dean of Graduate Studies to deposit two copies of my thesis/report entitled Development and Subsequent Demise of an Oceanic Spreading Center: the Troodos Ophiolite, Cyprus

in the University Library, on the following conditions. I understand that I may choose only ONE of the Options here listed, and may not afterwards apply for any additional restriction. I further understand that the University will not grant any restriction on the publication of thesis/report abstracts.

(After reading the explanatory notes at the foot of this form, delete TWO of (a), (b) and (c), whichever are inapplicable.)

The conditions of deposit are:

(a) that two copies are to be made available to users at the discretion of their custodians,

OR

~~(b) that access to, and quotation from, this thesis/report is to be granted only with my written permission for a period of one year from the date on which the thesis/report, after the approval of the award of a degree, is entrusted to the care of the University, namely, 19\_\_\_, after which time the two copies are to be made available to users at the discretion of their custodians,~~

OR

~~(c) that access to, and quotation from, this thesis/report is to be granted only with my written permission for a period of \_\_\_ years from the date on which the thesis/report, after approval for the award of a degree, is entrusted to the care of the University; namely, 19\_\_\_, after which time two copies are to be made available to users at the discretion of their custodians.~~

Date Feb 27 / 91  
[Signature]  
Dean of Graduate Studies

Signed [Signature]  
Witnessed by [Signature]

NOTES

1. Restriction (b) will be granted on application, without reason given. However, applications for restriction (c) must be accompanied with a detailed explanation, indicating why the restriction is thought to be necessary, and justifying the length of time requested. Restrictions required on the grounds that the thesis is being prepared for publication, or that patents are awaited, will not be permitted to exceed three years. Restriction (c) can be permitted only by a Committee entrusted by the University with the task of examining such applications, and will be granted only in exceptional circumstances.
2. Thesis writers are reminded that, if they have been engaged in contractual research, they may have already agreed to restrict access to their thesis until the terms of the contract have been fulfilled.

## Abstract

The sequence of magmatic events present within the lower plutonic crustal section exposed in the Amiandos area of the Troodos ophiolite records the death of a once active oceanic spreading center. At least three and possibly four magmatic episodes are evident on the of basis field relationships. The progressive variation in geometry, scale, composition and texture of these successive magmatic events appears to have resulted from a "decaying" or lowering oceanic geothermal gradient.

Earliest identified crustal processes record the development of a relatively large (at least 3 to 4 km) open-system magma chamber which is defined by a differentiated plutonic suite of ultramafic to mafic cumulates.

Lowering geotherms result in a freezing of the axial magma chamber and a lowering of the brittle-ductile transition zone into the lower crust and upper mantle. The axial magma chamber which is initially affected by high temperature ductile deformation accommodates extension by brittle failure which in turn controls the geometry and distribution of subsequent magmatic episodes. These are defined by much smaller fault controlled dike-like bodies that are lithologically and texturally highly variable, but temporally gradational.

Accompanying the structural change is a significant reduction in the supply of magma to the ridge system. Chemically these magmas become progressively more depleted (REEs and  $\text{TiO}_2$ ) and increasingly refractory (enriched in Mg, Cr and Ni) through time and appear to be correlative with the Troodos lava sequence.

A definitive explanation for the death of the ridge system at this stage is not possible, however "ridge jumping" or a locking up of the subduction system from which the Troodos crust was being generated due to collision, are possible candidates.

## Acknowledgments

The writer is most grateful to John Malpas for guidance and support throughout the field, research and write-up stages of this thesis. His jet-legged reviews significantly benefitted this work.

Thanks are extended to Costas Xenophontos and the Geological Survey of Cyprus for their hospitality and logistical support during field work.

A field visit and insightful discussions with Tom Calon of Memorial University broadened the author's understanding of the study area.

Editorial review by Bill McMillan benefitted this work. The patience and understanding of both Bill McMillan and Ron Smyth of the British Columbia Ministry of Energy, Mines and Petroleum Resources is greatly appreciated.

My most heartfelt gratitude goes to Brenda for her devotion, understanding and moral support during the many long hours and the months of separation. This and her assistance in drafting, typing and editing all played a fundamental role in the completion of this thesis.

Funding was provided by Memorial University of Newfoundland through an NSERC operating grant to Dr. John Malpas.

## Table of Contents

	Page
Abstract.....	i
Acknowledgements.....	ii
List of Figures .....	vi
List of Maps .....	vii
List of Tables .....	vii
List of Plates .....	viii
Abbreviations Used .....	xi
<b>Chapter 1. Introduction</b>	
1.1 Introduction .....	1
1.2 Regional Geological Setting.....	1
1.3 Local Geological Setting.....	6
1.4 Troodos Ophiolite.....	9
1.5 The Cyprus Crustal Study Project.....	13
1.6 Early Thoughts on the Plutonic Section of the Troodos Ophiolite	13
1.7 Location and Physiography of Study Area.....	17
1.8 Scope and Purpose.....	20
<b>Chapter 2. Geology of the Amiandos Map Area</b>	
2.1 Introduction.....	22
2.2 Residual Mantle Harzburgite Tectonites .....	26
2.3 Banded Dunite-Orthopyroxenite.....	28
2.4 The Early Plutonic Suite.....	34
2.4.1 Dunites .....	35
2.4.2 Wehrlite.....	39

	Page
2.4.3 Plagioclase-Bearing Ultramafic Cumulates .....	39
2.4.4 Melagabbros.....	42
2.4.5 Olivine Gabbros .....	42
2.4.6 Gabbro-Orthopyroxene Gabbro.....	50
2.5 Layered Ultramafic Cumulate Section.....	52
2.6 Structure and Distribution of the Early Plutonic Suite .....	58
2.7 Late Magmatic Suite .....	61
2.7.1 Clinopyroxenite.....	61
2.7.2 Gabbro .....	65
2.7.3 Trondhjemite.....	65
2.8 Diabase Dikes.....	68
2.8.1 Aphanitic Dike Suite .....	68
2.8.2 Late Porphyritic Dike Suite .....	71
2.9 Faulting.....	71
2.10 Discussion .....	73

### **Chapter 3. Geochemistry**

3.1 Geochemistry of the Layered Cumulate Section.....	77
3.1.1 Sampling and Analytical Techniques .....	77
3.1.2 Phase Chemistry .....	78
3.1.3 Whole Rock Chemistry .....	84
3.1.4 Discussion .....	86
3.2 Chrome-Spinel Chemistry.....	88
3.2.1 Mechanism producing Compositional Zonation in Chromite.....	92
3.2.2 Cryptic Variations in Chrome-Spinel .....	94

	Page
3.2.3 Discussion .....	94
3.3 Dike Chemistry .....	96
3.3.1 Geochemical Characteristics of the Dike Suites .....	96
3.2.2 Comparison with the Troodos Lavas .....	101
3.2.3 Discussion .....	105
 <b>Chapter 4. Implications for Crustal Evolution</b>	
4.1 Model .....	107
4.2 Conclusions.....	112
 <b>REFERENCES.....</b>	 <b>114</b>
 <b>APPENDICES</b>	
Appendix A Tables of Analyses.....	124
Appendix B Analytical Methods and Sample Preparation.....	138
B.1 AA (atomic absorption) .....	138
B.2 XRF (X-ray fluorescence) .....	142
B.3 ICPMS (inductively coupled plasma mass spectrometry). .....	143
B.4 Electron Microprobe Analysis	
B.4.1 Jeol JXA 50A Electron Microprobe.....	146
B.4.2 Jeol 733 Superprobe.....	147
B.5 Sample Preparation.....	148
B.5.1 Whole Rock Powders.....	148
B.5.2 Thin Sections .....	148

### List of Figures

<b>Figure 1.1</b> Ophiolites of the Peri-Arabic belt. ....	2
<b>Figure 1.2</b> Geological subdivisions of Cyprus. ....	7
<b>Figure 1.3</b> Geology of the Troodos Ophiolite.....	10
<b>Figure 1.4</b> Location of the Amiandos Map Area. ....	18
<b>Figure 3.1</b> Phase chemical variation profiles of the Ultramafic Cumulate Section..... (in back pouch)	
<b>Figure 3.2</b> Whole rock chemistry variation profiles of the Ultramafic Cumulate Section..... (in back pouch)	
<b>Figure 3.3</b> Composition of pyroxenes from the layered cumulate section. ....	83
<b>Figure 3.4</b> Mineral chemistry variation profiles of chrome-spinel from the base of the cumulate section..... (in back pouch)	
<b>Figure 3.5</b> Compositional core to rim variation in chrome-spinel grains .....	93
<b>Figure 3.6</b> Variation diagrams of major, minor and trace elements vs MgO, displaying compositional fields of the depleted and non-depleted dike suite.....	97
<b>Figure 3.7</b> Variation diagrams of immobile trace elements a) Zr vs Y and b) Cr vs Yb illustrating differentiation characteristics within the dikes.....	99
<b>Figure 3.8a</b> Rare-earth element distribution patterns of the dikes normalized to chondrite rare-earth abundances.....	100
<b>3.8b</b> Geochemical abundance patterns for the individual dike suites normalized to MORB.....	100
<b>Figure 3.9</b> Variation diagram of TiO <sub>2</sub> vs MgO for the aphyric and porphyritic dike suites compared to the Troodos volcanics.....	102
<b>Figure 3.10</b> Chondrite normalized rare-earth element distribution patterns of the aphyric and porphyritic dike suites compared to the compositional fields for the extrusive volcanic and sheeted dikes of the Troodos Ophiolite.....	103
<b>Figure 4.1 A-C</b> Schematic representation of the magmatic evolution of the Troodos oceanic crust. ....	108

<b>Figure B1</b> ICP-MS detection limits (average of several runs) in ppm for elements of the MUN trace element package. For the REE and less abundant trace elements, detection limits are generally about 0.01 ppm.....	144
---	-----

### List of Maps

<b>Map 1.</b> Geology of the Amiandos area, Cyprus.....	(in back pouch)
<b>Map 2.</b> Geology of the Ultramafic Cumulate Section.....	(in back pouch)

### List of Tables

<b>Table 1.1</b> Ophiolites of the Peri-Arabic belt.....	4
<b>Table 2.1</b> Magmatic History of the Amiandos Area.....	24
<b>Table A1</b> Olivine phase chemistry of chrome dunites.....	125
<b>Table A2a</b> Olivine phase chemistry of banded orthopyroxenite-dunite.....	125
<b>Table A2b</b> Orthopyroxene phase chemistry of banded orthopyroxenite-dunite.....	125
<b>Table A3</b> Olivine phase chemistry of layered section.....	126
<b>Table A4</b> Clinopyroxene phase chemistry of layered section.....	128
<b>Table A5</b> Orthopyroxene phase chemistry from layered section.....	130
<b>Table A6</b> Plagioclase phase chemistry of layered section.....	130
<b>Table A7</b> Chrome-spinel phase chemistry of layered section.....	131
<b>Table A8</b> Whole rock major element chemistry of layered section.....	132
<b>Table A9</b> Whole rock trace element chemistry of layered section.....	134
<b>Table A10</b> Whole rock major element chemistry of diabase dike suites.....	136
<b>Table A11</b> Whole rock trace element chemistry of diabase dike suites.....	136
<b>Table A12</b> REE analysis of diabase dike suites.....	137

## List of Plates

	Page
<b>Plate 1.1</b> The Amiandos Asbestos Mine, viewed from the west. ....	19
<b>Plate 2.1</b> Contact between residual mantle harzburgite and ultramafic cumulate rocks along the Amiandos fault zone. View looking south from Pano Amiandos. ....	23
<b>Plate 2.2</b> Nature of banded serpentized dunite-orthopyroxenite unit. Located immediately east of Pano Amiandos. ....	29
<b>Plate 2.3</b> Isoclinally folded banded serpentized dunite-orthopyroxenite. Located immediately east of Pano Amiandos. ....	29
<b>Plate 2.4</b> Photomicrograph of well developed recrystallized polygonal texture in orthopyroxenite layer. ....	30
<b>Plate 2.5</b> Polished slabs of serpentized dunite-orthopyroxenite unit illustrating the layer-parallel foliation fabric defined by the prefold dimensional orientation of orthopyroxene. Thin vertical dark bands perpendicular to layering in T26 represent serpentization along later fractures. ....	30
<b>Plate 2.6</b> Photomicrograph displaying interstitial nature of clinopyroxene poikilitically enclosing orthopyroxene. Note the polygonal nature of orthopyroxene in the lower left corner of the photo. ....	31
<b>Plate 2.7</b> Well washed exposure of banded serpentized dunite-orthopyroxenite demonstrating the interstitial nature of clinopyroxene, weathering a distinctive white colour in contrast to the darker rust brown host. ....	31
<b>Plate 2.8</b> Polished slabs illustrating transitional nature between dunite, clinopyroxene-dunite, and wehrlitic units, resulting from a progressive increase in intercumulate clinopyroxene. ....	37
<b>Plate 2.9</b> Weathered exposure of clinopyroxene (white)-dunite (brown). ....	38
<b>Plate 2.10</b> Photomicrograph of euhedral chromite, poikilitically enclosed by intercumulate clinopyroxene. ....	38
<b>Plate 2.11</b> Weathered exposure of olivine-rich wehrlite with intercumulate clinopyroxene. ....	40
<b>Plate 2.12</b> (Sample 028b) Polished slab of poikilitic wehrlite. ....	40

<b>Plate 2.13</b> (Samples 078, 078.2) Polished slabs of coarse grained herzolite with cumulate olivine, intercumulate clinopyroxene and oikocrysts of orthopyroxene.....	41
<b>Plate 2.14</b> (Sample 103) Polished slab of coarse grained plagioclase-bearing wehrlite with cumulate olivine (black), adcumulate clinopyroxene (grey) and intercumulate plagioclase (white). .....	41
<b>Plate 2.15</b> Polished slab of coarse grained melagabbro with moderately developed cm scale layering defined by a variation in olivine content. ....	43
<b>Plate 2.16</b> Polished slab displaying grain size reduction and the development of gneissic banding within the melagabbro. ....	43
<b>Plate 2.17</b> Close-up view of olivine gabbro illustrating pitted nature as a result of weathered out olivine grains. Feldspar rich cm scale layer present. ....	44
<b>Plate 2.18</b> Well developed penetrative ( $S_1$ ) tectonite fabric in olivine gabbro defined by elongation of olivine.....	45
<b>Plate 2.19</b> Photomicrograph of a plastically deformed olivine grain containing inclusions of plagioclase. ....	47
<b>Plate 2.20</b> Photomicrograph of clinopyroxene and plagioclase aggregate contained in deformed olivine grain (enlarged area of Plate 2.21).....	47
<b>Plate 2.21</b> Photomicrograph of deformed olivine grain enclosing surrounding plagioclase and clinopyroxene.....	48
<b>Plate 2.22</b> Photomicrograph of plastically deformed olivine grain enclosing surrounding plagioclase and clinopyroxene.....	48
<b>Plate 2.23</b> Photomicrograph of orthopyroxene oikocryst in deformed olivine gabbro. ....	49
<b>Plate 2.24</b> Outcrop of recrystallized mylonitic gabbro, located 400 meters NE of Pano Amiandos. ....	51
<b>Plate 2.25</b> Weathered surface of medium grained equigranular isotropic gabbro.....	51
<b>Plate 2.26</b> Polished slab displaying phase layering in gabbro. Light coloured layers composed almost entirely of plagioclase, darker layers composed of clinopyroxene and plagioclase.....	53
<b>Plate 2.27</b> Isoclinally folded mafic layer, locally developed within the gabbro. ....	53
<b>Plate 2.28</b> Location of the ultramafic cumulate line of section viewed from the west.....	54

<b>Plate 2.29</b> View of ultramafic cumulate rock in the southwestern area of the map sheet displaying a high percentage of intrusive clinopyroxenite with screens of darker ultramafic cumulate. ....	54
<b>Plate 2.30</b> T45: Massive wehrlitic unit with well developed clinopyroxene oikocrysts.....	56
<b>Plate 2.31</b> T48: Well layered wehrlite-olivine clinopyroxenite (detail in Plate 2.32). ....	56
<b>Plate 2.32</b> T48: Exposure of cm scale modal layering in wehrlite, olivine-clinopyroxenite and clinopyroxenite. ....	57
<b>Plate 2.33</b> T57 Wehrlite-olivine clinopyroxenite-clinopyroxenite modal layering with minor intercumulate plagioclase (white). 57	
<b>Plate 2.34</b> Variations in the content of plagioclase from approximately 1 (T57) to 10 (T60) modal percent.....	59
<b>Plate 2.35</b> Detailed view of the compositional layering. Sample T28.3 - displays a typical ductile flow fabric which is sporadically developed throughout the section.....	59
<b>Plate 2.36</b> Clinopyroxenite (light grey) intruding cumulate poikilitic wehrlite (black). Xenolith of wehrlite in center of photo is roughly 3 m wide.....	63
<b>Plate 2.37</b> Pegmatitic texture of intrusive clinopyroxenite. Located on ridge east of Pano Amiandos. ....	63
<b>Plate 2.38</b> Polished slab of intrusive clinopyroxene-rich dike. 025 - Pyroxenite with orthopyroxene oikicrysts. 0.62 - olivine clinopyroxenite with interstitial plagioclase. ....	64
<b>Plate 2.39</b> Exposure of Late magmatic suite varitextured gabbro. ....	66
<b>Plate 2.40</b> Polished slab of varitextured gabbro.....	66
<b>Plate 2.41</b> Late magmatic suite gabbro intruding fine-medium grained deformed olivine gabbro of the early plutonic suite. ....	67
<b>Plate 2.42</b> Late suite gabbro vein cross-cutting mylonitic fabric in early plutonic suite gabbro. ....	67
<b>Plate 2.43</b> Polished slab with a wide variety and high abundance of xenoliths.....	69
<b>Plate 2.44</b> Epidote-rich trondhjemite with diabase xenoliths.....	69
<b>Plate 2.45</b> Polished slabs of the non-depleted dike suite illustrating their darker aphanitic appearance.....	70

<b>Plate 2.46</b> Polished slabs of several porphyritic (depleted) dikes displaying general mesoscopic porphyritic texture. Sample 036 is relatively fresh compared to the others. ....	70
<b>Plate 2.47</b> Exposure of gabbro displaying the effects of crushing and the development of local fracture and shear zones. ....	74
<b>Plate 2.48</b> Thrust contact between harzburgite and gabbro exposed in road north of Pano Amiandos. ....	75
<b>Plate 3.1a</b> Typical grain size of chromite poikilitically enclosed by clinopyroxene in clinopyroxene-dunite. ....	89
<b>Plate 3.1b</b> As in 3.1a, X nicols. ....	89
<b>Plate 3.2a</b> Typical chromite grain size in serpentinized dunite. Also displays nature of remaining olivine kernels in serpentine matrix. ....	90
<b>Plate 3.2b</b> As in 3.2a, X nicols. ....	90

#### Abbreviations Used

Ol	-	Olivine
Cr	-	Chromite-Spinel
Cpx	-	Clinopyroxene
Opx	-	Orthopyroxene
Plag	-	Plagioclase
dun	-	Dunite
orthopy	-	Orthopyroxenite
web	-	Websterite
clinopy	-	Clinopyroxenite (also clpy)
gabnor	-	Gabbronorite

# Chapter 1

## INTRODUCTION

### 1.1 INTRODUCTION

Oceanic spreading centers are dynamic features which evolve through a close interplay of magmatic and deformational processes. The nature of these processes and how they relate to the evolution of the oceanic crust have received much attention in the last decade, particularly through the study of their on land equivalents - ophiolites. Such investigations indicate that the processes are extremely complex and require detailed study.

The following study focuses on the magmatic and structural evolution of a segment of the mantle-crust transition zone within the Troodos ophiolite, Cyprus.

### 1.2 REGIONAL GEOLOGICAL SETTING

The Troodos ophiolite, situated on the island of Cyprus, represents the western extension of a 3500 km belt of discontinuous ophiolites, the "Peri-Arabic" belt (Knipper et al., 1986), which extends from the Antalya complex in SW Turkey along the Eurasian - Afro-Arabian suture to the Semail Nappe in Oman (Figure 1.1).

Ophiolites along the belt vary in character from ophiolitic melanges (Bitlis Kermanshah and Neyriz) within the northern margin to relatively undeformed intact stratiform complexes located at the southern limits of the belt (Troodos, Hatay and Semail) (Hall, 1985). Comparative reviews of the various ophiolites along the belt, either as individual groups; Troodos, Antalya, Hatay, and Baer-Bassit (Robertson and Woodcock, 1979; Delaune-Mayere, 1985; 1980; Whitechurch et al., 1985); Hatay and Baer-Bassit (Delaloye and Wagner, 1985); Bitlis and Neyriz (Hall, 1980); Neyriz and Oman (Lippard, 1989), or as a whole, (Robertson and Dixon, 1985; Knipper et al., 1986) demonstrate the inherent



Figure 1.1 Ophiolites of the Peri-Arabic belt.

similarities throughout the belt in terms of an overall geotectonic framework.

A coherent picture with respect to the development and final emplacement of these ophiolites may be summarized as follows:

Rifting within the southern supercontinent of Gondwanaland during Permo-Triassic time resulted in the birth of the Mesozoic Neo-Tethyan ocean basin. Continuous sedimentation, ranging from shallow to deep water deposition, from Late Triassic to Mid-Cretaceous records the development of the Neo-Tethyan passive margin. Remnants of this are presently seen as either 1) tectonic slices of sedimentary and volcanic rocks occurring between the ophiolitic nappes or, 2) as autochthonous or parautochthonous continuations of the Arabian continental margin.

It has been suggested that Late Triassic alkalic-basic volcanic rocks common throughout the belt may reflect initial stages of rifting of either continental (Robertson and Woodcock, 1979; Mayere, 1985) or attenuated continental crust (Whitechurch et al., 1985); however it is more likely that they are remnants of intraoceanic islands tectonically incorporated with passive margin and ophiolitic rocks during accretion (Searle and Malpas, 1980, 1982; Malpas et al., in press).

From Mid to Late Cretaceous, northward subduction involving consumption of the Neo-Tethys took place. This subduction event is most commonly recorded by the presence of sedimentary melange units indicative of flysch basin or fore-deep successions containing both oceanic and continental detritus, and less commonly by isolated occurrences of blueschist-facies metamorphism as identified within the Bitlis ophiolite zone in eastern Turkey (Hall, 1985) and the Semail Complex in N.E. Oman (Lippard, 1983).

Most ophiolites were thrust southwards during Late Santonian time onto the Arabian continental margin, the same intra-Maastrichtian emplacement age

Table 1.1

## OPHIOLITES of the PERI-ARABIC BELT

Country/ Region	Individual complexes	Formation age <sup>a</sup>	Obduction <sup>b</sup> / emplacement <sup>c</sup> age	Remarks
1. Taurides	Antalya	KM?	85-95 Ma <sup>1</sup> [Metamorphics cut by Campanian (75 Ma) dykes]	Largely harzburgites. Layered sequence well exposed by Antalya. No sheeted dykes or lavas. Metamorphic soles and mantle sequences cut by tholeiitic dykes.
2. Cyprus	Troodos	90-93 Ma <sup>2</sup> (U-Pb, Zircon)	87-89 Ma Santonian - Pre Maastrichtian <sup>3</sup>	Intensely studied. Recent work on lavas suggests a supra- subduction zone setting.
3. NW Syria SE Turkey	(a) Hatay (b) Baer- Bassit	KM?	86-96 Ma Post Campanian - Pre Maastrichtian emplacement	Complete sequences exposed Harzburgitic. Island- arc tholeiite chemistry.
4. Zagros	(a) Khoy (b) Neyriz (c) Kermanshah	KM?	94.9 ± 7.6 Ma <sup>4</sup> Post Campanian - Pre Maastrichtian emplacement	Ophiolites strung out along Zagros fault zone (2000 km long). Harzburgite at Neyriz cut by low-K tholeiite dykes. Island arc tholeiite lavas in other complexes.
5. Oman Mts.	Semal (Samal)	98-94 Ma (U-Pb, Zircon)	96-85 Ma Post Campanian - Pre Maastrichtian	Harzburgitic mantle sequence Island-arc tholeiite chemistry. emplacement

## NOTES:

- a "Formation age" refers to isotopic ages of igneous minerals (usually of doubtful validity except in cases of U-Pb Zircon ages) and the palaeontologic age of interbedded or conformable sediments. KM - Middle Cretaceous
- b "Obduction ages" given in Ma in this column are isotopic ages of amphibolites in metamorphic soles taken to indicate the time of initial oceanic displacement.
- c "Emplacement age" is generally a minimum age of nappe emplacement bracketed by the age of the youngest rocks involved in the thrusting and the oldest continental or shallow marine beds.

Modified after Lippard *et al.* (1989). Changes are indicated by reference to source.

1. Whitechurch *et al.* (1984)
2. Mukasa and Ludden (1987)
3. Blome and Irwin (1985)
2. Knipper *et al.* (1986)

being more or less precisely bracketed everywhere (Table 1). The emplacement marks the zone of closure between the African and Eurasian plates and the almost complete disappearance of the Neo-Tethys Ocean.

A common feature at the base of the ophiolite nappes of the "Peri-Arabic belt", where exposed, is the presence of amphibolite facies metamorphic rocks (Malpas et al., in press; Coleman, 1988; Knipper, 1986; Whitechurch et al., 1985), interpreted to be the result of intraoceanic tectonic slicing. The age of these amphibolites relative to the age of the ophiolites indicates that the metamorphic events followed, almost directly, the formation of the ophiolites (Table 1).

Internally, the ophiolites along the belt display remarkable similarities with respect to age and environment of formation (Table 1). Both the Troodos and Semail ophiolites, situated at opposite ends of the belt, are directly overlain by radiolarian-bearing umbers which indicate a Turonian age (Blome and Irwin, 1985). Temporal similarities are also evident from reliable U-Pb isotopic age dates of zircons from plagiogranites occurring in both these ophiolite complexes. Mukasa and Ludden (1987) reported an average age of 92 Ma for Troodos, which is only slightly younger than the U-Pb zircon age of 95 Ma reported for the Semail ophiolite (Tilton et al., 1981).

Trace element characteristics of extrusive volcanic rocks associated with all the ophiolites of the "Peri-Arabic belt", indicate that the eruptive setting is most likely that of a suprasubduction zone (Moores et al., 1984). These authors proposed that all the ophiolites were formed in a marginal basin-island arc complex setting similar to the modern Andaman Sea. In this model the present discontinuous nature of the ophiolites is interpreted as a primary feature reflecting discrete spreading centers separated by a series of transform faults.

### 1.3 LOCAL GEOLOGICAL SETTING

The Island of Cyprus (Figure 1.2), covering an area of roughly 9,250 km<sup>2</sup>, is situated in the eastern corner of the Mediterranean sea, 70 km south of Turkey and 100 km west of Syria. The island is broadly divisible into four, slightly arcuate, east-west trending geologic zones (Figure 1.2).

Forming the structural and morphological backbone of the island, the *Troodos Ophiolite* and *Limassol Forest Complex* outcrop as a WNW-ESE oriented elongate dome of oceanic crust, which is geologically distinct from the geologic zones to the north and south. Both the adjoining *Kyrenia Range* to the north and *Mamonia Complex* to the south, include, in part, telescoped remnants of tectonically dismembered Mesozoic continental margin type sedimentary and igneous rocks. Since the Troodos Ophiolite is the centerpoint of the study it is described more fully below.

1. The *Limassol Forest Complex* represents a portion of the *Arakapas fault Zone*, a supposed oceanic transform (Moore and Vine, 1971; Simonian and Gass, 1978) which borders the Troodos ophiolite along its southwesterly exposed margin (Figure 1.2). The complex consists of an ultramafic core dominated by tectonized harzburgite with subordinate dunite invaded by near vertical intrusions of wehrlite and isotropic gabbro, surrounded by a discontinuous envelope of dikes and lavas. East-west trending vertical mylonitic and serpentized shear zones throughout the complex, cut by dikes, suggest intrusion into the active part of a leaky transform fault domain (Murton and Gass, 1986).
2. The *Kyrenia Range* comprises a 160 km long arcuate mountain belt, dominated by a steep northward dipping composite thrust pile of four main

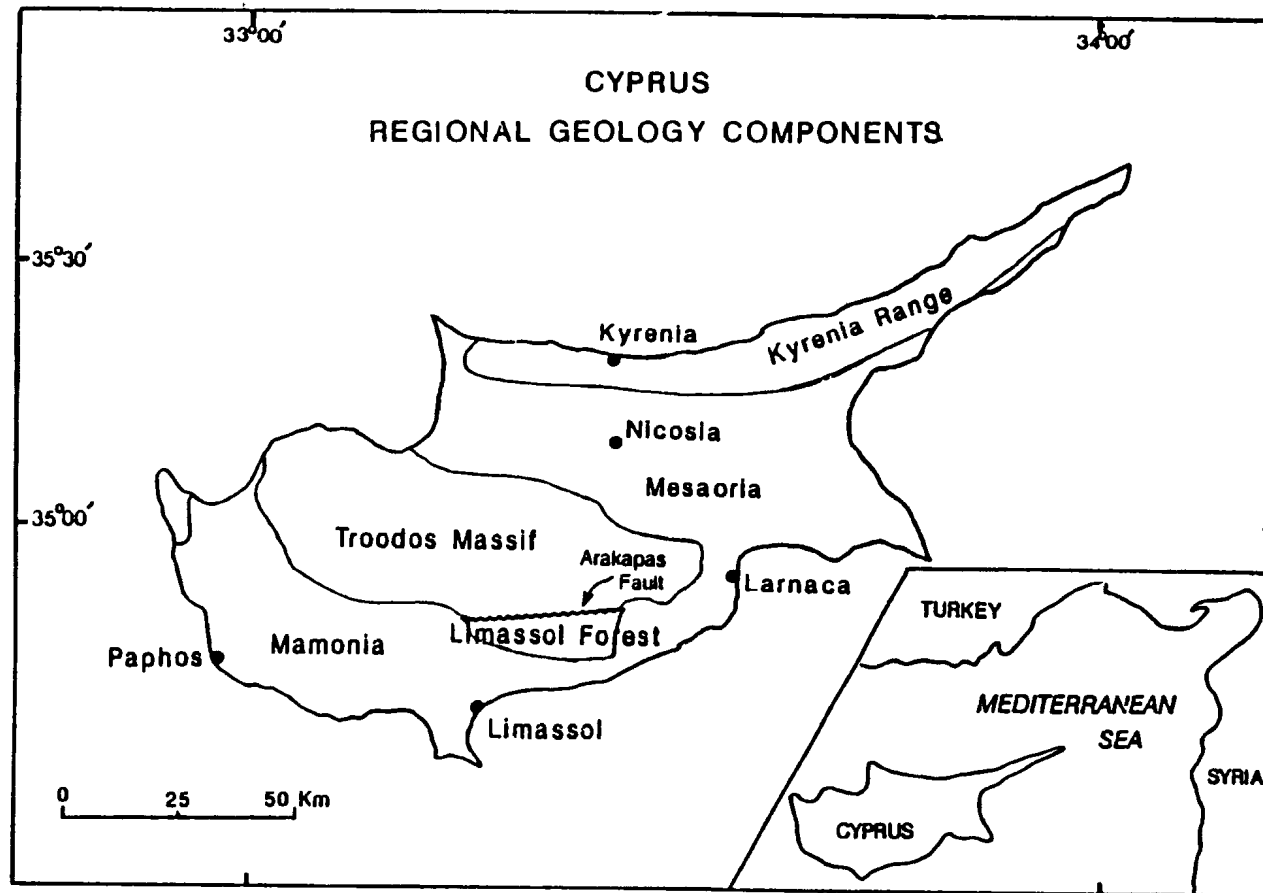


Figure 1.2 Geological subdivisions of Cyprus.

thrust-assemblages separated by major unconformities (Robertson and Woodcock, 1986). The oldest rocks exposed in the core of the range are Permian to Late Cretaceous massive shallow water limestones of the Trypa Group. These limestones are unconformably overlain, first by patchy volcanoclastic sediments (Kiparissovouno Formation) and then by an overlying Cretaceous to Early Eocene sequence of pelagic limestones, carbonate breccias and bimodal acid-basic volcanics (Lapithos Group) (Robertson and Woodcock, 1980, 1986). During Middle Miocene emplacement of the Kyrenia Range into its present position, a thick clastic sequence (Kythrea Flysch) was deposited on both the north and south flanks of the range (Robertson and Woodcock, 1980).

3. The *Mamonia Complex* of southwest Cyprus comprises an imbricate thrust stack of igneous, sedimentary and metamorphic units broadly divisible into largely volcanic and sedimentary packages.
  - a) First, a Late Triassic alkaline mafic volcanic unit, including minor intrusive and sedimentary rocks, the *Dhiarizos Group* (Swarbrick, 1980; Swarbrick and Robertson, 1980) represents development of a within plate off-axis oceanic island series (Malpas et al., in press).
  - b) Second, a Late Triassic to Mid Cretaceous sedimentary sequence the *Ayios Photios Group* documents the build up of the Mesozoic passive continental margin (Robertson and Woodcock, 1980; Swarbrick, 1980).
  - c) A volumetrically minor but geologically significant unit, the *Ayia Varvara Formation*, consists of tectonic slivers of amphibolite schist with intercalated metasediments that occur as fault bounded lenses within the Mamonia sequence along a serpentinite contact. These amphibolitic rocks are dated at 83 to 90 Ma by  $^{40}\text{Ar}/^{39}\text{Ar}$  methods (Spray and Roddick,

1981) and are suggested by Malpas et al. (in press) to represent portions of the Mamonia Complex, metamorphosed during subduction, by the overriding young Troodos crust. This age and interpretation is consistent with that of similar amphibolitic units throughout the "Peri Arabic" belt (Knipper et al., 1986), indicating that the timing of detachment followed very closely the age of formation of the oceanic crust.

4. The *Mesaoria Plain* is a broad valley of circum-Troodos, Upper Maastrichtian to recent sedimentary rocks. The sedimentary succession is divisible into three main sequences whose boundaries coincide with periods of uplift of the island (Cluntuar et al., 1977). The basal Lefkara Formation forms up to 700 m of Upper Maastrichtian to Lower Miocene pelagic chalks. The Lefkara Formation is unconformably overlain by the Pakhna Formation comprising up to 600 m of pelagic marls and limestones from Lower Miocene to Lower Pliocene in age. The Pliocene deposits, represented by the Myrtou and Nicosia Formations, are dominated by marls and clays which give way upward to coarse detrital calcareous and igneous material generated when the Troodos Massif was elevated to its present position.

#### 1.4 TROODOS OPHIOLITE

The Troodos ophiolite (Figure 1.3) displays a complete ophiolite stratigraphy (Penrose Conference, 1972) which, as a result of Late Tertiary domal uplift (Robertson, 1977) centered on Mount Olympus, is now reflected in a roughly annular outcrop pattern in which extrusives of the ophiolite occupy the periphery of the dome and give way inward to progressively lower structural units, with tectonized harzburgite outcropping at the summit of Mount Olympus.

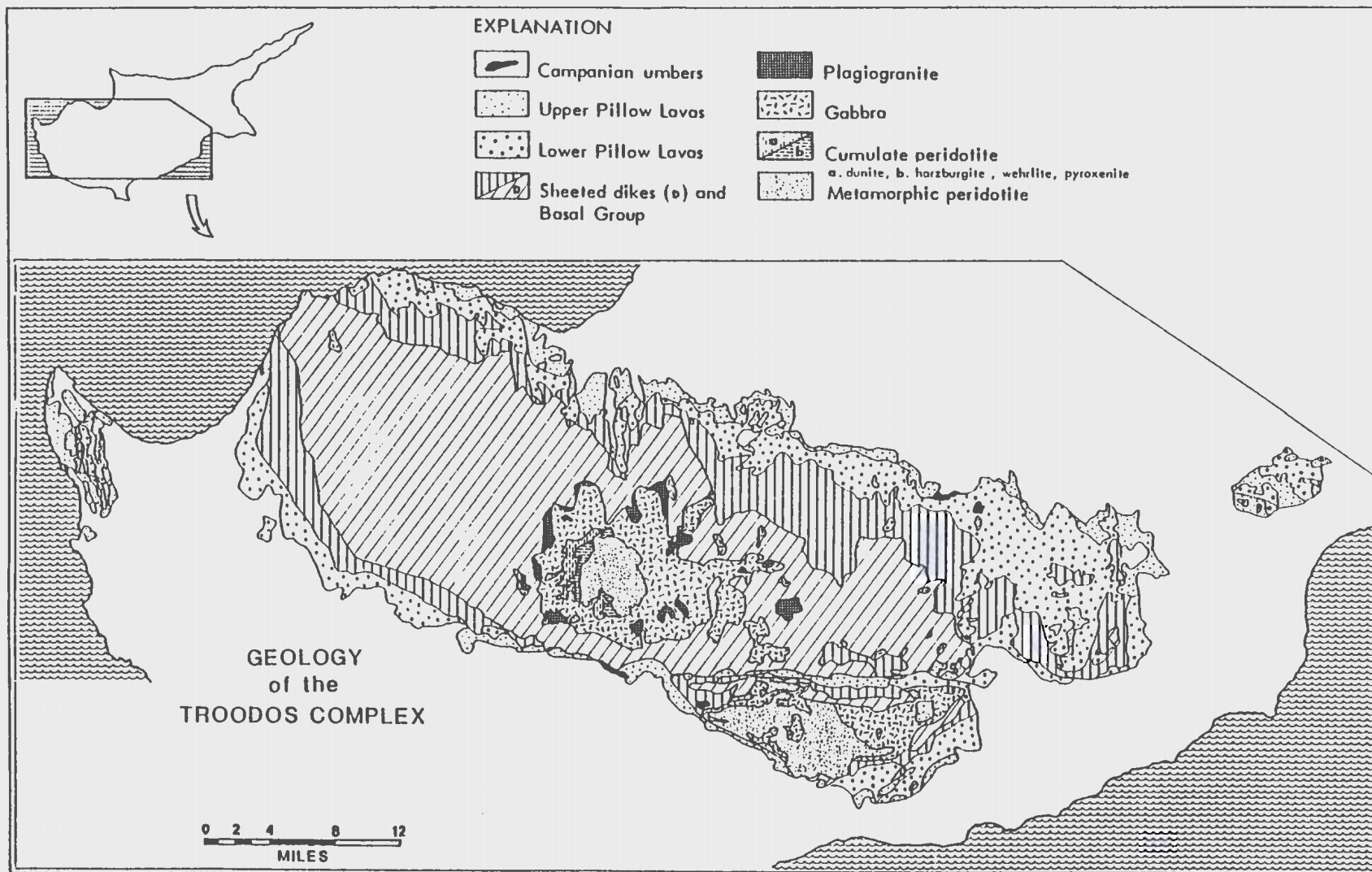


Figure 1.3 Geology of the Troodos Ophiolite (Bear, 1960).

The gross stratigraphy of the ophiolite displays pillowed mafic volcanic rocks, capped by deep oceanic cherts which give way downward through a sheeted dike unit into a plutonic sequence, represented first by the high level intrusives, comprising generally isotropic trondjemites, diorite and ferrogabbros which overlie a more mafic differentiated sequence of gabbros, peridotites and dunites. Residual mantle harzburgite tectonites containing lenticular pods of cumulate chrome-spinel bearing dunite form the exposed base of the ophiolite.

In detail, relationships within and between the various lithologies of the ophiolite sequence demonstrate a complex magmatic history. Plutonic units, display abundant evidence of multiple intrusion that are clearly identified in the field by a variety of cross-cutting relationships.

Extrusive rocks include pillow lavas, pillow breccias and massive flows. Pillowed volcanic rocks are divisible into a number of petrologically and geochemically distinct lava units (Robinson et al., 1983; Schminke et al., 1983). The Lower Pillow Lavas (LPLs) which directly overlie the Sheeted Dike Complex are generally aphyric andesites, dacites and rhyolites of an evolved-arc tholeiite suite. Subvertical picritic dikes cut the LPLs and feed the overlying Upper Pillow Lava (UPL) sequence. The UPLs are dominated by olivine-phyric basalts and basaltic andesites with boninitic affinities. This unit has itself been divided into four lava types on the basis of texture and macroscopic phenocryst mineralogy (Malpas and Langdon, 1984). In addition, UPLs on the southern flank of Troodos, close to and within the Arakapas Fault are typically more depleted than those to the North and may be considered as a third geochemical suite of lavas (Cameron, 1985).

The LPLs pass downward through a transition or mixed zone of dikes and lava screens several tens of meters thick (Basal Group) into the steeply dipping N-S trending Sheeted Dike Complex. Baragar et al. (1987, 1989) describe the

interior of the complex as an intricate plexus of subparallel dikes intrusive only into one another. On the basis of chilling relationships four categories of dikes were identified by these authors, and include; 1) both contacts chilled, 2) West contact chilled, 3) East contact chilled or 4) no contacts chilled, with the majority of the dikes having both contacts chilled. Based on these observations it was proposed that dike emplacement was intermittent, and from multiple discrete centers along a spreading ridge, each possibly 50 to over 100 meters in width.

Contact relationships between the Sheeted Dike Complex and the underlying plutonic sequence are highly variable. Dikes may intrude and also be intruded by, or less commonly arise directly from the "high level<sup>1</sup>" plutonic rocks (Malpas and Brace, 1989).

Recent detailed and systematic field investigations within the plutonic section of the Troodos ophiolite (Dunsworth, 1989; Benn, 1986; Benn and Laurent 1987; Malpas and Brace, 1989; Malpas et al., 1989a, b) have been fundamental in recognizing the multiple magmatic nature of the plutonic crust generated by prolonged intermittent igneous activity. Notably, these investigations have been able to demonstrate the complexity and variability of the different magmatic events. Such observations support the cross-cutting relationships noted throughout the sheeted dyke section which Baragar et al. (1987, 1989) concluded must be generated by intermittent intrusion from discrete centers, and are further commented on throughout this thesis.

---

<sup>1</sup> The term *high level intrusives* used throughout refers to the most differentiated of the oceanic plutonic rocks; these rocks are most commonly identified at high crustal level of the plutonic section. They are commonly isotropic coarse to pegmatitic and varitextured and include gabbro, hornblende gabbro, diorite and plagiogranite. In the present map areas these rocks are seen at basal crustal levels.

## **1.5 THE CYPRUS CRUSTAL STUDY PROJECT**

In 1981 a major re-investigation of the Troodos ophiolite was undertaken by a multinational consortium of scientists known as the International Crustal Research Drilling Group (Geotimes, 1983). This research project involved over 4.5 km of deep crustal drilling and detailed field and laboratory studies. Many publications have resulted from this combined research effort, of which this study is a part.

Initial investigations of this research project focused on petrological and geochemical aspects of the volcanic rocks of the ophiolite (Robinson et al., 1983; Schmincke et al., 1983; Thy, 1984; Malpas and Langdon, 1984). These studies were successful in confirming the earlier suspicions of Miyashiro (1973), that the volcanic rocks formed within a subduction zone environment. More recently, with the drilling of hole CY-4 which sampled a continuous section through the sheeted dike and upper plutonic section, work has focused on subvolcanic and magma chamber processes of ophiolitic crustal formation (Gibson et al., 1989). This work has demonstrated that, as in the case of the lavas, a similar bimodal distribution is present throughout the sheeted dikes (Baragar et al., 1987, 1988) and the plutonic section (Benn, 1986; Malpas and Brace, 1987, Malpas et al., 1989a,b; Thy, 1987a, 1987b; Thy et al., 1988) supporting the concept of multiple magma chambers.

## **1.6 EARLIER THOUGHTS on the PLUTONIC SECTION of the TROODOS OPHIOLITE**

The map area was originally included in a 1:31,680 (2 inch to 1 mile) scale geology map of the Xeros-Troodos area accompanying Memoir No. 1 of the Geological Survey Department, Cyprus (Wilson, 1959). This mapping represented the first detailed account of the geology of Troodos. Since that time the immediate map area has received little attention.

Wilson (op. cit.) was the first to recognize that the pillow lavas, diabase and gabbros were cogenetic and he attributed their formation to extrusion in an ocean basin. The underlying ultramafic rocks were considered to be derived from a peridotite layer in the earth, which was emplaced when the continental crust moved aside due to great tensional stress. Wilson also noted features which distinguished the plutonic rocks from layered basic intrusions, in particular, the lack of a basement to the complex and the nature of the vertical banding and igneous layering in the ultramafic rocks.

Gass and Masson-Smith (1963), following a detailed gravity survey, suggested that the ophiolite represented a thick (11 km) slab of upthrust oceanic crust. They interpreted all of the plutonic rocks to be differentiates of one parent magma which was emplaced into the Sheeted Dike Complex. They attributed the vertical banding to a period of remobilization and large-scale flow of quasi-solid magmas.

Moores and Vine (1971) suggested that the harzburgites and dunites are residual upper mantle tectonites and that the peridotites and gabbros were the products of fractional crystallization of a melt derived from the partially fused mantle material. These authors also, on the basis of mutually intrusive relationships between gabbro and sheeted diabase, concluded the existence of nested magma chambers suggesting multiple intrusive events.

Greenbaum (1972) studied the petrology of the western border of the harzburgite and the extensive belt of ultramafic cumulate rocks. He identified contacts between successively less mafic rock types and constructed a composite stratigraphic section suggesting that the plutonic complex crystallized in a large (> 20 kilometers in width) steady-state magma chamber. The dunites were considered to be of cumulate and not residual origin as previously suggested by Moores and Vine (1971).

George (1975, 1978) conducted a detailed petrofabric analysis of the structures present in the plutonic rocks and concluded that the penetratively deformed lower level ultramafic cumulates, "*ultramafic metacumulates*" were affected by synmagmatic deformation. The vertical orientation of the penetratively deformed residual mantle and ultramafic metacumulates was attributed to upward mantle flow at a spreading center.

Menzies and Allen (1975) demonstrated that the harzburgite is chemically homogeneous and lacks any cryptic mineralogic or bulk variation in  $Mg/(Mg + Fe)$ , confirming that the unit is a residuum of partial fusion.

Nicolas and Prinzhofer (1983) evaluated the structural nature of eight ophiolite complexes, including the Troodos ophiolite in order to establish whether the crust-mantle transition zone in ophiolites is of a cumulate or residual origin. They concluded that the dunites in most transition zones are of a residual origin and that the wehrlites and feldspathic dunites result from magmatic impregnation of the dunites.

Dunsworth and Calon (1984) suggested, on the basis of intrusive and deformation relationships, that the plutonic complex in the northwest of the Olympus ultramafic complex is divisible into early and late suites.

Benn (1986) studied the southernmost exposure of the Olympic ultramafic complex in the Caledonian Falls area. He demonstrated the presence of two distinct magmatic suites on the basis of field relationships and geochemical criteria.

Thy and Moores (1988) suggested on the basis of lithological and phase chemical character of the CY-4 drill core that the plutonic section of the ophiolite was generated by two distinct magmatic events. An Early Magmatic Suite which is represented by the upper gabbros, Sheeted Dike Complex and the Lower Pillow Lavas and a later suite, constituting the lower ultramafic cumulates and

### Upper Pillow Lavas.

Malpas et al. (1989a) described the geology in the vicinity of the CY-4 drill hole and demonstrated on the basis of multiple intrusive relationships that the gabbro and sheeted dike units present were generated by the intrusion of a number of magma chambers.

Malpas et al. (1989b) presented detailed field evidence of cross-cutting relationships throughout the plutonic section, supporting the view of multiple magma chambers. These authors also studied the phase chemistry of the CY-4 drill core and confirmed the presence of two distinct magma bodies in the section, that correlate with the lava subdivisions.

Hebert and Laurent (1989) investigated the mineral chemistry of the various rock types throughout the plutonic complex. They compared the phase chemistry to that published for the various oceanic environments collected by deep sea drilling and dredge hauls. They concluded that the mineralogical parameters correlate very well with those of plutonic sequences and xenoliths found in present arcs or active margins. The complex magmatic and tectonic relationships in the plutonic sequence are discussed in a series of papers appearing in the Reports of the Cyprus Crustal Study Project (Gibson et al., 1989).

## 1.7 LOCATION and PHYSIOGRAPHY of STUDY AREA

The present study area overlies the ophiolitic transition zone<sup>2</sup> on the southeastern segment of the Mount Olympus Ultramafic Complex (George 1975, 1978).

The center of the map area is located approximately 5.5 km ESE from the summit of Mt. Olympus (Figure 1.4). It covers an area of roughly 16 square kilometers, encompassing the Amiandos Asbestos Mine and the towns of Pano (Upper) and Kato (Lower) Amiandos, here termed the *Amiandos Map Area*. Tailings from the asbestos mine cover a large portion (roughly 5 km<sup>2</sup>) of the NE sector of the map area (Plate 1.1), and restrict detailed mapping to a zone east and south, marginal to the mine camp.

Mapping was conducted using 1:500 scale topographic maps obtained from the Amiandos Asbestos Mine Ltd. These maps were compiled by photogrammetric methods from 1970 aerial photography using a vertical contour interval of 8 m and provided excellent mapping control.

In the area of investigation the topographic elevation has a 800 meter range, varying from 900 meters, within the Troodos River valley approximately half a kilometer southeast of Kato Amiandos, to a maximum altitude of 1700 meters on the southwest margin of the map sheet. Topographic expression across the map sheet is dramatic, characterized by rounded spurs surrounded by deeply incised valleys and fault scarps. In faulted areas where steep gradients occur, extensive scree slopes are commonly developed. Relief is most extreme along the boundary of the ultramafic complex where the ultramafic rocks rise abruptly above the rounded hills of the surrounding gabbroic rocks.

---

<sup>2</sup> The term *Transition Zone* is used here in a similar respect to that applied by Wilson (1959) for the Troodos Ophiolite, "the margins of the ultrabasic rocks where it forms a transition zone (intermediate zone also used) between the harzburgite and dunite and the surrounding gabbro."

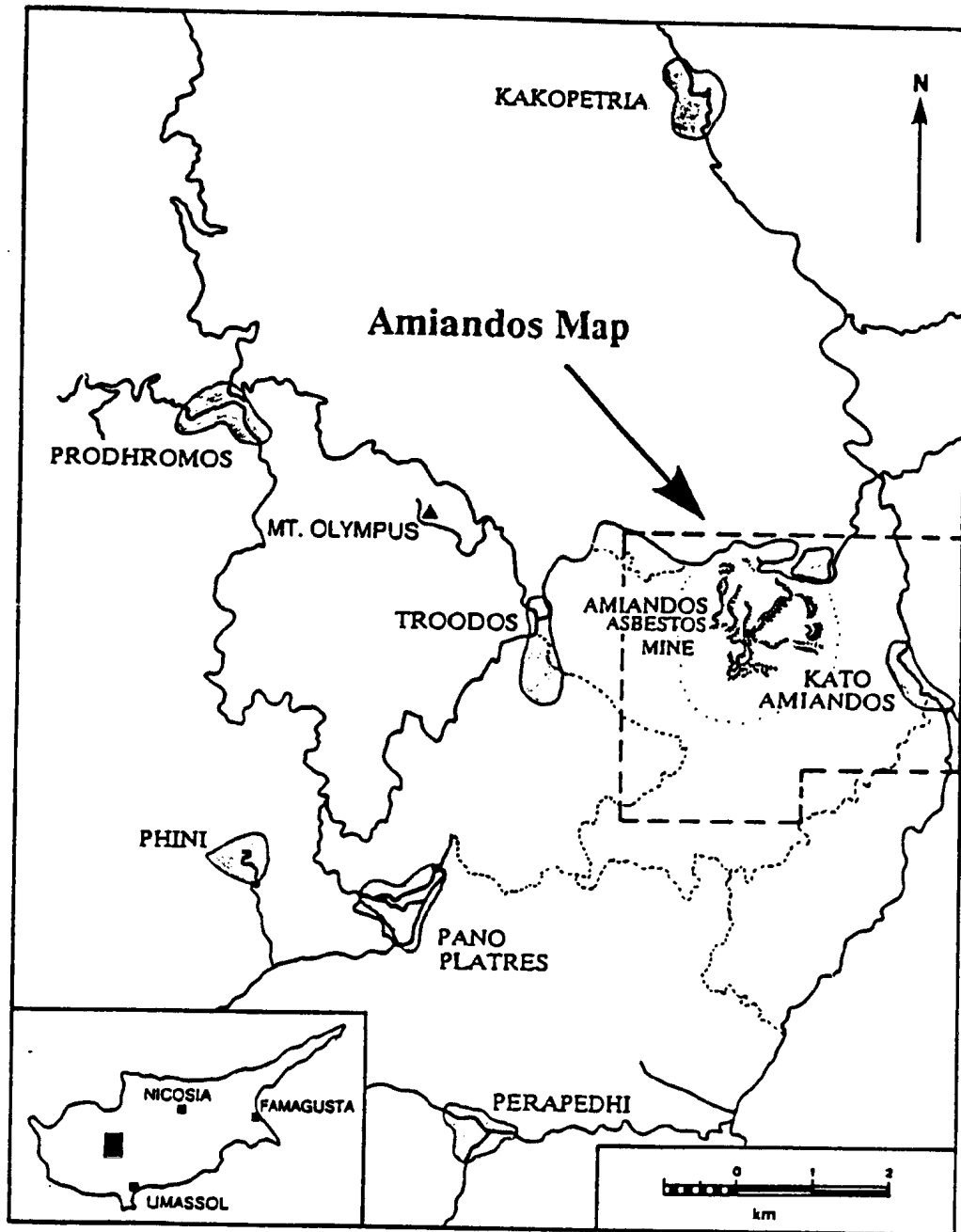


Figure 1.4 Location of the Amiandos Map Area.

The area is easily accessible by a network of mountain roads. A large number of these roads post date the 1970 photography and have been placed as accurately as possible on Map 1 (in back pouch) during the present field investigation using station posts and local topographic variations as frames of reference.



**PLATE 1.1** The Amiandos Asbestos Mine Viewed from the East.

## 1.8 SCOPE and PURPOSE

This thesis provides detailed field, petrological, geochemical and structural information for a section of the oceanic crust-mantle transition zone and mafic plutonic section of the Troodos Ophiolite. This data is used to address two series of questions pertaining to aspects of oceanic-crustal formation.

1. The first series is fundamental to the development of any acceptable model that adequately attempts to address the processes operative during the formation of oceanic crust. It may be simply stated "Exactly where is the mantle - crust boundary located ?" i.e. What is the origin of the ultramafic section commonly occurring at the mantle - crust transition zone within most ophiolite complexes (Coleman, 1977)? Are the dunitic units
  - a) residua produced by resorption of orthopyroxene during partial melting (Boudier and Nicolas, 1977; Nicolas et al., 1980; Johan and Auge, 1985) and the variably layered to banded to massive ultramafic rocks occurring between the dunite and gabbro units within ophiolites the result of magmatic impregnation of partial melt into residual mantle dunite (Boudier and Nicolas, 1977; Cassard, 1980; Nicolas et al., 1980; Nicolas and Boudier, 1980; Prinzhofer et al., 1980; Violette, 1980; Violette, 1980; Boudier and Coleman, 1981; Nicolas and Violette, 1982; Nicolas and Prinzhofer, 1983; Salisbury and Christensen, 1985; Nicolas, 1986; Lorange, 1987; Nicolas et al., 1988; Boudier et al., 1989)? Or, are they,
  - b) magnesium-rich cumulates generated by early olivine, chrome-spinel fractionation from a basaltic liquid with the overlying ultramafic rocks representing magmatic differentiates gradational from the dunitic units into less magnesium rich varieties (Greenbaum, 1972, 1977; Malpas, 1978; Stolper, 1980; George, 1975, 1978; Smewing et al., 1984)?

Current schools of thought regarding the genesis of the ultramafic rocks within the ophiolitic crust-mantle transition zone are clearly divided. These two distinct and opposing views are in a general way separable into a metamorphic and magmatic school.

Cryptic chemical and petrological variations within the mantle-crust transition zone of the Troodos ophiolite will be presented for a section of well layered ultramafic rocks from the Amiandos area. This data will be evaluated and compared to the existing database and pertinent arguments from the metamorphic and magmatic viewpoints.

2. The second series comprises two major questions: What is the relationship between deformation and magmatic events in the formation of oceanic crust? What is their relative importance and are magmatism and deformation synchronous or otherwise?

This work will attempt to place temporal and spatial significance on the progressive variation in the textural and compositional character of the multiple magmatic events and how they reflect the structural behavior of the crust during the development of the plutonic section in the Amiandos Area. On the basis of both chemistry and age relationships the individual magmatic suites will be correlated with the known lava groups of the Troodos ophiolite.

## CHAPTER 2

### GEOLOGY OF THE AMIANDOS MAP AREA

#### 2.1 INTRODUCTION

The Amiandos map area (Map 1., in back pouch) is divisible to the east and west into oceanic crust and mantle rocks respectively. Crust and mantle are in fault contact along a high angle reverse structure, the *Amiandos Fault* (Plate 2.1). West of the fault the mantle section is dominated by residual harzburgite tectonites which display an extreme variability in intensity of secondary alteration and deformation throughout the map area from north to south.

The crustal plutonic section to the east of the fault is divisible on the basis of multiple intrusive relationships into at least three distinct suites (Table 2.1). A differentiated sequence of medium grained ultramafic to mafic cumulates, termed "The Early Plutonic Suite" (M2) forms the bulk of the crustal section in the map area (roughly 80 to 85 percent). Compositionally the suite ranges from dunites through to gabbro and displays heterogeneously developed overprints of high temperature ductile deformation. The gross stratigraphy of the differentiated suite is such that less mafic, more differentiated rock types outcrop towards the east away from the the mantle section. Contained within the lower ultramafic portions of the Early Plutonic Suite are deformed and recrystallized xenoliths of banded orthopyroxenite-dunite that occur as isolated rectangular bodies, meters to tens of meters in size. These are volumetrically minor representing much less than one percent of the exposed area and are much more intensely deformed than their surrounding ultramafic host rocks. They are inferred to be remnants of cumulate layering from an earlier magmatic event (M1).



**Plate 2.1** Contact between residual mantle harzburgite and ultramafic cumulate rocks along the Amiandos fault zone. View looking south from Pano Amiandos.

Table 2.1

PLUTONIC HISTORY OF THE AMIANDOS MAP AREA

	Rock Type	Description	Magmatic Suite	Contact Relationships
	OI - Cpx (10-15%) Porphyritic Dikes	Highly altered. Displays chilled margins.	M4	INTRUDES EARLY AND LATE SUITES
L A T E  S M U A I G T M E A T I C	Aphyric Diabase	Chilled margins. Spatially associated with Trondhjemite and high level gabbro.		
	Trondhjemite	Dikes and small bodies, intrusive breccia.	M3	INTRUDES EARLY PLUTONIC SUITE
	Gabbro Clinopyroxenite	Coarse to pegmatitic, no chilled margins, minor penetrative S <sub>1</sub> deformation generally isotropic.		
E A R L Y  I P T L E  U T O N I C	Gabbro	Medium grained, isotropic to moderately deformed, locally mylonitic.		
	Olivine Gabbro	S <sub>1</sub> tectonite fabric, well developed		
	Melagabbro		M2	DIFFERENTIATED SUITE OF ULTRAMAFIC TO MAFIC CUMULATES INTRUDED BY M3 AND M4
	Clinopyroxenite, Olivine- Clinopyroxenite	medium to coarse grained, commonly -undeformed. Local recrystallized shear zones developed.		
	Wehrlite			
	Clinopyroxene- dunite, Dunite,	Highly altered, presence or absence of S <sub>1</sub> , deformation unclear.		
	Chrome-dunite			
	Banded Dunite- Orthopyroxenite	Recrystallized and deformed, locally folded	M1	OCCURS AS XENOLITHS IN THE EARLY PLUTONIC SUITE



The *Early Plutonic Suite* is intruded throughout by a petrologically variable suite of clinopyroxenite-rich peridotites, gabbros, diorites and trondhjemites termed "*The Late Magmatic Suite*" (M3). Intrusive rocks of the *Late Magmatic Suite* are massive, isotropic, coarse grained to pegmatitic and vary from centimeter scale vein networks and meter scale dikes to small intrusive bodies up to 100 meters in size. By volume, the suite represents roughly 15 to 20 percent of the crustal section in the map area. These intrusive rocks lack chilled margins, commonly cross-cut penetrative fabrics or layering developed within the *Early Plutonic Suite* and locally display xenolith-bearing margins.

Two petrologically distinct diabase dike suites were also identified throughout the map area. One dike type "*The Aphyric Dike Suite*" is characteristically fine grained, displays a distinct spatial association with the late magmatic suite and is relatively unaffected by secondary alteration. The second dike type "*The Porphyritic Dike Suite*" (M4) in contrast is porphyritic, intrudes all other elements of the plutonic section and is characterized by intense and pervasive alteration. Combined, both dike types represent roughly one to two percent of the crustal section mapped.

As extensive reviews of the petrography and associated secondary alteration of the rock types present throughout the plutonic complex have been given previously (Benn, 1986; Greenbaum, 1972, 1977; George, 1975, 1977; Wilson, 1959) they will only be discussed briefly below. Characteristics which distinguish the individual suites, and evidence of their multiple intrusive nature will be the focus of the discussion which follows.

## 2.2. RESIDUAL MANTLE HARZBURGITE TECTONITES (Map Unit 1)

As noted above, exposures of harzburgite throughout the map area from north to south are highly variable owing to the effects of secondary alteration and brittle deformation.

Harzburgite exposed south of the Asbestos Mine is the least altered (60-80% serpentinized) and displays a relict high temperature mineralogy characteristic of residual mantle and ductile deformation fabrics.

Texturally, the unit is coarse grained with a xenomorphic granular texture, and a remarkably homogeneous modal mineralogy containing 70 to 85 % olivine and 15 to 30 % orthopyroxene with accessory amounts of chrome-spinel and clinopyroxene. The orthopyroxene grains weather a light to dark brown color in contrast to the buff color of the weathered olivine. A rough surface is also imparted to the outcrop due to differential erosion of the more resistant orthopyroxene grains. On fresh surfaces the rock is dark green to black in color, with the orthopyroxene crystals displaying a characteristic luster in contrast to the dull dark green serpentinized olivine groundmass.

Tectonite foliation is defined by 5 to 15 mm elongate aggregates of uniformly distributed orthopyroxene displaying a characteristic preferred crystallographic orientation which is consistent with that developed in the harzburgite core throughout the ultramafic complex (George, 1975, 1978), that is, steeply dipping to vertical with a uniform NNW-SSE strike. Development of this penetrative fabric ( $S_1$ ) is attributed to hyper solidus to subsolidus plastic ductile deformation caused by mantle flow (George, 1975, 1978; Nicolas et al., 1980). A dominance of subvertical  $S_1$  fabrics is suggestive of their development within the upwelling convective limb of an oceanic spreading center (Nicolas and Violette, 1982).

Harzburgite, north and west of the Asbestos Mine, is intensely and pervasively altered. Exposures generally weather to a smooth surface containing

completely serpentinized olivine and diffuse black spots of bastite after orthopyroxene and display no apparent tectonite fabric.

Wilson (1959) described the central exposure of the Asbestos Mine as a "smashed bastite-serpentine area characterized by intense faulting and serpentinite brecciation." This area is host to the presently mined chrysotile asbestos which is extremely fine and occurs in a stockwork of highly irregular cross-fibre veins. These are usually less than one mm in width but rarely reach one cm. Serpentinite is composed of lizardite, chrysotile, brucite and magnetite; antigorite is restricted to veins (Magaritz and Taylor, 1974). Oxygen and hydrogen isotopic compositions of the lizardite and chrysotile suggest that the serpentine was formed by near surface, low temperature interaction of meteoric water with the host harzburgite (Magaritz and Taylor, 1974). Chemically, harzburgite occurring throughout the ultramafic complex is remarkably homogeneous and exhibits no cryptic mineralogic or bulk variation in  $Mg/(Mg + Fe)$  (Menzies and Allen, 1974). Phase chemical investigations of the harzburgite mineralogy (Greenbaum, 1972, 1977; Benn, 1986; Herbert and Laurent, 1988) have demonstrated that the unit is highly refractory in nature, with both olivine and orthopyroxene having high magnesium compositions ( $Fo_{89-91}$ ,  $En_{89-91}$ ). These authors have also shown that accessory chrome-spinels in the harzburgite are depleted in both  $TiO_2$  and  $Fe^{3+}$ .

### 2.3 BANDED DUNITE-ORTHOPYROXENITE M1 (Map Unit 2)

This unit is represented by a petrologically and structurally distinctive rock type of questionable origin which occurs as xenoliths within the ultramafic portion of the *Early Plutonic Suite*. The unit is characterized by centimeter scale alternating bands of serpentinized dunite and orthopyroxenite or websterite with subordinate olivine (Plate 2.2). Volumetrically the unit is the least common in the Amiandos map area, representing less than 1 percent of the exposed outcrop. The most significant exposure occurs immediately east of Pano Amiandos along a NW-SE trending elevated ridge (Map 1). The unit outcrops as a series of laterally discontinuous banded, steeply dipping rectangular blocks several meters to several tens of meters in width, hosted by clinopyroxene-bearing dunite of the early plutonic suite. The banded blocks are easily identifiable, as they are more resistant to weathering than the surrounding serpentinized host. Banding is, in general, laterally uniform. Locally however, layers are disrupted or pinch out. At one location the bands are isoclinally folded (Plate 2.3) with the axial plane of the fold paralleling the dominant orientation of the banding.

The orthopyroxene-rich bands are typically recrystallized (Plate 2.4) and exhibit a strong crystallographic fabric defined by prismatic orthopyroxene grains which are consistently parallel to banding (Plate 2.5). Clinopyroxene is a common accessory phase throughout the unit, representing on average, two to five modal percent of the rock. Locally, on the scale of a thin section, interstitial clinopyroxene may increase to 15 modal percent poikilitically enclosing orthopyroxene (Plate 2.7). In contrast to the recrystallized polygonal nature of the orthopyroxene, clinopyroxene is clearly undeformed (Plate 2.6).

Banded orthopyroxenite-dunite was also identified within the layered ultramafic cumulate section (Map 2, section 2.5). Exposure of the unit in this area



**Plate 2.2** Nature of banded serpentinized dunite-orthopyroxenite unit. Located immediately east of Pano Amiandos.

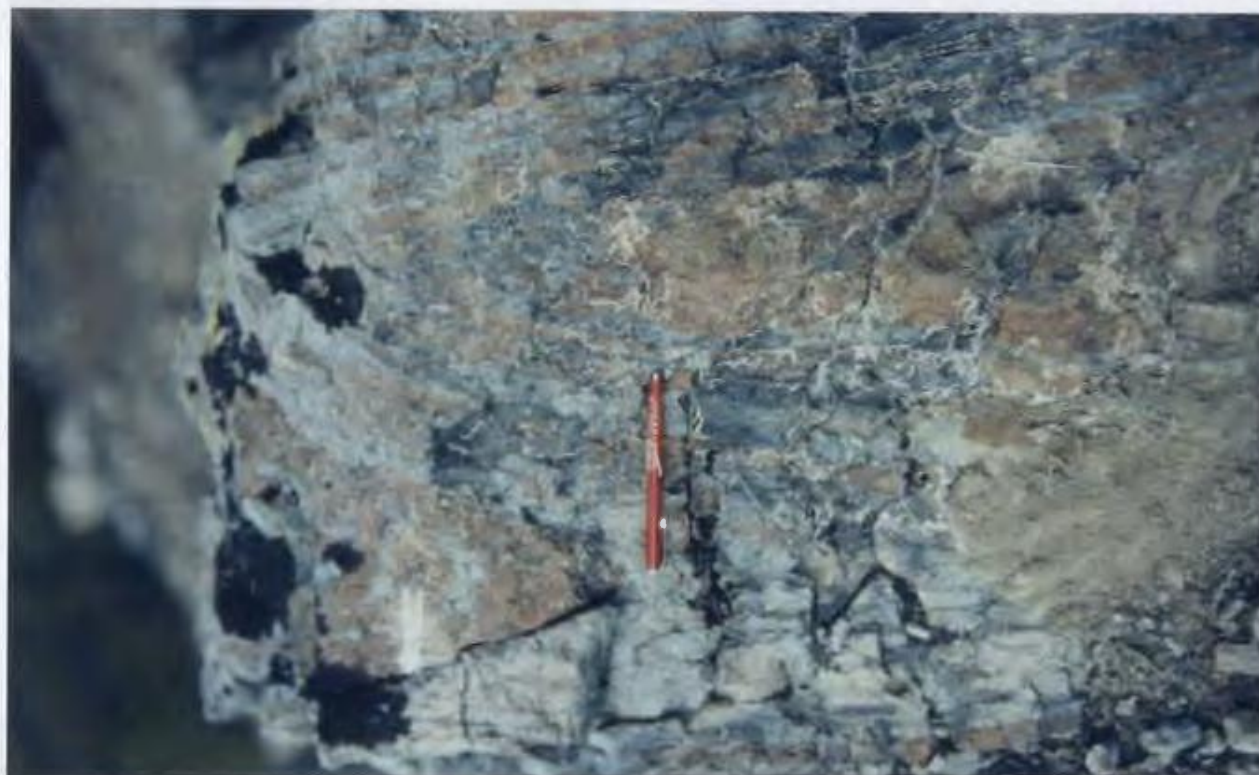


**Plate 2.3** Isoclinally folded banded serpentinized dunite-orthopyroxenite. Located immediately east of Pano Amiandos.

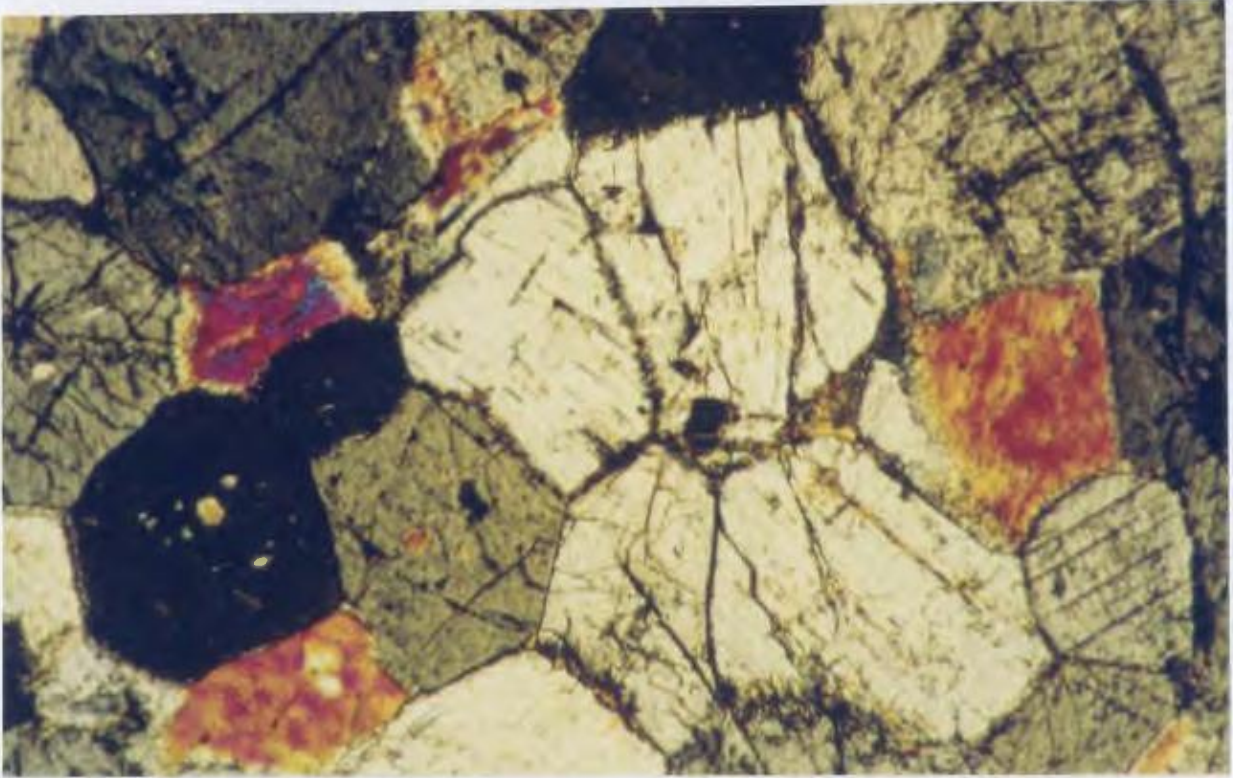


**Plate 2.4** Photomicrograph of well developed recrystallized polygonal texture in orthopyroxenite layer (field of view 2mm wide).



**Plate 2.5** Polished slabs of serpentinized dunite-orthopyroxenite unit illustrating the layer-parallel foliation fabric defined by the pre-fold dimensional orientation of orthopyroxene. Thin vertical dark bands perpendicular to layering in T26 represent serpentinization along later fractures.

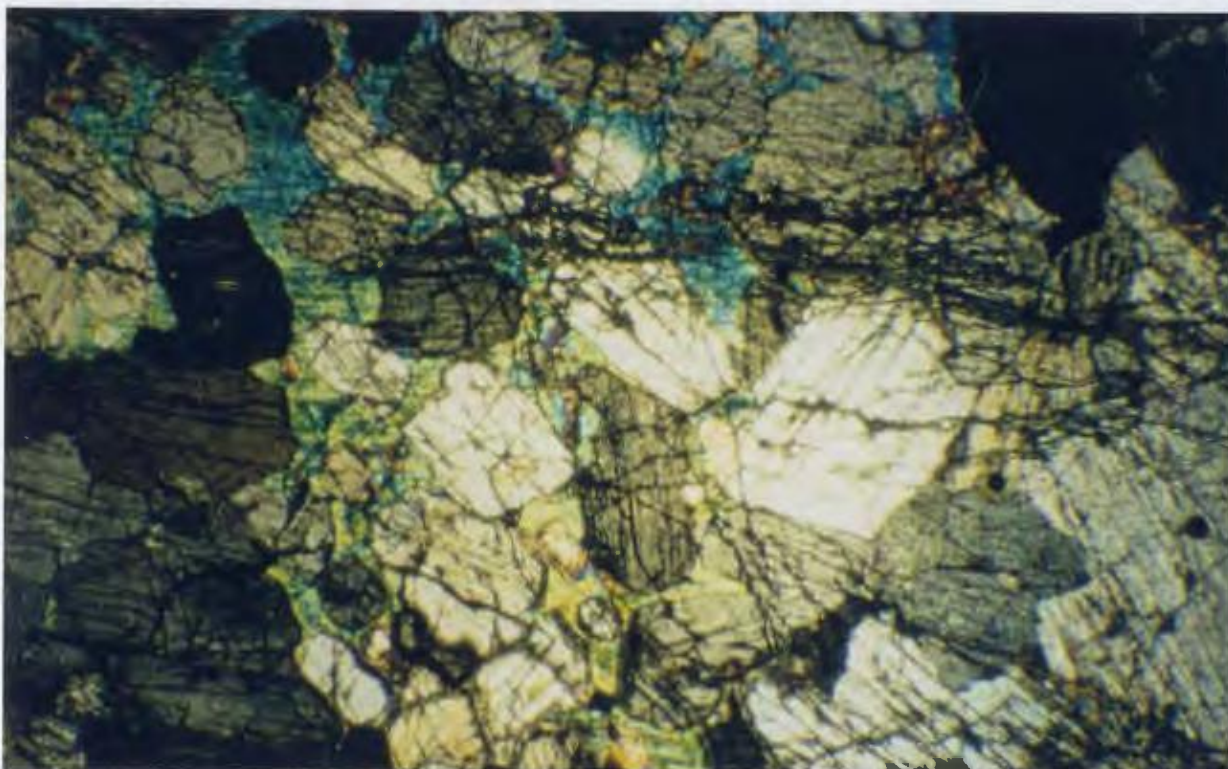


**Plate 2.6** Photomicrograph displaying interstitial nature of clinopyroxene poikilitically enclosing orthopyroxene. Note the polygonal nature of orthopyroxene in the lower left corner of the photo (field of view is 2mm).

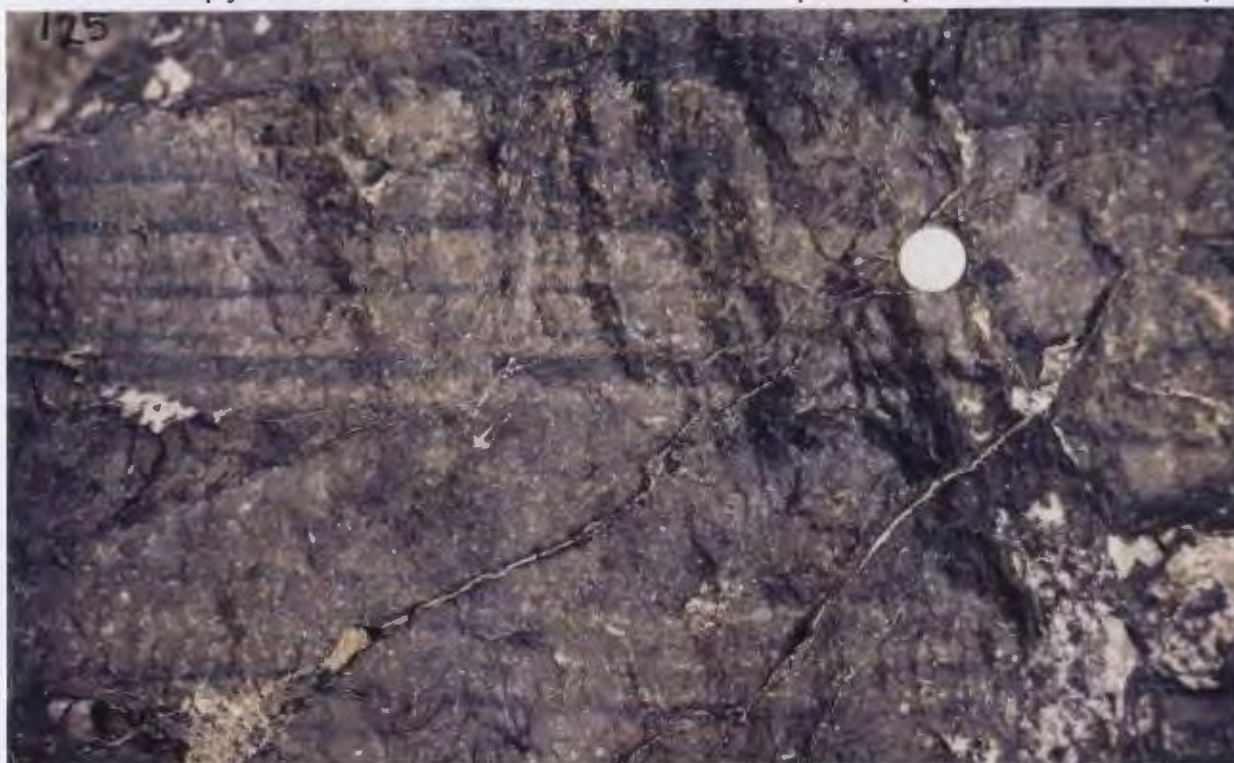


**Plate 2.7** Well washed exposure of banded serpentinized dunite-orthopyroxenite demonstrating the interstitial nature of clinopyroxene, weathering a distinctive white colour in contrast to the darker rust brown host. (Coin is approximately 1.5 cm in diameter).

was laterally limited to a well washed outcrop located within a steep stream valley. The interstitial nature of the clinopyroxene at one location was clearly evident (Plate 2.7), weathering a much lighter colour than the darker banded host. The unit at this location, as is the case near Pano Amiandos, occurs near the upper limits of the clinopyroxene-dunite unit and thus appears to maintain a pseudostratigraphic position within the ultramafic cumulate sequence.

It is presently unclear whether the unit represents xenoliths of 1) a banded residual mantle origin, or 2) an older primary igneous layered sequence which has been subsequently deformed and recrystallized. Evidence suggestive of a mantle origin is supported, primarily, by the degree of deformation and recrystallization combined with the overall mineralogical composition of the unit, consisting predominantly of olivine and orthopyroxene with accessory clinopyroxene. Both the deformational and compositional features contrast with the ultramafic cumulates hosting the unit, containing only minor amounts of orthopyroxene, as a late cumulate phase and showing only minor effects of penetrative deformation.

Compositionally banded dunite-orthopyroxenite is known to occur throughout the mantle sequence. One isolated exposure was identified within the tectonite unit in the present map area. This exposure occurs just south of Pano Amiandos, and consists of 1 to 2 centimeter wide bands over a distance of 10 centimeters. Hebert and Laurent (1988) noted that well developed banding, characterized by bands of orthopyroxene a few centimeters thick, alternating with dunitic layers, is a characteristic feature of the harzburgites throughout the mantle section. However, the overall extent and relationship of this layering to the host tectonite has not been discussed. Similar units have also been identified throughout the residual mantle sections in other ophiolites, commonly in the uppermost harzburgites (Nicolas and Jackson, 1983; Gregory, 1985). As in the present

case, they are described as consisting of dunitic, orthopyroxenitic and websteritic layers with a normal thickness of 1-10 cm and being strictly parallel and normally continuous at the scale of the outcrop. In these cases the banding is believed to have resulted from the transposition of intrusive pyroxenite dikes which produced a banded unit concordant to the foliation of the harzburgite tectonite.

Mineral phase chemistry for both olivine and orthopyroxene from the banded unit in the two areas described fall within a very limited range with respect to En and Fo content. Four samples collected along the discontinuous belt of the unit near Pano Amiandos ranged in composition from Fo 87.6-88 and En 88.3-88.4, for olivine and orthopyroxene, respectively. Six samples collected perpendicular to the layering, over a distance of approximately 50 m from the exposure south of the Amiandos Asbestos Mine indicated a compositional range of Fo 87.2-89.2 and En 88.5-89.6. Five of the samples contained olivine with a compositional range of Fo 87.2-87.8. No systematic variation in either the olivine or orthopyroxene composition as a function of stratigraphic position was identified.

It is thus mineral chemistry that proves a problem since it appears to support a cumulate origin, the composition of both the olivine and orthopyroxene being slightly more iron (Fe) rich (with the exception of one sample) than the compositional range of the phases characteristic of the residual mantle harzburgite, Fo 89-91 and En 89-91 (Hebert and Laurent, 1988).

The occurrence of undeformed accessory clinopyroxene is a common feature in both residual mantle harzburgite and deformed ultramafic cumulates (Greenbaum, 1972; George, 1975, 1978). Two possible scenarios could explain the presence of the undeformed clinopyroxene in the banded unit. The first mechanism invokes synmagmatic ductile deformation (deformation during crystallization in the presence of a fluid) in which the remaining fluid crystallized clinopyroxene after the deformational event. The second mechanism involves the

introduction of clinopyroxene by magmatic impregnation of a liquid fraction into a deformed olivine orthopyroxenite xenolith i.e. from the magma.

Although the present data is not conclusive in distinguishing as to whether or not the banded unit represents residual mantle or deformed layered cumulates the phase chemistry weighs more in favor of a cumulate origin. This relies on the recognition of "low" Fo and En contents compared to mantle compositions and the fact that clinopyroxene is an unlikely first crystallization product of cognate liquid trapped in residual harzburgite mantle. It is suggested that the unit represents deformed and recrystallized layered cumulate rocks, "*ultramafic metacumulates*" (George, 1975, 1978) from an older magmatic suite. Xenoliths of deformed banded orthopyroxenite occurring roughly 5 kilometers northwest of the present map area (Malpas et al., 1987) have likewise been interpreted as xenoliths of an older magmatic suite.

## **2.4 EARLY PLUTONIC SUITE (M2)**

The Early Plutonic Suite is represented by a differentiated sequence of ultramafic to mafic cumulate rocks.

Mineralogically the ultramafic cumulate (UMC) rocks are dominated by olivine and clinopyroxene, with dunite, wehrlite and olivine clinopyroxenite representing the most dominant rock types. A gradual transition involving a reduction in the modal abundance of cumulate olivine, combined with an increase in the modal abundance of intercumulate clinopyroxene followed by the introduction and subsequent build up of interstitial plagioclase defines a pseudo-stratigraphy locally and on the map scale. Textural relationships within the ultramafic cumulates indicate a crystallization history involving, from the base upward, Ol + Cr, Ol + Cr + Cpx, Ol + Cpx  $\pm$  Opx, Ol + Cpx  $\pm$  (Opx, Plag). Plagioclase is the last mineral phase to appear stratigraphically upward in the UMC cumulate

sequence developing plagioclase-bearing ultramafic rocks followed by the mafic cumulates. Within the mafic cumulates, including; melagabbro, olivine gabbro and gabbro, plagioclase becomes a dominant cumulate phase. The crystallization history of the mafic cumulate is represented by Ol, Ol + Cpx + Plag, Ol + Cpx + Plag  $\pm$  Opx.

Orthopyroxene is a common phase throughout most of the UMC and gabbroic rocks as a late interstitial poikilitic phase. Locally the modal abundance of orthopyroxene may increase above 5 to 10 percent, producing lherzolithic, olivine websteritic and orthopyroxene-gabbroic varieties.

Centimeter scale primary igneous phase layering is well developed locally throughout the *Early Plutonic Suite*. Within the ultramafic cumulates layering is most pronounced in exposures where they border the mantle harzburgite unit south of the Amiandos asbestos mine.

Early Plutonic Suite lithologies are discussed in detail below.

#### **2.4.1 Dunites (Map Unit 3)**

Sufficient variation exists within the dunite (90-100 modal percent olivine) in the map area with respect to the presence or absence as a constituent phase of either cumulate chromite or postcumulate clinopyroxene to warrant subdivision of the unit. Three distinct dunite subtypes, including; 1) chrome-spinel dunite, 2) dunite, and 3) clinopyroxene dunite, have been mapped in the Amiandos area.

##### **Chrome-Spinel Dunite (Unit 3c)**

Chrome-Spinel dunite is clinopyroxene-free and contains on average 2-5 percent chrome-spinel occurring as disseminated 0.5 to 2 millimeter euhedral to subhedral grains which are easily identifiable in hand sample. Locally, areas with up to 10 modal percent chromite are present. Concentrated zones of chromite

are up to 1 meter in area and are characterized by an increase in grain size, with chromite grains ranging from 2 to 6 millimeters. Olivine kernels in optical continuity within a serpentine matrix, indicate grain sizes of 2 to 4 millimeters and a granular texture. Compositionally, the olivine is highly magnesian with Fo 91.4-92 (Compositional range obtained from analysis of five separate samples, complete analyses reported in Appendix 1, Table 2).

#### **Dunite (Unit 3b)**

Dunite is composed essentially of cumulate olivine with only trace amounts of both chrome-spinel and clinopyroxene. Chrome-spinel grains are generally less than 0.4 mm in size and represent less than 0.5 modal percent of the rock. Clinopyroxene where present occurs as interstitial selvages between the olivine grains and is only identifiable in thin section.

#### **Clinopyroxene Dunite (Unit 3a)**

This rock type is transitional between the dunite and wehrlitic units (Plate 2.8), and contains three to ten percent intercumulate clinopyroxene which is clearly visible in outcrop (Plate 2.9). Small (0.1-1 millimeter) subhedral to euhedral chrome-spinel grains are usually present as an accessory phase (1-3%). Chrome-spinel shows a close spatial association with clinopyroxene and is commonly poikilitically enclosed by it (Plate 2.10).

Locally within the clinopyroxene dunite, zones enriched in clinopyroxene, (up to 15 to 20 modal percent) were identified, producing olivine-rich wehrlites. Clinopyroxene in these zones displays a well developed intercumulate texture



**Plate 2.8** Polished slabs illustrating transitional nature between dunite, clinopyroxene-dunite, and wehrlitic units, resulting from a progressive increase in intercumulate clinopyroxene.



**Plate 2.9** Weathered exposure of clinopyroxene (white)-dunite (brown). (Coin is approximately 1.5 cm in diameter).

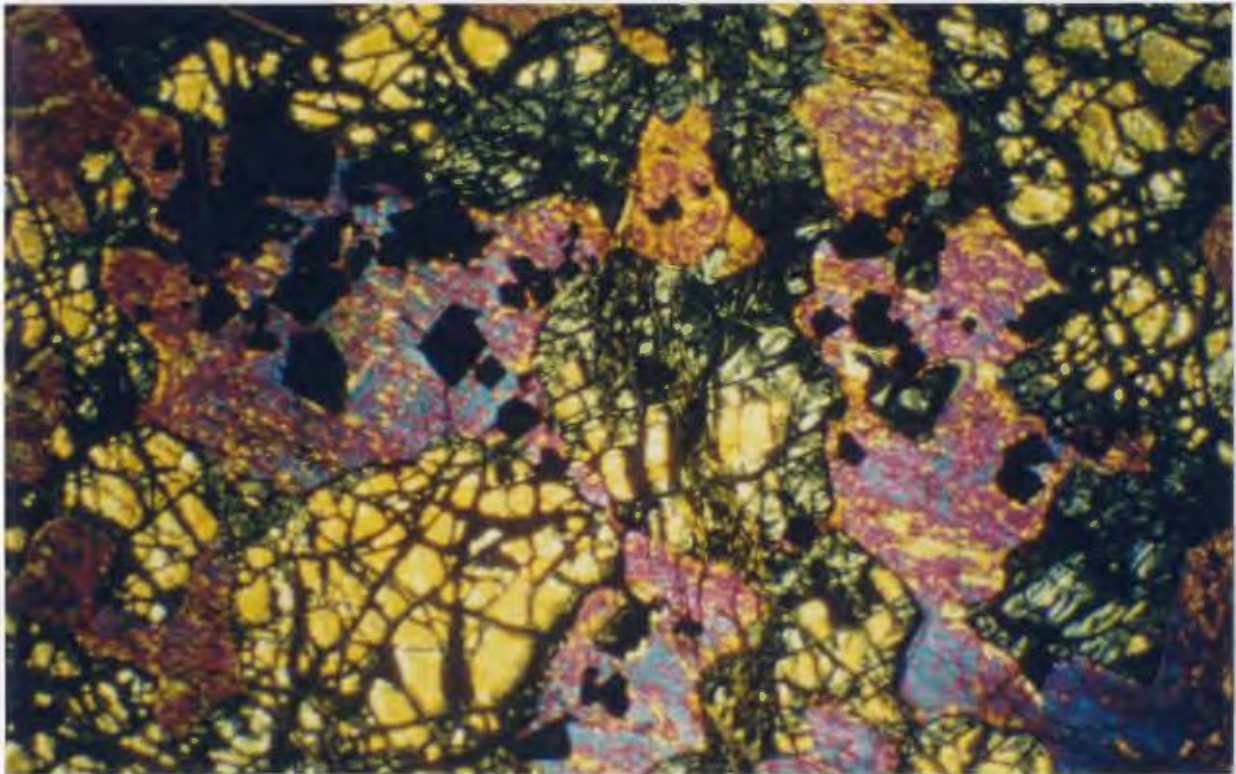


**Plate 2.10** Photomicrograph of euhedral chromite, poikilitically enclosed by intercumulate clinopyroxene (field of view is 6mm wide)

(Plate 2.11, Plate 2.8, Sample 033).

On weathered surfaces intercumulate clinopyroxene exhibits a deceptive chalky white colour which in the field, can be mistaken for plagioclase (Plates 2.9, 2.11). Thin section analysis however, reveals that the mineral is an alteration product of clinopyroxene, identified by Wilson (1959) as sephopite.

#### **2.4.2 Wehrlite (Unit 4)**

Wehrlite represents the dominant ultramafic cumulate rock type present in the Amiandos map area. This unit commonly contains 40 to 60 modal percent cumulate olivine (0.5 - 3 mm) as rounded grains poikilitically enclosed by 60 to 40 percent intercumulate clinopyroxene, commonly forming large (0.5-1.5 cm) oikocrysts (Plate 2.12). Highly weathered surfaces are extremely pitted due to weathering out of olivine grains. Well developed phase layering within the wehrlitic unit is common south of the Amiandos Asbestos Mine and is described below. Orthopyroxene is a common accessory phase throughout the unit and rarely increases to 10 or 20 modal percent where it occurs as large (1-1.5 cm) oikocrysts poikilitically enclosing both olivine and clinopyroxene (Plate 2.13).

#### **2.4.3 Plagioclase-Bearing Ultramafic Cumulate (Unit 5)**

This rock type is clearly transitional from the wehrlitic unit and is texturally similar to it, representing the introduction of plagioclase (1-10 %) as a late intercumulate phase. The unit ranges from plagioclase-bearing wehrlites (Plate 2.14) to plagioclase-bearing olivine websterites with variations in the modal abundance of both cumulate olivine and intercumulate orthopyroxene. In the field the intercumulate plagioclase is readily identifiable producing a characteristic white colour in contrast to the darker ferromagnesium rich phases.



**Plate 2.11** Weathered exposure of olivine-rich wehrlite with intercumulate clinopyroxene.



**Plate 2.12** (Sample 028b) Polished slab of poikilitic wehrlite.



**Plate 2.13** (Samples 078, 078.2) Polished slabs of coarse grained lherzolite with cumulate olivine, intercumulate clinopyroxene and oikocrysts of orthopyroxene.



**Plate 2.14** (Sample 103) Polished slab of coarse grained plagioclase-bearing wehrlite with cumulate olivine (black), adcumulate clinopyroxene (grey) and intercumulate plagioclase (white).

#### **2.4.4 Melagabbros (Unit 6c)**

This unit is represented by medium to coarse grained melanocratic gabbroic rocks with a plagioclase content greater than 10 modal percent and olivine in amounts exceeding 20 modal percent. The unit is transitional between the plagioclase bearing ultramafic cumulate rocks and the olivine gabbroic unit. Layering is commonly developed (Plate 2.15) and defined by a variation in both feldspar and olivine content. Throughout the unit, local well foliated to gneissic zones are present. These deformed zones are characterized by a grain size reduction in both clinopyroxene and plagioclase (Plate 2.16), and the rocks typically display a polygonal texture in thin section. Olivine grains appear plastically deformed and stretched out (aspect ratio of 5:1) defining a foliation fabric.

#### **2.4.5 Olivine Gabbros (Unit 6b)**

Olivine gabbros are medium grained and contain less than 20 modal percent cumulate olivine. Both cumulate plagioclase and clinopyroxene are present in amounts varying from 30-65 modal percent. Orthopyroxene is commonly present as a late intercumulate phase, forming oikocrysts (0.3-0.5 cm) which poikilitically enclose all other phases present.

Exposures weather a dark grey colour with the olivine grains producing rusty brown pits across the surface (Plate 2.17). Layering is developed as centimeter scale segregations of plagioclase, clinopyroxene, or olivine rich zones. Locally the olivine gabbro displays a well developed foliation defined by the preferred crystalligraphic orientation of olivine grains (Plate 2.18).

Based on first order petrographic observation of textural features in the foliated olivine gabbros, it appears that the development of the  $S_1$  fabric was produced by hypersolidus deformation (deformation during crystallization).

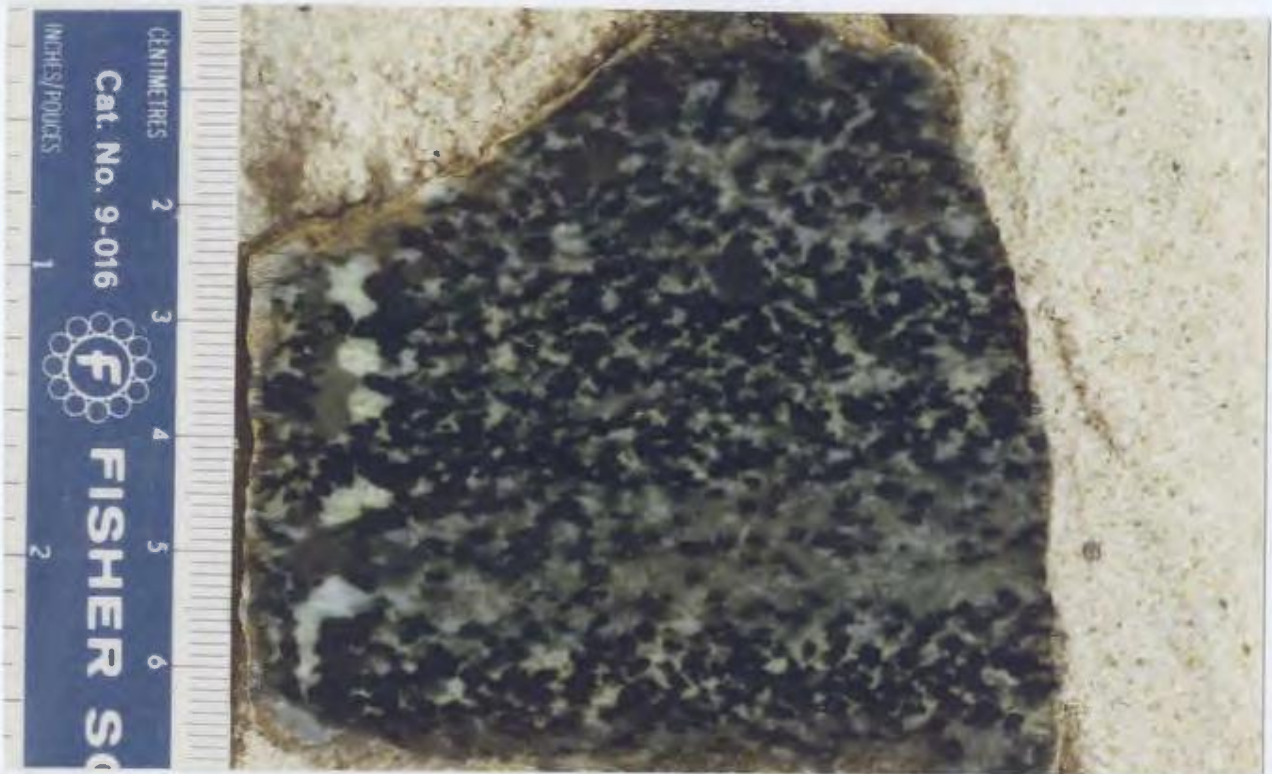


**Plate 2.15** Polished slab of coarse grained melagabbro with moderately developed cm scale layering defined by a variation in olivine content.

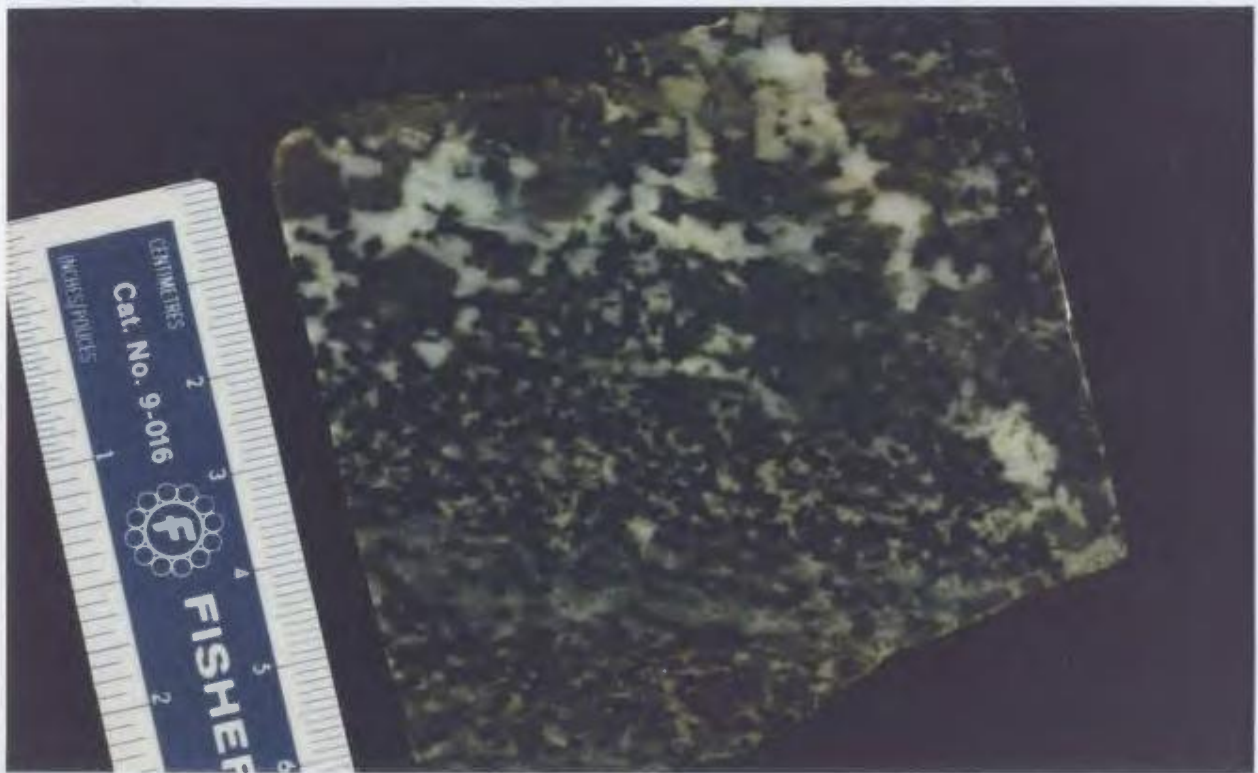


**Plate 2.16** Polished slab displaying grain size reduction and the development of gneissic banding within the melagabbro.



**Plate 2.17** Close-up view of olivine gabbro illustrating pitted nature as a result of weathered out olivine grains. Feldspar rich cm scale layer present.

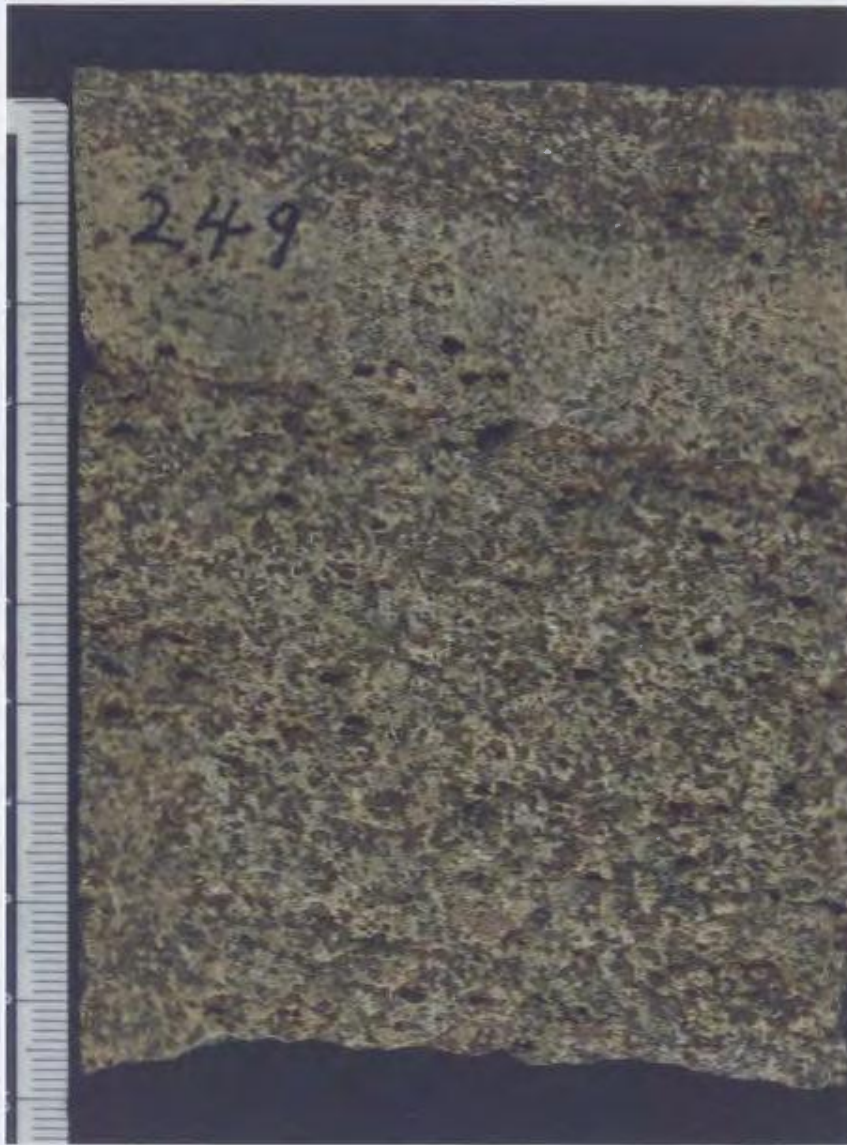


**Plate 2.17** Close-up view of olivine gabbro illustrating pitted nature as a result of weathered out olivine grains. Feldspar rich cm scale layer present.



**Plate 2.18** Well developed penetrative ( $S_1$ ) tectonite fabric in olivine gabbro defined by elongation of olivine. (Coin is approximately 1.5 cm in diameter).

Evidence in favor of this mechanism involves the mineralogical heterogeneities identified in thin section. Cumulate olivine grains act ideally as strain markers in demonstrating the effects of plastic deformation throughout the unit and commonly display the progressive development of large aspect ratios. A characteristic feature of these plastically deformed grains is the inclusion of both cumulate plagioclase and clinopyroxene as either individual crystals (Plate 2.19) or crystal aggregates (Plate 2.20). Individual olivine grains which are typically larger in size than the other mineral phases present consistently undergo uniform extinction with crossed nicols under transmitted light. Clinopyroxene and plagioclase crystals throughout the section are typically fine to medium grained equigranular and commonly display a recrystallized polygonal texture. A number of deformed olivine grains (Plates 2.21, 2.22) display features which suggest that the inclusion of the phases within the olivine is a mechanical one, in which the olivine grains plastically flow and encapsulate the surrounding crystals. Postcumulate orthopyroxene oikocrysts (Plate 2.23) present in the same thin section as the deformed olivine grains show no evidence of deformation. These features suggest that the postcumulate orthopyroxene, at the time of deformation, was represented by a liquid fraction.

The development of these fabrics in the olivine gabbros is best explained in terms of the liquid-crystal ratio which directly controls the rheological behavior of the mineral phases present (Arzi, 1978). Based on both experimental evidence and theoretical consideration Arzi (opt. cit.) demonstrated that below a particular melt percentage, known as the RCMP (rheological critical melt percentage), estimated to be in the range of 10-20 percent, deformation of a liquid-crystal mush requires strain in the solid fraction.

The modal percent of intercumulate orthopyroxene in the deformed olivine gabbros generally ranges from 2-15 percent. This indicates that a sufficiently high

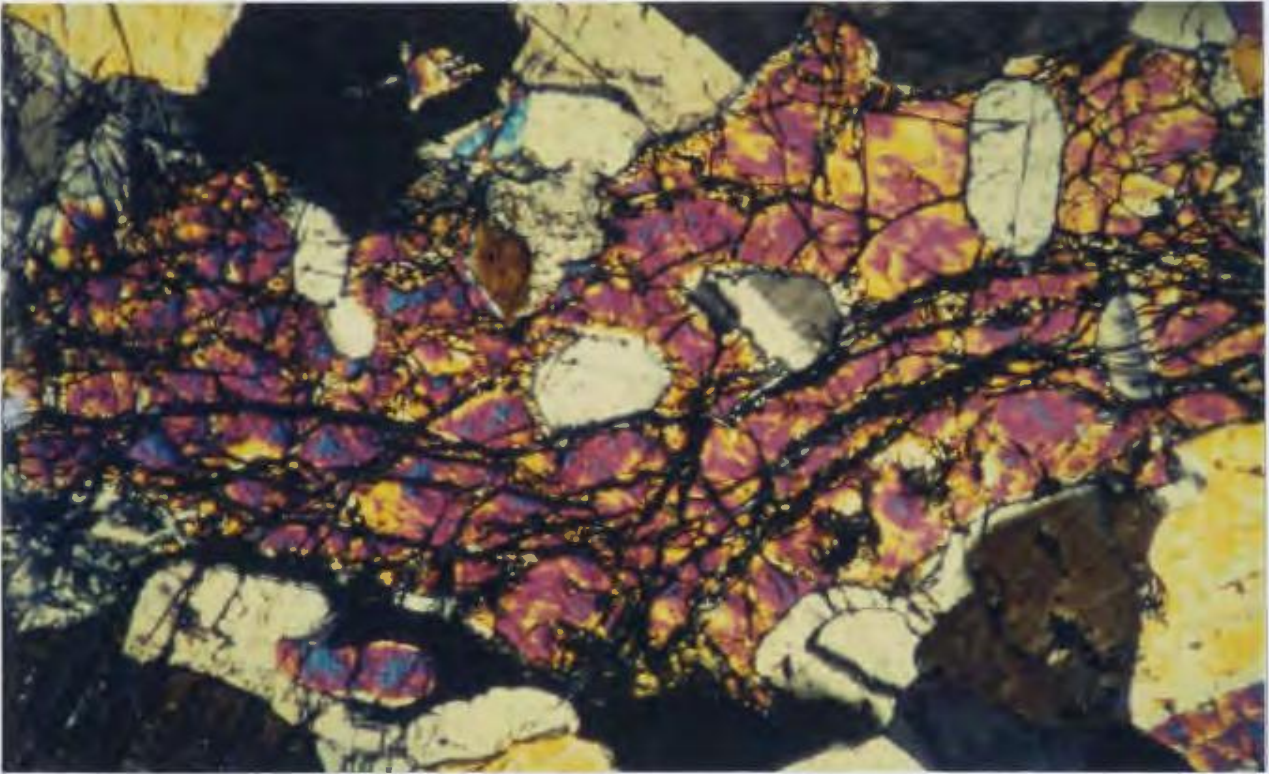


**Plate 2.19** Photomicrograph of a plastically deformed olivine grain containing inclusions of plagioclase (field of view is 6mm wide).

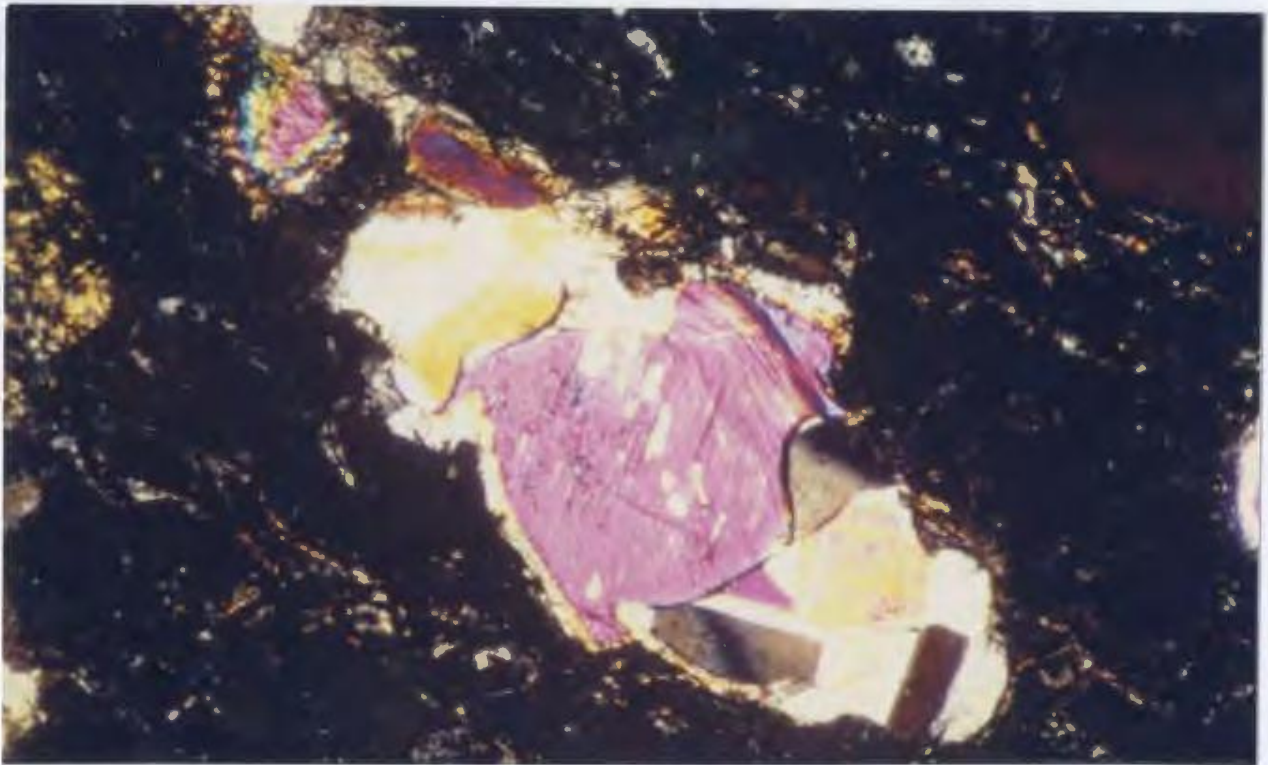


**Plate 2.20** Photomicrograph of clinopyroxene and plagioclase aggregate contained in deformed olivine grain (enlarged area of Plate 2.21, field of view is 2mm across).

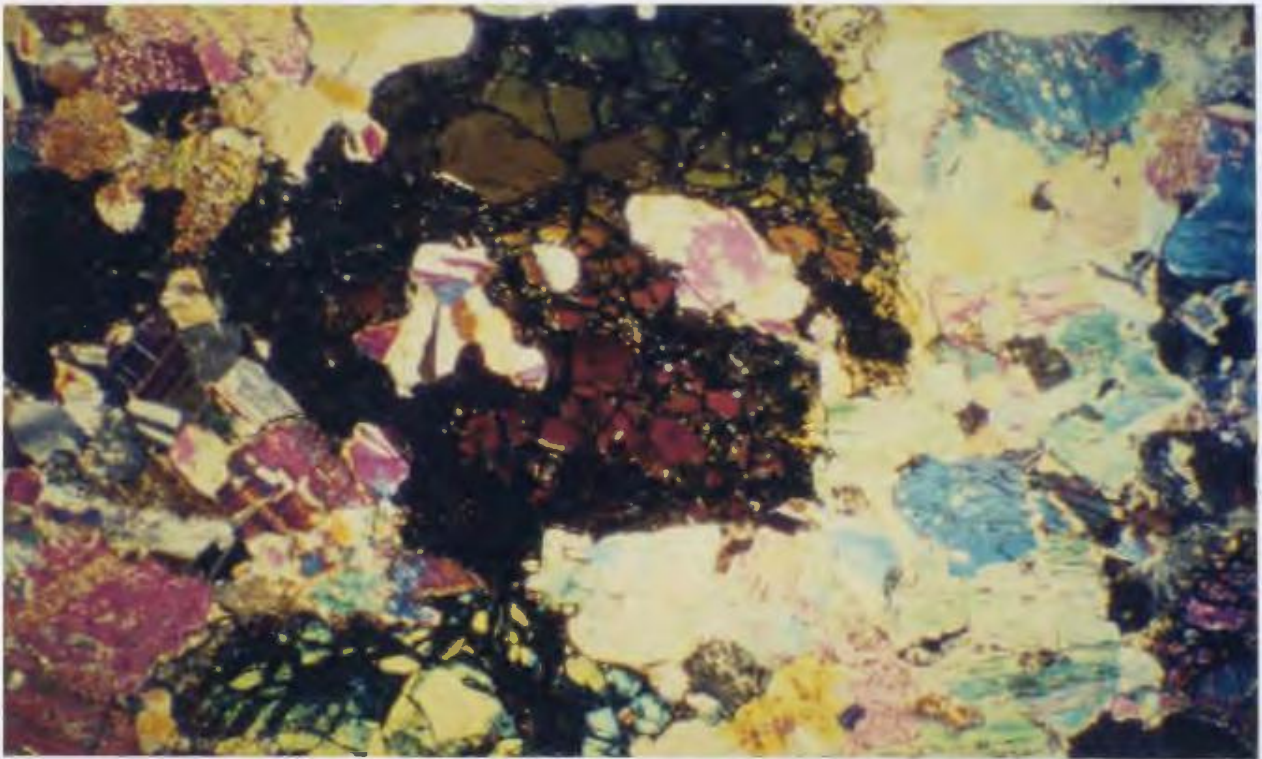


**Plate 2.21** Photomicrograph of deformed olivine grain enclosing surrounding plagioclase and clinopyroxene (field of view is 6mm across).

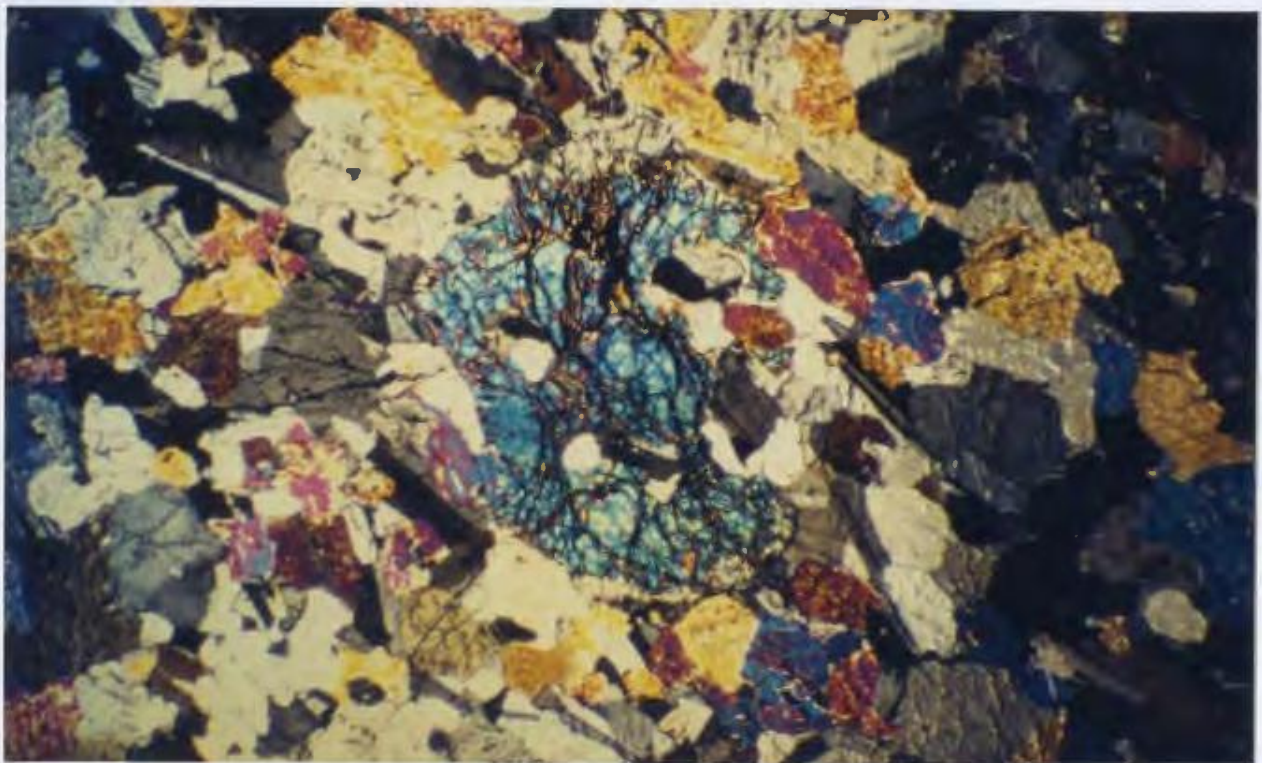


**Plate 2.22** Photomicrograph of plastically deformed olivine grain enclosing surrounding plagioclase and clinopyroxene (field of view is 6 mm across).

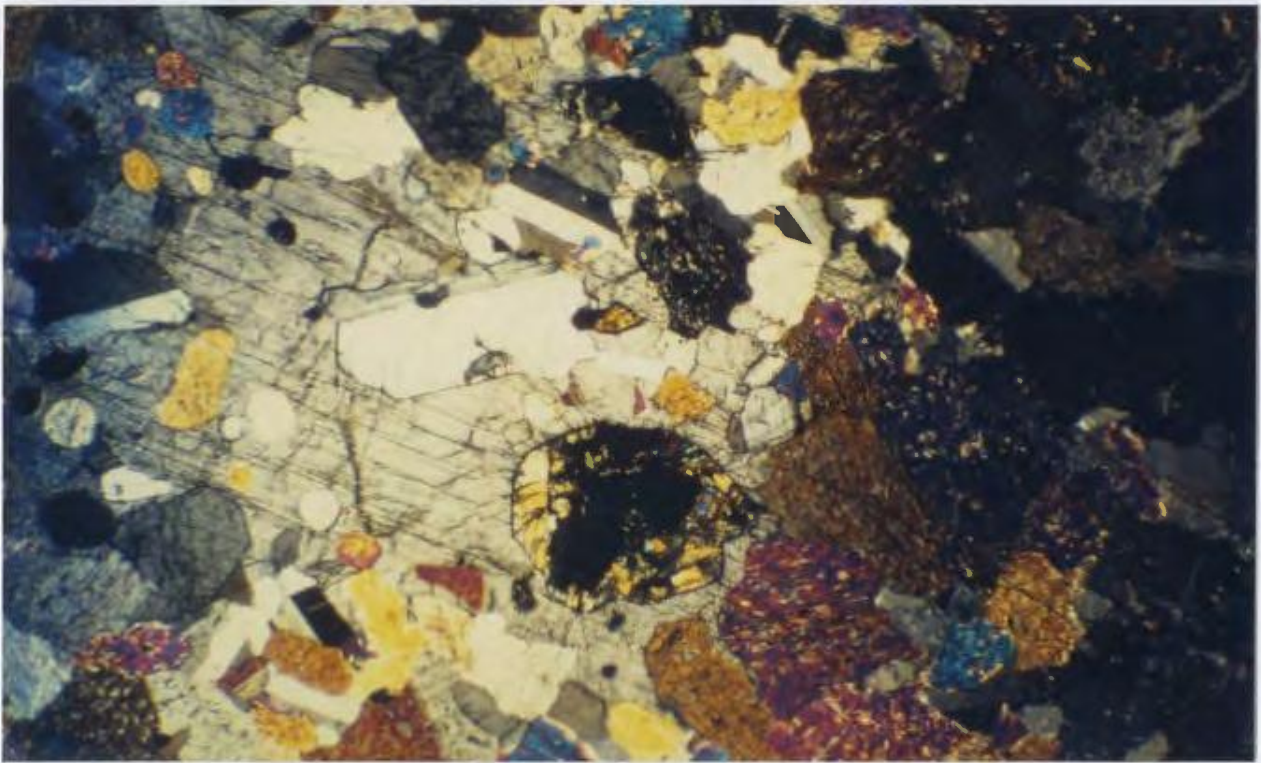


**Plate 2.23** Photomicrograph of orthopyroxene oikocryst in deformed olivine gabbro (field of view is 6mm across).

percentage of the magma must have crystallized in order for it to acquire typical solid-state deformation textures, and that hypersolidus deformation occurred at volumes of melt below the RCMP. To characterize the geometrical shape of these deformed, inclusion-bearing olivine grains, combined with their suggested mechanism of development, the term "*Pac Man*" structure is introduced.

Plastically deformed olivine grains as described above, were also identified intermittently throughout the layered cumulate section from which 86 samples, ranging from dunite to olivine gabbros, were petrographically studied. As in the deformed olivine gabbros, ultramafic cumulates display similar fabrics depicting elongate olivines. These deformed rocks are also characterized by low modal abundances of undeformed poikilitic orthopyroxene, supporting the concept that penetrative deformation is controlled by the RCMP.

Locally within the gabbro unit, mylonite zones (Plate 2.24) are developed indicating syntectonic recrystallization, which suggests that the early plutonic suite was initially deformed under low strain high temperature conditions (hypersolidus) and continued at possibly higher crustal levels into conditions of lower temperature higher strain conditions (subsolidus).

#### **2.4.6 Gabbro-Orthopyroxene Gabbro (Unit 6a)**

Gabbro-orthopyroxene gabbro is devoid of olivine and composed essentially of cumulate plagioclase and clinopyroxene with subordinate post cumulate orthopyroxene. The orthopyroxene content is highly variable, in some cases it is totally absent, while in others it may represent up to 20 percent of the mode. The unit is medium grained equigranular and ranges from totally isotropic (Plate 2.25) to weakly or moderately foliated types in which the foliation is defined by the orientation of both plagioclase and clinopyroxene. Locally the unit may be completely recrystallized and mylonitic (Plate 2.24). Layering, which is relatively



**Plate 2.24** Outcrop of recrystallized mylonitic gabbro, located 400 meters NE of Pano Amiandos. (Coin is approximately 1.5 cm in diameter).



**Plate 2.25** Weathered surface of medium grained equigranular isotropic gabbro. (Coin is approximately 1.5 cm in diameter).

rare in this unit, is represented by centimeter scale phase layering defined by alternating abundances of both plagioclase and clinopyroxene (Plate 2.26). Locally throughout the sequence the darker mafic layers display well developed isoclinal folding. (Plate 2.27).

## 2.5 LAYERED ULTRAMAFIC CUMULATE SECTION

An ultramafic cumulate section within the *Early Plutonic Suite* ranging from dunite to olivine gabbro, displaying well developed igneous layering was identified due south of the Amiandos Asbestos Mine and studied in detail (Map 2, location illustrated on Map 1). This section represents the first documented occurrence of near continuous exposure of well layered ultramafic cumulates within the Troodos ophiolite. The section outcrops over a distance of roughly 460 meters along a narrow, steeply inclined stream valley (Plate 2.28). Orientation of the line of section is on average east-west, nearly perpendicular to the strike of the igneous layering, which varies from NNW to NNE, and is steeply dipping to vertical. Exposure along the section is fairly continuous, lateral extent however, as a result of talus cover, is restricted to widths of one to five meters.

The section is intruded by numerous dikes of both clinopyroxenite and gabbro of the *Late Magmatic Suite* (Plate 2.29).

The base<sup>1</sup> of the section begins in highly serpentinized and brecciated dunite which is in fault contact with intensely altered and brittlely deformed residual mantle harzburgite.

The section is divisible on a large scale into three distinct lithostratigraphic components:

---

<sup>1</sup> The term base is used in the stratigraphic sense, applying to the most mafic unit which, as a result of doming of the complex, occurs at the highest elevation.



**Plate 2.26** Polished slab displaying phase layering in gabbro. Light coloured layers composed almost entirely of plagioclase, darker layers composed of clinopyroxene and plagioclase.



**Plate 2.27** Isoclinally folded mafic layer, locally developed within the gabbro.



**Plate 2.28** Location of the ultramafic cumulate line of section viewed from the west.

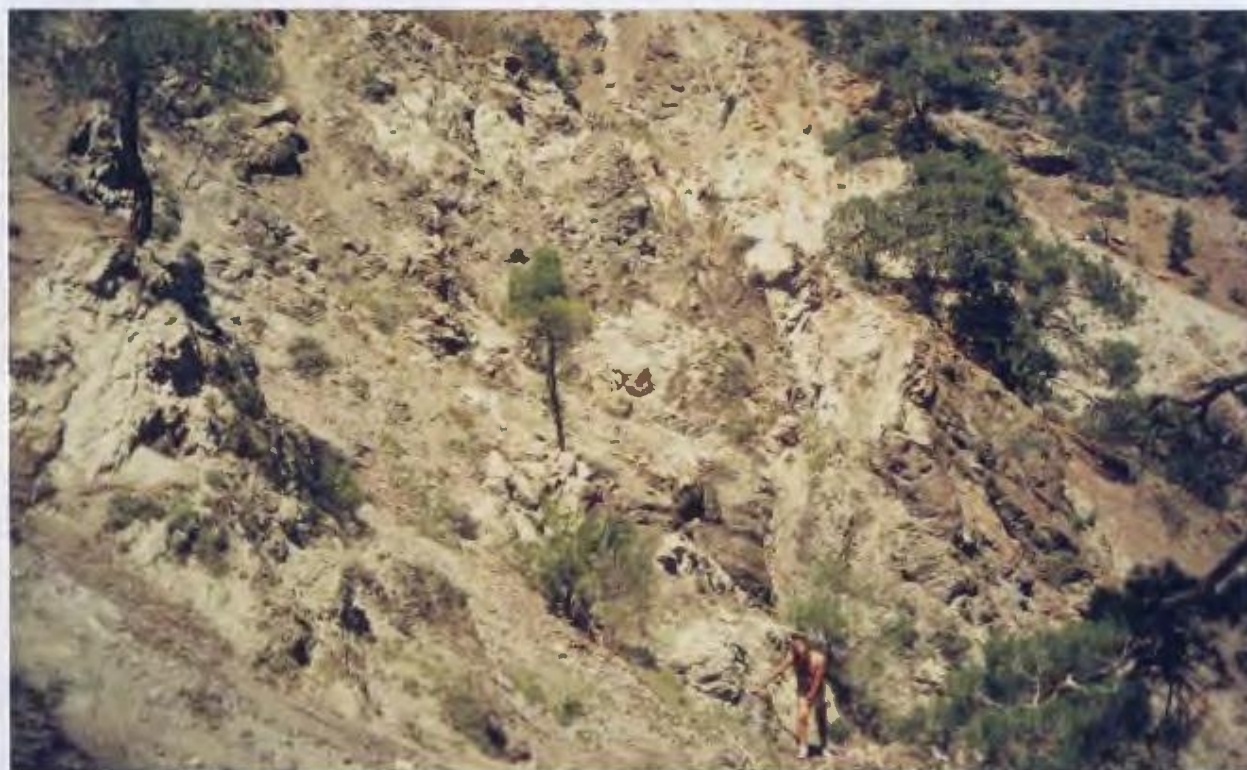


**Plate 2.29** View of ultramafic cumulate rock in the southwestern area of the map sheet displaying a high percentage of intrusive clinopyroxenite with screens of darker ultramafic cumulate.

1) the basal zone, comprising the first 100 meters of the section, is dominated by olivine-rich cumulates with variable amounts of intercumulate clinopyroxene and accessory amounts of cumulate chrome-spinel. Internally the zone displays a stratigraphy progressing upward from dunite to olivine-rich wehrlite with 10-20% clinopyroxene (Plate 2.11) to clinopyroxene-dunite (Plate 2.9). Contacts between the individual units of the basal zone are represented by localized shear zones.

2) The intermediate zone comprises the bulk of the section. It is dominated by wehrlite with lesser amounts of olivine clinopyroxenite, olivine-bearing clinopyroxenite, and dunite. Wehrlite varies from massive outcrops displaying beautifully developed poikilitic texture, with oikocrysts of clinopyroxene ranging from 0.5 to 1.5 centimeters in size (Plate 2.30), to well layered zones (Plate 2.31), outcropping over distances of less than one meter to tens of meters. Layering is commonly developed on centimeter scale (1-10 cm) and is represented by modal variations in the abundance of both cumulate olivine and intercumulate clinopyroxene (Plates 2.32, 2.33). Individual layers are generally uniform, lacking size or modal-grading.

3) The upper-zone, comprising the top 45 meters of the section, is dominated by clinopyroxene-rich gabbro and olivine-bearing gabbro. The transition from the dominantly ultramafic intermediate zone of the section described above into the upper mafic portion is defined by a sudden increase in the content of intercumulate plagioclase. The only occurrence of grain size layering identified along the entire section is at one isolated location in the upper zone. Layering is defined by an increase in olivine grain size from several millimeters to over a centimeter within a distance of roughly a meter in olivine gabbro.

Petrologically, the ultramafic cumulate section is dominated by both cumulate olivine and intercumulate clinopyroxene. Orthopyroxene is generally a



**Plate 2.30** T45: Massive wehrlitic unit with well developed clinopyroxene oikocrysts. (Coin is approximately 1.5 cm in diameter).



**Plate 2.31** T48: Well layered wehrlite-olivine clinopyroxenite (detail in Plate 2.32).



**Plate 2.32** T48: Exposure of cm scale modal layering in wehrlite, olivine-clinopyroxenite and clinopyroxenite. (Coin is approximately 1.5 cm in diameter).



**Plate 2.33** T57: Wehrlite-olivine clinopyroxenite-clinopyroxenite modal layering with minor intercumulate plagioclase (white). (Coin is approximately 1.5 cm in diameter).

late intercumulate minor phase (4-5%) throughout. Locally orthopyroxene is present in larger amounts within 1 to 2 centimeter scale, well banded and recrystallized orthopyroxenite-dunite (unit 2, described following) which occurs as xenoliths, meters to tens of meters in size near the base of the intermediate zone of the layered section. Plagioclase is rare, and where present forms a late intercumulate phase ranging from 2 - 10 modal percent (Plate 2.34).

As previously discussed, penetrative deformation throughout wehrlitic and olivine clinopyroxenitic portions of the ultramafic cumulate rocks is in general minimal and heterogeneously developed. Plate 2.35 displays the common undeformed nature of the layered unit within three of the slabs illustrated, sample T28.3 for comparison, demonstrates the effect of the ductile deformation.

## **2.6 Structure and Distribution of the Early Plutonic Suite**

The occurrence of chrome-spinel dunite (unit 3c) is restricted to the southwest corner of the map sheet (Map 1) where it is hosted by residual mantle harzburgite. The most continuous exposure forms a lensoid or podiform shaped (Thayer, 1969) body roughly 0.5 kilometers in width at its center. It is oriented NW-SE with its longer dimension essentially parallel to the foliation in the tectonized host rocks. Exposure of the chromitiferous dunite continues beyond the map sheet for some 400 to 500 m along strike to the north-west where the width of exposure is considerably narrowed. Subsequent normal faulting has displaced the southeastern portion of the body, allowing a rough estimate of a two kilometer half-length. Isolated tabular lenses (2-4 m in width) of the foliated harzburgite occur within the chrome-spinel dunite body as inclusions (xenoliths). The margins of the sheet-like harzburgite bodies in the dunite display gradational contacts defined by orthopyroxene which is totally absent in the dunite and increases up to 25 percent over distances of 5-10 cm. Foliation fabrics in these



**Plate 2.34** Variations in the content of plagioclase from approximately 1 (T57) to 10 (T60) modal percent.



**Plate 2.35** Detailed view of the compositional layering. Sample T28.3 - displays a typical ductile flow fabric which is sporadically developed throughout the section.

residual mantle xenoliths also parallel the dominant tectonite fabric present in the surrounding harzburgite. One of these dunite hosted harzburgite xenoliths is well exposed in a road cut at the southwestern corner of the map sheet. Also well exposed in this cut are zones rich (up to 10%) in chrome-spinel.

In contrast to the penetrative fabric in the mantle tectonites, chromites within these concentrated areas are randomly oriented and show no evidence of a preferred dimensional orientation.

This body is the only unit in the map area which displays an unfaulted contact with the residual mantle harzburgite unit. The contact, where exposed is very sharp, defined by the presence or absence of enstatite. The overall trend of the contact is steep and parallels the tectonite fabric in the harzburgite but in detail displays sheet-like veins and irregular bodies intruding the harzburgite.

Ultramafic cumulate (UMC) rocks form a nearly continuous belt up to 6 kilometers in overall length, varying from 200 to 500 meters in width (Map 1). The outcrop distribution pattern of the belt defines a large scale isoclinal fold with a wavelength of roughly one kilometer. Penetrative  $S_1$  fabric elements associated with the synmagmatic deformational event (D1) are best developed within the olivine gabbro unit marginal to the UMC rocks in the core of the western fold hinge. This tectonite foliation is in general steeply dipping and parallels both igneous layering ( $S_0$ ) and geological boundaries ( $S_L$ ). All these planar elements are folded about a NNW-SSE trending subvertical fold axis ( $F_A$ ). There is no  $S_2$  foliation or cleavage representative of the folding event identified, yet the constructed axes are invariably parallel to  $S_1$  in the mantle tectonites. Development of this geometrical configuration is attributed transposition of the lower plutonic crust during convective mantle flow above the spreading center.

Penetrative synmagmatic deformation clearly affects the upper (olivine gabbroic, gabbroic) units as previously described. Within the ultramafic

cumulates, S<sub>1</sub> fabrics are inhomogeneously developed. Deformation fabrics, where noted are indicated by a weak to moderate fabric defined by elongated cumulate olivine grains or the presence of recrystallized zones which are finer grained (0.25-0.5 millimeter mean grain size) than the generally coarser grained relatively undeformed sequence.

## **2.7 LATE MAGMATIC SUITE (M3)**

For the most part units of the *Late Magmatic Suite*, either crosscut S<sub>1</sub> fabrics or are discordant with respect to the igneous layering in the early plutonic suite and clearly post-date the ductile deformational event that affected the early suite. The suite is characterized by clinopyroxenite and olivine-clinopyroxenite, varitextured gabbros and a high level intrusive zone dominated by trondjhemites and diabase with screens of diorite and gabbro. These units are represented by dikes and small intrusive bodies, the enveloping surfaces of which commonly cross-cut the S<sub>1</sub> fabrics developed in the early suite and display xenolith-bearing contacts.

### **2.7.1 Clinopyroxenite (Unit 7)**

Intrusive clinopyroxenite is a ubiquitous feature throughout the belt of ultramafic cumulate rocks bordering the harzburgite along the *Amiandos Fault* and for the most part appears restricted to the belt. Abundant clinopyroxenite dikes are clearly evident cutting the wehrlite unit in Plate 2.2 to the left of the fault. Clinopyroxenite was not observed intruding the stratigraphically higher mafic units of the early plutonic suite. Clinopyroxenite intrusions are in general represented by steeply inclined dike-like to irregular shaped bodies. A number of somewhat larger variably stratified bodies up to 100 meters in size, were identified in the southwestern corner of the map area within both dunite and residual mantle

harzburgite. A well defined intrusive contact is exposed along the northern margin of the most westerly body where intrusive olivine-bearing clinopyroxenite contains xenoliths of the host dunite. Primary igneous layering is also well developed in this body defined by alternating centimeter scale layers of dunite and clinopyroxenite. To the west, just outside the present map sheet, a much larger body of clinopyroxenite was noted.

Most dikes range from several centimeters to several meters in width. They weather a distinctive light grey colour, easily visible against the much darker weathering ultramafic cumulate rocks (Plates 2.36, 2.29).

On fresh surfaces clinopyroxene weathers a distinctive olive-green colour; most are medium grained and equigranular. Along the NW-SE trending ridge near Pano Amiandos several bodies (10 to 30 m in size) of pegmatitic clinopyroxenite (Plate 2.37) cut ultramafic cumulates of the *Early Plutonic Suite*.

Petrologically the unit is characterized by well developed cumulate textures. Accumulate diopsidic clinopyroxene is the dominant mineral phase present. Cumulate olivine is a common accessory phase and some veins contain as much as 15 modal percent olivine (Plate 2.38, Sample 062). Also present, within the larger intrusive bodies, is a centimeter-scale layering of relatively olivine-rich and olivine-poor layers. Olivine, where present, is relatively fresh, locally however, it may be completely altered to iddingsite and weathers to a rusty brown colour.

Orthopyroxene is generally present but not abundant varying from 3 to 5 modal percent. It occurs as a late intercumulate phase forming oikocrysts (Plate 2.38, Sample 025). Minor amounts of plagioclase (2-4%), occur as an interstitial phase (Plate 2.38, Sample 062). Locally clinopyroxenite dikes contain segregations of coarse grained gabbro.



**Plate 2.36** Clinopyroxenite (light grey) intruding cumulate poikilitic wehrlite (black). Xenolith of wehrlite in center of photo is roughly 3 m wide.



**Plate 2.37** Pegmatitic texture of intrusive clinopyroxenite. Located on ridge east of Pano Amiandos. (Coin is approximately 1.5 cm in diameter).



**Plate 2.38** Polished slab of intrusive clinopyroxene-rich dike. 025 - Pyroxenite with orthopyroxene oikocrysts. 0.62 - olivine clinopyroxenite with interstitial plagioclase.

### 2.7.2 Gabbro (Unit 8)

Intrusive gabbros vary from medium grained to pegmatitic and are commonly highly variable in grain size on the outcrop scale. Thus the gabbros are characteristically referred to as "varitextured" (Plates 2.39, 2.40). Mineralogically the unit is dominated by both plagioclase and clinopyroxene and may contain primary uraltic amphibole.

The intrusive nature of *Late Magmatic Suite* gabbro into deformed gabbro of the *Early Plutonic Suite* is clearly identifiable in the field on the basis of cross cutting relationships (Plate 2.41 and 2.42). Where the *Early Plutonic Suite* gabbro is undeformed the intrusive nature of the *Late Magmatic Suite* may be recognized by marked textural variation between the two. Separation of the two distinct gabbro suites along the eastern sector of the map sheet (Map 1) is confounded however, by both a lack of deformation in the Early Suite and lack of continuous outcrop throughout most of the low lying areas underlain predominantly by these units. Characteristically, textures of the gabbro vary from one outcrop to the next, and although some outcrops are clearly net veined by the Late Magmatic Suite gabbro it was not possible to clearly distinguish early and late suite gabbro in a large portion of the eastern sector of the map sheet (Map 1)

### 2.7.3 Trondhjemite (Unit 9a)

The most significant exposures of trondhjemite (or plagiogranite) occur in the central eastern sector of the map sheet, within a roughly oval-shaped area containing abundant dikes and more massive irregular bodies of both diabase and trondhjemite with screens of coarse to pegmatitic gabbro and diorite, termed the "High Level Intrusive Zone". Locally within the zone, an intrusion breccia is exposed over an area of approximately 10 meters. This intrusion breccia contains abundant xenoliths of gabbro and diabase within a matrix of epidote-rich



**Plate 2.39** Exposure of Late Magmatic Suite varitextured gabbro.



**Plate 2.40** Polished slab of varitextured gabbro.



**Plate 2.41** Late Magmatic Suite gabbro intruding fine-medium grained deformed olivine gabbro of the Early Plutonic Suite. (Coin is approximately 1.5 cm in diameter).



**Plate 2.42** Late suite gabbro vein cross-cutting mylonitic fabric in early plutonic suite gabbro.

trondhemite (Plates 2.43 and 2.44). Trondhemite is also cut by younger diabase dikes.

An irregularly shaped body of medium grained hornblende trondhemite several meters in size with a well developed cumulate texture intrudes ultramafic cumulate of the *Early Plutonic Suite* on the north west - southeast trending ridge due east of Pano Amiandos.

## **2.8 DIABASE DIKE SUITES**

Mafic dikes identified throughout the Amiandos are divisible, on the basis of field criteria including texture, colour, and degree of alteration into aphyric and porphyritic dike types. Both are, in general, steeply inclined.

### **2.8.1 Aphyric Dike Suite**

These dikes are typically fine grained, aphyric and massive (Plate 2.45). They weather a characteristic dark grey colour and are relatively unaffected by secondary alteration. Dikes vary from several centimeters to over a meter in width, but are in general 0.5 to 1 meter wide. Aphyric dikes maintain a consistent spatial association with late differentiates of the *Late Magmatic Suite*, including areas of gabbro and trondhemite, and appear to be cogenetic with the late suite.

Dikes are composed essentially of fine grained interstitial plagioclase, augite and intergranular magnetite. Primary silicate phases may be partially altered to sericite and amphibole. Both plagioclase and augite in some places occur as microphenocrysts 0.5 to 1 millimeter in size.



**Plate 2.43** Polished slab with a wide variety and high abundance of xenoliths.

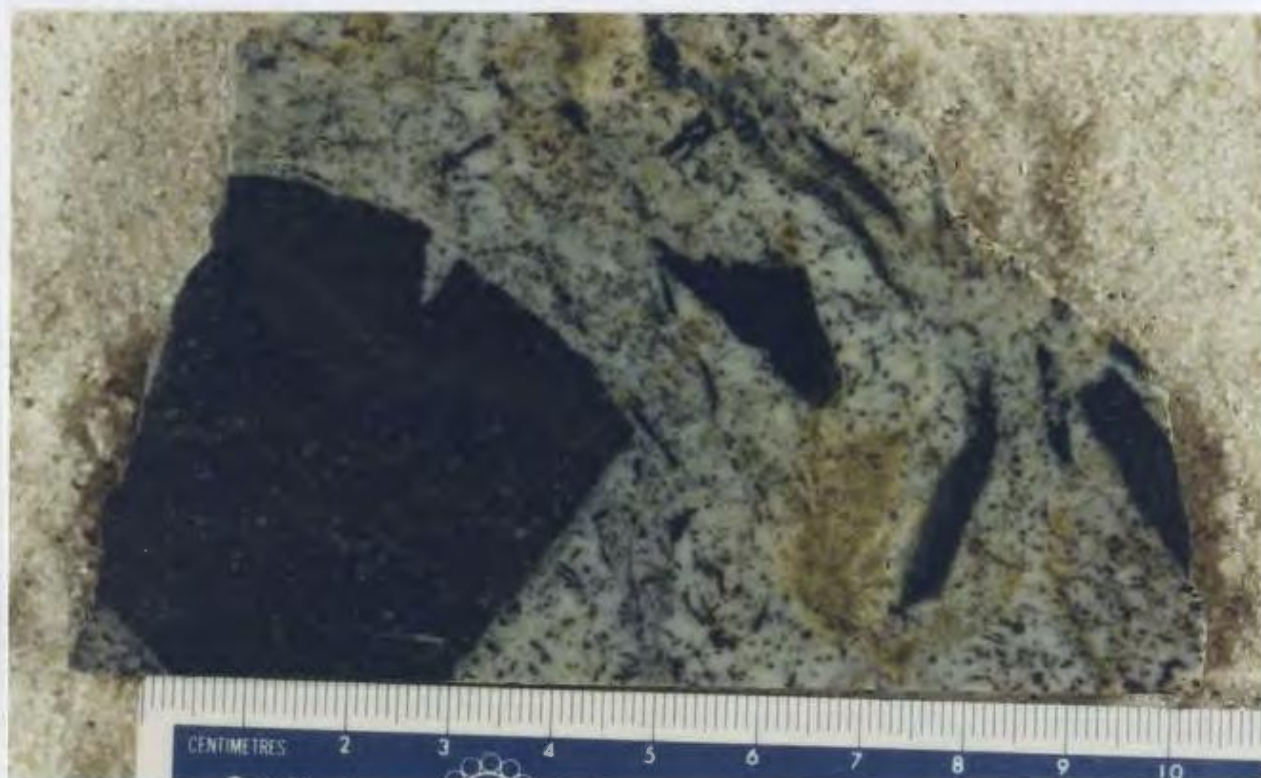


**Plate 2.44** Epidote-rich trondhjemite with diabase xenoliths.



**Plate 2.45** Polished slabs of the non-depleted dike suite illustrating their darker aphanitic appearance.

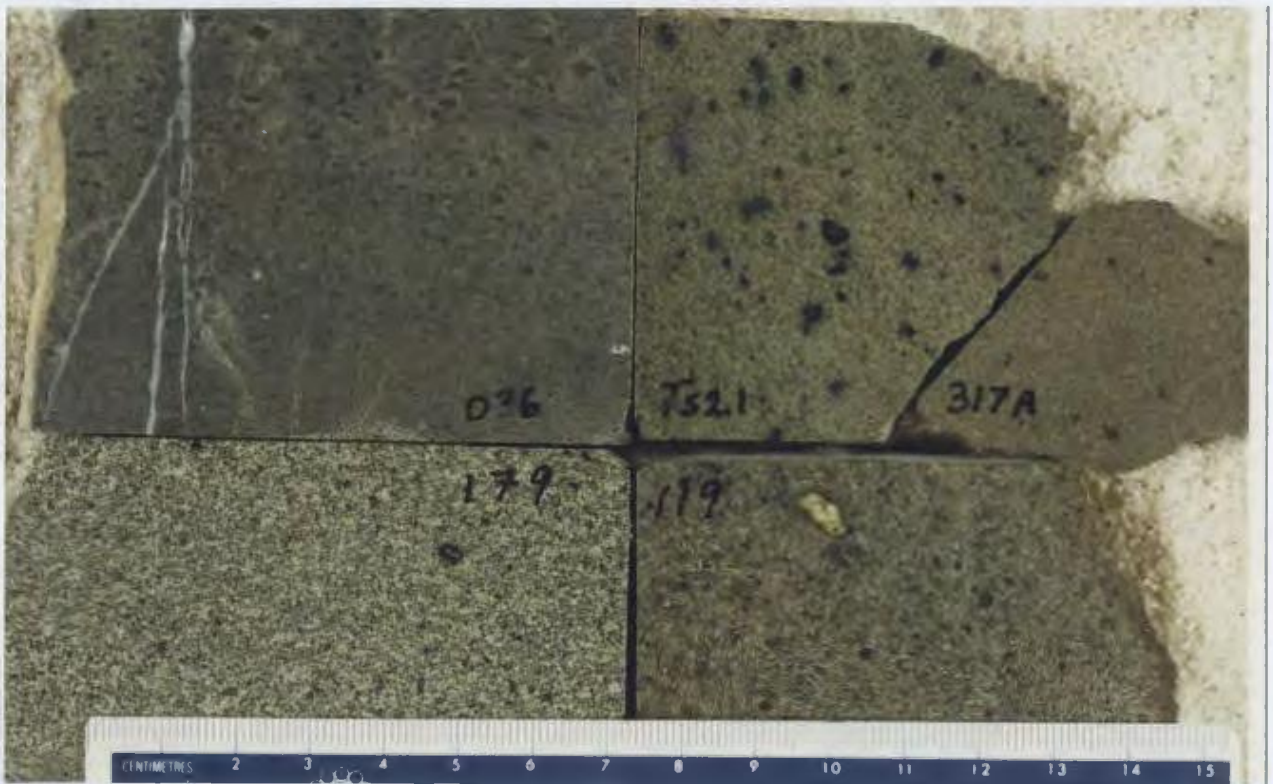


**Plate 2.46** Polished slabs of several porphyritic (depleted) dikes displaying general mesoscopic porphyritic texture. Sample 036 is relatively fresh compared to the others.

### **2.8.2 Late Porphyritic Dike Suite (M4)**

This dike suite is characterized by a porphyritic texture (Plate 2.46), weathers a bleached yellow to tan colour and in general displays intense and pervasive alteration. Dikes vary from 0.5 to 1.5 meters in width. Chilled contacts are evident as a reduction in phenocryst grain size towards the margin of the dikes.

Porphyritic dikes intrude all the crustal elements present, and unlike the aphyric suite, they are commonly noted intruding the ultramafic cumulate rocks.

Similar types of dikes have also been reported along the southern boundary of the ultramafic complex in the Caledonian Falls area (Benn, 1986). In this case however, Benn grouped both dike types as aphyric and porphyritic varieties of the same unit. However, Benn did note that the porphyritic diabase dikes occurred mainly in the dunite and olivine pyroxenite units.

Porphyritic dikes contain 5 to 15 percent phenocrysts (1 to 3 mm), dominated by antigorite pseudomorphs after olivine. Augite phenocrysts, commonly altered to amphibole and chlorite, are also present. The groundmass is fine grained and composed of crystalline plagioclase and augite which, in general, are extensively replaced by antigorite, chlorite and magnetite. Chromite euhedra (0.5 mm) are occasionally present within the olivine pseudomorphs.

## **2.9 FAULTING**

Emplacement and subsequent uplift of the central core of the ophiolite caused extensive crushing and brittle failure and has thus generated numerous fault zones throughout the map area. Faults have been indicated for the most part where they represent structural contacts or represent prominent structural features; numerous localized faults are present throughout the harzburgite and gabbroic units and have not been indicated. The Amianos Fault is the most prominent brittle deformation feature in the area; it separates residual mantle

harzburgite from the ultramafic plutonic rocks (Plate 2.2). The fault trends roughly N-S and dips steeply toward the east. Intermittent exposures, occurring in narrow streams along a broad river valley south of Pano Amiandos, consist of serpentinite breccia that forms a zone of unknown width containing blocks of residual harzburgite in a serpentinite matrix. The faulted contacts are best exposed where they cross ridges and promontories.

To the east, topographic depressions in two north-south flowing river valleys are inferred faults paralleling the Amiandos fault. The central fault, north of Kato Amiandos, accounts for the displacement of the ultramafic cumulate belt. Ultramafic cumulates on the west side of the valley are exposed at road level. The ultramafic cumulate rocks are positioned approximately 50 meters above the eastern side of the stream valley and beyond that they are continuous, forming the western limb of the "megafold". The easterly inferred fault marks an abrupt lithological change from mela- and olivine gabbros on the western side to mainly high level gabbro with abundant diabase dikes to the east. Additional evidence of a fault are N-S brittle fractures in the diabase adjacent to the river valley.

These faults break the plutonic section into a series of crustal-scale blocks. Exposure of deeper crustal levels, westward along the individual faults, indicates a reverse movement of unknown displacement.

It is assumed that the individual crustal blocks have not been significantly tilted during or after emplacement. This is a reasonable assumption based on the overall continuity of the various  $S_1$  structural elements. Internally each block forms a relatively homogeneous mass and is characterized by abundant local fractures of minor displacement which affected, in particular, the gabbros. As suggested by Wilson (1959), the ultramafic massif acted as a buttress against which the gabbros have been crushed thus making it extremely difficult to trace a particular fault line within the gabbro unit. This crushing and the subsequent

development of local fractures and shear zones is clearly evident where gabbro is well exposed (Plate 2.47). Along the southern margin of the harzburgite unit are numerous steeply inclined faults which bound isolated blocks of ultramafic cumulate rocks. In each fault-bounded block the orientation of the igneous layering consistently strikes NNE-SSW, suggesting that it has not been significantly tilted during uplift.

Emplacement-related faulting is represented by a single NW-SE trending thrust fault which structurally emplaces both the harzburgite and ultramafic cumulate units above the gabbro unit. This fault contact is clearly exposed in a road just north of Pano Amiandos (Plate 2.48). Further south the thrust contact is largely obscured by debris along the eastern face of the NW-SE trending ridge of ultramafic cumulate rocks. The contact on the face is exposed for several meters at only one location.

## 2.10 DISCUSSION

The geological relationships described above document a section of the lower oceanic crust that has evolved through a highly variable magmatic and deformational history. The probable remnants of an older magmatic event (M1) have been subjected to the effects of high temperature ductile deformation, involving both recrystallization and folding.

The *Early Plutonic Suite* (M2) forms an extensive differentiated pluton on the scale of kilometers in size. Textures clearly suggest evolution by cumulate processes that are periodically affected by heterogeneously developed overprints of synmagmatic ductile deformation. This process produces a wide textural variability which ranges from completely isotropic cumulates (both layered and massive) to progressively higher stress and lower temperature strain fabrics



**Plate 2.47** Exposure of gabbro displaying the effects of crushing and the development of local fracture and shear zones.



**Plate 2.48** Thrust contact between harzburgite and gabbro exposed in road north of Pano Amiandos.

appearing and grading into fine grained porphyroclastic textures with locally mylonitic fabrics developed.

The texture and geometry of the *Late Magmatic Suite* (M3) intrusives occurring predominantly as coarse grained dike-like bodies which lack chilled margins suggests that this portion of the crust, at the time of intrusion was still near solidus temperature with extension controlled by brittle fracture. Also evident in the *Late Magmatic Suite* rocks is the systematic presence of more differentiated rock types intruding at progressively lower stratigraphic levels within the *Early Plutonic Suite*. Clinopyroxenite intrusives are restricted to the mantle and ultramafic cumulate sections. Late differentiates of the *Late Magmatic Suite* intrude the complete range of lithologies represented by the *Early Plutonic Suite*.

Intrusion of the diabase dikes clearly demonstrates that the crust had continued to cool, resulting in brittle failure and extreme textural variability between dike and host.

Thus the deformation path for this section of the crust appears to progress from an area dominated by high temperature ductile deformation into the field of extension, controlled by brittle behavior. This is considered in more detail later.

## Chapter 3

### GEOCHEMISTRY

#### 3.1 GEOCHEMISTRY of the LAYERED CUMULATE SECTION

Identification of a nearly continuous ultramafic cumulate section oriented perpendicular to intermittently developed cumulate layering provided an excellent opportunity to conduct the first study of a continuous chemical evolution of the lower crustal section of the Early Plutonic Suite within the Troodos Ophiolite.

##### 3.1.1 Sampling and Analytical Techniques

In order to investigate whole rock and mineral chemistry variations as a function of stratigraphic position a total of 90 samples were collected at five meter intervals along the section. The location of these samples along the line of section are illustrated on Map 2 (located in back pocket). In some instances, the sample density was increased, particularly in areas of well developed layering, to test for finer-scale chemical variations. Several samples were also collected from the clinopyroxenite and gabbroic intrusive rock types for comparison between the the *Early Plutonic* and *Late Magmatic* suites.

Whole rock concentrations of the transition elements (Cr, Ni, Ti, V, and Sc), and Ca were analyzed by X-ray fluorescence spectrometry methods using pressed powder pellets bound with polyvinyl alcohol binder. Major element abundances were analyzed by atomic absorption (AA). Details of sample preparation and the analytical methods employed are given in Appendix B, and the complete analyses, listed in order of stratigraphic position, are given in Tables A8 and A9.

Compositions of the mineral phases were determined using an electron microprobe. Minerals analyzed included olivine, clinopyroxene, orthopyroxene, plagioclase and chrome-spinel. All analyses of the individual phases are listed

according to stratigraphic position along the ultramafic cumulate section in Tables A3, A4, A5, A6 and A7 respectively. Probe specifications and procedural details are given in Appendix B. The phase chemistries of olivine, clinopyroxene and orthopyroxene as a function of stratigraphic position, are illustrated in Figure 3.1 (in back pouch). Modal mineralogy of the individual samples displayed along the left margin of the profiles was estimated visually from the thin sections used for probe analysis. Whole rock major and trace element abundances are illustrated in Figure 3.2 (in back pouch). It is important to note that the ordinate on both figures is not to scale because all samples have been equally spaced along the sectional plot, including intervals of high density sampling, for clarity of presentation.

### 3.1.2 Phase Chemistry

The purpose of the mineral chemistry investigation is to determine how the composition of both the cumulus phase, olivine and the intercumulate phases clinopyroxene and orthopyroxene varies as a function of stratigraphic position. Documentation of the cryptic chemical variations within the layered cumulates of the *Early Plutonic Suite* will facilitate evaluation of the fractionation processes operative during magma chamber evolution.

Microprobe analyses of olivine, clinopyroxene and orthopyroxene, the most common and significant phases throughout the section, are near complete. Gaps in analysis at certain levels are the result of extreme degrees of alteration affecting particular samples or individual minerals, resulting in a lack of the primary phases available for analysis.

Analysis of plagioclase, which occurs too infrequently to yield a continuous profile, is not complete. Results on plagioclase are briefly discussed but have not been plotted due to the limited number of analyses obtained.

Mineral chemistry of chrome-spinel, which occurs only within the first 100 meters of the section is treated separately in the following section (Section 3.3).

The first notable feature in the profiles of cryptic chemical variation (Figure 3.1) is that a change in the composition of any particular phase, from one sample to the next, is apparently not associated with the modal proportions of the mineral phases present. The dominant feature evident in the chemical variations is the overall geochemical pattern of successive normal and reverse trends, which define a number of cyclic units.

"Normal" trends are defined by negative geochemical gradients with height for compatible elements (ie. Fo and NiO in olivine, Mg# and Cr<sub>2</sub>O<sub>3</sub> in clinopyroxene, Cr<sub>2</sub>O<sub>3</sub> in orthopyroxene) and positive geochemical trends with height for incompatible elements (ie. MnO in olivine, Na<sub>2</sub>O and TiO<sub>2</sub> in clinopyroxene) (Browning, 1984). These normal trends, in which Mg numbers of ferromagnesian silicates and compatible elemental abundances decrease with height as incompatible element contents increase, indicate the progressive evolution of the magma towards a more evolved liquid composition due to fractional crystallization (Irvine, 1980).

"Reverse" trends, also referred to as "*Cryptic Regressions*" (Irvine pers. comm. in Komor et al., 1985) display the opposite behavior to that of the normal trends, with compatible elements displaying sustained enrichment with height and incompatible elements showing progressive depletion (Browning, 1984). *Cryptic regressions*, unlike "rapid resets", which suggest the instantaneous mixing of a primitive replenishing magma are suggested to indicate a gradual resetting of the magma chamber chemistry due to a prolonged influx of a more 'primitive' magma without catastrophic mixing. Similar reverse trends have been referred to as; "sustained reverse gradients", by Browning (1984, 1989), "gradual inverse fractionation trends" by Komor et al. (1985) and "progressive reversals", by Thy

(1987).

**Olivine:**

Olivine phase chemistry is reported (Table A3, Appendix 1) and graphically illustrated (Figure 3.1) for a total of 68 samples. Individual values reported per sample are averages of 2 to 4 analyses. No chemical heterogeneities were identified within individual grains or between grains within single rock samples.

Fo contents (mole %) of olivine throughout, vary from a high of 92.4 in the dunitic unit at the base of the section, to a low of 83.1 in olivine gabbro near the top. A systematic decrease to lower Fo content is discernible with increasing stratigraphic position to a height of approximately 250 meters, illustrating a well defined fractionation trend or normal gradient. Upward from 250 meters in the section this normal trend is affected by a number of successive cryptic regressions as indicated by gradual resets to higher Fo contents.

The Ni content of olivine varies from 0.14 to 0.32 wt. % and portrays both normal and reverse gradients, consistent with the trends defined by Fo content. The behavior of MnO is variable and displays a normal positive gradient characterized by a progressive enrichment with decreasing Fo and Ni for the lower portion of the section. In the upper portion of the section, MnO displays a geochemical trend which mimics the normal and reverse gradients defined by Fo and Ni. This type of incoherent geochemical behavior is referred to as "decoupling" (Browning, 1984) and may be attributed to some late stage intercumulus process, in which the incompatible element is most likely affected, due to its affinity for the intercumulate liquid.

Olivine present in the intrusive clinopyroxenite dikes is dramatically lower in Fo content than that in the surrounding host. The Mn and Ni contents are, in general, higher and lower, respectively, reflecting the more evolved nature of the

intrusives of the late magmatic suite relative to their surrounding hosts

### **Clinopyroxene:**

Clinopyroxene phase chemistry is reported Table A4, and graphically illustrated (Figure 3.1) for a total of 77 samples. Individual values reported are averages of 2 to 4 analyses. No chemical heterogeneities were identified within individual grains or between grains within individual thin sections.

All the clinopyroxenes analyzed lie in either the diopside or endiopside fields of the Ca-Mg-Fe pyroxene classification scheme (Figure 3.3).

The Mg# (mole %) of the clinopyroxene [ $Mg\# = (100 \times Mg)/(Mg + Fe)$ ] ranges from 86.3 to 95.4, and as in the case of Fo in olivine, it is highest in the basal dunite and lowest in the upper gabbros. A systematic reduction to lower Mg# content with increasing height is also evident, however the onset of the first cryptic regression is at a lower stratigraphic position than that observed in olivine.

The Cr<sub>2</sub>O<sub>3</sub> content (wt. %) of the clinopyroxene varies from 0.18 to 0.91 and portrays combined normal negative and reversed positive gradients, clearly consistent with the gradients defined by the Mg#.

The content of both TiO<sub>2</sub> and Na<sub>2</sub>O is low, TiO<sub>2</sub> ranges from 0.05 to 0.25 wt. percent and Na<sub>2</sub>O ranges from 0.004 to 0.35 wt. percent. Both Na<sub>2</sub>O and TiO<sub>2</sub> display similar variation patterns of normal positive and reverse negative gradients. These variation patterns are however, less well defined throughout the profile than the compatible element (Cr<sub>2</sub>O<sub>3</sub>) and elemental ratio (Mg #). These vague trends may simply reflect a lack of precision at the low abundance of these trace elements (oxides) in the clinopyroxenes. Alternatively it may reflect the fact that both Na and Ti are highly incompatible with respect to clinopyroxene and are therefore most likely affected by intercumulus melt migration. McKenzie (1984) has suggested that the incompatible elements should be much more prone to

partition into the migrating intercumulus melt relative to the more strongly retained compatible elements. The recorded divergence from well defined trends of the compatible elements and the much vaguer trends of the incompatible elements reflect such a mechanism here.  $\text{TiO}_2$  and  $\text{Na}_2\text{O}$  contents within the lower 100 meter olivine-rich zone of the section display a chaotic distribution with no consistent trend. For  $\text{TiO}_2$ , the subsequent crystallization of chromite at low modal abundances of clinopyroxene may also have some bearing on this variation pattern. Alternatively the high degree of alteration affecting this zone may be a cause.

#### **Orthopyroxene:**

Orthopyroxene phase chemistry for a total of 28 samples is reported in Table A5, and graphically illustrated (Figure 3.1). Two of these values are from olivine clinopyroxenite dikes with intercumulate orthopyroxene from the *Late Magmatic Suite*. Individual values reported are averages of at least 2 and more commonly 3 to 4 analyses. No chemical heterogeneities were identified in individual grains or between grains within individual thin sections.

All the orthopyroxenes analyzed lie in the enstatite field within Ca-Mg-Fe space of the pyroxene classification scheme (Figure 3.3).

The Mg# of orthopyroxene [ $\text{Mg\#} = (100 \cdot \text{Mg}) / (\text{Mg} + \text{Fe})$ ] varies from 90.78 to 85.52 and displays an overall trend toward less magnesian values from the base upward. Initiation of the first pronounced regressive trend is apparent at approximately 230 meters.

Analyses of orthopyroxene in the upper portion of the section above approximately 250 meters are insufficient to yield a profile from which to

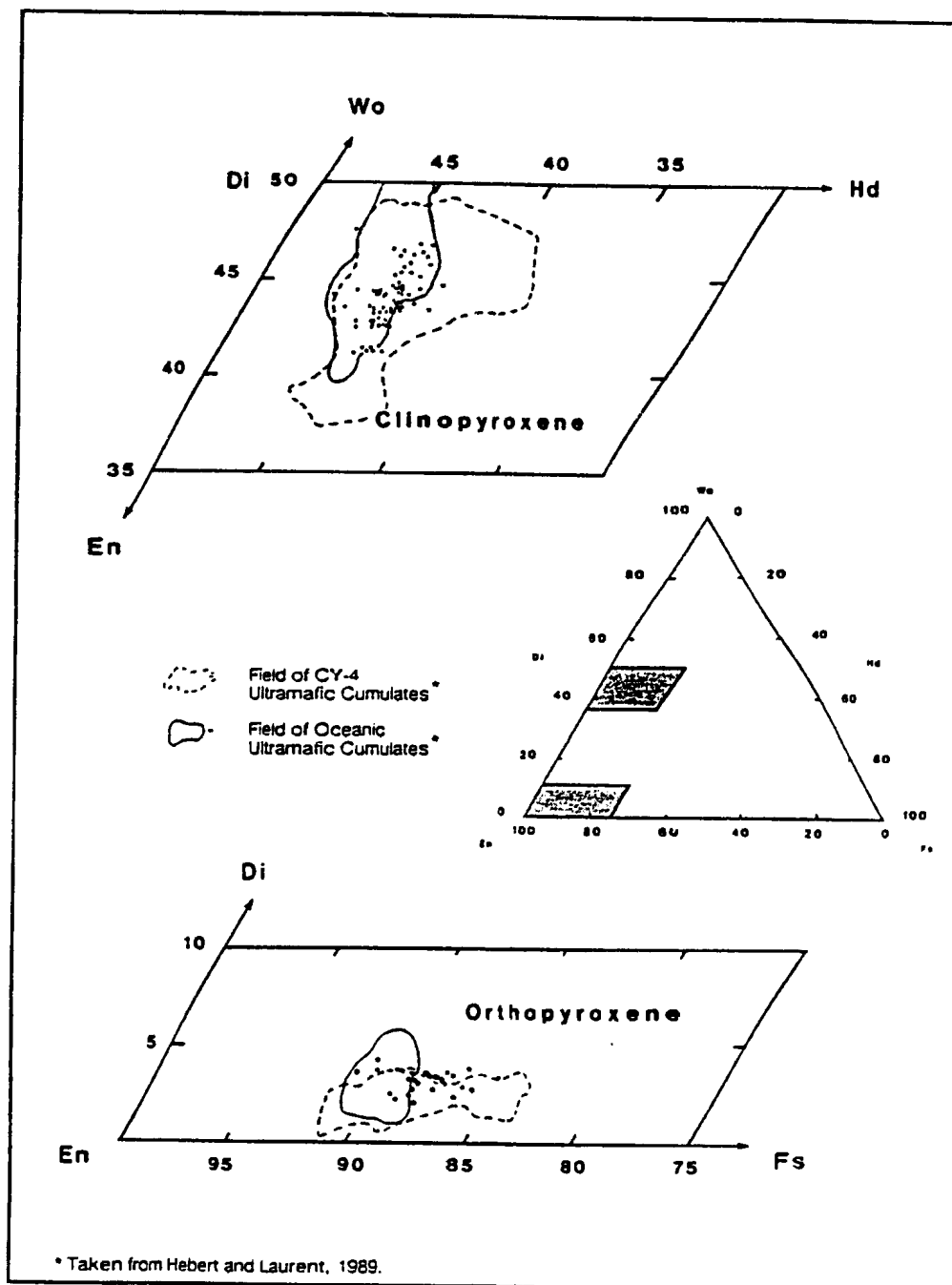


Figure 3.3 Composition of pyroxenes from the layered cumulate section.

conclusively identify the cyclic events seen in the other two ferromagnesian minerals, olivine and clinopyroxene.

Cr<sub>2</sub>O<sub>3</sub> content (weight %) in orthopyroxene varies from 0.17 to 0.63. Within the lower half of the section a number of cryptic regressive cycles are present. Above this none can be identified, due to the low abundance of data. The available data however, do indicate a progressive reduction to lower Cr contents with height.

The cryptic regressive trends indicated by the Cr content are not readily apparent in the Mg number profile, however a number of more subtle variations may be superimposed on the gradual normal negative trend in Mg number, associated with the pronounced regressive trends defined by Cr<sub>2</sub>O<sub>3</sub> occurring between 130 and 180 meters.

#### **Plagioclase:**

Plagioclase phase chemistry is reported for only six samples (Table A6). Four analyses are of plagioclase from the *Early Plutonic Suite* and two are of plagioclase from intrusive gabbroic dikes of the *Late Magmatic Suite*. Each value reported is based on a single analysis. The only conclusive statement that can be made from these limited results, is that all the plagioclases analyzed are highly calcic and of anorthite composition. There is no notable difference in composition between plagioclases of the early or late suites.

### **3.1.3 Whole Rock Chemistry**

The following discussion focuses on Figure 3.2 which displays selected whole rock elemental abundances as a function of stratigraphic position and modal mineralogy. In contrast to the phase chemistry, the whole rock element abundances are directly controlled by the modal mineralogy. Relative

abundances of the individual elements are clearly a result of their affinity for either the cumulate minerals or the intercumulate liquid. This relationship is best illustrated in the lower 100 meters of the section. Ni is clearly compatible with the cumulate mineral olivine while incompatible elements (eg. Ti) display a strong correlation with the intercumulate phase (clinopyroxene). The amount of Cr within the first 100 meters of the section is obviously related to the modal abundance of chromite and does not show a distribution pattern similar to the other incompatible elements (with respect to cumulate phase) at this level.

Remarkably consistent and rapid compositional gradients imposed on the larger scale gradual trends, reflect the modal mineralogical variations of the individual samples. The broad trends are thought to reflect bulk compositional variations within the magma from which the minerals are crystallizing. The cryptic regressions defined by Mg # are associated with an increase in incompatible elements and a reduction in the compatible element Ni with crystallization of cumulate olivine; both these features are likely associated with addition of a more primitive liquid into the system.

Of particular interest is the bulk rock Mg # [ $Mg \# = (100 \times MgO) / (MgO + FeO)$ ]. This displays a systematic reduction with increasing height up to approximately 250 m above the base, as does the Fo, (mole %) of the olivine (Figure 3.1) before the first major reset is encountered. Above this interval resets are common and provide additional evidence for the cryptic regressions identified in the mineral chemistry indicating that more primitive magma was periodically leaked into the system. Several somewhat more subtle resets may exist below this level as indicated.

### 3.1.4 Discussion

Cryptic variations in olivine and clinopyroxene differ in the number of obvious compositional resets. This may be the result of differences in the sample density between the two phases such that some compositional resets have remained unrecognized or are overshadowed by the major resets. Clearly there are also inconsistencies in the expected trends of elements and elemental ratios within individual phases. In some cases this may be the result of "decoupling" (Browning et al., 1988), but this is, at this stage, equivocal. In general, the existence of gradual resets are clearly evident throughout the section. These trends are best defined by the compatible elements or elemental ratios, as would be expected with the affinity of these elements for the cumulate minerals, (Mckenzie, 1984). They are also best defined within the upper two thirds of the section.

Another feature of interest is that the Mg numbers of the first olivines and clinopyroxenes to crystallize following each successive reset, are lower with increasing height in the stratigraphy. This feature suggests that the replenishing magmas are mixed with progressively more evolved residual magmas up section. (It is also possible that the replenishing magma is itself becoming more evolved with time due to continuing early olivine fractionation in the mantle source region). Cryptic variation patterns characterized by periodic resets to higher Mg numbers and compatible element contents, suggesting magma replenishment have been well documented in other ophiolitic sections, such as the Semail ophiolite in Oman (Pallister and Hopson, 1981; Smewing, 1981; Browning, 1984) and the Bay of Islands ophiolite in Western Newfoundland (Malpas, 1976; Elthon et al., 1984; Komor et al., 1985). A number of these studies (Pallister and Hopson, 1981; Smewing, 1981; Elthon et al., 1984) have identified for the most part "rapid resets" in the cryptic variation profiles under investigation, suggesting the instantaneous

mixing of primitive replenishing magmas. Studies by Komor et al. (1985) in the Bay of Islands and Browning (1985) in Oman have demonstrated, as in the present case, magma replenishments defined by cryptic regressions. These authors have offered a number of mechanisms to account for these progressive reversals. In general it is agreed that some process of gradual magma mixing must take place to account for the geochemical gradients. The actual process however, remains unclear. A primitive magma entering an evolving magma chamber would most likely be hotter and denser and therefore inhibited from mixing if the densities between the primitive and residual magmas were significantly different (Sparks and Huppert, 1980, 1984). Several processes operating independently or together, may overcome such a density contrast. Early olivine fractionation of the primitive magma will act to progressively reduce the density of the melt, the effect of which will become more pronounced as the Fe content increases in the cumulate phase (Sparks and Huppert, 1984). Browning (1984), has suggested that eruption of magma from the chamber (to be expected in an open system) will temporarily reduce the density of the magma in the chamber allowing primitive magma from below to reset the mixed liquid compositions to more primitive compositions. Komor et al. (1985) has suggested that progressive reversals are the result of slow gradual mixing which allows crystallization to occur during mixing.

Extensive magma replenishment combined with limited fractional crystallization as depicted by the present data set clearly suggest open-system evolution of the *Early Magmatic Suite* cumulates.

It has been suggested from a study of cryptic variations of mineral chemistry for the lower gabbroic and websteritic portion of the CY-4 drill core (Thy, 1987a, b; Thy and Moores, 1988; Thy et al., 1989) that the ultramafic and gabbroic cumulate sequence overlying the mantle rocks in the Troodos ophiolite have

crystallized in a relatively closed-system magma chamber within a slow spreading tectonic environment. This conclusion is clearly inconsistent with the present data. Browning et. al.(1989) have recently reevaluated the detailed phase chemical variations in the lower websteritic cumulate section of the CY-4 drill core and have demonstrated that finer scale variation, apparently missed by other workers, clearly does indicate open-system evolution. These findings (Browning et. al., 1989) indicate that the Late Magmatic Suite also evolved as an open-system.

Such multiple magma injections and associated mixing of magmas explain certain geochemical trends in oceanic basalts (Komor et al., 1985 and references therein).

### **3.2 CHROME-SPINEL CHEMISTRY**

Small (0.05-0.9 millimeter) subhedral to euhedral cumulate chrome-spinel grains are a ubiquitous accessory phase (1-3 modal percent) throughout the lowermost 100 meters (basal zone) of the ultramafic cumulate section. In thin section chrome-spinel grains display a close spatial association with interstitial clinopyroxene, and are commonly poikilitically enclosed by it (Plate 2.12). Where clinopyroxene is absent grains occur along the intergrain boundaries of olivine. The phase chemistry of the chrome-spinel grains is analyzed in detail as it is considered to provide a reliable indication of the chemical behavior of the intercumulate melt during crystallization. The vertical variations in the chrome-spinel chemistry are graphically illustrated in Figure 3.4 (in back pouch), and the analyses, listed according to stratigraphic position within the section, in Appendix A, Table A7. Values plotted on the graph represent the average of two analyses per grain. Values joined by tie-lines represent core to rim variations in individual grains and likewise each value plotted is the average of two analyses for both

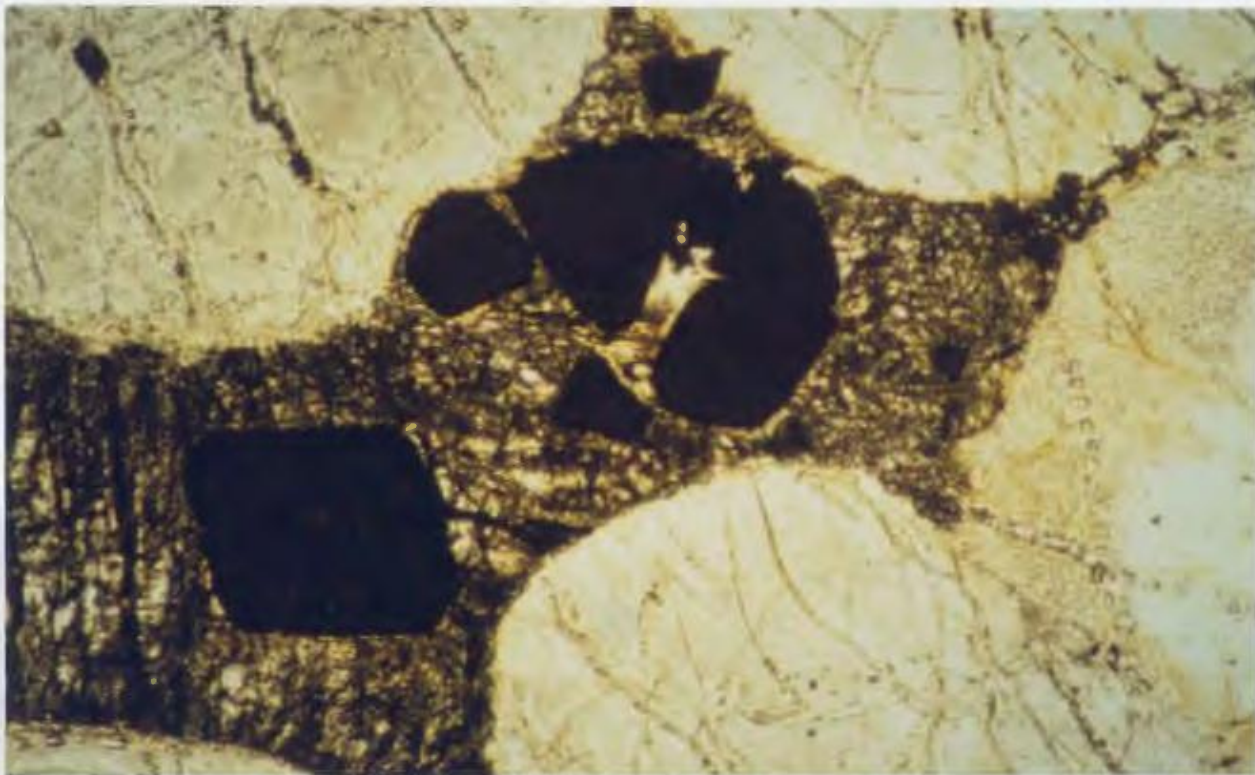


**Plate 3.1a** Typical grain size of chromite poikilitically enclosed by clinopyroxene in clinopyroxene-dunite (field of view is 2mm across).

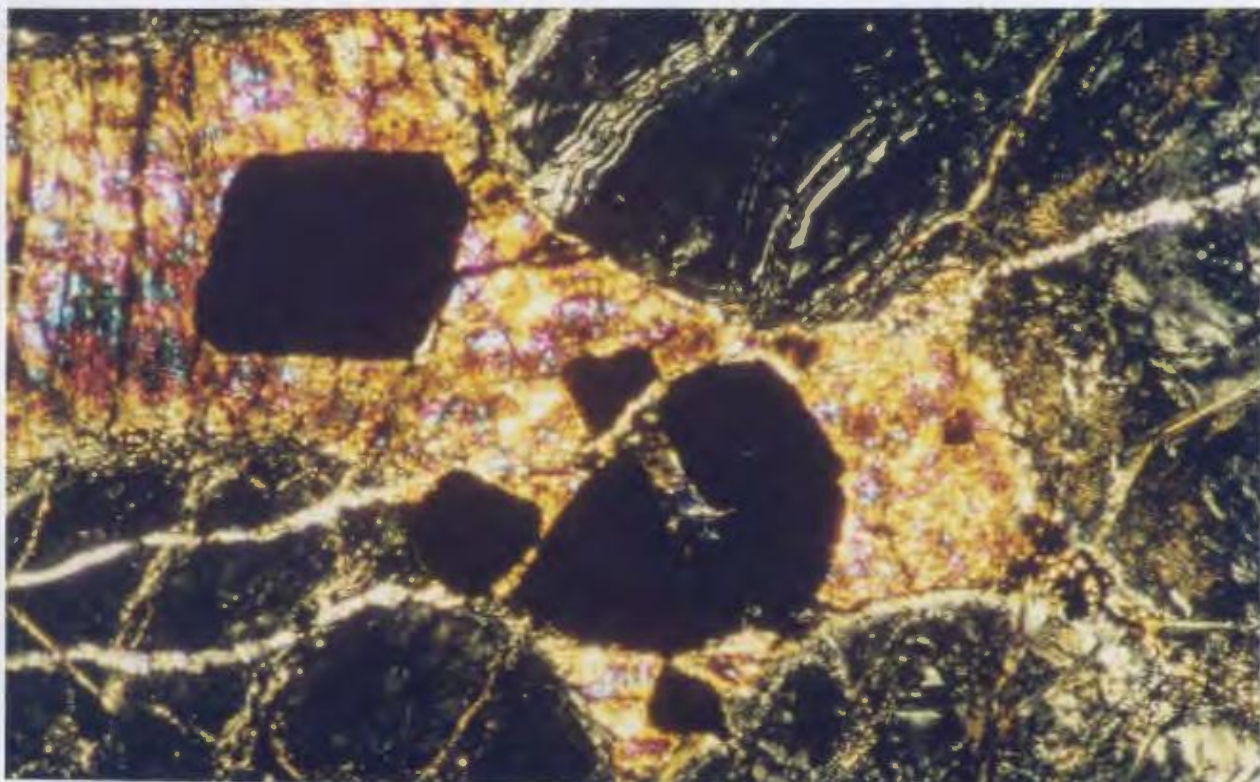


**Plate 3.1b** As in 3.1a, X nicols (field of view is 2mm across).



**Plate 3.2a** Typical chromite grain size in serpentinized dunite. Also displays nature of remaining olivine kernels in serpentine matrix (field of view is 2 mm across).

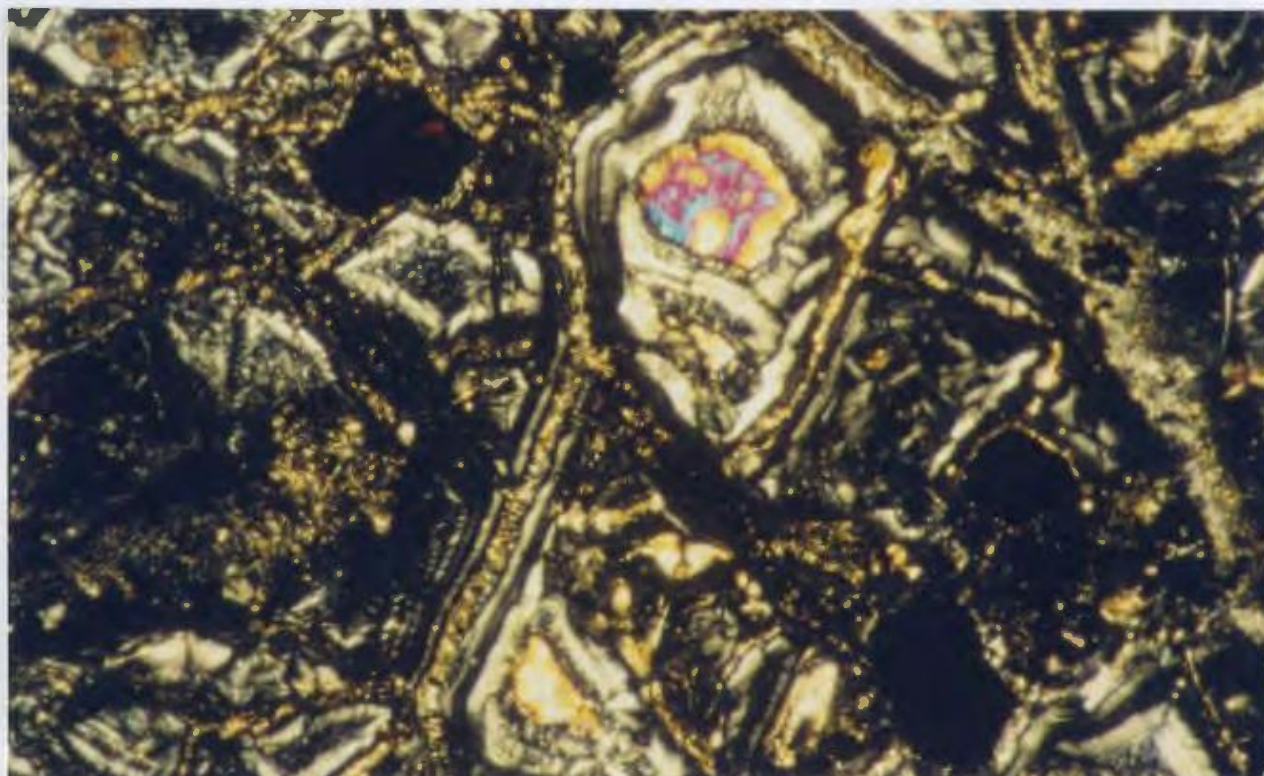


**Plate 3.2b** As in 3.2a, X nicols (field of view is 2mm across)

core and rim. Cr#'s of the chrome-spinel grains vary from 58.5 to 78.1 [ $\text{Cr \#} = (100 \times \text{Cr})/(\text{Cr} + \text{Al})$ ], while the Mg numbers [ $\text{Mg \#} = (100 \times \text{Mg})/(\text{Mg} + \text{Fe}^*)$ ] vary from 40.1 to 59.4 and the TiO<sub>2</sub> contents, from 0.15 to 0.88 weight percent.

The most prominent feature is the apparent effect of intercumulate clinopyroxene on the physicochemical behavior of the chrome-spinel. Physically, there is an increase in the spinel grain size with the increased amounts of interstitial clinopyroxene (compare Plates 3.1 and 3.2). Ranges in grain size of each of the samples investigated are reported along the right margin of Figure 3.4. This relationship is most pronounced in sample T3 which shows the first appearance of intercumulate clinopyroxene (approximately 1-2 modal percent) within the dunitic unit. Spinel grains in this section are up to 1 millimeter in size compared to a maximum grain size of 0.2 to 0.3 millimeters in the dunite samples collected above and below T3 which contain no clinopyroxene. Likewise, there is a significant increase in grain size evident in samples T8 to T10 which contain the greatest amount of intercumulate clinopyroxene.

Chemically, individual grains show a pronounced compositional zoning which varies systematically with the amount of intercumulate clinopyroxene present. The whole rock elemental abundance, notably, calcium, is graphically illustrated in Figure 4.4 as a function of stratigraphic position to directly reflect the relative abundance of clinopyroxene in the bulk rock. Observation of Table A4, Appendix A, indicates that the CaO content (weight percent) of the clinopyroxene is fairly consistent, making the above comparison a reasonable one.

Core to rim zoning in the chrome spinel is reflected by a decreasing Cr#; represented by an increase in Al<sub>2</sub>O<sub>3</sub> of up to 3 weight percent, and a decrease in Cr<sub>2</sub>O<sub>3</sub> of up to 6.8 weight percent from core to rim. Significant increases are also present in TiO<sub>2</sub> content of the individual grains from core to rim, displaying a

---

\* All iron as Fe<sup>2+</sup>

maximum variation of 0.59 weight percent. Interestingly, the maximum variation occurs in the sample with the highest clinopyroxene content. There is no consistent core-rim variation evident in either the Mg number or MnO contents.

### **3.2.1 Mechanism of Compositional Zonation in Chromite**

The compositional zonation associated with an increase in grain size of chrome-spinel is best explained in terms of adcumulate growth which is controlled by the interstitial melt, the last remnants of which are now represented by intercumulate clinopyroxene. Initially the system is represented by a mixture of crystals with interstitial silicate melt at or near liquidus temperature. The trapped liquid then crystallizes to produce post cumulate overgrowths on the cumulate crystals (chrome-spinel) and intercumulate clinopyroxene. The elemental variations characterizing the zoned chromites, notably a progressive increase in both  $\text{TiO}_2$  and  $\text{Al}_2\text{O}_3$  accompanied by a progressive reduction in the  $\text{Cr}_2\text{O}_3$  content, would be the expected change in the melt composition during the crystallization of clinopyroxene. This process has been termed, the "trapped liquid shift" by Barnes (1986).

Additional evidence of an adcumulate origin may be obtained using the chemical variability between selected elemental ratios (mole percent), Al/Cr and Fe/Mg. Figure 3.5 depicts these ratios for a number of grains which display the greatest chemical zonation. These are from rocks with a larger proportion of intercumulate clinopyroxene. Tie lines connect the compositions for cores and rims of the individual grains selected. An increase in the Fe/Mg ratio associated with an increase in Al/Cr may be explained by the reaction of chromite with an interstitial liquid, similar to the mechanism identified for layered basic intrusions of continental areas (Cameron, 1975; Moutte, 1982). The chemical range of the

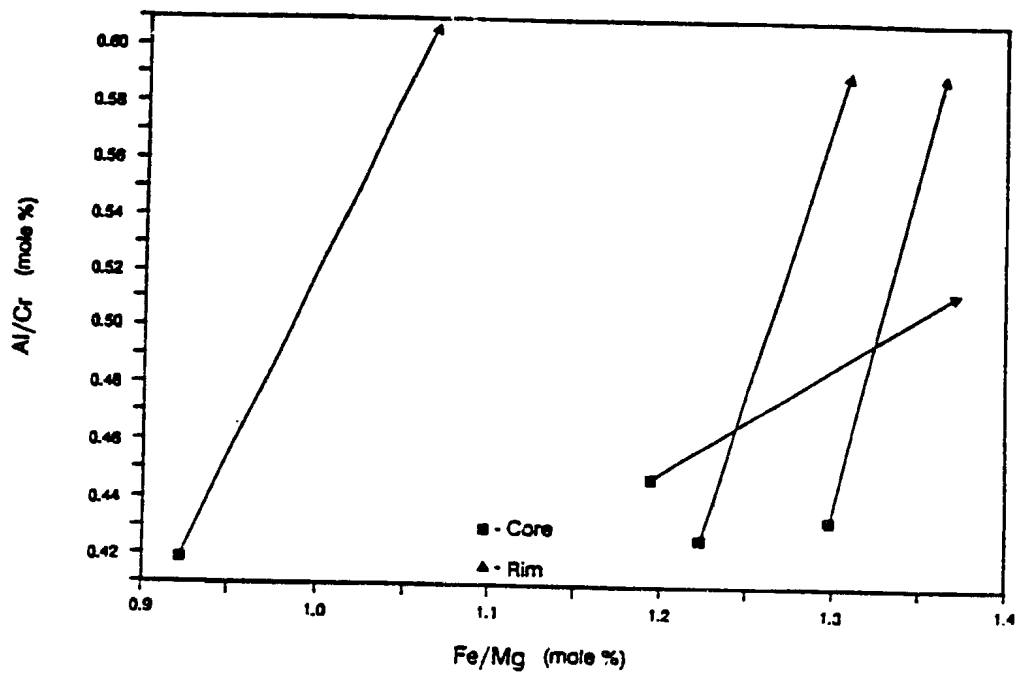


Figure 3.5 Compositional core to rim variation in zoned chrome-spinel grains. Tie-lines connect core to rim variation of individual grains.

individual grains, in 3 of the 4 samples, varies widely in the Al/Cr ratio but is limited in Fe/Mg ratios.

### **3.2.2 Cryptic Variations in Chrome Spinel**

The Cr number of chrome-spinel displays a well defined negative normal geochemical gradient consistent with the cryptic variation profile defined by Fo in olivine throughout the dunitic unit.

No cryptic variation, compatible with that identified in Cr number is evident in the Mg numbers of the chrome-spinels. The lack of such Mg # variation may be attributed to the effects of subsolidus reequilibration. Komor et al. (1985) have pointed out that spinels exchange Fe and Mg with olivine at temperatures well below the solidus.

### **3.2.3 Discussion**

The concentration of TiO<sub>2</sub> in ophiolitic chromite deposits has been traditionally recognized as being low and constant, generally less than 0.3 weight percent (Dickey, 1975), averaging 0.25 weight percent (Leblanc et al., 1980). TiO<sub>2</sub> is commonly used as a discriminant to distinguish ophiolitic from stratiform deposits, with TiO<sub>2</sub> being higher in the latter (Dickey, 1975). Figure 4.6 clearly demonstrates that disseminated chromite from the lower or dunitic portion of the section, with very little or no associated clinopyroxene, has less than 0.3 weight percent TiO<sub>2</sub> and little variation and so elsewhere would be interpreted to be ophiolitic according to Dickey's criteria. The adcumulate chromite grains however, are notably well above the range of typical ophiolitic chromite, the rims of several of the grains contain up to 0.88 weight percent TiO<sub>2</sub>.

Advocates in favor of a residual origin for the dunitic portions of ophiolites (Nicolas and Prinzhofer, 1983) suggest a mechanism of magmatic impregnation

to account for the presence of intercumulate clinopyroxene within the dunitic and wehrlitic units of the lower crust. Accordingly they suggest that the composition of the chrome-spinel grains should evolve from an aluminous spinel to a chromite, due to the incongruent melting of the orthopyroxene with concomitant magmatic growth of the spinel due to local percolation of basaltic magma. Clearly the data presented above show the opposite effect, an Al increase and a reduction in chrome content, suggesting evolution in a closed system apparently not affected by percolation of basaltic magma.

The normal negative gradients defined by both the cumulate olivine and chromite within the basal dunitic portion of the ultramafic cumulate provides additional evidence against a residual origin for the unit. Such compositional gradients are indicative of crystal fractionation (Irvine, 1980), suggesting a magmatic origin for the unit.

Thus the axial magma chamber appears to have been an essentially closed system during early stages of evolution, represented by chromite crystallization in the layered section, but was subsequently open to periodic magma influxes producing cryptic regressions seen higher in the section.

### 3.3 DIKE CHEMISTRY

In an attempt to further characterize the aphyric and porphyritic dike groups recognized on the basis of field and petrographic characteristics, their whole rock chemistry was investigated. A total of seventeen dikes, including both aphyric and porphyritic types, were analyzed by atomic absorption (AA) for major elements, and by x-ray fluorescence (XRF) for minor and trace elements (Sr, Y, Zr, Ni, Ti, V, and Cr). Several representative samples from each dike suite were analyzed by Inductively Coupled Plasma Mass Spectrometry (ICP-MS) for both rare earth and trace elemental abundances. Complete results of these analyses are reported in Tables A10, A11 and A12 and a detailed summary of the analytical methods is given in Appendix B.

#### 3.3.1 Geochemical Characteristics of the Dike Suites

A commonly used differentiation index, MgO is plotted against representative major, minor and trace elements to demonstrate the distinctive geochemical character of the individual dike suites (Figure 3.6). The samples clearly fall into two compositional fields defined by relatively high and low magnesium-rich end members which correspond to the petrographic subdivisions previously described. Elements of common chemical affinity behave in a similar fashion, that is, Ni and V display variation patterns comparable to those of Cr and Y, respectively.

Major elements of the porphyritic dikes, particularly CaO and Na<sub>2</sub>O, display extreme variability which is directly attributable to secondary metasomatic alteration, and therefore plots are not presented here. The oxides Al<sub>2</sub>O<sub>3</sub> and SiO<sub>2</sub> appear more stable but show a much wider range than the minor and

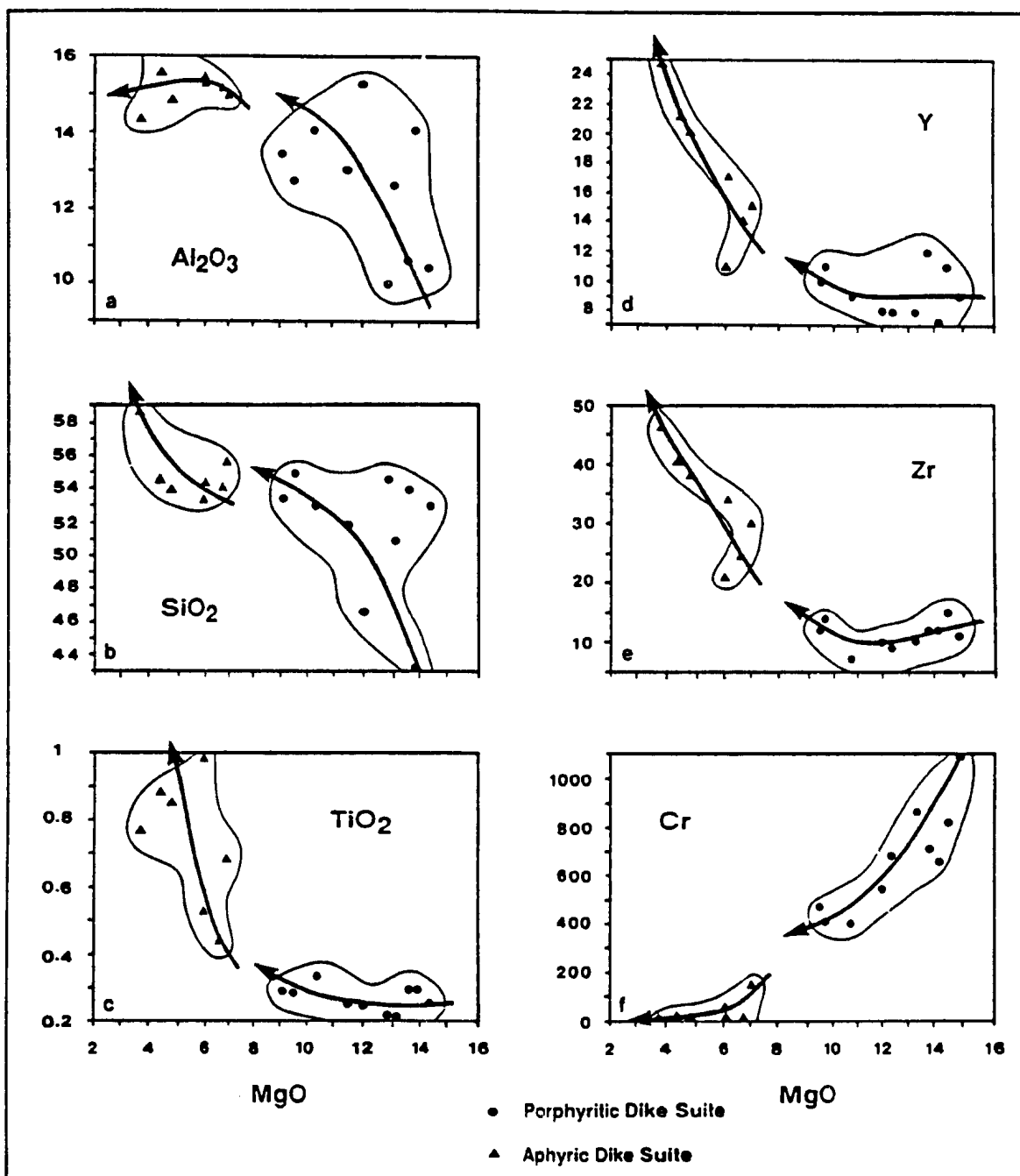


**Figure 3.6** Variation diagrams of major, minor and trace elements vs MgO, displaying compositional fields of the Aphyric and Porphyritic Dike Suites.

immobile trace elements, particularly in the highly altered porphyritic dikes (Figure 3.6 a and b).

The *Porphyritic Dike Suite* is characterized by low abundances of incompatible minor and trace elements (Ti, Zr and Y) suggesting derivation from a highly depleted mantle source. A high concentration of refractory trace (Cr, Ni) and major elements (MgO) displaying a positive colinear variation (Figure 3.6f) suggest derivation from a highly magnesian parental magma undergoing olivine and chrome spinel (and later clinopyroxene) fractionation. Reduction in Cr content at a constant Y concentration (Figure 3.7a) also supports a loss of olivine and chrome spinel from the melt (Alabaster et al. 1982).

In contrast the *Aphyric Dike Suite* is characterized by lower concentrations of refractory elements, and higher abundance of incompatible minor and trace elements. Incompatible element contents vary widely but a negative correlation with MgO (Figure 3.6c,d,e), suggest fractionation of olivine and/or pyroxene. A well defined positive colinear variation of the immobile-incompatible trace elements Zr vs Y (Figure 3.7) also supports a solid-liquid fractionation mechanism. The consistency in Zr/Y ratio throughout the suite is compatible with the crystallization of olivine, clinopyroxene and orthopyroxene phenocrysts phases as this has little affect on Zr/Y ratio, except to increase the absolute elemental abundances (Baragar et al., 1989). Relatively low abundances of Cr, Ni and MgO displaying limited variation suggests that both olivine and chrome-spinel are not dominant liquidus phases. Variation trends are therefore most likely controlled by pyroxene and plagioclase fractionation.

The geochemical data suggests the possibility of a separate highly refractory, depleted dike suite (porphyritic dikes) and a comparatively less depleted, more evolved suite (aphyric dikes). This distinction is clearly defined by representative chondrite normalized rare earth element (REE) distribution patterns

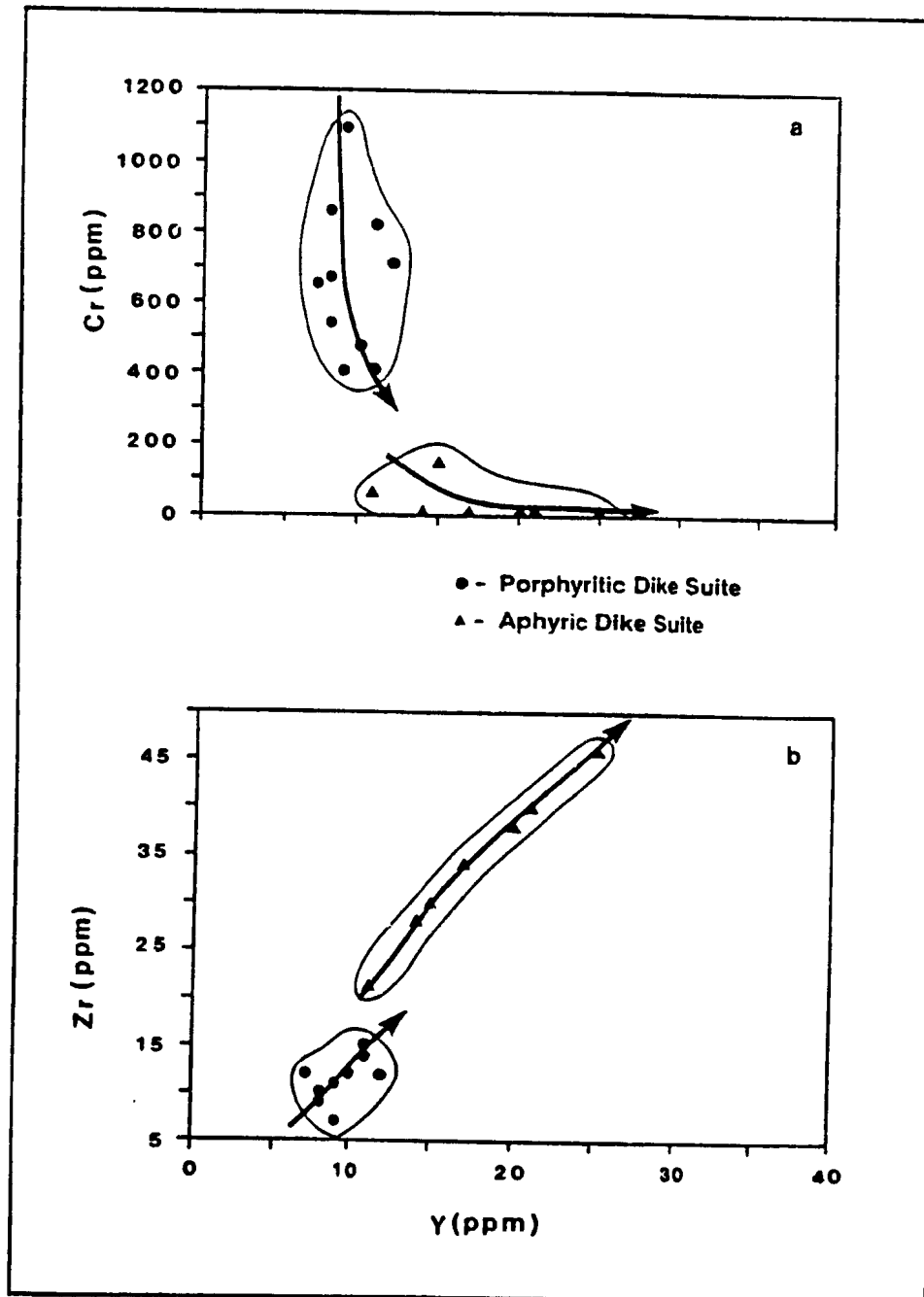
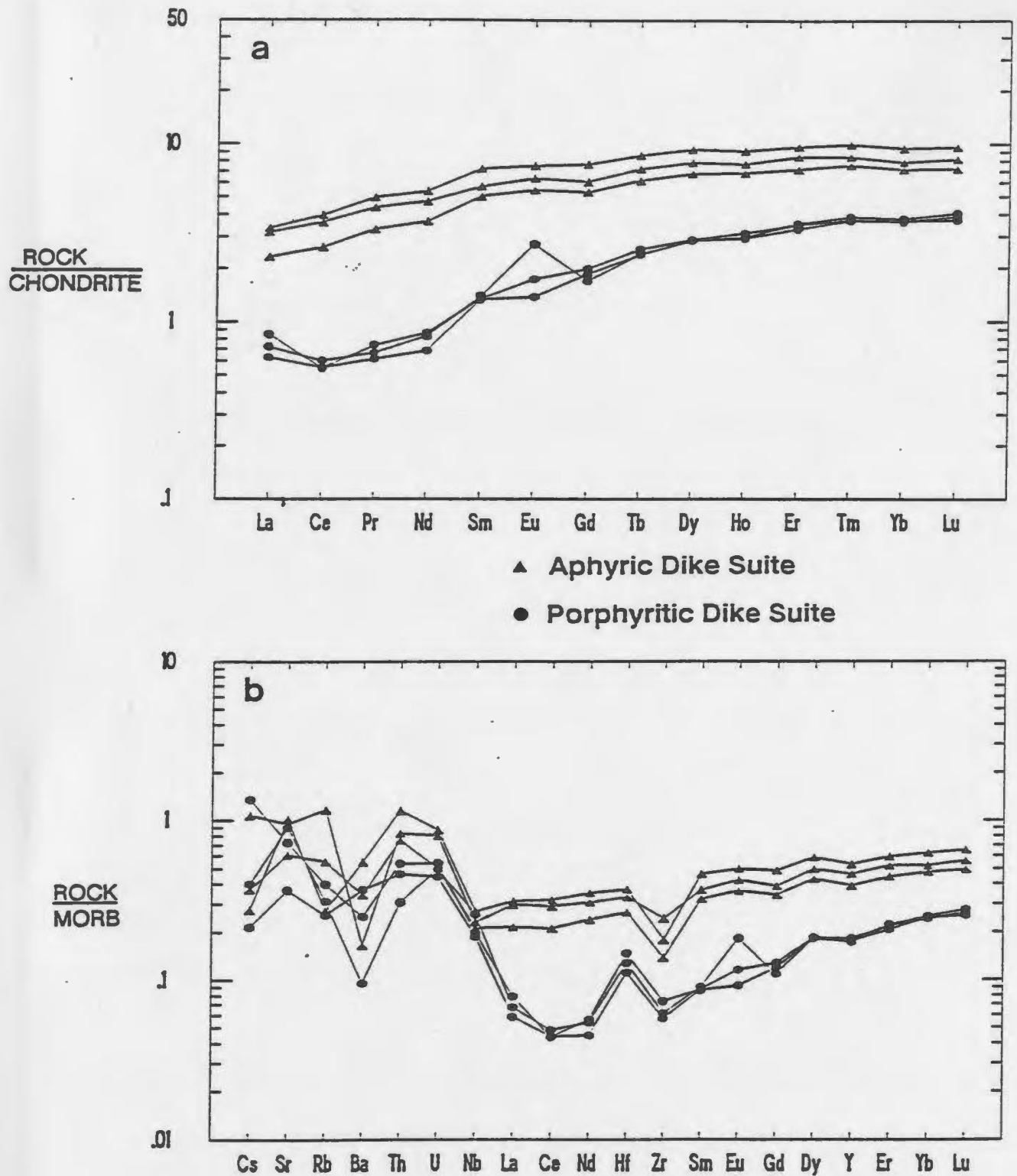


Figure 3.7 Variation diagrams of immobile trace elements a) Zr vs Y and b) Cr vs Yb illustrating differentiation features within the Aphyric and Porphyritic Dike Suites.



**Figure 3.8a** Rare-earth element distribution patterns of the individual dike suites normalized to chondrite rare-earth abundances.

**b** Geochemical abundance patterns of the individual dike suites normalized to MORB.

(Figure 3.8a). Aphyric dike patterns have about 5 to 10 times chondrite abundances for the HREE, with the LREE showing a relatively depleted pattern at 2.5 to 5 times chondrite. The distribution pattern for the porphyritic dikes is 3 to 6 times lower in overall REE abundance and there is a greater depletion in light REE (LREE) relative to the heavy REE (HREE). The porphyritic dikes also, in contrast to the aphyric suite display a distinctive upturn in La.

Both dike suites are characterized by selective enrichment in the large ion lithophile (LIL) elements. Such features are commonly attributed to the influence of an underlying subducting slab which during partial melting enriched the source region in incompatible elements (Alabaster et al. 1982; Cameron, 1985; MuCulloch and Cameron, 1983; Rautenschlein et al. 1985). Enrichment is only slightly greater in the porphyritic dikes relative to the aphyric suite. The relative depleted pattern of Ba is suspected to be the result of secondary processes comparable to those affecting both CaO and Na<sub>2</sub>O.

### **3.2.2 Comparison with the Troodos Lavas**

Comparison of selective compositional fields defined by the two dike suites with published chemical fields for the various volcanic units of the Troodos ophiolite (Figures 3.9 and 3.10) enables correlation between the volcanics and the dikes.

Figure 3.10 clearly demonstrates that the porphyritic and aphyric dike suites are compositionally similar to the Upper Pillow Lavas (UPL) and Arakapas Fault basalts (Thy, 1984) respectively. The Upper Pillow Lavas are identified as a silica-rich, basalt-basaltic andesite assemblage displaying boninitic affinities (Cameron et al., 1979; Cameron, 1985; Robertson et al., 1983; Thy, 1984; Malpas and Langdon, 1984). The Arakapas Fault basalts or the type III subdivision of the

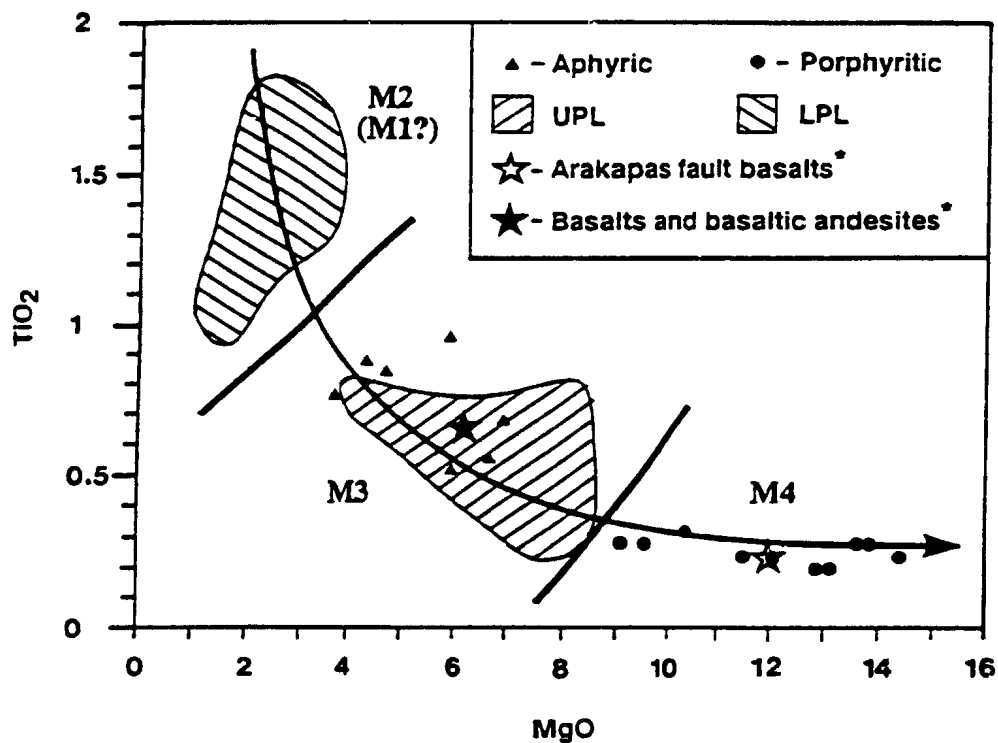


**Figure 3.9** Variation diagram of  $\text{TiO}_2$  vs  $\text{MgO}$  for the aphyric and porphyritic dike suites compared to the Troodos volcanics. Average of primitive Arakapas fault basalts is taken from Thy et al. (1984) using the data of Simonian and Gass (1978). Average of basalts to basaltic andesite glasses from the Troodos Ophiolite are from Thy et al. (1984). Fields of analysis for the Upper and Lower Pillow Lavas are from Robinson et al. (1983). Arrow indicates progressive depletion of the source region through time.

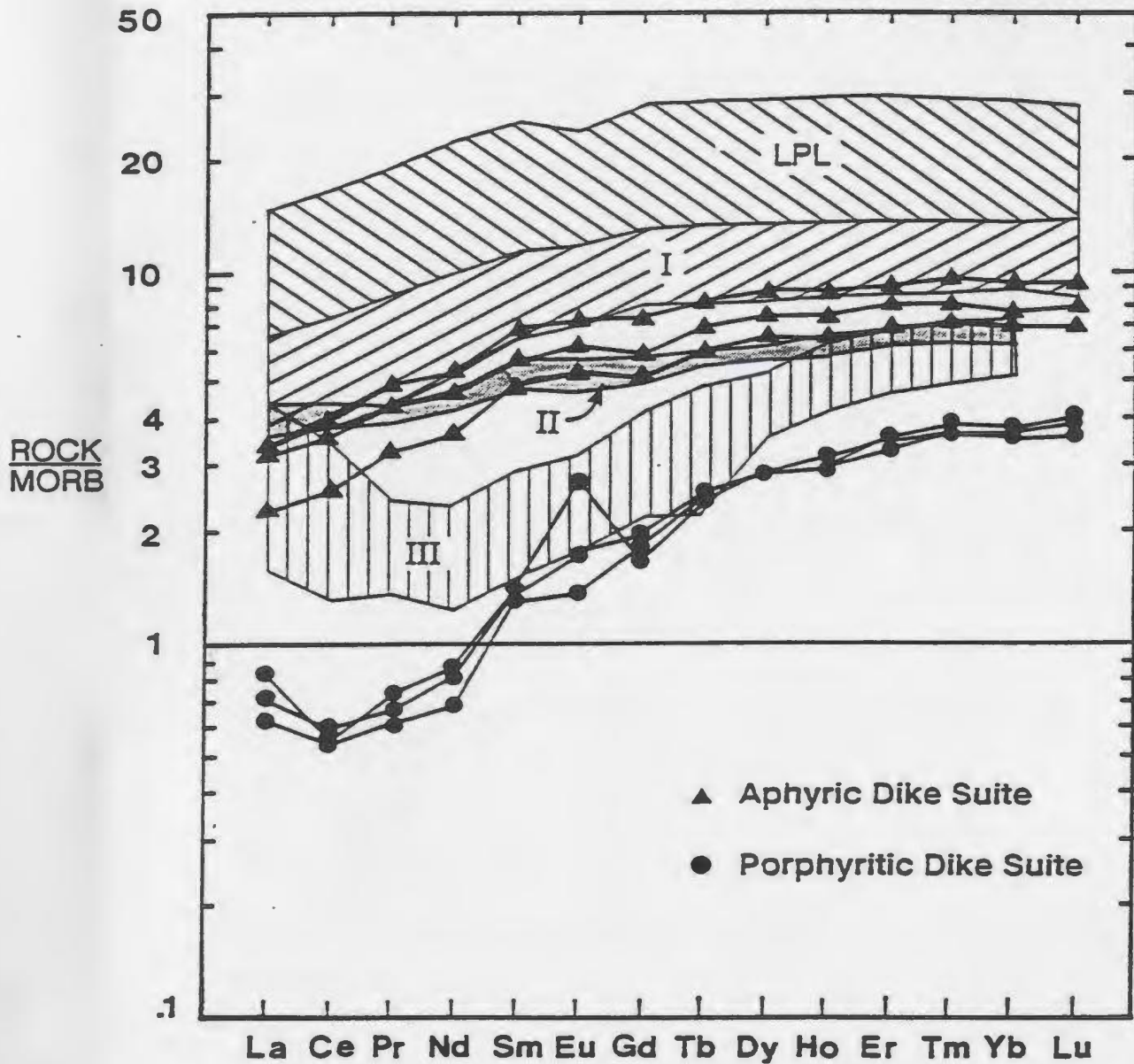


**Figure 3.10** Chondrite normalized rare-earth element distribution patterns of the aphyric and porphyritic dike suites compared to the compositional fields for the extrusive volcanic and sheeted dikes of the Troodos Ophiolite. Data for the LPL are from Rautenschlein et al. (1985) and for the UPLs groups I to III are taken from Cameron (1985).

primitive Troodos lavas (McCulloch and Cameron, 1983; Cameron, 1985) represents the most depleted and refractory member for the three-fold subdivision defined by these authors. Type III lavas have only been previously identified along the Arakapas Fault Belt (AFB) and were thus termed the Arakapas fault basalt by Thy (1984) (Figure 3.9). The type I and II lava subdivisions of McCulloch and Cameron (1983) and Cameron (1985) have been shown by Taylor and Nesbitt (1985) on the basis of  $Al_2O_3/TiO_2$  ratios (depletion index) to be transitional. REE abundances of the Aphyric Dike Suite (Figure 3.10) clearly overlap those of the Type I and II lava groups and support their transitional nature. Zr/Y ratios of the aphanitic suite vary from 1.9 to 2 which is intermediate to the range of 1.7 to 2.4 reported by Cameron (1985) for the type I and II lavas respectively.

The Porphyritic Dike Suite and the Arakapas Fault basalts display comparable abundances of both Ti and MgO (Figure 3.9). Similarly Zr/Y values for the dikes are close to 1 which is consistent with that reported for type III lavas (Cameron, 1985). REE abundances are, however, in several ways distinct from those of the type III lavas. The Porphyritic dikes, although displaying a somewhat similar REE distribution pattern, are clearly more depleted in overall abundances. They also lack the distinctive U-shaped, LREE enriched pattern characteristic of the type III lavas (Cameron, 1985; Rautenschlein et al., 1985; Taylor and Nesbitt, 1988) which are attributed to the introduction of a LREE enriched component into the source region, possibly derived from a subducting slab. Taylor and Nesbitt, (1988) proposed that fusion of a refractory source accompanied by the introduction of a hydrous silicate melt carrying LREEs indicates either higher degrees of batch melting or melting of a highly refractory source material. These boninitic U-shaped patterns show enrichment in La, Ce and Nd unlike the single La 'kick' identified in the porphyritic dikes. Since La is a mobile element in hydrous

environments, any comparison may not be valid here. Both dike suites do however, show enrichment in LFS elements (notably more so in the porphyritic or most depleted dike suite) suggesting a subduction related influence may have influenced dike composition.

### 3.2.3 Discussion

Notably none of the dikes sampled at the lower crustal levels currently under investigation, fall within the compositional fields defined for the Lower Pillow Lavas (LPLs). The LPL represent an andesite-dacite-rhyolite assemblage interpreted as an evolved arc-tholeiite suite (Robinson et al., 1983; Schmincke et al., 1983). The absence of dikes representative of this composition at this level of the crust suggest that they were most likely generated by the *Early Plutonic Suite* (M2 and possibly M1). Any dikes generated by this suite at the time of its evolution would be extruded well above the ultramafic section of the pluton (M2). Chrome-spinels associated with the *Early Plutonic Suite* are anomalously high in TiO<sub>2</sub> relative to typical oceanic chromites. Relatively high TiO<sub>2</sub> content is also a characteristic feature of the LPLs and the majority of the Sheeted Dike Complex, adding additional evidence for a comagmatic origin.

A close spatial relationship in the field between the Late Magmatic and Aphyric Dike Suites combined with geochemical information indicates these dikes were derived from a differentiating plutonic suite undergoing pyroxene and plagioclase fractionation supports the inference that the two are cogenetic. The fractionation trend defined by the dikes however, is not thought to represent differentiation of an isolated liquid confined to a single magma body. The variation is more likely the result of the faults tapping a number of magma bodies producing a wide petrological and compositional variability at differing stages of magmatic evolution. All derived from a similar initial source region.

The porphyritic dikes are clearly tapping a more depleted mantle source region. It is generally agreed on the basis of differences in incompatible element content (in particular  $\text{TiO}_2$  and REE) that the variation in lava chemistry is a function of a heterogeneous source rather than shallow-level crustal processes (ie. crystal fractionation). The preferred mechanism of producing this heterogeneous mantle is repeated incremental melting of the source region (Baragar et al., 1988, 1989; Cameron, 1985; Taylor and Nesbitt, 1988).

The sequence of the multiple magmatic events as defined by the intrusive and tectonic contact relationships throughout the plutonic section suggests that each successive intrusive event is related to progressive mantle melting. Thus the line on Figure 3.9a indicates the progressive depletion through time of the source region and the change recorded by successive magmatic events **M2** to **M4** and corresponding lava sequences.

## CHAPTER 4

### 4.1 MODEL

Data presented in this thesis indicates that the portion of lower oceanic crust represented in the Amiandos area of the Troodos ophiolite evolved through a close interplay of varying magmatic and deformational processes. These are recognized by a progressive change in texture, composition, geometry and magnitude of individual magmatic episodes. These progressive variations are schematically illustrated in Figures 4 A to C and discussed below.

The earliest clearly recognizable magmatic event (**M2**) was the development of a well differentiated plutonic suite of dunites, wehrlites and mafic gabbros (Figure 4.1A). These rocks are massive to layered and are overprinted by a heterogeneous synmagmatic ductile deformational event. Evolution through predominantly olivine, clinopyroxene and plagioclase crystallization produced a well defined lithostratigraphy, the extent of which suggests batholithic dimensions on the order of at least 3 to 4 kilometers. Phase chemical variations of the mafic minerals indicate a fractionating magma chamber that underwent several episodes of primitive magma replenishment or, open system evolution. Dunite and associated chromitite bodies contained within the residual mantle section are interpreted as representing early fractionation products of olivine and chromite within ascending magma batches or "mini chambers" (Neary and Brown, 1979) of basaltic liquid (Malpas, 1976; Talkington and Malpas, 1980; Brown, 1980; Pallister and Gregory, 1983; Duke, 1984; Christiansen, 1984; 1985; Hock and Fredrich, 1985; Hock et al., 1986). The mineralogical character of these bodies indicates that the melts were in the olivine phase volume during and after their ascent through the mantle sequence (Pallister and Gregory, 1983). The absence

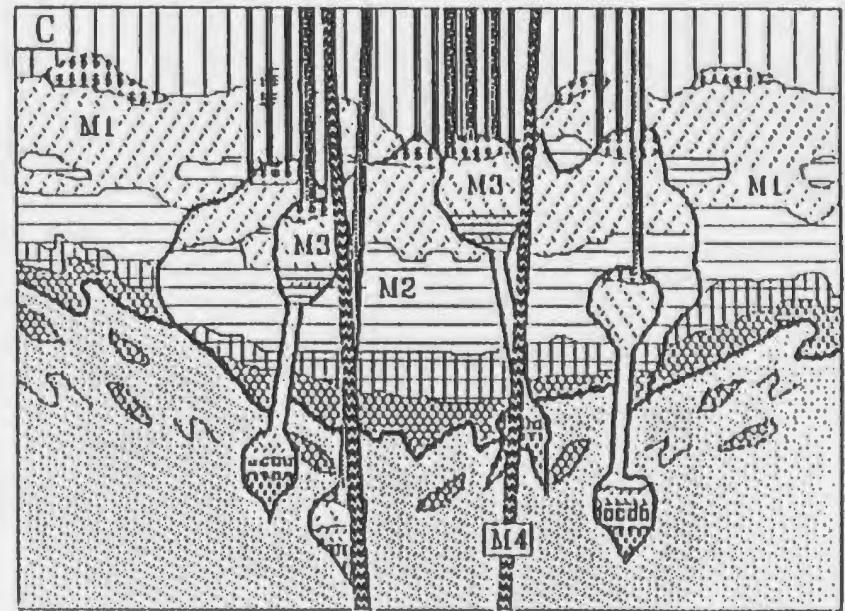
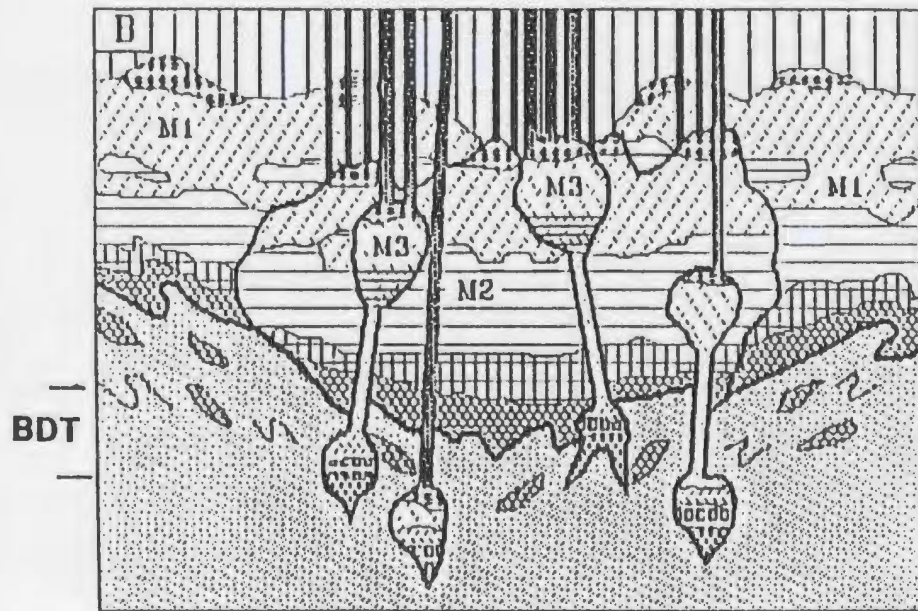
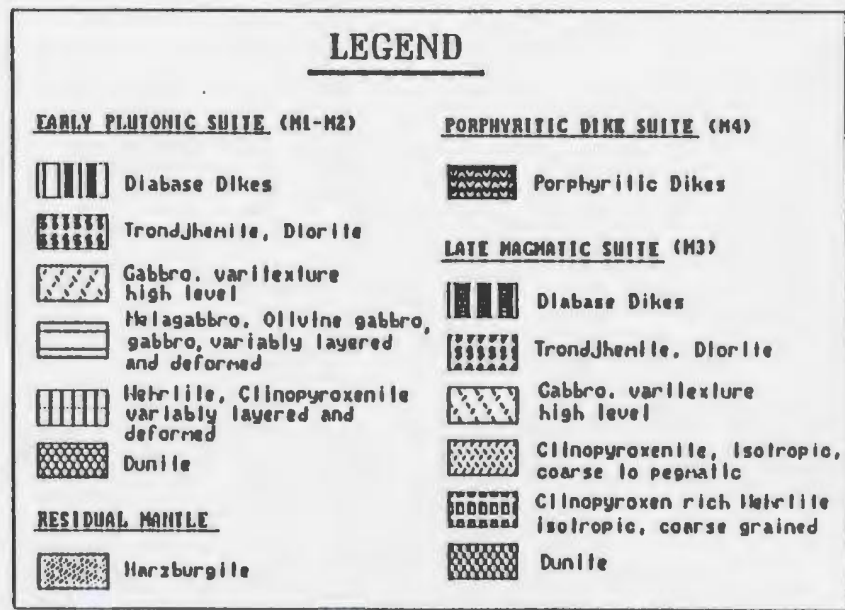
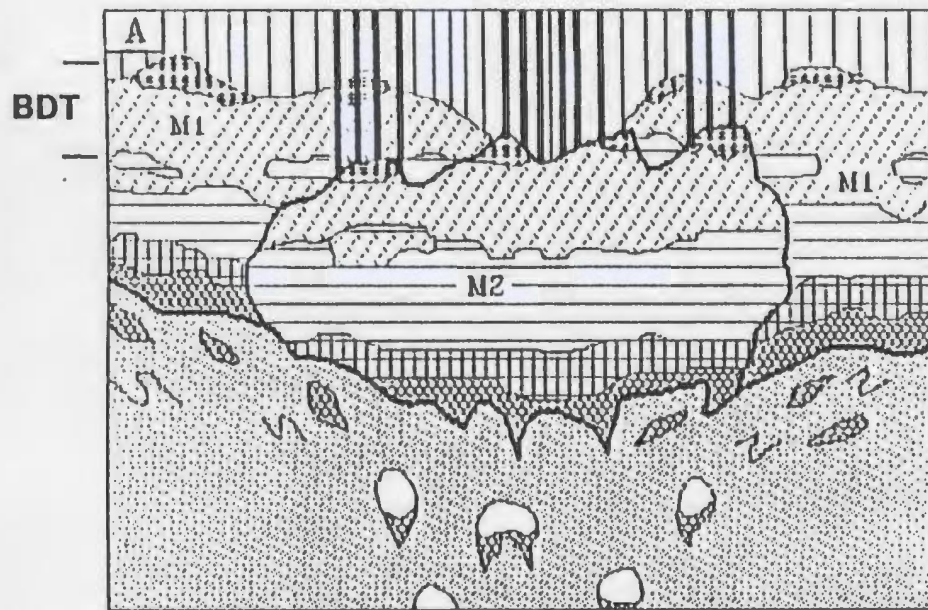


Figure 4.1 Schematic representation of the magmatic evolution of the Troodos oceanic crust. Individual stages A to C discussed in text. BDT- brittle ductile transition.

BDT  
↓

?

of gabbro in these bodies suggests that the chambers were open systems in which the melt was separated from the retained precipitates (Duke, 1984). Periodic tapping and release of melt from these mini chambers during episodes of magma fracturing\* (Yoder, 1976) may account for the cryptic regressions identified in the ultramafic cumulate section (Chapter 3.1). Relative timing and composition of both the *Early Magmatic Suite* and Lower Pillow Lavas suggest the two may have been cogenetic.

Xenoliths contained within this Early Plutonic Suite, of pervasively deformed and recrystallized banded dunite and orthopyroxenite suggest the probability of a preexisting plutonic phase (M1).

The *Early Plutonic Suite* was episodically intruded by a petrologically variable suite of pyroxenite-rich peridotites, gabbros, diorites, trondhjemite and diabase - the *Late Magmatic Suite* (M3) (Figure 4.1B). This suite is represented by a series of small, fault-controlled, irregular masses and dike-like bodies. These are isotropic, coarse grained to pegmatitic and display features characteristic of "high level" intrusives. A wide petrological range suggests that the melts supplying the individual structures were affected by varying degrees of differentiation. Chemistry of associated aphyric diabase dikes indicates that the suite may have been cogenetic with portions of the extrusive Upper Pillow Lava unit (Figures 3.9 and 3.10)

The latest and least represented magmatic episode (M4) (Figure 4.1C) occurs as isolated, fine grained, magnesian-rich, olivine and clinopyroxene phyrlic dikes which vary from less than a meter to several meters in width. These dikes cross-cut and are chilled against all other plutonic rocks. Geochemical data suggests that the dike suite is generated from magmas undergoing olivine and

\* *Magma fracturing* represents fracturing caused by an increase in the effective stress to a critical value so that extensional failure and upward migration of melt takes place. The process is a form of hydraulic fracturing, but used in its present context, as the fluid pressure is created by magma.

chrome-spinel fractionation, which were derived from a previously depleted mantle source region. The geochemical signature of this suite is in some respects similar to the depleted, primitive lavas characteristic of the Arakapas Fault Belt (Figure 3.9 and 3.10).

The sequence of events in this section of the lower crust and upper mantle is best explained in terms of a lowering of the geothermal gradient beneath the spreading center accompanied by progressive cooling and a subsequent deepening of the brittle-ductile boundary. The deepening of this boundary caused the lower crust and upper mantle initially affected by ductile flow, to accommodate extension by fissuring and fracturing. Batches of ascending basaltic liquid which initially fed a relatively large fractionating magma chamber were subsequently tapped by independent deep crustal fractures. Continued cooling of the lower crust and upper mantle had the effect of producing higher degrees of crystal fractionation of magma at progressively lower levels in the mantle. This relationship is demonstrated by the wide range of compositions in the Late Magmatic Suite lithologies identified cross-cutting the ultramafic cumulate rocks of the Early Plutonic Suite. The presence of highly differentiated dike lithologies intruded at the base of the crust would clearly indicate the evolution of magma bodies below that level.

Such a magma body was described by Malpas et al. (1987) as a small 300 to 400 meter fault controlled postkinematic differentiated pluton within the mantle harzburgite section roughly 4 to 5 kilometers to the west of the present map area. Lithologies of the intrusion range from dunite to variably layered and massive wehrlites to plagioclase wehrlites and pyroxenites and more differentiated phases including magnetite gabbros, pegmatitic leucogabbros and diorites.

The fine grained nature of the porphyritic dike suite combined with consistently developed chilled margins clearly indicates that the lower parts of the

crust had significantly cooled by the time of their intrusion.

A progressive lessening in the magnitude of the individual magmatic events as defined by decreasing size of plutonic suites and decreasing number of hypabyssal intrusions (Dilek et al., 1990) suggests that the amount of available melt was becoming significantly less through time.

Acceptance of this mechanism to explain the development of lower crust and upper mantle in the Amiantos area requires evaluation of the proposed mechanism for the progressive cooling of the crust and mantle. The possibility that lower crust and upper mantle have been cooled by lateral lithospheric drift (Rabinowicz et al., 1984) in which the material flow lines cross the narrowly spaced isotherms associated with a spreading center (Bottinga and Allegre, 1978) can be ruled out on the basis of consistent subvertical  $S_1$  tectonite fabrics present throughout the mantle section of the ophiolite, i.e. the area is a sample of the ridge itself.

The normal position of the brittle-ductile transition at the oceanic spreading center is at the base of the sheeted dike complex. Brittle processes such as normal faulting and dilational fracturing are dominant above the boundary; ductile deformational processes are dominant below. It is clear that the only mechanism which can explain the brittle features in the lower crust exposed in the present map area is a lowering of that boundary.

The existence of a fluctuating geothermal gradient within an oceanic spreading center is also supported by existing geophysical data from present day ridge systems. Harper (1985) has provided microseismic and refraction data indicating that isotherms beneath a spreading ridge system rise and fall with time producing a large variation in the thickness and strength of the brittle layer. Ephemeral magma chambers will periodically freeze changing the thermal structure. Microearthquakes detected to depths of 10 to 15 km below present

day ridge axis indicate that near axis faults will deepen as the brittle/ductile transition lowers and extends into the upper mantle.

The model presented in Figure 4.1 explains the highly varied and diverse field relationships present in the Amiandos area. Specifically the model relates the sequence of magmatic events both temporally and chemically to the Troodos lava sequence and also provides a tangible mechanism of generating the sequence of events for the environment in question.

The reason for the death of the spreading center is not clear, however, several mechanisms may be invoked to account for its demise. These include either ridge jumping or subduction locking due to collision, or more likely a combination of the two mechanisms. Vara and Moores (1985) have documented at least 3 spreading centers on Troodos which young from north to south. These ridge jumps may be attributed to a migration of the locus of partial melting through changes in the angle of the down going slab (C. Xenophonos, personal communication). It is therefore suggested that these older spreading ridges met their demise through ridge jumping and that the final death of the ridge system resulted from collision of the subduction zone with possibly a microcontinent (Eratosthenes Seamount) or the Arabian continental margin (Moores et al., 1984).

#### **4.2 CONCLUSIONS**

This work demonstrates the necessity of combining geochemical data with detailed field relationships to define a comprehensive model for oceanic crustal development. The main conclusions regarding the magmatic and structural evolution of crustal plutonic rocks in the Amiandos area of the Troodos ophiolite are:

1. The crust-mantle ultramafic transition zone formed by processes of magmatic differentiation within a relatively large (on the order of at least 3 to 4

kilometers) axial magma chamber. A systematic decrease in both the Fo content of olivine and the Cr number of chrome-spinel throughout the basal dunites of the ultramafic rocks indicate that they are not residual but formed as early differentiates during crystal fractionation. Cryptic variation patterns defined in both olivine and clinopyroxene throughout the upper half of the transition zone indicate periodic replenishment by primitive magmas into an open-system axial magma chamber.

2. On the basis of intrusive and tectonic contact relationships at least three and possibly four distinct magmatic episodes are identified. Each successive magmatic episode displays a systematic change in composition and scale becoming progressively more depleted chemically and significantly smaller through time.
3. The transition from ductile to brittle styles of deformation affecting the lower crust suggests continuous cooling during the tectonic and magmatic history of the plutonic suite. A "decaying" or lowering geothermal gradient is the proposed operative mechanism which causes the axial magma chamber to freeze and the brittle-ductile zone to transgress the section of crust under review. Associated with this depression of geotherms is a reduction in the supply of magma as the ridge system itself eventually dies.

## REFERENCES

- Alabaster, T., Pearce, J.A. and Malpas, J. 1982. The volcanic stratigraphy and petrogenesis of the Oman Ophiolite complex. *Contrib. Mineral Petrol.*, Vol. 81, 168-183.
- Anonymous, 1982. Penrose field conference on ophiolites. *Geotimes*, Vol. 17, 24-25.
- Arzi, A.A. 1978. Critical Phenomena in the rheology of partially melted rocks. *Tectonophysics*, Vol.44, 173-184.
- Baragar, W.R.A, Lambert, M.B., Baglow, N. and Gibson, I.L., 1988. Sheeted dykes of the Troodos ophiolite, Cyprus. *In*: Hall, H.C. and Fahrig, W.F. (eds.), *Mafic dyke Swarms*, Geol. Assoc. of Canada Special Paper 34, 257-272.
- Baragar, W.R.A, Lambert, M.B., Baglow, N. and Gibson, I.L. 1989. Sheeted dykes from CY-4 and surface sections: Troodos ophiolite. *In*: I.L. Gibson, J. Malpas, P.T. Robinson and C. Xenophontos (eds.), *Cyprus Crustal Study Project: Initial Report, Hole CY-4*. Geol. Surv. of Canada, Paper 88-9. 69-106.
- Barnes, S.J. 1986. The effects of trapped liquid crystallization on cumulus mineral compositions in layered intrusions. *Contrib. Mineral Petrol.*, Vol. 93, 524-531.
- Bear, L.M., 1960. The geology and mineral resources of the Akaki - Lythrodondha Area. Geol. Surv. Dept., Cyprus, Memoir No. 3, 122 pp.
- Benn, K. 1986. Petrology of the Troodos plutonic complex in the Caledonian Falls area, Cyprus. B.Sc. Thesis, Laval University, Montreal, Quebec. 226 pp.
- Benn, K and Laurent, R., 1987. Intrusive suite documented in the Troodos ophiolite plutonic complex, Cyprus. *Geology*, Vol. 15, 821-824.
- Benn, K., Nicolas, A., and Reuber, I. 1988. Mantle-Crust transition zone and origin of wehrlitic magmas: Evidence from the Oman Ophiolite. *Tectonophysics*, Vol. 151, 75-85.
- Blome, C.D. and Irwin, W.P. 1985. Equivalent radiolarian ages from ophiolitic terranes of Cyprus and Oman. *Geology*, Vol. 13, 401-404.
- Boudier, F. and Nicolas, A., 1977 Structural controls on partial melting in the Lanzo peridotites, *In*: H.J.B. Dick (ed.), *Magma Genesis*. State Oregon Dep., Geol. Min. Ind. Bull., Vol. 96, 63-78.
- Boudier, F., Le Sueu, E., Nicolas, A., 1989. Structure of an atypical ophiolite: The Trinity complex, eastern Kalamath Mountains, California, *Geol. Soc. of Amer. Bull.*, Vol. 101, 820-833.
- Bottinga, Y.W. and Allegre, C.J. 1978. Partial melting under spreading ridges. *Phil. Trans. R. Soc. Lond. A.*, Vol. 288, 501-525.

- Brown, M. 1980. Textural and geochemical evidence for the origin of some chromite deposits in the Oman ophiolite. In: A. Panaylotou (ed.) Ophiolites. Proc. Int. Ophiolite Symp., Cyprus, 1979 Geol. Survey Dept., Nicosia, 714-721.
- Browning, P. 1984. Cryptic variation within the cumulate sequence of the Oman ophiolite: magma chamber depth and petrological implications. In: I.G. Gass, S.J. Lippard and A.W. Shelton (eds.), Ophiolites and Oceanic Lithosphere. Geol. Soc. Lond. Special Publ., Vol. 13, 71-81.
- Browning, P., Roberts, S. and Alabaster, T. 1989. Fine Scale Modal Layering and Cyclic Units in Ultramafic Cumulates from the CY-4 Borehole, Troodos Ophiolite: Evidence for an Open System Magma Chamber. In: I.L. Gibson, J. Malpas, P. T. Robinson and C. Xenophontos (eds.), Cyprus Crustal Study Project: Initial Report, Hole CY-4. Geol. Surv. of Canada Paper 88-9, 193-220.
- Burgath, K. and Welsch, Th. 1980. Primary features and genesis of Greek podiform chromite deposits. In: A. Panaylotou (ed.), Ophiolites. Proc. Int. Ophiolite Symp., Cyprus, 1979 Geol. Survey Dept., Nicosia, 675-689.
- Cameron, W.E., Nisbet, E.G. and Dietrich, V.J. 1979. Boninites, komatites and ophiolitic basalts. Nature, Vol. 280, 550-553.
- Cameron, W.E. 1985. Petrology and origin of primitive lavas from the Troodos ophiolite, Cyprus. Contrib. Mineral. Petrology, Vol. 89, 239-255.
- Cassard, D., Nicolas, A., Rabinovitch, M., Moutte, J., Leblanc, M. and Prinzhofer, A. 1981. Structural classification of chromite pods in southern New Caledonia. Econ. Geol., Vol. 76, 805-831.
- Ceuleneer, G. and Nicolas, A. 1985. Structures in podiform chromite from the Maqсад district (Semail Ophiolite, Oman). Mineral Deposita, Vol. 20, 177-185.
- Christiansen, F.G. 1985. Structural classification of ophiolitic chromite deposits. In: Gallagher et. al. (eds.), Metallogeny of Basic and Ultrabasic Rocks, 279-289.
- Christiansen, F.G. 1985. Deformation fabric and microstructures in ophiolitic chromites and host ultramafics, Sultanate of Oman. Geologische Rundschau, Vol. 74/1, 61-76.
- Cleintuar, M.R., Knox, G.J. and Ealey, P.J. 1977. The Geology of Cyprus and its place in the East-Mediterranean framework. Geologie En Mijnbouw, Vol. 56 (1), 66-88.
- Coleman, R.G. 1977. Ophiolites. Springer-Verlag. New York. 229 pp.
- Delaloye, M., de Souza, H., Wagner, J.-J and Hedley, I. 1979. In: A. Panaylotou (ed.), Ophiolites. Proc. Int. Ophiolite Symp (Cyprus, 1979) Geol. Survey Dept., Nicosia, 292-295

- Dalaloye, M. and Wagner, J.-J. 1984. Ophiolites and volcanic activity near the western edge of the Arabian plate. In: J.E. Dixon and A.H.F. Robertson (eds.), *The geological evolution of the eastern Mediterranean*: Geol. Soc. Lond. Special Publ. 17, 225-233.
- Delaune-Meyere, M. 1984. Evolution of a Mesozoic passive continental margin: Baer-Bassit (NW Syria). In: J.E. Dixon and A.H.F. Robertson (eds.), *The geological evolution of the eastern Mediterranean*: Geol. Soc. Lond. Spec. Publication 17, 151-159.
- Dickey Jr., J.S. and Yoder Jr., H.S. 1972. Partitioning of chromium and aluminium between clinopyroxene and spinel. *Carnegie Inst. Wash. Yearbook*, Vol. 71, 384-392.
- Dickey Jr., J.S. 1975. A hypothesis of origin for podiform chromite deposits. *Geochemica et Cosmochimica Acta*, Vol. 30, 1061-1074.
- Dilek, Y., Thy, P., Moores, E.M. and Ramsden, W. 1990. Tectonic evolution of the Troodos ophiolite within the Tethyan framework. *Tectonics*, Vol. 4, 811-823.
- Dunsworth, S.M. and Calon, T. 1984. Relationships between deformation and magmatism in the plutonic complex, Troodos ophiolite, Cyprus. *Abstracts, Geol. Assoc. Can., Mineral. Assoc. Can. Joint Annual Meeting, London, Ontario, Canada*. p. 59.
- Dunsworth, S., Calon, T. and Malpas, J. 1986. Structural and magmatic controls on the internal geometry of the plutonic complex and its chromite occurrences in the Bay of Islands Ophiolite, Newfoundland. *Current Res., Pap. 86-1B*, 471-482.
- Ealey, P.J. and Knox, G.J. 1975. The pre-tertiary rocks of S.W. Cyprus. *Geologie en Mijnbouw*, Vol. 54 (1), 85-100.
- Elthon, D., Casey, J.F. and Komor, S. 1984. Cyptic mineral-chemistry variations in a Detailed Traverse through the Cumulate Ultramafic Rocks of the North Arm Mountain Massif of the Bay of Islands Ophiolite, Newfoundland. In: I.G. Gass, S.J. Lippard and A.W. Shelton (eds.), *Ophiolites and Oceanic Lithosphere*. Geol. Soc. London Spec. Pub., Vol. 13, 83-96.
- Gass, I.G. and Smewing, J.D. 1973. Intrusion, extrusion and metamorphism at constructive margins: evidence from the Troodos Massif, Cyprus. *Nature*, Vol. 242, 26-29.
- George Jr., R.P. 1975. The Internal structure of the Troodos Ultramafic Complex, Cyprus. Ph. D. Thesis, Department of Earth and Space Sciences, State University of New York. 122 pp.
- George Jr., R.P. 1978. Structural petrology of the Olympus ultramafic complex in Troodos Ophiolite, Cyprus. *Geol. Soc. Amer. Bull.*, Vol. 89, 845-865.
- Geotimes. 1983. Crustal Study drills and maps extrusives: November, p. 19.

- Greenbaum, D. 1972. The geology and evolution of the Troodos plutonic complex and associated chromite deposits, Cyprus. Ph.D. Thesis. Department of Earth Sciences, University of Leeds. 142 pp.
- Greenbaum, D. 1977. The chromitiferous rocks of the Troodos ophiolite complex, Cyprus. *Econ. Geol.*, Vol. 72, 1175-1194.
- Gregory, R.T. 1984. Melt percolation beneath a spreading ridge: evidence from the Semail peridotite, Oman. In: I.G. Gass, S.J. Lippard and A.W. Shelton (eds.), *Ophiolites and Oceanic Lithosphere*. Blackwell, Oxford, 55-62.
- Hall, R. 1980. Disrupted Tethyan ophiolites. In: A. Panayiotou (ed.), *Ophiolites*. Proc. Int. Ophiolite Symp., Cyprus, 1979 Geol. Surv. Dept., Nicosia, 287-291.
- Hall, R. 1980. Unmixing a Melange: the petrology and history of a disrupted and metamorphosed ophiolite, SE Turkey. *J. Geol. Soc. Lond.*, Vol. 137, 195-206.
- Hall, R. 1984. Ophiolites: Fragments of oceanic lithosphere? In: I.G. Gass, S.J. Lippard and A.W. Shelton (eds.), *Ophiolites and Oceanic Lithosphere*. Geol. Soc. Lond. Special Publ., Vol. 13, 393-404.
- Harper, G.D. 1985. Tectonics of slow spreading mid-ocean ridges and the consequences of a variable depth to the brittle/ductile transition. *Tectonics*, Vol. 4, 395-409.
- Hebert, R. and Laurent, In press R. Mineral chemistry of the plutonic section of the Troodos ophiolite: New constraints for genesis of arc-related ophiolites. In: I.L. Gibson, J. Malpas, P.T. Robinsen and C. Xenophontos (eds.), *Geol. Surv. of Canada*, Paper 88-9.
- Hock, M. and Friedrich, G. 1985. Structural features of ophiolitic chromites in the Zambales Range, Luzon, Philippines. *Mineral. Deposita (Berl.)*, Vol. 9, 253-259.
- Hock, M., Friedrich, G., Pluger, W.L. and Wichowski, A. 1986. Refractory-and metallurgical-type chromite ores, Zambales ophiolite, Luzon, Philippines. *Mineral Deposita*, Vol. 21, 190-199.
- Irvine, T.M. 1980. Magmatic infiltration metasomatism, double-diffusive fractional crystallization, and adcumulus growth in the Muskox intrusion and other layered intrusions. In: Hargraves, R.B. (ed.), *Physics of magmatic processes*. Princeton University Press, 325-383.
- Irvine, T.N. 1987. Processes involved in the formation and development of layered igneous rocks. In: I. Parsons (ed.), *Origins of Igneous Layering*. D. Reidel Publishing Company, Dordrecht. 649-656.
- Johan, Z. and Auge, T. 1985. Ophiolitic mantle sequences and their evolution: mineral chemistry constraints. In: Gallagher et. al. (eds.), *Metallogeny of Basic and Ultrabasic Rocks*, 305-317.

- Knipper, A., Ricou, L.-E and Dercourt, J. 1986. Ophiolites as indicators of the geodynamic evolution of the Tethyan Ocean. *Tectonophysics*, Vol. 123, 213-240.
- Komer, S.C., Elthon, D. and Casey, J.F. 1985. Mineralogic variation in a layered ultramafic cumulate sequence at the North Arm Mountain Massif, Bay of Islands ophiolite, Newfoundland. *J. Geophys. Res.*, Vol. 90, No. B9, 7705-7736.
- LaBlanc, M. 1980. Chromite growth, dissolution and deformation from a morphological view point: SEM Investigations. *Mineral. Deposita (Berl.)*, Vol. 15, 201-210.
- LaBlanc, M. and Violette, J.F. 1983. Distribution of aluminum-rich and chromium-rich chromite pods in ophiolitic peridotites. *Econ. Geol.*, Vol. 78, 293-301.
- Lago, B.L., Rabinowicz, M. and Nicolas, A. 1982. Podiform chromite ore bodies: a genetic model. *J. Petrol.*, Vol. 23, 103-125.
- Laurent, R. and Hebert, R. 1989. Petrological features of gabbroic and ultramafic rocks from deep drill CY-4, Cyprus. In: I.L. Gibson, J. Malpas, P.T. Robinson and C. Xenophontos (eds.), *Cyprus Crustal Study Project: Initial Report, Hole CY-4*. *Geol. Surv. of Canada*, 115-145.
- Lippard, S.J. 1983. Cretaceous high pressure metamorphism in N.E. Oman and its relationship to subduction and ophiolite nappe emplacement. *J. Geol. Soc. Lond.*, Vol. 140, 97-104.
- Lippard, S.J., Shelton, A.W. and Gass, I.G. 1986. *The ophiolite of Northern Oman*. Blackwell Scientific Publications. London. pp.
- Lorand, J.P. 1987. Cu-Fe-Ni-S mineral assemblages in upper-mantle peridotites from the Table Mountain and Blow-Me-Down Mountain ophiolite massifs (Bay of Island area, Newfoundland): Their relationships with fluids and silicate melts. *Lithos*, Vol. 20, 59-76.
- Magaritz, M. and Taylor, P.H. 1974. Oxygen and hydrogen isotope studies of serpentinization in the Troodos ophiolite complex. *Earth & Planet. Sci. Lett.*, Vol. 23, 8-14
- Malpas, J. 1976. *The Petrology and petrogenesis of the Bay of Islands ophiolite suite, Western Newfoundland*. Unpubl. Ph. D. Thesis, Memorial University.
- Malpas, J., Xenophontos, C. and Williams, D., *The Ayia Varvara formation of S.W. Cyprus; a product of Complex microplate interaction*, In prep.
- Malpas, J. and Strong, D.F. 1975. A comparison of chrome-spinels in ophiolites and mantle diapirs of Newfoundland. *Geochimica et Cosmochimica Acta*, Vol. 39, 1045-1060.
- Malpas, J. 1978. Magma generation in the upper mantle, field evidence from ophiolite suites, and application to the generation of oceanic lithosphere. *Phil. Trans. R. Soc. Lond. A.*, Vol. 288, 527-546.

- Malpas, J. and Langdon, G. 1984. Petrology of the Upper Pillow Lava suite, Troodos ophiolite, Cyprus. In: I.G. Gass, S.J. Lippard and A.W. Shelton (eds.), *Ophiolites and Oceanic Lithosphere*. Geol. Soc. Lond. Special Publ., Vol. 13, 155-167.
- Malpas, J., Calon, T. and Xenophontos, C. 1987. Plutonic rocks of the Troodos ophiolite. In: C. Xenophontos and J.G. Malpas (eds.), *Field Excursion Guidebook, Troodos 87, Ophiolites and Oceanic Lithosphere*, Geol. Surv. Dept., Nicosia, 158-181.
- Malpas, J., Brace, T. and Dunsworth, S.M. 1989. Structural and petrologic relationships of the CY-4 drill hole of the Cyprus Crustal Study Project. In: I.L. Gibson, J. Malpas, P.T. Robinson and C. Xenophontos (eds.), *Cyprus Crustal Study Project: Initial Report, Hole CY-4*, Geol. Surv. of Canada, Paper 88-9, 39-67.
- Malpas, J., Case, G. and Moore, P. 1989. The Geology of the Area immediately surrounding the CY-4 borehole of the Cyprus Crustal Study Project. In: I.L. Gibson, J. Malpas, P.T. Robinson and C. Xenophontos (eds.), *Cyprus Crustal Study Project: Initial Report, Hole CY-4*. Geol. Surv. of Canada, Paper 88-9, 31-37.
- McKenzie, D. 1984. The generation and compaction of partially molten rock. *Jour. Petrol.*, Vol. 25, Part 3, 713-765.
- Menzies, M. and Allen, C.A. 1974. Plagioclase lherzolite: residual mantle within the eastern Mediterranean ophiolites. *Contrib. Mineral. Petrol.*, Vol. 45, 197-213.
- Misseri, M. and Boudier, F. 1985. Structures in the Canyon Mountain ophiolite indicate an island-arc intrusion. *Tectonophysics*, Vol. 120, 191-209.
- Miyashiro, Akiho. 1973. The Troodos ophiolite complex was probably formed in an island arc. *Earth Planet. Sci. Lett.*, Vol. 19, 218-224.
- Moores, E.M. and Vine, F.J. 1971. The Troodos Massif, Cyprus and other ophiolites as oceanic crust: Evaluation and implications. *Phil. Trans. R. Soc. Lond. Ser. A*, Vol. 268, 443-466.
- Moores, E.M., Robinson, P.T., Malpas, J. and Xenophontos, C. 1984. Model for the origin of the Troodos massif, Cyprus, and other mideast ophiolites. *Geology*, Vol. 12, 500-503.
- Moutte, J. 1982. Chromite deposits of the Tiebaghi Ultramafic Massif, New Caledonia. *Econ. Geol.*, Vol. 77, 576-591.
- Mukasa, S.B. and Ludden, J.N. 1987. Uranium-lead isotopic ages of plagiogranites from the Troodos ophiolite, Cyprus, and their tectonic significance. *Geology*, Vol. 15, 825-828.
- Murton, B.J. and Gass, I.G. 1986. Western Limassol forest complex, Cyprus: part of an Upper Cretaceous leaky transform fault. *Geology*, Vol. 14, 255-258.

- Nicolas, A. 1986. Structure and petrology of peridotites: Clues to their geodynamic environment. *Reviews of Geophysics*, Vol. 24, No. 4, 875-895.
- Nicolas, A., Boudier, F. and Bouchez, J-L. 1980. Interpretation of peridotite structures from ophiolitic and oceanic environments. *Amer. J. Sci.*, Vol. 280-A, 192-210.
- Nicolas, A. and Violette, J.F. 1982. Mantle flow at oceanic spreading centers: Models derived from ophiolite. *Tectonophysics*, Vol. 81, 319-339.
- Nicolas, A. and Jackson, M. 1982. High temperature dikes in peridotites: Origin by hydraulic fracturing. *J. Petrol.*, Vol. 23, 568-582.
- Nicolas, A. and Prinzhofer, A. 1983. Cumulative or residual origin for the transition zone in ophiolites: structural evidence. *J. Petrol.*, Vol. 24, 188-206.
- Nicolas, A. and Rabinowicz, M. 1985. Mantle flow at oceanic spreading centers: relation with ophiolitic and oceanic centers. Massif, New Caledonia. *Econ. Geol.*, Vol. 77, 576-591.
- Nicolas, A., Reuber, I. and Benn, K. 1988. A new magma chamber model based on structural studies in the Oman ophiolite. *Tectonophysics*, Vol. 151, 87-105.
- Oxburgh, E.R. 1980. Heat flow and magma genesis. In: Hargraves, R.B. (ed.), *Physics of magmatic processes*. Princeton University Press. 161-199.
- Pallister, J.S. and Hopson, C.A. 1981. Semail ophiolite plutonic suite: Field relations, phase variations, cryptic variation and layering, and a model of a spreading ridge magma chamber. *J. of Geophys. Res.*, Vol. 86, 2593-2645.
- Pallister, J.S. and Gregory, R.T. 1983. Composition of the Semail ocean crust. *Geology*, Vol. 11, 638-642.
- Prinzhofer, A., Nicolas, A., Cassard, D., Moutte, J., Leblanc, M., Paris, J.P. and Rabinovitch, M. 1980. Structures in the New Caledonia peridotites-gabbros: implications for oceanic mantle crust. *Tectonophysics*, Vol. 69, 85-112.
- Rabinowicz, M., Nicolas, A. and Vigneresse, J.L. 1984. A rolling mill effect in asthenosphere beneath oceanic spreading centers. *Earth Plan. Sci. Lett.*, Vol. 67, 97-108.
- Rautenschlein, M., Jenner, G.A., Hertogen, J., Hoffmand, A.W., Kerrich, R., Schmincke, H.-U., and White, W.M. 1985. Isotopic and trace element composition of volcanic glasses from the Akaki Canyon, Cyprus: Implications for the origin of the Troodos ophiolite. *Earth Plan. Sci. Lett.*, Vol. 75, 369-383.
- Robertson, A.H.F. 1977. The Moni Melange, Cyprus: an olistostrome formed at a destructive plate margin. *J. Geol. Soc.*, Vol. 133, 447-466.

- Robertson, A.H.F. and Dixon, J.E. 1980. Introduction: aspects of the geological evolution of the Eastern Mediterranean. In: J.E. Dixon and A.H.F. Robertson (eds.), *The geological evolution of the eastern Mediterranean*: Geol. Soc. Lond. Special Publ. 17, 1-23.
- Robertson, A.H.F. and Woodcock, N.H. 1980. Tectonic Setting of the Troodos massif in the east Mediterranean. In: A. Panayiotou (ed.), *Ophiolites*. Proc. Int. Ophiolite Symp., Cyprus, 1979 Geol. Surv. Dept., Nicosia, 36-46.
- Robertson, A.H.F. and Dixon, J.E. 1984. Introduction: Aspects of the Geological Evolution of the Eastern Mediterranean. In: J.E. Dixon and A.H.F. Robertson (eds), *The Geological Evolution of the Eastern Mediterranean*. Geol. Soc. Lond. Special Publ., Vol. 17, 1-74.
- Robertson, A.H.F. and Woodcock, N.H. 1986. The role of the Kyrenia range lineament, Cyprus, in the geological evolution of the eastern Mediterranean area. *Phil. Trans. R. Soc. Lond.*, Vol. 317, 141-177.
- Robinson P.T., Melson, W.G., O'Hearn, T. and Schmincke, H.-U. 1983. Volcanic glass compositions of the Troodos ophiolite, Cyprus. *Geology*, Vol. 11, 400-404.
- Salisbury, M.H. and Christensen, N.I. 1985. Olivine fabrics in the Bay of Islands Ophiolite: implications for oceanic mantle structure and anisotropy. *Can. J. Earth Sci.*, Vol. 22, 1757-1766.
- Schmincke, H.-U, Rätutenschlein, M., Robinson, P.T., and Mehegan, J.M. 1983. Troodos extrusive series of Cyprus: A comparison with oceanic crust: *Geology*, Vol. 11, 405-409.
- Searle, M.P. and Malpas, J., 1980. Structure and metamorphism of rocks beneath the Semail ophiolite of Oman and their significance in ophiolite obduction. *Trans. R. Soc. Edinburgh*, 71, 247-262.
- Searle, M.P. and Malpas, J., 1982. Petrochemistry and origin of subophiolitic metamorphic and related rocks in the Oman Mountains. *J. Geol. Soc. Lond.*, Vol. 139, 235-248.
- Shaw, H.R. 1980. The fracture mechanisms of magma transport from the magmatic mantle to the surface. In: Hargraves, R.B. (ed.), *Physics of magmatic processes*. Princeton University Press. 201-263.
- Simonian, K.O. and Gass, I.G. 1978. Arakapas fault belt, Cyprus: A fossil transform fault. *Geol. Soc. Amer. Bull.*, Vol. 89, 1220-1230.
- Smewing, J.D. 1981. Mixing characteristics and compositional differences in mantle-derived melts beneath spreading axes: Evidence from cyclically layered rocks in the ophiolite of North Oman. *J. of Geophys. Res.*, Vol. 86, 2645-2659.

- Smewing, J.D., Christensen, N.I., Bartholomew, I.D. and Browning, P. 1984. The structure of the oceanic upper mantle and lower crust as deduced from the northern section of the Oman ophiolite. In: I.G. Gass, S.J. Lippard and A.W. Shelton (eds.), *Ophiolites and Oceanic Lithosphere*. Blackwell, Oxford, 41-53.
- Spray, J.G. and Roddick, J.C. 1981. Evidence for Upper Cretaceous transform fault metamorphism in West Cyprus. *Earth Plan. Sci. Let.*, Vol. 55, 273-291.
- Stephen, R., Sparks, J. and Huppert, H.E. 1984. Density Changes during the fractional crystallization of basaltic magmas: Fluid dynamic implications. *Contrib. Mineral Petrol.*, Vol. 85, 300-309.
- Swarbrick, R.E. 1979. The Mamonia complex of S.W. Cyprus: a Mesozoic continental margin and its relationship to the Troodos complex. In: A. Panayiotou (ed.), *Ophiolites*. Proc. Int. Ophiolite Symp., Cyprus, 1979 Geol. Surv. Dept., Nicosia, 86-92.
- Swarbrick, R.E. and Robertson, H.F. 1980. Revised stratigraphy of the Mesozoic rocks of southern Cyprus. *Geol. Mag.*, Vol. 117 (6), 547-563.
- Talkington, R. and Malpas, J. 1980. Spinel phases of the White Hills peridotite, St. Anthony Complex, Newfoundland: Part 1 Occurrence and Chemistry. In: A. Panayiotou (ed.), *Ophiolites*. Proc. Int. Ophiolite Symp., Cyprus, 1979 Geol. Surv. Dept., Nicosia, 607-619.
- Taylor, R.N. and Nesbitt, R.W. 1988. Light rare-earth enrichment of supra subduction-zone mantle: Evidence from the Troodos ophiolite, Cyprus. *Geology*, Vol. 16, 448-451.
- Thayer, T.P. 1980. Syncrystallization and subsolidus deformation in ophiolitic peridotite and gabbro. *Amer. J. Sci.*, Vol. 280, 269-283.
- Thy, P. 1984. On the nature of the Troodos boninites, Cyprus. *Ophiolite*, Vol. 9, 555-568.
- Thy, P. 1987a. Magmas and magma chamber evolution, Troodos Ophiolite, Cyprus. *Geology*, Vol. 15, 316-319.
- Thy, P. 1987b. Petrogenetic implications of mineral crystallization trends of Troodos cumulates, Cyprus. *Geol. Magazine*. Vol. 124, No. 1., 1-11.
- Thy, P. and Moores, E.M. 1988. Crustal accretion and tectonic setting of the Troodos Ophiolite, Cyprus. *Tectonophysics*, Vol. 147, 221-245.
- Thy, P., Schiffman, P. and Moores, E.M. 1989. Igneous mineral stratigraphy and chemistry of the Cyprus Crustal Study Project Drill Core in the Plutonic Sequences of the Troodos Ophiolite. In: I.L. Gibson, J. Malpas, P.T. Robinson and C. Xenophontos (eds.), *Cyprus Crustal Study Project: Initial Report, Hole CY-4*, Geol. Surv. of Canada, Paper 88-9, 147-180.
- Tilton, G.R., Hopson, C.A., and Wright, J.G., 1981, Uranium-Lead isotopic ages of the Samail ophiolite with applications to Tethyan ocean ridge tectonics. *J. of Geophys. Res.*, Vol. 86, 165-178.

- Varga, R.J. and Moores, E.M. 1985. Spreading structure of the Troodos Ophiolite, Cyprus. *Geology*, Vol. 13, 846-850.
- Whitechurch, H., Juteau, T. and Montigny, R. 1984. Role of the Eastern Mediterranean ophiolites (Turkey, Syria, Cyprus) in the history of the Neo-Tethys. In: J.E. Dixon and A.H.F. Robertson (eds.), *The geological evolution of the eastern Mediterranean: Geol. Soc. Lond. Special Publ. 17*, 301-317.
- Wilson, R.A.M. 1959. *The Geology of the Xeros-Troodos Area*. Ministry of Agriculture and Natural Resources, Geol. Surv. Dept, Cyprus. 184 pp
- Woodcock, N.H. and Robertson, A.H.F. 1980. The structural variety in Tethyan ophiolite terrains. In: J.E. Dixon and A.H.F. Robertson (eds.), *The geological evolution of the eastern Mediterranean: Geol. Soc. Lond. Special Publ. 17*, 321-330.

# APPENDIX A

## Tables of Analyses

TABLE A1

## Olivine Phase Chemistry of Chrome-Dunites

Sample Number	Rock type	MgO	Al <sub>2</sub> O <sub>3</sub>	SiO <sub>2</sub>	CaO	TiO <sub>2</sub>	Cr <sub>2</sub> O <sub>3</sub>	MnO	FeO	NiO	Total	Fo mole %
		(weight %)										
CA 332	chrome dunite	50.60	0.02	41.71	0.09	0.01	0.02	0.11	7.84	0.30	100.70	92.00
CA 295	chrome dunite	50.45	0.00	41.16	0.05	0.02	0.00	0.13	8.60	0.31	100.19	91.75
CA 185	chrome dunite	50.27	0.00	41.05	0.09	0.01	0.00	0.11	7.51	0.31	100.35	91.37
CA 267	chrome dunite	49.84	0.00	41.60	0.34	0.00	0.02	0.20	8.41	0.16	100.57	91.41
CA 241B	chrome dunite	50.20	0.00	41.18	0.04	0.03	0.02	0.12	8.37	0.30	100.27	91.49

TABLE A2

## 2a) Olivine Phase Chemistry of Banded Orthopyroxenite-Dunite

Sample Number	Rock type	MgO	Al <sub>2</sub> O <sub>3</sub>	SiO <sub>2</sub>	CaO	TiO <sub>2</sub>	Cr <sub>2</sub> O <sub>3</sub>	MnO	FeO	NiO	Total	Fo mole %
		(weight %)										
CA 308	dun/orthopy.	47.38	0.00	40.39	0.05	0.01	0.02	0.18	11.97	0.30	100.31	87.61
CA 308B	dunite layer	47.32	0.00	40.29	0.06	0.00	0.00	0.13	11.98	0.24	100.03	87.56
CA 180	dun/ol. web.	47.58	0.02	40.03	0.07	0.02	0.00	0.19	11.55	0.27	99.73	88.04
CA 180C	dun/orthopy.	48.13	0.02	39.26	0.06	0.00	0.04	0.24	11.77	0.30	99.75	87.94
CA S2	dunite	49.45	0.00	40.70	0.07	0.03	0.01	0.15	9.56	0.22	100.20	90.24
CA S3	cpx. dunite	49.14	0.02	40.82	0.02	0.01	0.02	0.11	9.52	0.26	99.91	90.24
CA S5	dunite	49.64	0.00	40.58	0.04	0.02	0.03	0.13	9.79	0.22	100.45	90.03

## 2b) Orthopyroxene phase chemistry of banded orthopyroxenite-dunite

Sample Number	Rock type	MgO	Al <sub>2</sub> O <sub>3</sub>	SiO <sub>2</sub>	CaO	TiO <sub>2</sub>	Cr <sub>2</sub> O <sub>3</sub>	MnO	FeO	NiO	Total	Mg# mole %
		(weight %)										
CA 180	dunite/ol. web.	32.23	1.66	55.37	1.44	0.05	0.61	0.23	7.64	0.05	99.28	88.28
CA 180C	dun/orthopy.	32.26	1.68	55.51	1.49	0.02	0.54	0.17	7.66	0.06	99.33	88.28
CA 308B	dun/orthopy.	32.84	1.13	56.67	1.23	0.05	0.38	0.16	7.70	0.05	100.21	88.44

Individual listings represent an average of 2 to 4 analysis

$$Fo = (100 \times Mg)/(Mg + Fe)$$

$$Mg\# = (100 \times Mg)/(Mg + Fe)$$

TABLE A 3

## Olivine Phase Chemistry of Layered Section

Sample Number	Distance (meters)	Rock Type	MgO	Al <sub>2</sub> O <sub>3</sub>	SiO <sub>2</sub>	CaO	TiO <sub>2</sub>	Cr <sub>2</sub> O <sub>3</sub>	MnO	FeO	NiO	Total	Fo
			(weight %)										mole %
CA-T1	0.00	dunite	50.48	0.02	40.88	0.15	0.01	0.03	0.17	7.97	0.18	99.89	91.88
CA-T3	25.00	dunite	50.86	0.02	40.90	0.07	0.01	0.03	0.12	7.50	0.29	99.80	92.39
CA-T8	55.00	dunite	49.47	0.02	41.30	0.13	0.01	0.02	0.16	9.16	0.31	100.58	90.65
CA-T9	60.00	wehrlite	48.91	0.00	41.45	0.08	0.00	0.02	0.16	9.52	0.29	100.43	90.20
CA-T10	65.00	wehrlite	48.89	0.04	41.23	0.14	0.03	0.02	0.13	9.30	0.26	100.04	90.40
CA-T12	80.00	wehrlite	48.77	0.00	41.61	0.11	0.01	0.05	0.17	9.50	0.28	100.50	90.17
CA-T13	85.00	wehrlite	48.63	0.00	41.28	0.06	0.00	0.09	0.14	9.63	0.19	100.02	90.04
CA-T14	90.00	dunite	48.25	0.00	41.55	0.06	0.00	0.01	0.32	9.74	0.31	100.24	89.87
CA-T15	95.00	dunite	48.42	0.00	40.44	0.10	0.00	0.04	0.15	10.91	0.25	100.31	88.79
CA-T16	100.00	dunite	47.95	0.00	40.82	0.10	0.00	0.05	0.22	9.95	0.12	99.21	89.58
CA-T17	105.00	ol. webst.	47.32	0.04	41.41	0.08	0.00	0.03	0.18	10.36	0.18	99.60	89.07
CA-T18	105.00	clinopy.	47.85	0.02	40.34	0.12	0.03	0.08	0.18	10.80	0.16	99.58	88.78
CA-T19	110.00	ol. webst.	47.53	0.02	39.88	0.12	0.00	0.04	0.18	11.91	0.25	99.93	87.67
CA-T20	115.00	ol. clinopy.	44.59	0.00	40.25	0.12	0.01	0.02	0.19	14.64	0.12	99.94	84.47
CA-T22	120.00	ol. clinopy.	46.84	0.00	40.37	0.09	0.02	0.00	0.17	12.53	0.18	100.20	86.97
CA-T22	120.00	ol in opx	47.93	0.02	41.00	0.07	0.00	0.03	0.14	10.54	0.19	99.92	89.05
CA-T23	125.00	clinopy.	43.89	0.00	39.99	0.16	0.00	0.08	0.26	15.93	0.19	100.50	83.13
CA-T24	130.00	wehrlite	48.27	0.02	40.76	0.12	0.00	0.01	0.14	10.59	0.18	100.09	89.07
CA-T25	135.00	ol. orthopy.	47.38	0.02	39.38	0.12	0.02	0.01	0.17	11.93	0.22	99.25	87.65
CA-T25.1	135.05	ol. webst.	47.39	0.00	40.03	0.09	0.00	0.01	0.17	12.29	0.14	100.12	87.33
CA-T26	140.00	dun/orthopy.	47.33	0.00	40.50	0.09	0.00	0.04	0.17	11.74	0.22	100.09	87.81
CA-T27	145.00	clinopy.	45.74	0.15	40.18	0.48	0.04	0.09	0.19	13.07	0.15	100.09	86.17
CA-T28.1	151.00	orthopy.	47.49	0.03	40.23	0.11	0.06	0.08	0.14	11.65	0.24	100.03	87.94
CA-T28.2	151.25	ol. clinopy.	46.57	0.03	40.04	0.12	0.06	0.08	0.21	12.42	0.22	99.75	87.00
CA-T28.3	151.50	wehrlite	45.85	0.04	40.76	0.11	0.06	0.10	0.21	12.66	0.21	100.00	86.61
CA-T28.4	151.80	wehrlite	46.48	0.03	40.72	0.12	0.07	0.09	0.20	12.29	0.14	100.14	87.09
CA-T28.5	152.10	ol. clinopy.	47.46	0.02	39.29	0.12	0.00	0.01	0.18	11.96	0.19	99.23	87.62
CA-T28.6	152.50	ol. clinopy.	46.62	0.02	40.24	0.14	0.07	0.09	0.19	12.43	0.19	99.99	86.98
CA-T29.1	165.00	herzolite	47.48	0.06	40.05	0.18	0.07	0.07	0.22	11.93	0.18	100.24	87.67
CA-T30	175.00	wehrlite	46.09	0.00	40.20	0.12	0.02	0.01	0.19	13.53	0.24	100.40	85.87
CA-T31	180.00	wehrlite	46.65	0.01	40.12	0.07	0.02	0.03	0.16	12.19	0.26	99.51	87.21
CA-T33	200.00	ol. gabnorite	43.83	0.02	39.44	0.11	0.00	0.02	0.23	15.35	0.22	99.22	83.57
CA-T34	210.00	ol. clinopy.	45.77	0.00	39.89	0.07	0.04	0.04	0.29	13.46	0.16	99.72	85.83
CA-T35	215.00	wehrlite	45.49	0.02	40.00	0.07	0.02	0.05	0.22	14.00	0.22	100.09	85.30
CA-T36	220.00	clinopy.	45.63	0.00	39.63	0.09	0.01	0.00	0.22	13.89	0.28	99.75	85.43
CA-T37.1	225.00	wehrlite	44.48	0.01	39.42	0.14	0.05	0.04	0.27	15.36	0.31	100.08	83.75
CA-T37.2	225.50	wehrlite	45.25	0.01	39.80	0.13	0.03	0.02	0.20	14.89	0.23	100.56	84.41
CA-T37.4	226.50	herzolite	45.59	0.03	39.82	0.10	0.00	0.00	0.27	14.40	0.26	100.47	84.97
CA-T38	230.00	wehrlite	45.74	0.03	40.02	0.09	0.02	0.02	0.23	13.55	0.26	99.96	85.74
CA-T39	235.00	wehrlite	45.09	0.00	39.57	0.14	0.02	0.04	0.25	14.82	0.22	100.15	84.43
CA-T40.1	240.00	webst./dun.	45.80	0.00	39.89	0.15	0.03	0.00	0.21	14.11	0.26	100.45	85.27
CA-T40.2	240.50	webst.	45.46	0.03	39.77	0.12	0.04	0.01	0.25	14.80	0.24	100.72	84.54

Individual listing represent an average of 2 to 4 analysis

$$Fo = (Mg \times 100)/(Mg + Fe)$$

TABLE A 3 (con't)

## Olivine Phase Chemistry of Layered Section

Sample Number	Distance (meters)	Rock Type	MgO	Al <sub>2</sub> O <sub>3</sub>	SiO <sub>2</sub>	CaO	TiO <sub>2</sub>	Cr <sub>2</sub> O <sub>3</sub>	MnO	FeO	NiO	Total	Fo
			(weight %)										mole %
CA-T41	250.00	ol. clinopy.	44.68	0.03	39.33	0.16	0.03	0.04	0.27	15.49	0.30	100.33	83.71
CA-T42	260.00	ol. gabnor.	44.46	0.02	39.67	0.17	0.10	0.02	0.22	15.36	0.24	100.26	83.76
CA-T44	270.00	wehrlite	44.12	0.03	39.68	0.13	0.00	0.00	0.29	16.02	0.30	100.57	83.10
CA-T45	275.00	wehrlite	45.11	0.04	39.19	0.13	0.06	0.05	0.29	14.68	0.26	99.81	84.57
CA-T47	285.00	wehrlite	45.03	0.02	39.44	0.15	0.03	0.04	0.28	15.32	0.26	100.57	83.97
CA-T48.1	288.00	wehrlite	46.04	0.03	39.84	0.12	0.03	0.00	0.29	14.00	0.26	100.81	85.41
CA-T48.2	289.00	wehrlite	47.69	0.04	40.42	0.12	0.06	0.03	0.22	12.19	0.26	101.03	87.47
CA-T48.3	298.00	wehrlite	45.95	0.02	39.52	0.15	0.01	0.04	0.28	13.61	0.32	99.90	85.75
CA-T48.4	290.50	wehrlite	47.22	0.03	40.15	0.12	0.00	0.03	0.25	12.62	0.29	100.71	86.95
CA-T48.5	291.00	clinopy.	46.10	0.02	39.76	0.14	0.03	0.03	0.26	13.55	0.31	100.20	85.83
CA-T49.1	300.00	wehrlite	46.97	0.03	40.22	0.15	0.04	0.01	0.25	12.89	0.33	100.89	86.67
CA-T49.2	300.50	clinopy.	45.83	0.06	39.68	0.15	0.02	0.03	0.29	14.21	0.32	100.59	85.20
CA-T53	330.00	gabnor.	44.54	0.00	39.19	0.09	0.00	0.01	0.23	15.80	0.19	100.05	83.42
CA-T54	340.00	web/ol. clpy	45.02	0.02	39.41	0.10	0.02	0.00	0.18	14.40	0.19	99.34	84.82
CA-T55	345.00	wehrlite	45.88	0.00	39.86	0.06	0.01	0.00	0.18	14.43	0.18	100.60	85.03
CA-T56	350.00	wehrlite	46.53	0.00	39.82	0.07	0.01	0.02	0.21	13.98	0.14	100.78	85.59
CA-T57	355.00	wehrlite	46.68	0.02	39.87	0.09	0.01	0.01	0.21	13.13	0.19	100.21	86.41
CA-T58	360.00	clinopy.	45.05	0.00	39.83	0.11	0.01	0.01	0.19	14.25	0.24	99.69	85.25
CA-T59	365.00	wehrlite	45.88	0.02	39.91	0.13	0.02	0.02	0.21	13.64	0.21	100.04	85.75
CA-T60	380.00	wehrlite	44.26	0.00	39.51	0.12	0.02	0.02	0.23	15.26	0.17	99.59	83.78
CA-T62	405.00	wehrlite	45.24	0.02	39.77	0.20	0.01	0.00	0.17	13.91	0.21	99.53	85.30
CA-T63	410.00	wehrlite	45.39	0.00	39.81	0.09	0.02	0.02	0.19	14.20	0.16	99.88	85.11
CA-T66	430.00	ol. gabnor.	46.13	0.00	39.50	0.11	0.01	0.01	0.19	14.33	0.18	100.46	85.17
CA-T67	435.00	ol. gabbro	43.78	0.00	39.38	0.13	0.02	0.00	0.24	15.91	0.20	99.66	83.07
CA-T69	445.00	ol. gabbro	46.08	0.00	40.38	0.09	0.00	0.02	0.15	13.47	0.18	100.37	85.94

Individual listing represent an average of 2 to 4 analysis

$$Fo = (Mg \times 100) / (Mg + Fe)$$

TABLE A4

## Clinopyroxene Probe Data of Layered Section

Sample#	Distance (meters)	Rock Type	(weight %)											Total	Mg# mole %
			NaO	MgO	Al <sub>2</sub> O <sub>3</sub>	SiO <sub>2</sub>	CaO	TiO <sub>2</sub>	Cr <sub>2</sub> O <sub>3</sub>	MnO	FeO	NiO			
CA-T3	25.00	dunite	0.05	18.24	0.98	54.66	24.16	0.05	0.48	0.06	1.59	0.05	100.32	95.41	
CA-T5	35.00	dunite	0.07	18.88	2.64	53.21	22.26	0.20	0.79	0.11	2.36	0.01	100.53	93.44	
CA-T9	60.00	dunite	0.26	18.09	2.31	53.13	21.91	0.18	0.89	0.12	2.68	0.01	99.58	92.38	
CA-T12	80.00	wehrlite	0.04	18.02	2.73	52.77	21.71	0.14	0.80	0.07	3.24	0.08	99.60	90.90	
CA-T13	85.00	dunite	0.07	18.80	2.79	52.20	21.97	0.15	0.85	0.06	2.64	0.06	99.59	92.73	
CA-T17	105.00	websterite	0.12	18.87	1.70	53.81	21.29	0.05	0.62	0.07	3.23	0.05	99.81	91.23	
CA-T18	105.00	clinopyr.	0.13	18.12	1.06	54.24	21.58	0.09	0.59	0.10	3.26	0.00	99.17	90.82	
CA-T19	110.00	websterite	0.08	18.59	2.09	52.95	21.57	0.06	0.88	0.13	3.64	0.05	100.04	90.16	
CA-T20	115.00	ol. clinopy.	0.21	18.08	1.93	53.45	22.15	0.15	0.48	0.12	3.71	0.04	100.32	89.72	
CA-T21	120.00	gabbro	0.20	17.00	1.79	53.39	22.39	0.22	0.21	0.18	5.01	0.00	100.39	85.81	
CA-T22	120.00	ol. clinopy.	0.23	17.45	2.11	53.63	22.04	0.15	0.65	0.10	3.55	0.03	99.94	89.75	
CA-T23	125.00	clinopy.	0.26	17.89	1.75	54.33	20.81	0.11	0.42	0.10	4.19	0.05	99.91	88.39	
CA-T24	130.00	wehrlite	0.08	18.66	1.84	54.10	21.99	0.07	0.49	0.07	3.06	0.01	100.37	91.60	
CA-T25	135.00	ol. orthopy.	0.06	19.03	2.47	53.53	20.75	0.08	0.83	0.13	3.86	0.03	100.80	89.80	
CA-T25.1	135.05	ol. webst.	0.13	18.27	2.21	53.02	22.20	0.11	0.75	0.09	3.25	0.01	100.04	91.00	
CA-T26	140.00	dun/orthopy	0.16	18.48	2.46	52.86	21.38	0.07	0.95	0.12	3.80	0.04	100.32	89.69	
CA-T27	145.00	clinopy.	0.32	17.50	2.83	53.32	20.48	0.12	0.87	0.14	5.53	0.00	101.11	89.90	
CA-T28.1	151.00	orthopy.	0.18	16.88	2.88	53.93	20.88	0.16	0.85	0.16	3.24	0.10	99.06	90.34	
CA-T28.2	151.25	ol. clinopy.	0.26	17.64	2.40	53.65	21.03	0.14	0.87	0.12	3.86	0.00	99.97	89.09	
CA-T28.3	151.50	wehrlite	0.27	17.22	2.48	53.62	21.41	0.14	0.84	0.17	3.75	0.03	99.93	89.13	
CA-T28.4	151.80	wehrlite	0.19	17.29	2.51	52.84	22.30	0.13	0.95	0.12	3.58	0.00	99.91	89.62	
CA-T28.5	152.10	ol. clinopy.	0.14	18.55	2.18	52.84	21.63	0.08	0.69	0.13	3.76	0.08	100.08	89.82	
CA-T28.6	152.50	ol. clinopy.	0.28	17.01	2.25	53.66	22.57	0.15	0.78	0.19	3.33	0.01	100.23	90.11	
CA-T29.1	165.00	herzolite	0.26	17.21	2.58	53.92	22.03	0.19	0.76	0.18	3.52	0.10	100.75	89.71	
CA-T31	180.00	wehrlite	0.15	17.39	2.58	53.28	22.10	0.16	0.84	0.00	3.75	0.00	100.25	89.27	
CA-T32.1	187.00	clinopy.	0.09	17.05	2.09	53.09	22.65	0.14	0.22	0.10	3.80	0.10	99.33	88.93	
CA-T32.2	188.00	clinopy.	0.03	17.11	1.81	53.48	23.27	0.14	0.18	0.13	3.89	0.10	100.14	88.66	
CA-T32.3	188.00	gabbro	0.13	17.22	2.09	53.17	21.91	0.12	0.50	0.15	4.41	0.09	99.79	87.50	
CA-T32.4	190.00	gabbro	0.13	16.46	2.42	53.56	22.91	0.15	0.23	0.10	3.87	0.05	99.88	88.35	
CA-T33	200.00	ol. gabnor.	0.09	18.66	1.96	53.06	21.69	0.12	0.40	0.16	3.99	0.00	100.13	89.32	
CA-T34	210.00	ol. clinopy.	0.08	17.78	2.25	52.38	22.29	0.12	0.57	0.12	4.05	0.07	99.69	88.68	
CA-T35	215.00	wehrlite	0.23	17.15	2.14	52.83	22.36	0.18	0.56	0.11	3.88	0.10	99.54	88.73	
CA-T36	220.00	clinopy.	0.09	18.29	1.86	53.58	22.26	0.04	0.32	0.18	4.03	0.07	100.72	88.97	
CA-T37.1	225.00	wehrlite	0.15	17.26	2.57	52.21	23.16	0.11	0.78	0.10	3.70	0.08	100.12	89.28	
CA-T37.2	225.50	wehrlite	0.13	18.80	2.31	52.66	21.40	0.09	0.74	0.14	3.72	0.08	100.07	89.66	
CA-T37.3	226.00	webst.	0.10	16.64	2.74	51.92	23.03	0.07	0.72	0.15	3.70	0.08	99.15	88.92	
CA-T37.4	226.50	herzolite	0.08	18.69	1.74	53.73	20.08	0.08	0.89	0.10	3.66	0.13	99.18	89.99	
CA-T38	230.00	wehrlite	0.05	17.34	1.36	53.79	23.08	0.06	0.62	0.14	3.10	0.15	99.69	90.94	
CA-T39	235.00	wehrlite	0.15	18.40	2.61	52.97	20.49	0.16	0.78	0.19	4.22	0.08	100.05	88.62	

Individual listings represent an average of 2 to 4 analysis.

$$\text{Mg\#} = (100 \times \text{Mg}) / (\text{Mg} + \text{Fe})$$

TABLE A4 (cont.)

## Clinopyroxene Probe Data from the Layered Section

Sample#	Distance (meters)	Rock Type	NaO	MgO	Al <sub>2</sub> O <sub>3</sub>	SiO <sub>2</sub>	CaO	TiO <sub>2</sub>	Cr <sub>2</sub> O <sub>3</sub>	MnO	FeO	NiO	Total	Mg#
			(weight %)											mole %
CA-T40.1	240.00	webst/dun.	0.16	18.48	2.45	52.94	20.31	0.07	0.80	0.18	4.18	0.09	99.64	88.78
CA-T40.2	240.50	webst.	0.07	16.74	2.97	52.31	22.49	0.08	0.88	0.20	4.18	0.12	100.04	87.70
CA-T42	260.00	ol. gabnor.	0.08	18.11	2.44	52.72	21.44	0.09	0.49	0.13	3.82	0.15	99.47	89.49
CA-T43	265.00	clinopy.	0.15	17.78	2.20	52.85	22.07	0.14	0.51	0.18	4.60	0.16	100.64	87.34
CA-T44	270.00	wehrlite	0.11	16.98	2.43	52.89	22.94	0.12	0.57	0.18	4.12	0.12	100.48	88.06
CA-T45	275.00	wehrlite	0.13	18.25	1.94	52.22	22.27	0.10	0.85	0.20	3.49	0.00	99.45	90.33
CA-T47	285.00	wehrlite	0.06	18.74	2.50	52.56	20.81	0.09	0.77	0.17	4.15	0.15	100.00	88.91
CA-T48.1	288.00	wehrlite	0.13	17.19	1.44	53.77	23.02	0.10	0.85	0.18	3.39	0.13	100.20	90.07
CA-T48.2	289.00	wehrlite	0.10	18.23	1.95	53.44	21.74	0.08	0.80	0.17	3.38	0.11	100.00	90.58
CA-T48.3	290.00	wehrlite	0.34	17.30	2.30	53.04	22.00	0.26	0.63	0.22	3.95	0.16	100.20	88.68
CA-T48.4	290.50	wehrlite	0.15	18.19	2.36	52.93	21.34	0.13	0.75	0.19	3.82	0.14	100.00	89.49
CA-T48.5	291.00	clinopy.	0.18	17.65	2.36	53.04	21.80	0.16	0.62	0.23	4.01	0.13	100.18	88.70
CA-T48.6	292.00	wehrlite	0.20	18.00	2.43	52.85	22.05	0.20	0.68	0.20	3.95	0.15	100.71	89.02
CA-T49.1	300.00	wehrlite	0.12	18.02	2.44	53.23	21.72	0.23	0.52	0.18	4.02	0.13	100.81	88.86
CA-T49.2	300.50	clinopy.	0.18	17.67	2.30	52.13	21.56	0.22	0.57	0.18	4.32	0.21	99.34	87.94
CA-T50	315.00	clinopy.	0.20	17.52	2.46	52.69	21.82	0.18	0.49	0.21	4.37	0.13	100.07	87.68
CA-T51	320.00	clinopy.	0.22	18.04	2.06	52.86	21.73	0.11	0.49	0.15	4.03	0.12	99.81	88.39
CA-T52	325.00	clinopy.	0.13	18.22	2.53	52.67	21.36	0.13	0.56	0.21	4.07	0.15	100.03	68.87
CA-T53	330.00	gabnor.	0.06	17.27	2.25	53.29	22.60	0.10	0.33	0.12	4.26	0.01	100.29	87.90
CA-T54	340.00	wehr/ol.cipy	0.26	17.43	2.04	53.46	21.83	0.17	0.52	0.16	3.99	0.05	99.91	88.66
CA-T55	345.00	wehrlite	0.07	17.83	1.93	53.87	21.81	0.15	0.68	0.10	4.13	0.04	100.61	88.56
CA-T56	350.00	wehrlite	0.12	18.12	2.38	52.72	21.04	0.07	0.91	0.20	4.10	0.02	99.68	88.84
CA-T57	355.00	wehrlite	0.12	18.01	2.37	53.05	21.95	0.09	0.87	0.10	3.27	0.02	99.85	90.80
CA-T58	360.00	clinopy.	0.18	17.51	2.55	53.41	21.80	0.17	0.73	0.13	3.83	0.03	100.34	89.08
CA-T59	365.00	wehrlite	0.08	18.22	2.16	53.20	21.00	0.11	0.77	0.09	3.75	0.06	99.44	89.77
CA-T60	380.00	wehrlite	0.07	18.38	1.98	53.68	21.32	0.10	0.44	0.12	4.27	0.02	100.38	88.57
CA-T61	400.00	ol. clinopy.	0.23	17.87	1.99	53.44	21.86	0.14	0.50	0.10	3.98	0.01	100.12	88.97
CA-T62	405.00	wehrlite	0.17	17.87	1.96	53.42	21.63	0.22	0.57	0.05	4.19	0.05	100.13	88.40
CA-T64	415.00	gabnor.	0.05	18.20	1.77	53.48	22.31	0.09	0.35	0.11	3.74	0.02	100.12	89.72
CA-T65	420.00	gabbro	0.18	17.46	1.80	53.73	21.62	0.18	0.18	0.12	4.95	0.05	100.27	86.33
CA-T66	430.00	ol. gabnor.	0.21	17.85	1.85	53.37	21.74	0.15	0.39	0.12	4.40	0.04	100.12	87.92
CA-T67	435.00	ol. gabbro	0.05	18.16	2.05	53.99	21.09	0.09	0.38	0.15	4.16	0.01	100.13	88.70
CA-T68	440.00	gabbro	0.05	18.85	2.30	53.66	20.50	0.07	0.48	0.12	3.94	0.01	99.98	89.52
CA-T69	445.00	ol. gabbro	0.08	18.76	1.98	53.40	20.63	0.08	0.47	0.15	4.46	0.00	100.01	88.28
CA-T70	460.00	clinopy	0.11	17.70	2.04	54.09	21.98	0.09	0.51	0.13	4.00	0.04	100.69	88.82

Individual listings represent an average of 2 to 4 analysis.

Mg # = (100\*Mg)/(Mg + Fe)

TABLE A 5

## Orthopyroxene Phase Chemistry Data of Layered Section

Sample #	Distance (meters)	Rock Type	(weight %)										Total	Mg# mole %
			MgO	Al <sub>2</sub> O <sub>3</sub>	SiO <sub>2</sub>	CaO	TiO <sub>2</sub>	Cr <sub>2</sub> O <sub>3</sub>	MnO	FeO	NiO			
CA-T10	65.00	wehrlite	32.85	1.55	56.70	1.84	0.05	0.55	0.14	5.97	0.09	99.74	90.78	
CA-T17	105.00	ol. webst.	32.21	1.14	56.64	2.16	0.03	0.36	0.14	6.44	0.06	99.18	89.92	
CA-T19	110.00	ol. webst.	31.90	1.70	56.78	1.89	0.02	0.47	0.18	7.16	0.07	100.17	88.79	
CA-T20	115.00	ol. clinopy.	31.34	1.44	55.39	1.52	0.08	0.28	0.21	9.10	0.04	99.40	86.01	
CA-T23	125.00	clinopy.	30.27	1.14	55.13	1.70	0.10	0.19	0.27	10.02	0.00	98.82	84.42	
CA-T24	130.00	wehrlite	33.27	1.38	57.07	2.00	0.05	0.30	0.13	6.45	0.04	100.69	90.26	
CA-T25	135.00	ol. orthopy.	32.02	1.65	55.86	1.53	0.05	0.44	0.20	7.73	0.07	99.55	88.08	
CA-T25.1	135.05	ol. webst.	31.98	1.50	55.49	1.88	0.06	0.37	0.18	7.43	0.08	99.97	88.57	
CA-T26	140.00	dun/orthopy	32.38	1.80	56.17	1.14	0.10	0.47	0.21	7.44	0.07	99.78	88.71	
CA-T28.1	151.00	orthopy	32.26	1.87	56.75	1.30	0.09	0.57	0.13	7.20	0.00	100.17	88.89	
CA-T28.3	151.50	wehrlite	31.70	1.49	56.73	1.23	0.11	0.40	0.15	7.78	0.03	99.62	87.94	
CA-T28.6	152.50	ol. clinopy	31.81	1.85	56.19	1.64	0.12	0.51	0.20	7.82	0.00	100.14	87.86	
CA-T29.1	165.00	herzolite	31.93	1.78	56.22	1.93	0.01	0.63	0.13	7.04	0.00	99.67	88.96	
CA-T30	175.00	wehrlite	31.81	1.78	56.69	1.27	0.06	0.37	0.18	8.31	0.00	100.47	87.31	
CA-T31	180.00	wehrlite	32.08	1.82	56.19	1.62	0.07	0.45	0.21	7.75	0.00	100.19	88.47	
CA-T33	200.00	ol. gabnor.	31.84	1.52	56.23	1.59	0.07	0.07	0.23	7.95	0.07	99.57	87.74	
CA-T36	220.00	clinopy.	31.45	1.68	55.69	1.83	0.04	0.30	0.26	8.18	0.09	99.52	87.29	
CA-T37.1	225.00	wehrlite	31.10	1.70	55.53	1.45	0.11	0.27	0.21	9.40	0.09	99.86	85.52	
CA-T37.3	226.00	webst.	31.56	1.83	55.29	1.58	0.08	0.39	0.24	8.61	0.12	99.70	86.69	
CA-T37.4	226.50	herzolite	31.02	1.56	55.60	1.50	0.09	0.32	0.27	9.04	0.06	99.46	85.97	
CA-T38	230.00	wehrlite	31.20	1.35	55.78	2.04	0.08	0.21	0.23	8.91	0.17	99.97	86.18	
CA-T40.1	240.00	webst./dun	31.60	1.56	56.02	1.84	0.06	0.23	0.22	8.52	0.00	100.05	86.83	
CA-T40.2	240.50	webst.	31.57	1.53	55.99	1.75	0.04	0.44	0.32	8.02	0.15	99.81	87.57	
CA-T48.1	288.00	wehrlite	31.44	1.72	56.03	1.59	0.09	0.35	0.24	8.49	0.11	100.06	86.85	
CA-T49.2	300.50	clinopy.	32.82	1.51	55.44	1.08	0.07	0.28	0.28	8.18	0.19	99.85	87.72	
CA-T54	340.00	web/ol. cpx	31.38	1.45	55.41	1.25	0.06	0.25	0.19	8.93	0.03	98.95	86.25	
CA-T55	345.00	wehrlite	31.46	1.52	55.72	1.77	0.06	0.30	0.19	8.73	0.02	99.77	86.63	
CA-T66	430.00	ol. gabnor	31.59	1.22	56.95	1.85	0.05	0.17	0.17	8.00	0.04	100.04	87.65	

Individual listing represent 2-4 analysis.

$$\text{Mg\#} = (\text{Mg} \times 100) / (\text{Mg} + \text{Fe})$$

TABLE A6

## Plagioclase Phase Chemistry of Layered Section

Sample Number	Rock Type	Distance (meters)	(weight %)										
			Na <sub>2</sub> O	MgO	Al <sub>2</sub> O <sub>3</sub>	SiO <sub>2</sub>	K <sub>2</sub> O	CaO	TiO <sub>2</sub>	Cr <sub>2</sub> O	FeO	Total	An
CA-T21	gabbro	120.00	1.21	0.06	34.75	45.94	0.03	18.10	0.03	0.05	0.52	99.50	93.73
CA-T32.2	clinopy.	188.00	0.70	0.03	36.17	44.45	0.00	18.89	0.00	0.00	0.33	99.87	96.43
CA-T33	ol. gabnor	200.00	0.85	0.00	35.56	44.06	0.00	18.72	0.00	0.00	0.46	98.80	95.66
CA-T40.2	webster	240.50	2.00	0.02	34.12	47.01	0.00	16.98	0.03	0.00	0.38	98.54	89.46
CA-T42	ol. gabnor	260.00	0.74	0.00	36.29	44.57	0.00	18.64	0.03	0.00	0.40	99.93	96.18
CA-T49.2	clinopy	300.50	0.91	0.00	36.00	45.25	0.00	18.07	0.04	0.03	0.44	99.83	95.21

TABLE A7

## Chrome-Spinel Phase Chemistry from the Basal Dunite of Layered Section

Sample #	Distance (meters)	ROCK TYPE	MgO	Al <sub>2</sub> O <sub>3</sub>	TiO <sub>2</sub>	Cr <sub>2</sub> O <sub>3</sub>	MnO	FeO	Total	Cr#	Mg#
			(weight %)							(mole %)	
CA-T1	0.50	dunite I	11.92	12.31	0.18	56.52	0.24	19.23	100.40	78.09	51.06
	0.50	dunite I	11.08	11.69	0.16	56.70	0.24	20.21	100.08	76.52	49.45
CA-T2	10.00	dunite I	11.53	11.59	0.15	58.32	0.30	17.82	99.71	76.83	50.63
	10.00	dunite I	12.07	12.36	0.16	56.92	0.28	18.70	100.49	75.57	53.54
CA-T3	25.00	dunite C	14.09	13.80	0.23	54.55	0.23	17.24	100.14	72.62	59.36
	25.00	R	14.24	15.46	0.22	52.74	0.22	17.48	100.36	69.58	59.22
CA-T4	30.00	dunite I	12.75	15.54	0.17	52.06	0.21	19.63	100.36	69.23	56.11
CA-T5	35.00	dunite I	14.14	16.63	0.27	50.70	0.23	17.89	99.86	67.14	58.44
CA-T6	40.00	dunite I	13.73	16.72	0.26	50.55	0.23	18.36	99.85	67.02	57.13
CA-T7	45.00	dunite I	13.87	16.16	0.26	52.14	0.23	17.15	99.81	68.50	58.53
	45.00	dunite I	13.93	17.59	0.23	50.47	0.23	17.59	100.04	66.79	58.51
CA-T8	55.00	dunite I	13.35	14.07	0.21	51.74	0.25	20.62	100.24	71.14	53.63
	55.00	dunite C	10.75	13.60	0.20	52.53	0.32	23.16	100.56	72.18	45.24
	55.00	R	11.98	17.70	0.50	46.51	0.29	23.63	100.61	63.81	47.46
	55.00	dunite C	12.61	14.60	0.16	51.91	0.25	20.70	100.23	70.46	52.02
CA-T9	60.00	wehrlite C	11.27	14.33	0.25	50.36	0.32	23.95	100.48	69.08	45.58
	60.00	R	10.96	15.83	0.84	45.86	0.26	26.69	100.44	66.05	42.22
CA-T10	65.00	wehrlite C	10.84	14.29	0.58	49.20	0.28	25.11	100.30	69.76	43.51
	65.00	R	11.20	17.16	0.88	43.31	0.25	27.02	99.82	62.89	42.29
CA-T11	65.00	wehrlite C	11.34	14.16	0.52	49.40	0.30	24.72	100.44	70.10	45.00
	65.00	R	11.25	17.30	0.88	43.54	0.30	26.19	99.46	62.85	43.34
	70.00	chromite	12.94	15.96	0.18	48.59	0.29	22.14	100.10	67.16	50.74
CA-T12	70.00	chromite	11.46	16.18	0.17	47.78	0.29	23.97	99.85	66.47	46.03
	70.00	chromite	13.52	17.66	0.61	45.85	0.27	21.80	99.71	63.54	52.53
	80.00	chromite	11.13	15.29	0.64	47.69	0.32	25.76	100.83	67.70	43.50
CA-T13	80.00	chrom. core	12.5	16.54	0.24	47.50	0.22	23.43	100.50	65.87	49.64
	80.00	rim	12.76	17.46	0.32	45.54	0.27	22.43	98.78	63.63	50.37
	80.00	chrom. core	12.45	18.02	0.34	45.49	0.29	23.00	99.59	62.86	49.09
	80.00	rim	13.32	19.96	0.30	44.20	0.29	22.20	100.27	59.79	53.28
	85.00	cpx dunite C	12.23	16.23	0.52	47.18	0.29	23.52	99.97	66.12	48.08
CA-T14	85.00	R	11.82	18.54	0.55	43.61	0.25	24.84	99.61	61.23	45.88
	85.00	cpx dunite C	13.71	17.04	0.36	47.77	0.29	20.87	100.04	65.29	53.98
	85.00	R	13.37	20.32	0.36	42.75	0.20	22.49	99.49	58.52	51.43
	90.00	cpx dunite C	11.36	16.34	0.71	45.32	0.31	25.79	99.83	65.07	43.98
CA-T15	95.00	R	11.72	19.34	0.65	41.07	0.27	25.83	98.88	58.75	44.72
	95.00	wehrlite C	11.47	15.07	0.39	48.00	0.30	25.05	100.28	68.11	44.93
CA-T16	95.00	R	11.86	16.43	0.46	46.34	0.29	25.02	100.40	65.42	45.80
	100.00	chrom. core	10.61	15.03	0.64	46.96	0.34	27.16	100.74	67.71	40.09
	100.00	rim	10.70	17.49	0.78	43.30	0.26	27.09	99.62	62.41	41.28
	100.00	chrom. core	11.75	14.82	0.33	48.34	0.21	24.79	100.24	68.66	45.75
	100.00	rim	10.88	17.89	0.47	43.07	0.29	27.60	100.20	61.76	41.27
100.00	rim	11.62	16.65	0.41	45.27	0.33	25.35	99.63	64.60	44.95	

Individual listings represent an average of at least two analysis.

Cr# =  $(100 \times \text{Cr}) / (\text{Cr} + \text{Al})$ , Mg# =  $(100 \times \text{Mg}) / (\text{Mg} + \text{Fe})$

C - Core, R - rim, I - small grain

TABLE A8

**Whole Rock Major Element Chemistry of Layered Section  
Oxide (weight %)**

Sample#	Dist. (m)	Rock Type	SiO <sub>2</sub>	Al <sub>2</sub> O <sub>3</sub>	Fe <sub>2</sub> O <sub>3</sub>	MnO	MgO	CaO	Na <sub>2</sub> O	K <sub>2</sub> O	P <sub>2</sub> O <sub>5</sub>	LOI	Total	Mg #
CA-T1	0.00	dunite	33.20	0.00	7.26	0.09	40.98	0.40	0.01	0.00	0.00	15.79	97.73	84.95
CA-T2	10.00	dunite	37.30	0.00	7.36	0.09	38.83	0.22	0.01	0.00	0.04	15.01	98.86	84.07
CA-T3	25.00	dunite	34.30	0.22	6.53	0.09	41.95	0.70	0.01	0.00	0.01	15.27	99.08	86.53
CA-T4	30.00	dunite	33.60	0.18	6.48	0.08	42.22	0.12	0.01	0.00	0.00	15.93	98.62	86.69
CA-T5	35.00	dunite	34.70	0.36	6.42	0.08	41.60	0.28	0.01	0.00	0.01	15.00	98.46	86.63
CA-T6	40.00	dunite	33.60	0.26	6.63	0.09	41.51	0.10	0.01	0.00	0.00	15.27	97.47	86.23
CA-T7	45.00	dunite	34.00	0.18	6.70	0.09	41.86	0.06	0.01	0.00	0.00	15.34	98.24	86.20
CA-T8	55.00	wehrlite	35.50	1.50	7.69	0.10	38.41	0.94	0.02	0.00	0.00	14.63	98.79	83.32
CA-T9	60.00	wehrlite	36.70	1.84	7.56	0.11	38.32	2.20	0.03	0.00	0.01	13.05	99.62	83.52
CA-T10	65.00	wehrlite	36.40	1.84	8.05	0.11	37.66	1.32	0.03	0.00	0.00	13.26	98.67	82.39
CA-T11	70.00	dunite	35.60	0.90	8.43	0.11	39.81	0.32	0.01	0.00	0.01	14.16	99.35	82.52
CA-T12	80.00	dunite	35.10	0.94	8.26	0.10	39.81	0.62	0.10	0.00	0.05	13.79	98.77	82.82
CA-T13	85.00	dunite	35.00	0.68	8.38	0.11	39.91	0.96	0.01	0.00	0.03	13.69	98.77	82.65
CA-T14	90.00	dunite	35.50	0.74	7.52	0.09	40.00	0.88	0.02	0.00	0.00	13.53	98.28	84.18
CA-T15	95.00	dunite	34.80	0.66	9.73	0.13	39.39	0.32	0.01	0.00	0.01	14.15	99.16	80.19
CA-T16	100.00	dunite	34.30	0.60	8.99	0.11	39.81	0.18	0.01	0.00	0.00	14.65	98.85	81.58
CA-T17	105.00	ol. webst.	52.10	1.50	6.23	0.14	28.78	7.32	0.10	0.01	0.01	2.35	98.60	82.21
CA-T18	106.00	clinopy.	51.50	1.68	4.67	0.10	22.03	17.06	0.11	0.01	0.01	2.51	99.74	82.51
CA-T19	110.00	ol. webst.	51.90	2.08	5.82	0.13	23.94	13.14	0.07	0.01	0.00	1.47	98.00	80.44
CA-T20	115.00	ol. clinopy.	48.60	2.28	7.21	0.13	23.83	14.06	0.13	0.01	0.00	3.45	99.80	76.77
CA-T21	120.00	gabbro	44.40	17.03	4.54	0.09	11.68	17.16	0.43	0.04	0.01	4.54	100.00	72.01
CA-T22	120.00	ol. clinopy.	47.90	2.14	5.95	0.11	24.00	13.88	0.10	0.01	0.00	4.74	98.93	80.13
CA-T23	125.00	clinopy.	50.70	2.08	6.27	0.12	21.80	17.12	0.15	0.01	0.00	1.36	99.75	77.66
CA-T24	130.00	wehrlite	44.80	1.54	6.29	0.11	28.87	10.64	0.06	0.01	0.00	6.09	98.45	82.11
CA-T25	135.00	ol. orthopy.	48.10	1.36	8.84	0.15	32.78	2.36	0.04	0.01	0.01	4.70	98.35	78.76
CA-T26	140.00	dun/orthopy	45.10	1.24	8.78	0.15	33.57	1.98	0.04	0.01	0.00	8.03	98.90	79.27
CA-T27	145.00	clinopy.	50.60	2.68	5.76	0.12	20.67	16.84	0.16	0.01	0.01	2.41	99.30	78.21
CA-T28.1	151.00	orthopy.	53.10	2.14	7.55	0.15	30.17	4.84	0.08	0.01	0.00	1.91	99.99	79.98
CA-T28.2	151.30	ol. clinopy.	50.60	2.12	5.46	0.12	22.02	16.66	0.12	0.00	0.01	2.29	99.44	80.13
CA-T28.3	151.60	wehrlite	43.70	2.48	8.84	0.14	31.25	7.70	0.07	0.01	0.00	5.56	99.75	77.95
CA-T28.4	151.90	wehrlite	46.10	2.64	7.49	0.13	27.18	11.08	0.10	0.01	0.01	4.99	99.77	78.40
CA-T28.5	152.20	ol. clinopy.	47.40	2.02	6.31	0.14	25.77	13.02	0.09	0.00	0.01	4.56	99.45	80.33
CA-T28.6	152.50	ol. clinopy.	47.50	2.40	6.49	0.13	24.71	13.96	0.10	0.00	0.00	3.59	98.92	79.20
CA-T29.1	165.00	hercynite	44.80	1.32	8.67	0.13	32.22	6.20	0.10	0.00	0.02	5.48	98.94	78.80
CA-T30	175.00	wehrlite	46.10	2.98	7.37	0.13	25.05	12.18	0.11	0.01	0.00	4.41	98.38	77.27
CA-T31	180.00	wehrlite	44.40	1.82	8.63	0.14	29.36	7.66	0.07	0.00	0.00	6.85	98.93	77.28
CA-T32.1	187.00	clinopy.	42.50	19.00	3.60	0.07	11.43	15.16	0.92	0.03	0.00	7.44	100.15	76.05
CA-T32.2	188.00	clinopy.	41.40	2.76	2.19	0.03	4.43	16.34	1.08	0.12	0.00	5.26	98.45	66.92
CA-T32.4	190.00	gabbro	44.80	22.30	2.94	0.05	6.81	16.86	1.08	0.07	0.01	3.98	98.90	69.85
CA-T33	200.00	ol. gabnor.	52.90	4.56	6.99	0.14	21.53	11.56	0.22	0.01	0.00	1.08	99.11	75.49
CA-T34	210.00	ol. clinopy.	47.80	2.12	7.57	0.14	25.01	13.42	0.11	0.01	0.00	2.74	98.96	76.76
CA-T35	215.00	wehrlite	45.60	2.00	8.30	0.14	26.57	11.98	0.13	0.01	0.00	4.23	98.96	76.20

All analysis obtained by AA (atomic absorption spectrometry)

Mg# =  $(100 \times \text{MgO}) / (\text{MgO} + \text{FeO})$ , LOI = Lost on ignition

TABLE A8 (con't)

**Whole Rock Major Element Chemistry of Layered Section**  
**Oxide (weight %)**

Sample#	Dist. (m)	Rock Type	SiO <sub>2</sub>	Al <sub>2</sub> O <sub>3</sub>	Fe <sub>2</sub> O <sub>3</sub>	MnO	MgO	CaO	Na <sub>2</sub> O	K <sub>2</sub> O	P <sub>2</sub> O <sub>5</sub>	LOI	Total	Mg #
CA-T36	220.00	clinopy.	52.20	2.84	5.72	0.12	19.82	17.36	0.14	0.01	0.00	2.12	100.37	77.60
CA-T37.1	225.00	wehrlite	47.80	3.38	8.70	0.15	25.80	10.76	0.10	0.01	0.00	3.79	100.53	74.78
CA-T37.2	225.50	wehrlite	47.80	2.26	8.47	0.15	25.38	11.26	0.13	0.02	0.02	3.92	99.41	74.98
CA-T37.3	226.00	webst.	53.60	2.44	7.26	0.15	24.17	9.74	0.19	0.02	0.00	1.58	99.19	76.90
CA-T37.4	226.50	herzolite	47.00	3.04	8.22	0.15	26.08	11.54	0.11	0.01	0.00	3.61	99.80	76.03
CA-T38	230.00	wehrlite	38.30	1.72	12.78	0.13	35.55	1.88	0.04	0.00	0.00	8.59	99.03	73.56
CA-T39	235.00	wehrlite	44.20	2.54	9.44	0.15	27.85	9.70	0.09	0.00	0.00	5.16	99.13	74.68
CA-T40.1	240.00	webst/dun.	47.80	2.82	9.85	0.16	29.39	5.44	0.12	0.01	0.00	4.18	99.81	74.90
CA-T40.2	240.50	webst.	52.40	2.66	8.17	0.16	25.77	8.60	0.16	0.01	0.01	1.28	99.34	75.93
CA-T41	250.00	ol. clinopy.	48.60	2.88	7.90	0.11	22.27	13.76	0.14	0.01	0.02	3.92	99.73	73.82
CA-T42	260.00	ol. gabnor.	50.40	6.44	5.40	0.12	18.17	16.16	0.29	0.02	0.02	1.72	98.86	77.09
CA-T43	265.00	clinopy.	52.50	3.18	6.18	0.11	19.43	15.94	0.21	0.01	0.30	2.10	99.78	75.87
CA-T44	270.00	wehrlite	41.10	2.44	12.22	0.13	31.61	4.84	0.11	0.01	0.00	6.75	99.29	72.12
CA-T45	275.00	wehrlite	38.10	1.50	12.45	0.15	34.61	2.46	0.03	0.00	0.00	8.86	98.16	73.54
CA-T46	280.00	clinopy.	50.40	3.36	6.49	0.12	19.43	15.86	0.34	0.05	0.01	2.05	98.31	74.96
CA-T47	285.00	wehrlite	40.00	4.40	11.59	0.14	30.93	5.04	0.12	0.01	0.00	6.39	98.62	72.74
CA-T48.1	288.00	wehrlite	45.40	2.06	8.60	0.13	27.59	10.76	0.12	0.01	0.01	3.96	98.76	76.24
CA-T48.2	289.00	wehrlite	37.60	1.76	10.46	0.12	36.24	1.58	0.02	0.00	0.03	10.61	98.50	77.60
CA-T48.3	290.00	wehrlite	43.90	1.92	8.92	0.14	28.72	9.70	0.08	0.00	0.01	5.99	99.46	76.30
CA-T48.4	290.50	wehrlite	39.30	1.38	11.01	0.12	35.72	2.96	0.03	0.00	0.00	9.02	99.54	76.44
CA-T48.5	291.00	clinopy.	50.00	3.04	5.71	0.11	20.91	16.86	0.19	0.02	0.00	2.19	99.15	78.55
CA-T48.6	292.00	wehrlite	37.80	1.52	11.05	0.11	36.00	1.98	0.01	0.00	0.00	0.08	98.55	76.51
CA-T49	300.00	wehrlite	41.50	1.98	10.14	0.15	33.22	5.38	0.06	0.00	0.01	7.17	99.69	76.61
CA-T50	315.00	clinopy.	50.00	3.60	5.98	0.09	20.30	15.40	0.19	0.02	0.00	2.38	98.04	77.25
CA-T51	320.00	clinopy.	50.80	3.06	4.76	0.11	19.43	18.92	0.16	0.00	0.02	1.51	98.87	80.26
CA-T53	330.00	gabnor.	51.70	3.76	5.44	0.12	18.96	17.92	0.26	0.01	0.01	1.37	99.71	77.70
CA-T54	340.00	wehr/ol.cipy	45.20	2.26	8.28	0.15	27.72	10.24	0.10	0.01	0.00	3.97	98.03	77.04
CA-T55	345.00	wehrlite	44.50	2.38	8.58	0.16	28.06	10.50	0.07	0.00	0.00	4.20	98.51	76.58
CA-T56	350.00	wehrlite	39.20	1.24	11.35	0.14	35.83	3.48	0.03	0.00	0.01	8.77	100.09	75.94
CA-T57	355.00	wehrlite	45.10	2.62	7.85	0.15	28.17	10.34	0.09	0.00	0.01	5.50	99.91	78.21
CA-T58	360.00	clinopy.	49.60	4.08	5.85	0.12	20.62	16.26	0.26	0.02	0.01	2.43	99.45	77.90
CA-T59	365.00	wehrlite	41.10	2.02	10.41	0.16	33.60	4.60	0.09	0.00	0.02	7.27	99.27	76.35
CA-T60	380.00	wehrlite	41.10	5.14	10.75	0.13	29.55	5.42	0.19	0.01	0.01	7.23	99.57	73.33
CA-T61	400.00	ol. clinopy.	48.10	2.90	6.68	0.13	23.30	14.16	0.13	0.00	0.01	2.68	98.07	77.72
CA-T62	405.00	wehrlite	44.30	2.50	9.36	0.14	30.15	8.52	0.12	0.01	0.01	5.23	100.34	76.31
CA-T63	410.00	wehrlite	45.00	2.10	9.66	0.14	28.78	8.94	0.18	0.00	0.03	4.35	99.22	74.87
CA-T64	415.00	gabnor.	49.30	7.05	5.11	0.11	18.28	15.32	0.71	0.10	0.00	3.14	99.20	78.15
CA-T65	420.00	gabbro	48.20	16.80	3.25	0.07	10.32	15.34	1.17	0.63	0.00	3.17	98.83	76.05
CA-T66	430.00	ol. gabnor.	50.00	6.10	4.99	0.11	17.83	17.98	0.23	0.01	0.00	1.67	99.00	78.13
CA-T67	435.00	ol. gabbro	49.10	6.19	5.58	0.11	18.73	16.46	0.21	0.07	0.00	1.82	98.35	77.05
CA-T68	440.00	gabbro	51.60	4.86	5.05	0.12	17.39	19.34	0.21	0.02	0.00	1.06	99.77	77.50
CA-T70	460.00	clinopy	50.70	6.95	5.07	0.11	18.46	15.60	0.48	0.03	0.00	2.45	99.93	78.45

All analysis obtained by AA (atomic absorption spectrometry)

Mg# = (100 x MgO)/(MgO + FeO), LOI - Lost on ignition.

TABLE A9  
Trace Element Chemistry from Layered Section

Sample	Distance (meters)	Rock Type	GA	ZN	CU	NI	SC	CR	V	TI	CA
			(ppm)							(wt. %)	
CA-T1	0.00	dunite	0	18	0	961	3	2571	6	0.02	0.20
CA-T2	10.00	dunite	0	17	0	993	1	2295	13	0.02	0.06
CA-T3	25.00	dunite	0	19	0	1455	5	4138	21	0.02	0.69
CA-T4	30.00	dunite	0	17	0	1533	0	3312	17	0.02	0.06
CA-T5	35.00	dunite	1	17	0	1411	1	4584	22	0.03	0.23
CA-T6	40.00	dunite	2	17	0	1646	3	4417	19	0.03	0.05
CA-T7	45.00	wehrlite	1	13	0	1631	3	2368	12	0.02	0.05
CA-T8	55.00	wehrlite	1	18	0	1564	4	2295	34	0.04	1.02
CA-T9	60.00	wehrlite	2	22	0	1551	5	3772	47	0.04	2.24
CA-T10	65.00	dunite	3	23	0	1566	8	2991	43	0.04	1.41
CA-T11	70.00	dunite	1	18	0	1691	4	2929	35	0.04	0.36
CA-T12	80.00	dunite	1	17	0	1638	2	3441	34	0.03	0.65
CA-T13	85.00	dunite	1	22	0	1051	4	2805	29	0.03	1.08
CA-T14	90.00	dunite	1	16	0	1927	6	3077	39	0.03	0.95
CA-T15	95.00	dunite	2	28	0	1675	1	2724	33	0.04	0.37
CA-T16	100.00	dunite	0	15	0	1593	4	2978	35	0.03	0.23
CA-T17	105.00	ol. webst.	1	18	0	292	31	2764	122	0.06	8.59
CA-T18	105.00	clinopy.	2	5	0	229	45	2535	150	0.05	18.33
CA-T19	110.00	ol. webst	2	12	0	351	41	4361	152	0.06	14.70
CA-T20	115.00	ol. clinopy.	2	21	0	480	38	1995	145	0.10	14.16
CA-T21	120.00	gabbro	8	10	132	156	27	369	106	0.08	17.93
CA-T22	120.50	clinopy.	4	16	23	438	36	2318	139	0.09	15.00
CA-T23	125.00	wehrlite	3	11	7	328	44	2088	187	0.12	18.42
CA-T24	130.00	ol. orthopy.	3	17	0	535	28	1779	106	0.06	11.05
CA-T25	135.00	dun/orthopy	3	32	0	677	23	2590	94	0.06	2.58
CA-T26	140.00	clinopy.	1	29	0	670	23	2340	88	0.06	2.17
CA-T27	145.00	orthopy.	2	10	5	370	45	3353	183	0.11	18.28
CA-T28.1	151.00	ol. clinopy.	3	24	0	391	36	3846	137	0.07	5.46
CA-T28.2	151.25	wehrlite	0	8	0	430	44	3563	155	0.07	18.33
CA-T28.3	151.50	wehrlite	2	28	0	777	25	2056	101	0.07	8.27
CA-T28.4	151.80	ol. clinopy.	1	22	0	652	29	2619	128	0.08	12.01
CA-T28.5	152.10	ol. clinopy.	4	17	0	590	37	3124	140	0.06	13.74
CA-T28.6	152.50	herzolite	2	15	0	515	37	2868	145	0.07	15.20
CA-T29.1	165.00	rodingite	1	23	0	687	28	2436	109	0.06	6.73
CA-T29.2	165.00	wehrlite	5	14	11	57	12	199	40	0.03	27.19
CA-T30	175.00	wehrlite	2	18	4	589	36	2372	136	0.09	12.94
CA-T31	180.00	clinopy.	3	27	0	863	29	2203	116	0.09	8.53
CA-T32.1	187.00	clinopy.	5	4	0	135	26	459	87	0.06	16.59
CA-T32.2	188.00	gabbro	11	0	2	31	17	255	38	0.03	18.26
CA-T32.4	190.00	gabbro	9	0	1	60	27	483	70	0.04	19.34
CA-T33	200.00	ol. gabnor	4	22	2	245	42	1451	169	0.12	13.21
CA-T34	210.00	ol. clinopy.	1	20	6	480	40	2218	158	0.09	14.86

Analysis obtained by XRF (X-Ray Fluorescence)

TABLE A9 (cont)

## Trace Element Chemistry from the Layered Section

Sample	Distance (meters)	Rock Type	GA	ZN	CU	NI	SC	CR	V	Ti	CA
			(ppm)								(wt. %)
CA-T35	215.00	wehrlite	3	22	24	531	37	2012	143	0.10	12.93
CA-T36	220.00	clinopy.	4	10	5	307	46	2763	201	0.10	19.31
CA-T37.1	225.00	wehrlite	3	29	0	581	31	2280	126	0.10	11.94
CA-T37.2	225.50	wehrlite	4	25	0	496	39	2643	156	0.13	12.64
CA-T37.3	226.00	webst.	4	23	17	266	42	3427	189	0.10	11.30
CA-T37.4	226.50	lherzolite	2	25	23	488	37	2804	131	0.09	12.91
CA-T38	230.00	wehrlite	1	37	0	991	11	535	51	0.07	1.77
CA-T39	235.00	wehrlite	3	31	2	666	29	1922	112	0.08	9.97
CA-T40.1	240.00	webst/dun.	3	32	0	524	31	2215	125	0.10	5.78
CA-T40.2	240.50	webst.	1	27	9	352	42	3110	170	0.12	9.32
CA-T41	250.00	ol. clinopy.	3	16	0	454	41	2142	160	0.12	13.98
CA-T42	260.00	ol. gabnor.	5	12	10	211	43	2108	161	0.11	16.92
CA-T43	265.00	clinopy	2	10	0	255	54	2727	196	0.13	17.32
CA-T44	270.00	wehrlite	2	37	0	904	17	1048	65	0.06	5.31
CA-T45	275.00	wehrlite	2	38	0	1001	14	911	55	0.05	2.60
CA-T46	280.00	clinopy.	3	12	0	352	47	2447	204	0.19	17.13
CA-T47	285.00	wehrlite	4	35	0	883	14	740	57	0.07	5.48
CA-T48.3	290.00	wehrlite	0	34	28	786	31	2379	141	0.12	10.26
CA-T48.4	290.50	wehrlite	0	30	0	1100	16	937	53	0.05	2.96
CA-T49	300.00	wehrlite	2	29	0	904	24	1089	98	0.07	5.43
CA-T50	315.00	clinopy.	4	5	0	320	45	1868	169	0.11	15.37
CA-T51	320.00	clinopy.	3	5	0	249	50	2209	191	0.09	18.62
CA-T52.2	326.00	clinopy.	3	6	4	273	50	2519	189	0.09	18.61
CA-T53	330.00	gabnor.	3	11	7	238	50	2144	198	0.13	17.58
CA-T54	340.00	wehr/ol.cipy	1	31	0	618	39	2180	144	0.09	10.51
CA-T55	345.00	wehrlite	2	37	0	737	35	2209	125	0.08	10.70
CA-T56	350.00	wehrlite	1	31	0	1079	15	1244	66	0.05	3.06
CA-T57	355.00	wehrlite	3	24	0	693	29	2683	136	0.09	9.86
CA-T58	360.00	clinopy.	4	14	0	369	47	326	195	0.15	16.88
CA-T59	365.00	wehrlite	1	40	0	1065	20	1277	85	0.09	4.66
CA-T60	380.00	wehrlite	3	26	0	755	15	493	72	0.09	5.47
CA-T61	400.00	ol. clinopy.	3	17	1	462	38	2264	151	0.08	14.54
CA-T62	405.00	wehrlite	3	24	0	789	26	1562	106	0.07	8.19
CA-T63	410.00	wehrlite	1	27	0	671	31	2152	128	0.08	9.72
CA-T64	415.00	gabnor.	4	6	1	246	41	1697	156	0.08	15.86
CA-T65	420.00	gabbro	8	2	9	116	31	574	116	0.08	16.17
CA-T66	430.00	ol. gabnor.	6	7	15	207	47	1801	168	0.09	18.66
CA-T67	435.00	ol. gabbro	5	11	19	255	45	1726	162	0.09	17.10
CA-T68	440.00	gabbro	2	8	22	172	50	1990	193	0.11	19.72
CA-T69	445.00	ol. gabbro	4	4	6	149	42	1877	170	0.09	15.85
CA-T70	460.00	clinopy	4	5	6	150	47	1864	168	0.10	15.96

Analysis obtained by XRF (X-Ray Fluorescence)

TABLE A10

**Whole Rock Major Element Chemistry of the Diabase Dike Suites  
(oxide weight %)**

Sample	Rock Type	SiO <sub>2</sub>	TiO <sub>2</sub>	Al <sub>2</sub> O <sub>3</sub>	Fe <sub>2</sub> O <sub>3</sub>	MnO	MgO	CaO	Na <sub>2</sub> O	K <sub>2</sub> O	P <sub>2</sub> O <sub>5</sub>	LOI	Total
CA 126A	diabase	54.30	0.88	15.50	11.24	0.07	4.35	9.46	2.58	0.07	0.04	0.44	99.13
CA 166C	diabase	53.40	0.84	14.70	12.12	0.06	4.73	8.52	2.63	0.20	0.04	0.91	98.15
CA 217B	diabase	54.80	0.88	14.80	7.93	0.09	6.93	10.74	1.92	0.12	0.03	1.18	99.22
CA 239	diabase	53.90	0.52	15.30	9.87	0.14	5.97	10.82	1.09	0.07	0.02	0.79	98.49
CA 321	diabase	58.00	0.76	14.20	10.56	0.08	3.71	7.76	2.30	0.14	0.05	1.07	98.63
CA 322	diabase	51.90	0.96	14.90	11.42	0.06	5.92	8.18	3.00	0.26	0.04	2.63	99.05
CA 323	diabase	54.30	0.56	15.10	8.41	0.10	6.71	10.82	1.55	0.13	0.03	1.49	99.20
CA 036	Por. diab.	51.20	0.24	10.10	6.17	0.08	14.40	12.00	1.33	0.03	0.00	3.22	99.31
CA T52.1	Por. diab.	41.30	0.28	13.50	12.53	0.16	13.85	12.54	0.09	0.02	0.01	4.21	98.49
CA 119	Por. diab.	52.70	0.20	9.65	8.94	0.15	12.85	8.86	2.19	0.12	0.02	3.30	98.98
CA 179	Por. diab.	51.10	0.32	13.60	8.07	0.12	10.37	8.56	2.94	0.68	0.01	3.51	99.28
CA 289A	Por. diab.	45.40	0.24	14.90	10.52	0.09	12.05	12.56	0.58	0.07	0.00	2.58	98.99
CA 316	Por. diab.	51.50	0.28	13.00	8.51	0.13	9.10	10.10	2.74	0.07	0.01	3.57	99.01
CA 317A	Por. diab.	51.80	0.28	10.20	8.46	0.12	13.60	7.30	2.92	0.11	0.00	3.86	98.65
CA 317B	Por. diab.	54.20	0.28	12.60	8.87	0.15	9.53	10.66	0.97	0.14	0.00	1.28	98.68
CA 334	Por. diab.	48.30	0.20	12.00	9.04	0.13	13.10	8.34	2.78	0.17	0.00	5.05	99.11
CA 336C	Por. diab.	49.70	0.24	12.50	7.71	0.13	11.50	10.34	1.88	0.25	0.00	4.08	98.33

Analysis obtained by AA (atomic absorption spectrometry).

LOI - Lost on ignition

TABLE A11

**Whole Rock Trace Element Chemistry of the Diabase Dike Suites**

Sample	Rock Type	Sr	Y	Zr	Ni	V	Cr	Ti
		(ppm)						
CA 126A	diabase	126	21	40	120	386	12	0.30
CA 166C	diabase	120	20	38	0	510	0	0.94
CA 217B	diabase	102	15	30	32	306	147	0.56
CA 239	diabase	46	11	21	22	313	55	0.46
CA 321	diabase	95	25	46	0	257	0	0.69
CA 322	diabase	70	17	34	10	363	0	0.69
CA 323	diabase	130	14	28	20	252	7	0.43
CA 036	Por. diab.	112	9	11	227	203	1062	0.24
CA T52.1	Por. diab.	59	11	15	97	296	819	0.30
CA 119	Por. diab.	86	8	10	107	255	856	0.25
CA 179	Por. diab.	36	9	7	120	250	401	0.30
CA 289A	Por. diab.	105	8	9	97	256	674	0.23
CA 316	Por. diab.	92	10	12	47	276	474	0.28
CA 317A	Por. diab.	42	7	12	87	258	656	0.23
CA 317B	Por. diab.	26	11	14	51	252	409	0.28
CA 334	Por. diab.	26	12	12	93	271	712	0.23
CA 336C	Por. diab.	115	8	10	92	227	540	0.21

Analysis obtained by XRF (X-Ray Fluorescence).

TABLE A12

## Whole Rock Trace and REE Abundances of the Diabase Dike Suites

Sample	CA-116C	CA-289A	CA-336C	CA-126A	CA-317A	CA-119	CA-323	CA-289A*	CA-036
Li	2.893	0.919	2.425	1.052	4.262	5.200	3.369	0.921	10.701
Be	0.066	-0.236	-0.191	0.140	0.038	-0.100	-0.048	-0.132	-0.145
Sc	35.613	43.244	35.356	34.272	39.650	37.065	32.869	42.812	30.671
Rb	1.312	0.351	1.085	0.305	0.286	0.448	0.620	0.360	1.518
Sr	116.31	111.46	117.28	124.58	44.79	88.65	74.47	111.12	116.11
Y	15.682	5.865	5.367	18.056	5.969	6.205	13.261	6.186	7.072
Zr	21.778	5.526	4.611	15.994	5.134	6.542	12.393	7.524	6.312
Nb	0.823	0.927	0.672	0.962	0.667	0.707	0.759	0.926	1.062
Mo	0.216	0.899	0.153	0.212	0.132	0.137	0.164	0.136	0.141
Cs	0.014	0.005	0.009	0.004	0.003	0.018	0.005	0.004	6.904
Ba	2.36	1.37	2.97	7.84	5.26	3.57	4.90	1.29	3.62
La	1.173	0.266	0.199	1.234	0.231	0.311	0.852	0.272	0.577
Ce	3.468	0.576	0.421	3.795	0.527	0.522	2.522	0.588	0.980
Pr	0.588	0.090	0.071	0.667	0.083	0.099	0.444	0.092	0.133
Nd	3.370	0.590	0.472	3.840	0.489	0.615	2.616	0.576	0.753
Sm	1.320	0.324	0.252	1.660	0.310	0.313	1.163	0.334	0.406
Eu	0.551	0.238	0.124	0.648	0.120	0.151	0.473	0.221	0.210
Gd	1.849	0.521	0.507	2.321	0.566	0.608	1.624	0.575	0.704
Tb	0.413	0.139	0.123	0.493	0.139	0.148	0.356	0.145	0.168
Dy	2.960	1.085	0.930	3.489	1.086	1.099	2.564	1.156	1.254
Ho	0.646	0.251	0.222	0.765	0.249	0.286	0.575	0.271	0.303
Er	2.071	0.879	0.758	2.360	0.821	0.868	1.765	0.855	0.948
Tm	0.297	0.136	0.126	0.348	0.130	0.131	0.266	0.138	0.151
Yb	1.942	0.931	0.818	2.327	0.909	0.899	1.767	0.941	1.003
Lu	0.312	0.154	0.132	0.368	0.141	0.148	0.276	0.151	0.162
Hf	0.946	0.366	0.223	1.057	0.319	0.421	0.762	0.411	0.338
Ta	0.371	0.499	0.226	0.440	0.124	0.131	0.207	0.479	0.380
W	116.572	46.505	67.872	187.549	30.053	37.235	84.255	47.218	60.802
Tl	-0.004	0.005	-0.005	-0.005	-0.007	-0.006	-0.010	-0.012	-0.011
Pb	0.387	1.629	0.399	0.617	0.565	0.293	0.357	1.880	0.610
Bi	0.034	0.004	0.049	0.052	0.047	0.052	0.056	0.042	0.044
Th	0.150	0.055	0.132	0.208	0.084	0.096	0.135	0.140	0.087
U	0.060	0.037	0.031	0.065	0.033	0.040	0.038	0.040	0.050

Analysis Obtained by ICP-MS

## APPENDIX B

### ANALYTICAL METHODS AND SAMPLE PREPARATION

Whole rock powders were used to determine major, trace and rare earth elemental abundances using AA, XRD and ICP-MS respectively.

All whole rock analysis were carried out at the Department of Earth Sciences, Memorial University of Newfoundland.

Probe work was conducted in part at Memorial University and in part at Dalhousie University, Halifax, Nova Scotia.

#### B.1 AA (Atomic Absorption)

**ELEMENTS ANALYZED:** SiO<sub>2</sub>, Al<sub>2</sub>O<sub>3</sub>, TiO<sub>2</sub>, Fe<sub>2</sub>O<sub>3</sub>, MnO, MgO  
CaO, Na<sub>2</sub>O, K<sub>2</sub>O,

#### Procedure

0.1000 grams of rock powder (100 mesh) are placed on a steam bath with 5 ml of concentrated HF (ACS) in a digestion bottle for 30 minutes. After cooling 50 ml of saturated boric acid solution are added and the solution replaced on the steam bath until the solution is clear. After cooling 145ml of distilled water is added and the mixture shaken. This solution is then used for analysis of all elements excluding calcium and magnesium.

- 1) Digestion bottles used here are made of polymethylpentene, Nalge Catalogue No. 2107 (250ml).
- 2) Use Nalgene precise volume dispenser #3700 (5ml) for adding HF.
- 3) If black residue remains (other than organic matter or graphite) add 1 ml Aqua Regia along with the HF. Add only 144ml H<sub>2</sub>O afterwards.

- 4) Saturated boric acid: weigh 200g boric acid crystals (c.p). Add 1600ml distilled water and heat until dissolved. Dilute, while hot to 4l and store in polyethylene bottles.

Note: "Repipets" are used for addition of boric acid of water.

#### Standard Solutions

Prepare 1000ug/ml solutions of each of the oxides of the major elements except silica using Spec-pure chemicals. (Spex. Industries). Use compounds that can be dissolved in HCl. Store these solutions in tightly capped polyethylene bottles.

From these stock solutions a blend of all the elements is made. Further dilution will give a range of values for each oxide. Table B1 is given as an example of how the stock blend solutions is made:-

**TABLE B1**

Oxide	% Oxide in rock	ml 1000 y/me Standard solutions of oxides (pipet into 200ml volumetric flask)
SiO <sub>2</sub>	50.00*	30.00*
Al <sub>2</sub> O <sub>3</sub>	15.00	4.00
TiO <sub>2</sub>	2.00	24.00
Fe <sub>2</sub> O <sub>3</sub>	12.00	24.00
MnO	0.20	0.40
MgO	7.00	14.00
CaO	7.00	14.00
Na <sub>2</sub> O	5.00	5.00
K <sub>2</sub> O	2.00	2.00

\*Weigh 0.1000g Spec-pure SiO<sub>2</sub>, in a digestion flask add 5ml HF, when dissolved add 50ml boric acid. Add this solution carefully to the others in the volumetric flask, rinsing digestion flask with distilled water and fill up to the mark with distilled water.

This basic blend solutions can be diluted with blank solution

- (a) To give a range of values for each oxide.
- (a) Blank solution:- 5 ml HF, 50 ml saturated boric acid solution and 145 ml distilled water.

### Analysis

Using the settings given in the Atomic Absorption manual each element is determined on the basic solution except CaO and MgO. The sample solutions is bracketed between a higher and lower standard and the results are found by using the following formula.

$$\% \text{ oxide} = 2 \left\{ \% \text{ in low std.} + \frac{(\text{sample Abs.} - \text{low std. Abs.} \times (\text{high Std} - \% \text{ low std}))}{\text{High Std Abs.} - \text{low Std Abs.}} \right\}$$

### CaO and MgO

Pipette 5 ml sample solution into a 50 ml volumetric flask. Add 10 ml lanthanum oxide\* solution and make to mark with distilled water. Treat a series of standards in the same way. Stopper and shake and use these solutions for determination of CaO and MgO. \*Lanthanum Oxide Solution. Suspend 58.7g pure lanthanum oxide in 250ml distilled water, add 250ml concentrated HCl. When dissolved cool and make up to 1000ml in a volumetric flask using concentrated HCl.

In some cases when concentrations are too high the burner is turned side

ways to light path - e.g.  $\text{Na}_2\text{O}$ .

This method has been adapted from:-

- (1) Analysis of Silicate Rocks - F.J. Langymhr and P.E. Paus. Anal. Chem. Acta 43, (1968) pages 397-408.
- (2) Analysis of Rocks and Minerals by A.A.S. - Sidney Abbey- G.S.C. Bulletin, 1968.
- (3) Atomic Absorption Analysis of 18 elements from a single decomposition of Alumina Silica - D.E. Buckley and R.E. Cranston, Marine Geology Atlantic Oceanographic Laboratory, Bedford Institute, Dartmouth, N.S.

The accuracy of analysis for the various elemental oxides is given in Table B2.

**TABLE B2**

Accuracy of Analysis by Atomic Absorption Spectrophotometry

Oxides	Range of Values %	No. of Analysis	Mean	STD Deviation
$\text{SiO}_2$	68.1-69.6	12	68.8	0.46
$\text{TiO}_2$	0.84-0.92	8	0.87	0.03
$\text{Al}_2\text{O}_3$	15.0-15.4	12	15.2	0.11
$\text{Fe}_2\text{O}_3\text{T}$	0.75-0.77	12	0.76	0.008
$\text{CaO}$	0.52-0.64	12	0.56	0.04
$\text{MgO}$	1.62-1.73	12	1.70	0.03
$\text{Na}_2\text{O}$	7.95-8.50	12	8.23	0.17
$\text{K}_2\text{O}$	0.48-0.49	12	0.49	0.005
$\text{MnO}$	0.1-0.1	12	0.10	0.00

**B.2 XRF (X-Ray Fluorescence)**

<b>ELEMENTS ANALYSED:</b>	Sr, Y, Zr, Ni, V, Cr, Ti
<b>SAMPLE TYPE:</b>	Pressed powder pellets (10.000 g) bound with polyvinyl alcohol binder.
<b>SPECTROMETER TYPE:</b>	Phillips's PW1450
<b>Crystals Used:</b>	Lif200, Lif220, Ge, Pet, Tlap
<b>POWER INPUT:</b>	2400 watts (60 kv 40 ma)
<b>COMPUTING SYSTEM:</b>	Hewlett Packard HP 86

XRF analysis was conducted at Memorial University using a Phillip's PW1450 automatic sequential spectrometer. A water cooled, side window, rhodium target x-ray tube is employed as an energy source, with a constant power input of 2400 watts (60 kv 40 ma). Five analysing crystals (Lif200, Lif220, Ge, Pet, Tlap) and two collimators (fine, coarse) are available for line selection and peak resolution. A gas flow proportional counter and a scintillation detector mounted in series produce voltage pulses directly proportional to the incident x-ray energies. The voltage pulses from the detectors are normalized by a sine wave potentiometer and first order lines are selected by a pulse height analyzer. A time constant of four seconds is used. All parameter settings are input to the XRF with a Hewlett Packard HP86 desk top computer via an interface designed and built at Memorial. Output of data can be sent directly to a printer or an IBM compatible PC.

### **B.3 ICPMS (Inductively Coupled Plasma Mass Spectrometry)**

**ELEMENTS ANALYSED:** Li, Rb, Sr, Y, Zr, Nb, Mo, Cs, Ba, La, Ce, Pr, Nd, Sm, Eu, Gd, Tb, Dy, Ho, Er, Tm, Yb, Lu, Hf, Ta, W, Ti, Pb, Bi, Th, U

#### **PROCEDURE:**

- 1) A standard HF/HNO<sub>3</sub> digestion of a 0.1 gram sample aliquot.
- 2) Any sample material that did not dissolve in HF/HNO<sub>3</sub> was attacked with HCl/HNO<sub>3</sub>.
- 3) Analysis of the solution by inductively coupled plasma mass spectrometry (ICP-MS) using the method of standard addition to correct for matrix effects.
- 4) Any sample that did not dissolve fully even after multi-acid attack (usually due to presence of graphite, chromite, ilmenite and other oxides) and required filtering of insoluble residue prior to analysis are indicated (F). Note that other resistant phases, most notably zircon, may not always dissolve completely (particularly in young, low Th and U rocks) and that Zr and Hf values should therefore be considered minimum concentrations. (An alternative digestion procedure which ensures solution of all minerals is now available for the analysis of Y, Zr, Hf and the REE only). Further information on the analytical procedures can be supplied on request.

Limits of detection and reagent blanks are typically about 10% of chondrite levels (Figure B1); ie. about 0.01 ppm for the REE and less abundant traces to 0.5-1 ppm for the more abundant elements (Table B2).

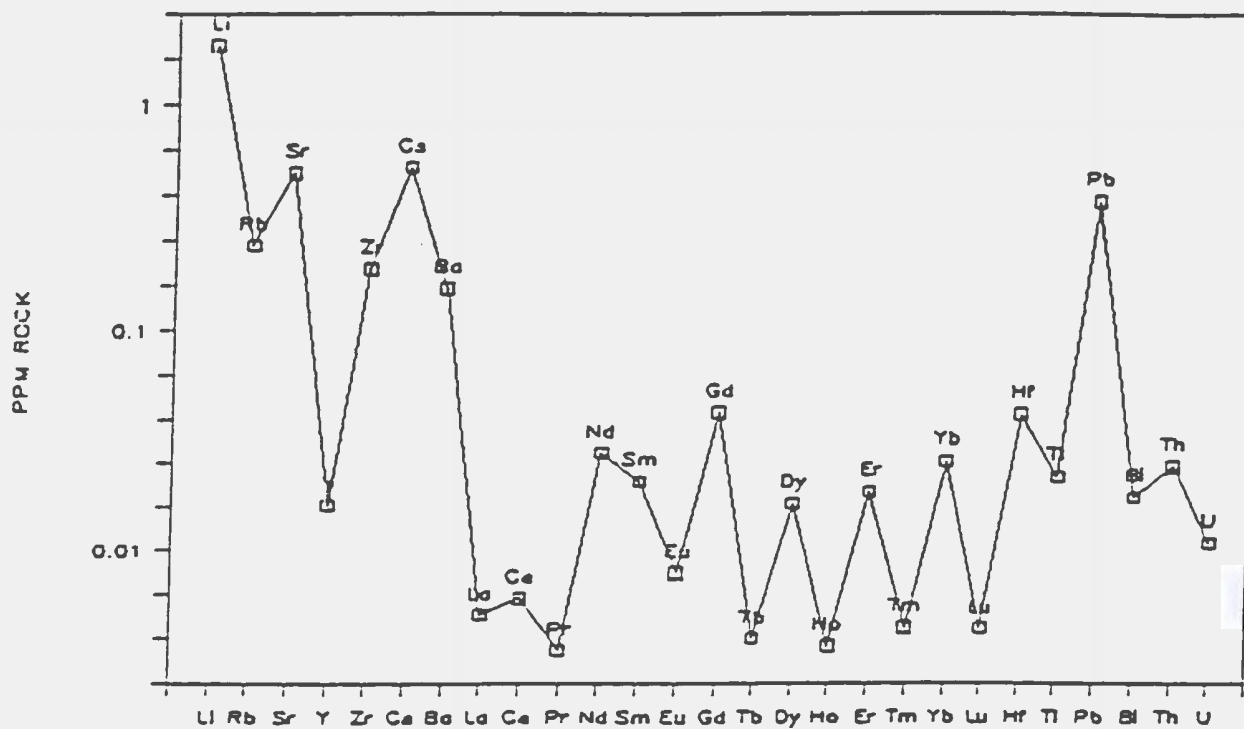


**Figure B1** ICP-MS detection limits (average of several runs) in ppm for elements of the MUN trace element package. For the REE and less abundant trace elements, detection limits are generally about 0.01 ppm.

**TABLE B3.** Results of 21 repeat ICP-MS determinations of the standard reference material SY-2. Literature values from (1) Geostandards Newsletter, 8, 1984, (2) Doherty and Vander Voet, Canadian Journal of Spectroscopy, 30, 135, 1985.

Element	ICP-MS mean ppm	Std dev ppm	rsd	literature (1) ppm (2)		rel. diff.
Li	93	7	8%	93		0%
Rb	221	11	5%	220		0%
Sr	270	14	5%	280		2%
Y	116	5	5%	130	126-131	12%
Zr	262	16	6%	280		7%
Cs	2.53	0.25	10%	2.3		-9%
Ba	454	16	4%	460		1%
La	67.6	2.1	3%	88	73-88	30%
Ce	152	6	4%	210	164-210	38%
Pr	19.0	0.6	3%	21	21	10%
Nd	72.0	1.5	2%	71	70-80	-1%
Sm	15.2	0.4	3%	15	15-16.5	-1%
Eu	2.35	0.11	5%	2.4	2.4-3	2%
Gd	14.9	1.5	10%	17	17	14%
Tb	2.84	0.14	5%	2	2-3	-30%
Dy	19.5	0.6	3%	20	20-21.3	3%
Ho	4.42	0.15	3%	5	5	13%
Er	14.7	0.4	3%	12	12-16	-18%
Tm	2.35	0.06	3%	2	2-2.6	-15%
Yb	17.2	0.5	3%	17	17-18.4	-1%
Lu	2.81	0.09	3%	3	3	7%
Hf	8.8	0.5	5%	8		-9%
Tl	1.49	0.07	5%			
Pb	99	4	6%	80		-20%
Bi	0.14	0.03	19%			
Th	338	38	11%	380		12%
U	258	25	10%	290		12%

## B.4 ELECTRON MICROPROBE ANALYSIS

Electron Microprobe analysis was conducted using two separate microprobes. A Jeol JXA 50A microprobe located at the Dept. of Earth Sciences, Memorial University of Newfoundland and a Jeol 733 Superprobe located at the Regional Electron Microprobe Laboratory, Dalhousie University, Halifax, Nova Scotia.

### B.4.1 JEOL JXA 50A Electron Microanalyzer.

<b>SPECTROMETERS:</b>	Wavelength Dispersive
<b>Type:</b>	Two sealed xenon detectors One gas flow argon detector
<b>Crystals Used:</b>	LiF, Rap and Pet.
<b>BEAM CURRENT:</b>	0.0220 DC microamperes
<b>ACCELERATING VOLTAGE:</b>	15 kv
<b>COUNTING TIME:</b>	30 seconds or 60,000 counts
<b>COMPUTING SYSTEM:</b>	Digital Equipment Corp. RX01

The electron microprobe used at Memorial University of Newfoundland was a Jeol JXA 50A electron probe microanalyzer. Three wavelength dispersive spectrometers with two analyzing crystals each allow for the analysis of all elements fluorine and heavier, and eliminate most line overlap problems. The three crystals most often in use are the LiF, Rap, and Pet. Two spectrometers contain sealed xenon detectors while the third is a gas flow argon detector. Voltage pulses from the detectors are filtered by a pulse height analyzer whose window settings are automatically set depending on which element is being analyzed. The beam current and counting time can be and often is set by the operator depending on

mineral type, but the most common settings are, .0220 DC microamperes for the beam current and 30 seconds or 60,000 counts for a count rate. The high voltage is set at 1.5 kv and the accelerating voltage is set at 15 kv. Both Bence-Albee and Ziebold-Ogilvie data reduction schemes are available for alpha-matrices corrections. The computer that runs the probe is a Digital Equipment Corp. RX01 with a teletype as its input/output device, but an interface has been attached that allows the hookup of and IBM compatible pc for output.

#### B.4.2 JOEL 733 Superprobe.

<b>SPECTROMETERS:</b>	Wavelength Dispersive
<b>BEAM CURRENT:</b>	5 nA
<b>BEAM DIAMETER</b>	$1 \times 10^{-6}$ m
<b>ACCELERATING VOLTAGE:</b>	15 kv
<b>COMPUTING SYSTEM:</b>	Traycor Northern ZAF software

The electron microprobe used at Dalhousie University in Halifax, Nova Scotia was a Jeol 733 Superprobe. A wavelength dispersive analytical technique was used, involving up to four simultaneous analysis and an automated spectrometer drive, to obtain analysis of ten major elements. An accelerating voltage of 15 kV, a probe current of 5 nA and a beam diameter of approximately  $1 \times 10^{-6}$  m were used. The data reduction converting raw counts per second to corrected weight percent of oxides was done using Traycor Northern ZAF software.

## **B.5 SAMPLE PREPARATION**

All sample preparation was conducted at the Department of Earth Sciences, Memorial University.

### **B.5.1 Whole Rock Powders**

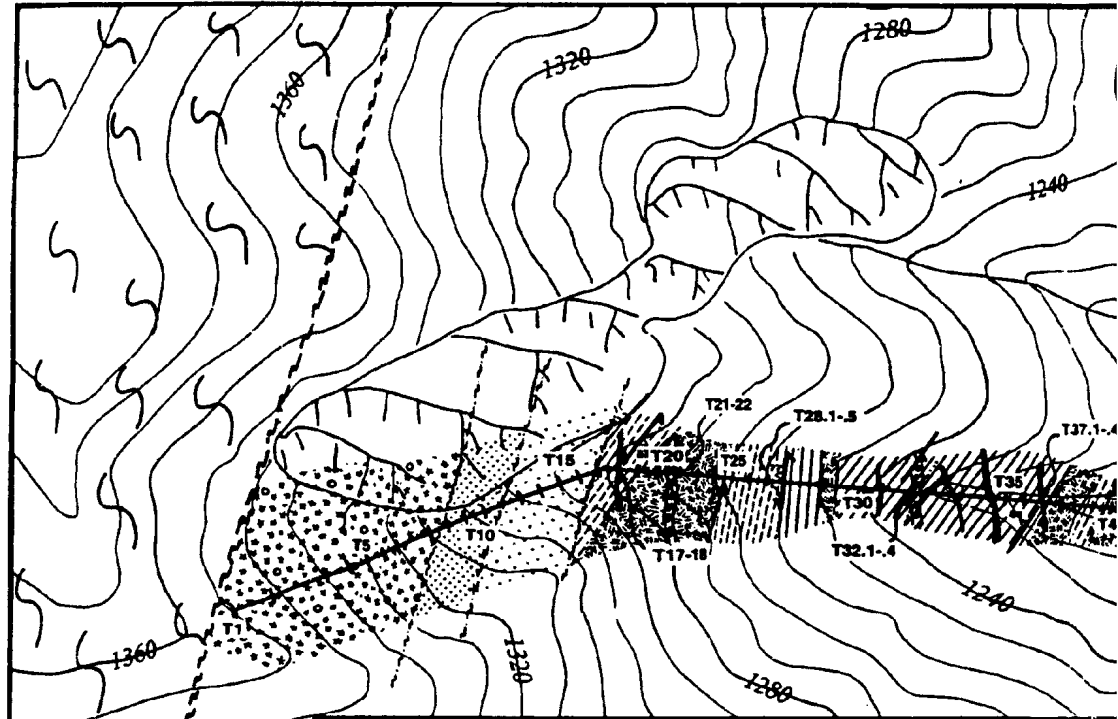
- 1) All samples were trimmed using a diamond-bladed table rock saw to remove weathered surfaces.
- 2) All samples were passed through a jaw crusher several times, with the exit gap of the jaw plates being progressively narrowed to a minimum width of roughly 0.5 cm.
- 3) Crushed samples were then powdered using a tungsten carbide pulverizing dish with ring and puck. Silica sand was powdered between the powdering of each sample to reduce the possibility of cross contamination.

### **B.5.2 Thin Sections**

Thin sections used for probe analysis were cut and polished at the lapidary shop, Dept. of Earth Sciences Memorial University.

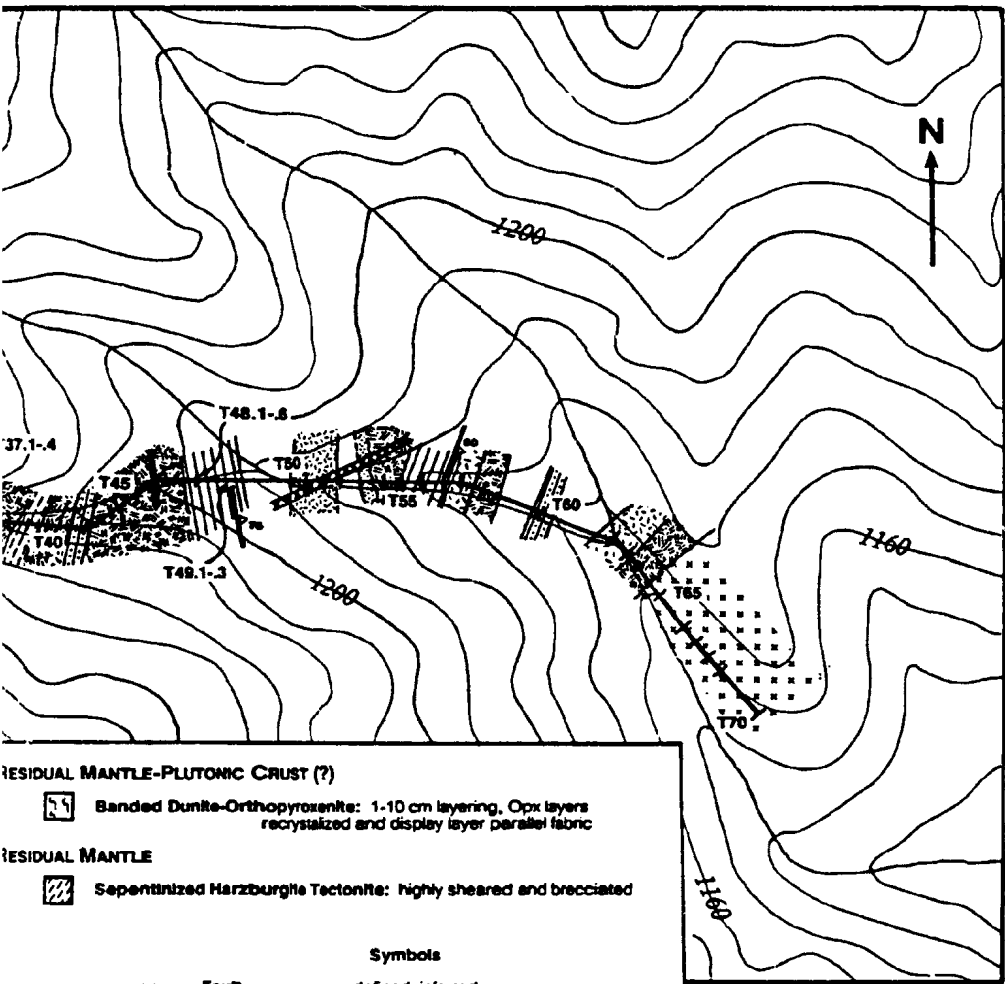
# MAP 2

# ULTRAMAFIC CUM



	<b>LEGEND</b>	RESIDU
<i>Late Cretaceous (Turonian)</i>	Diabase Dike: olivine phyric, intensely altered magnesian-rich diabase	RESIDU
<b>PLUTONIC CRUST (variably deformed)</b>		
<b>LATE-MAGMATIC INTRUSIVE SUITE</b>		
	Gabbro: coarse to pegmatitic, generally as dikes (cumulate plagioclase)	
	Clinopyroxenite: coarse grained, common as dikes, locally grades to gabbro	
<b>EARLY-PLUTONIC SUITE</b>		
	Olivine gabbro: Medium grained, intercumulate plagioclase	
	Olivine clinopyroxenite: locally grades to clinopyroxenite	
	Layered wehrlite-olivine clinopyroxenite-clinopyroxenite	
	Wehrlite: 40-75 % clinopyroxene, olivine commonly developed	
	Olivine wehrlite: 10-25 % clinopyroxene, intensely serpentinized	
	Clinopyroxene dunite: 2-10 % clinopyroxene, intensely serpentinized	
	Serpentinized Dunite: highly sheared and brecciated, veined by rodingite	

# UMULATE SECTION



**RESIDUAL MANTLE-PLUTONIC CRUST (?)**

 **Banded Dunite-Orthopyroxenite:** 1-10 cm layering, Opx layers recrystallized and display layer parallel fabric

**RESIDUAL MANTLE**

 **Serpentinized Harzburgite Tectonite:** highly sheared and brecciated

**Symbols**

 **Fault** defined, inferred

 **Geological contact**

 **Igneous layering** 2-10 cm scale, phase layering

 **Layer parallel fabric**

0 10 20 30 40 50 m

**Elevation in meters** **Location shown on Map 1.**

Chris Ash, 1990, M.Sc Thesis.

# Geology of the Amiandos Area, Cyprus

Chris H. Ash, 1970. Map 1. M.Sc. Thesis. Memorial University of Newfoundland, Canada.

## LEGEND

### Late Cretaceous (Turonian)

#### Dike Rocks

- Olivine clinopyroxene phync dike - brown weathering, highly altered, magnetite-rich diabase dike
- Aegirine dike - green to grey weathering, diabase dike

#### PLUTONIC ROCKS

##### Late-Magmatic Suite

- 9** High Level Intrusive Zone  
Abundant monzonite and diabase units including fine and coarse grained gabbro, trondhjemite dikes and small intrusive bodies
- 9a** Intrusion breccia of epidote rich trondhjemite containing abundant xenoliths of gabbro and diabase
- High Level Gabbro**  
Very altered, medium grained to pegmatitic gabbro-dike gabbro - common as dikes and veins may contain granite
- Clinopyroxene-Olivine Clinopyroxenite**  
Predominantly as dikes bearing clinopyroxene dikes, larger bodies commonly contain olivine clinopyroxenite

##### Early-Plutonic Suite

- 8** Gabbro-Orthopyroxene Gabbro  
8a Medium to fine grained gabbro-dike gabbro  
8b Medium grained olivine gabbro-dike gabbro  
8c Medium to coarse grained mesogabbro-dike gabbro (20-40% O)
- 5** Pigeonite-bearing Ultramafic Cumulates  
Medium to coarse grained pigeonite-bearing spinel-websterite, locally gradational to mesogabbro
- 4** Wehrlite  
Medium to coarse grained, commonly dolokitic, gradational to olivine clinopyroxenite with subordinate olivine websterite (on scale phase layering locally developed)
- 3** Dunite  
3a Clinopyroxene Dunite (2-10% clinopyroxene)  
3b Dunite (Trace clinopyroxene and chromite)  
3c Chrome spinel dunite (2-10% chrome spinel)
- Banded Dunite-Orthopyroxene**  
Orthopyroxene layers recrystallized with well developed layer parallel foliation fabric and contain from 2-15% unaltered clinopyroxene (on scale layering)

#### MANTLE-CRUST (?)

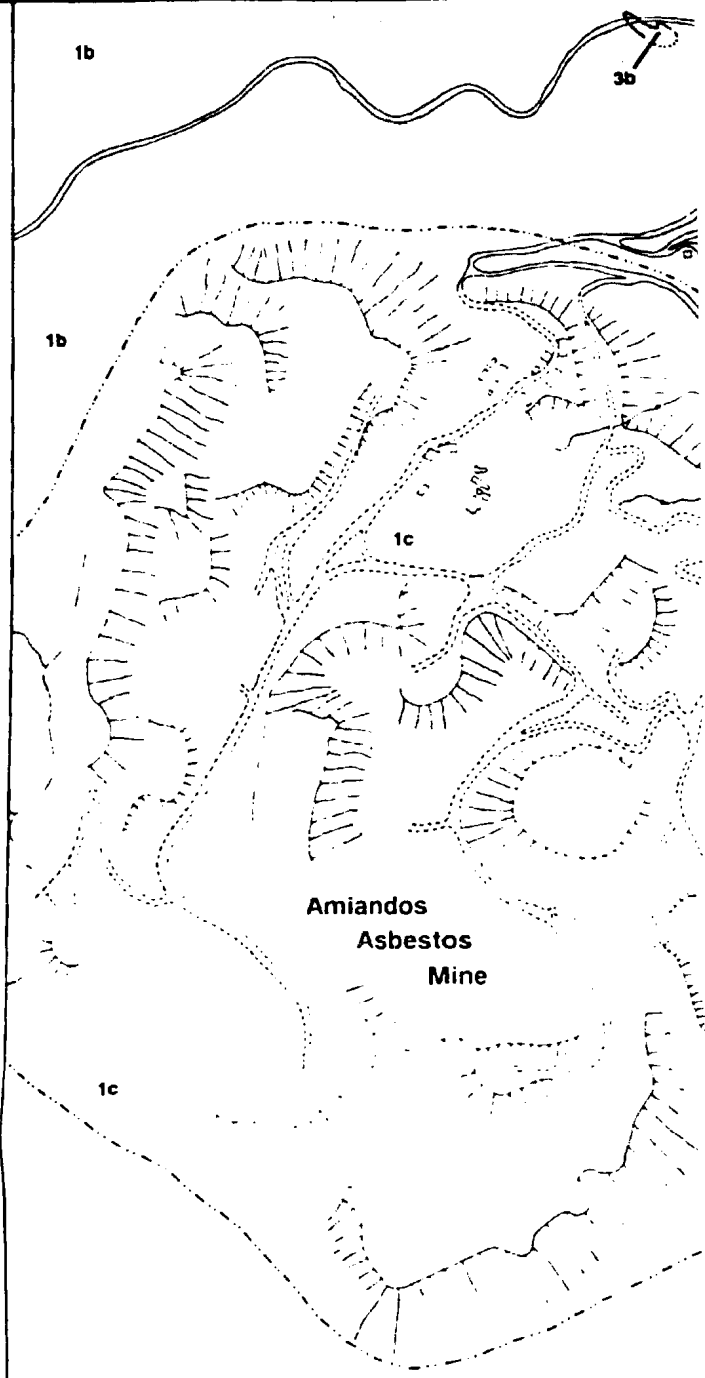
- Banded Dunite-Orthopyroxene**  
Orthopyroxene layers recrystallized with well developed layer parallel foliation fabric and contain from 2-15% unaltered clinopyroxene (on scale layering)

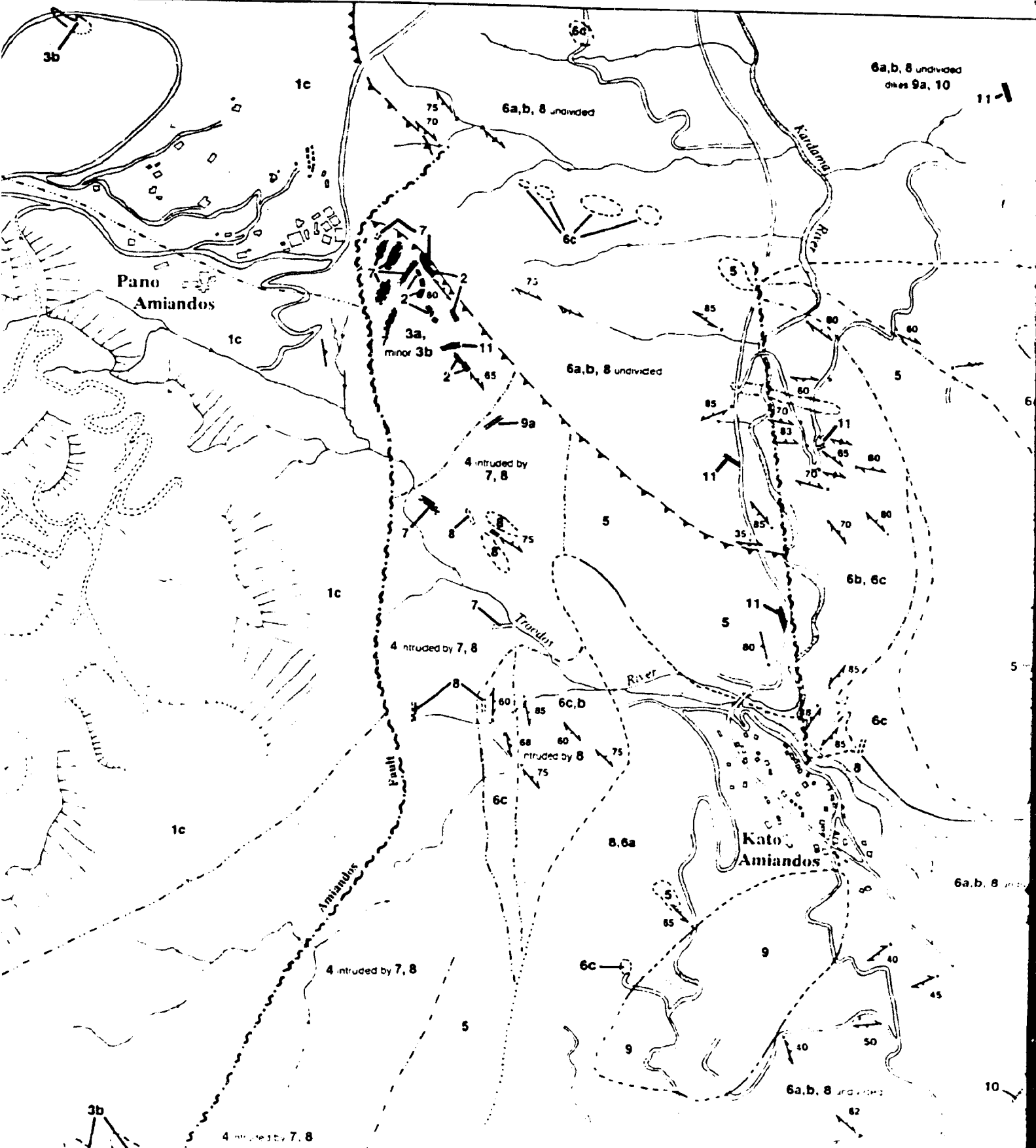
#### RESIDUAL MANTLE ROCKS

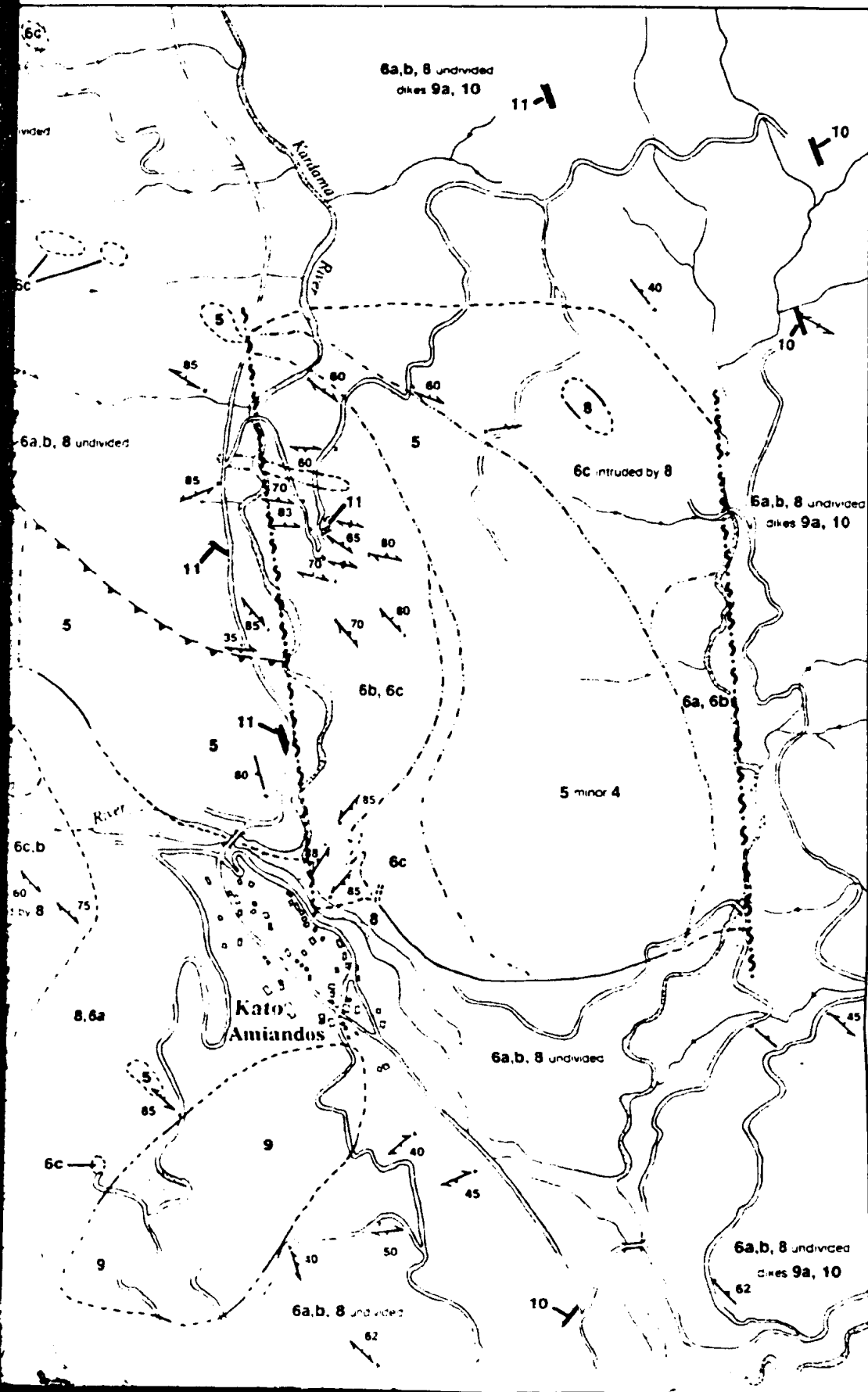
- Harzburgite**  
Well developed tectonite fabric
- Serpentine basine** - no fabric present
- 1c** Highly brecciated, abundant asbestos veins

#### Symbols

- Intrusive contact (approximate assumed)
- Gradational contact (approximate assumed)
- Inferred contact (relationship unknown)
- Reverse normal fault (approximate assumed)
- Thrust Fault (approximate assumed)
- Tectonite fabric (recrystallized)
- Igneous Layering
- Layer-parallel foliation fabric
- Weak to moderate foliation fabric



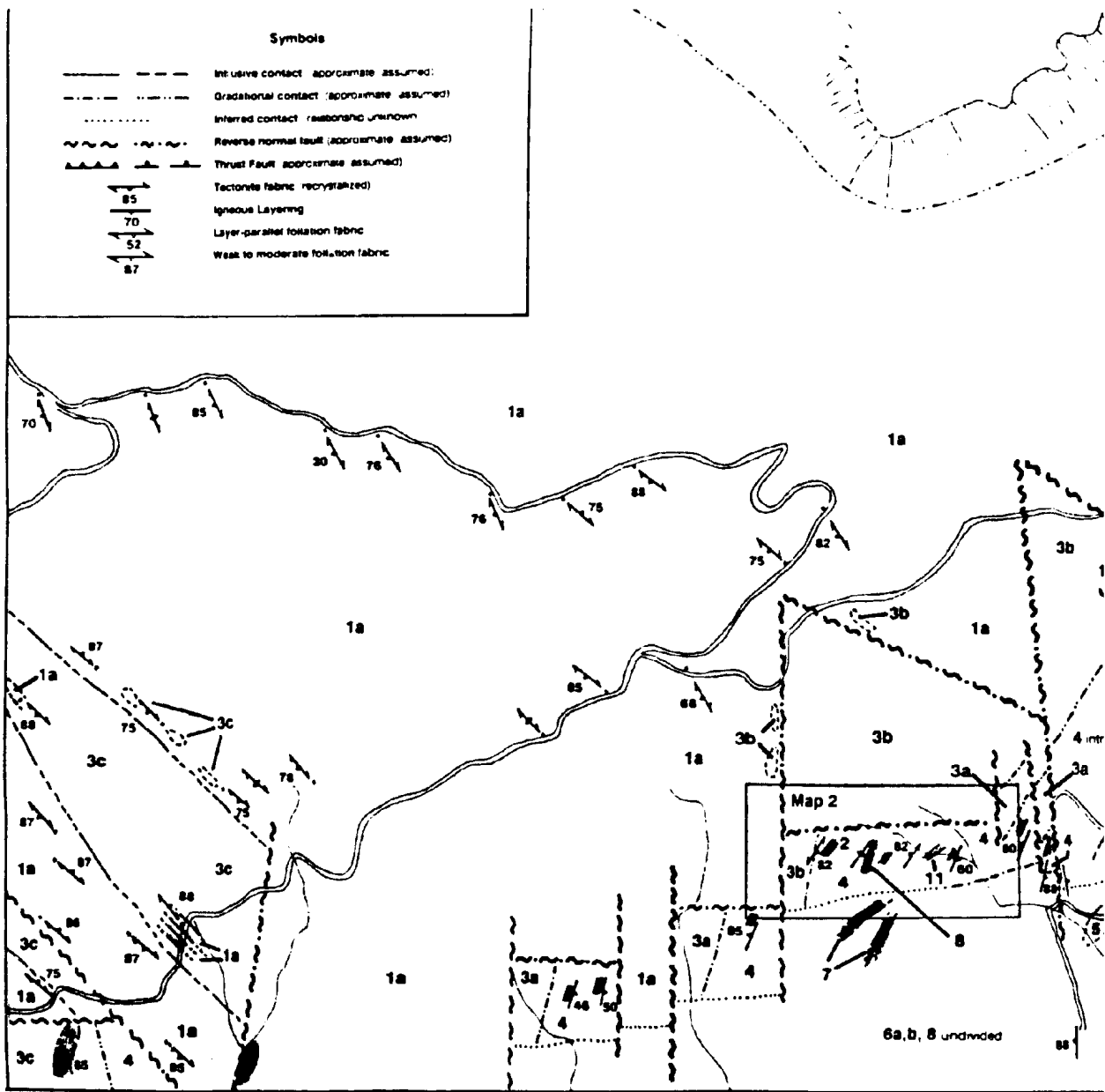


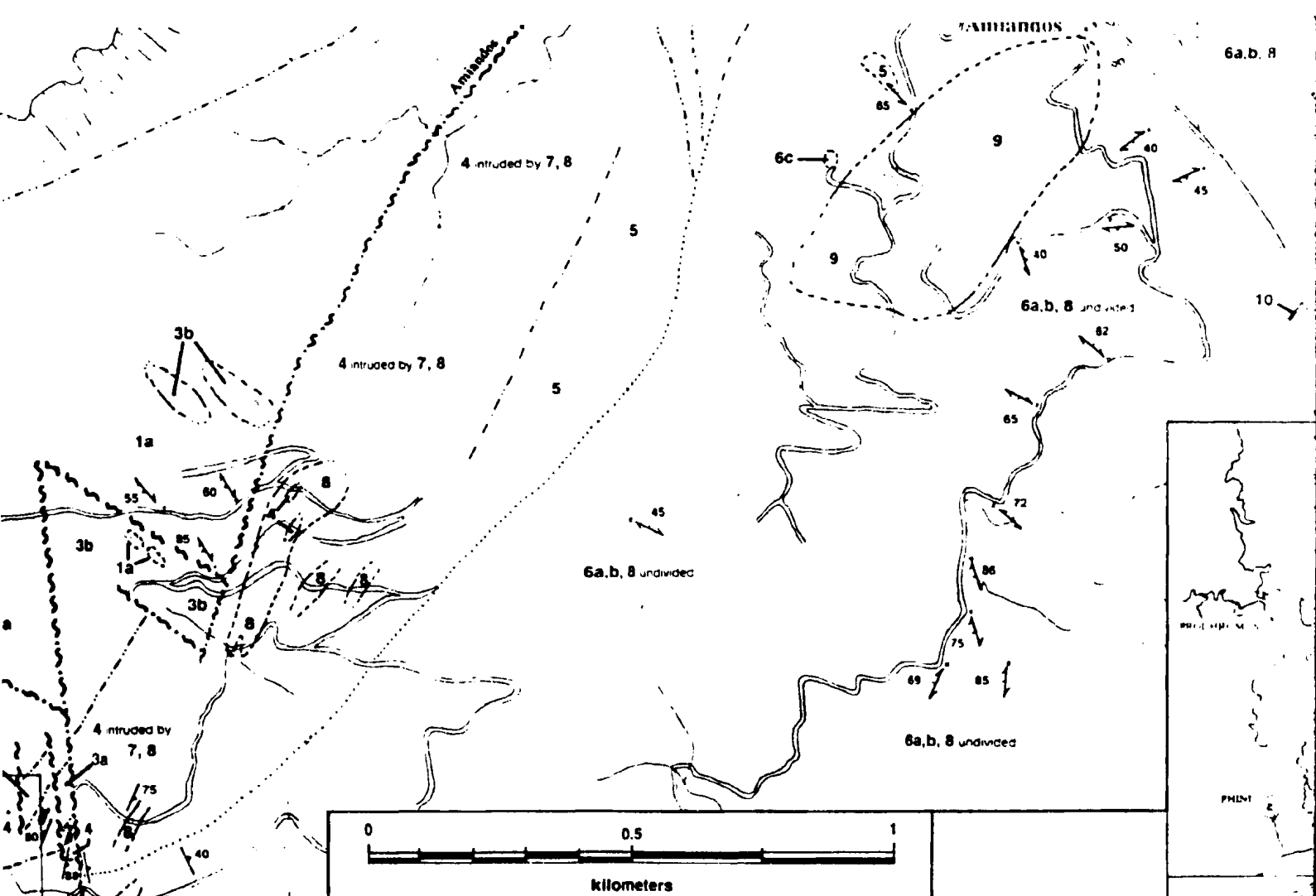




Symbols

	Intrusive contact (approximate assumed)
	Gradational contact (approximate assumed)
	Inferred contact (relationship unknown)
	Reverse normal fault (approximate assumed)
	Thrust Fault (approximate assumed)
	Tectonite fabric (recrystallized)
	Igneous Layering
	Layer-parallel foliation fabric
	Weak to moderate foliation fabric





**Marginal Notes:**

Serpentinization of the olivine rich rocks is extensive

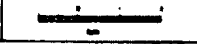
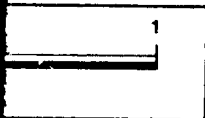
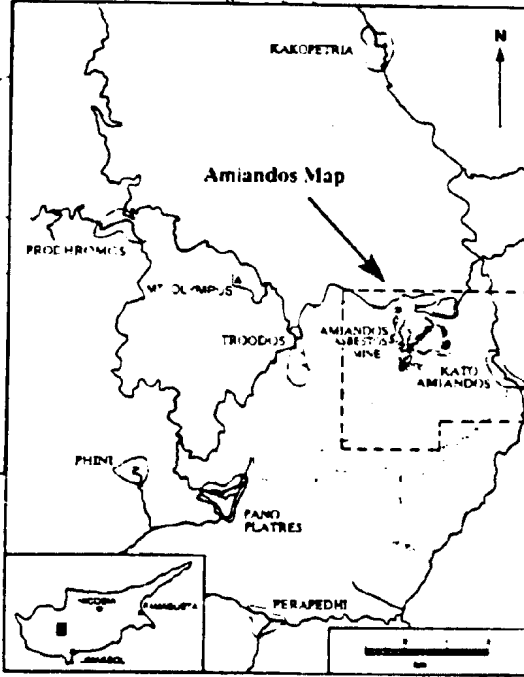
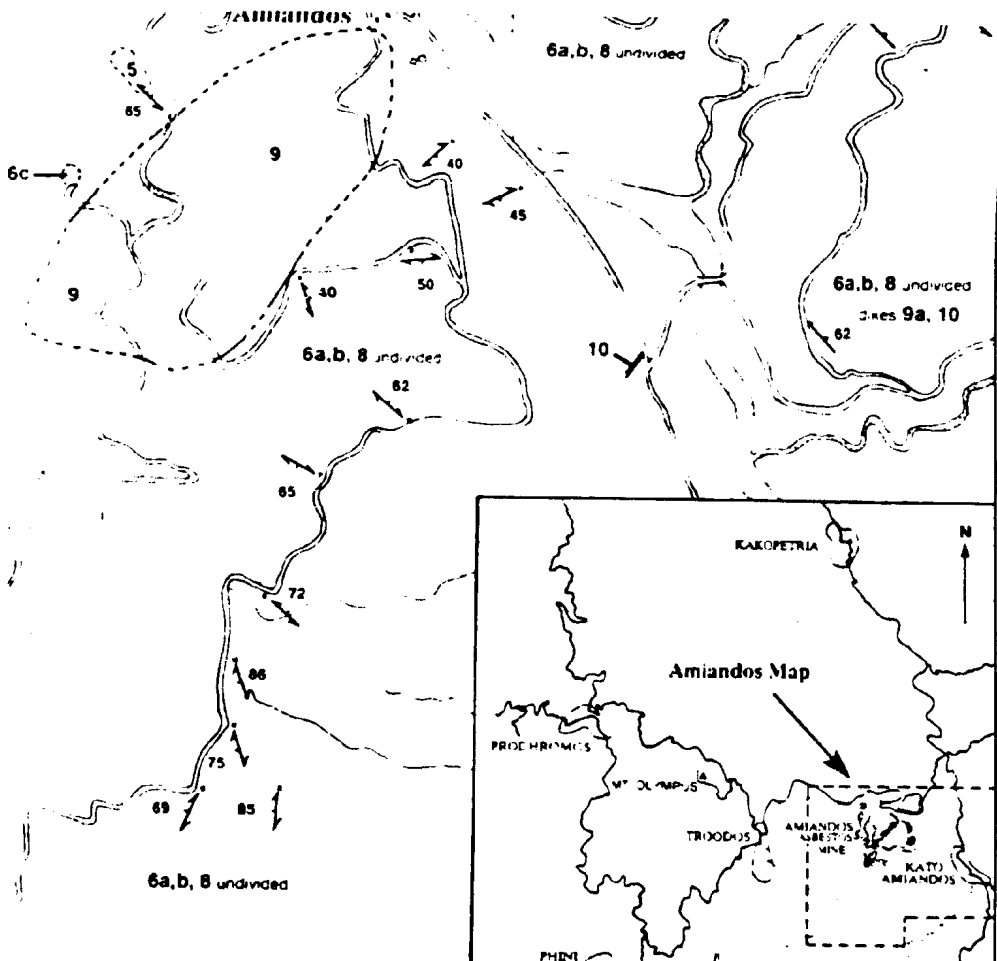
Gradational contacts are locally present throughout the complete range of the 'early plutonic suite' cumulate rocks. Moderate to intense deformational fabrics are locally present, and are particularly well developed in the olivine gabbros.

'Late magmatic suite' rocks are rarely deformed and clearly cross-cut both layering and foliation in early magmatic suite rocks, locally containing xenoliths.

Base maps used include D series maps 10000

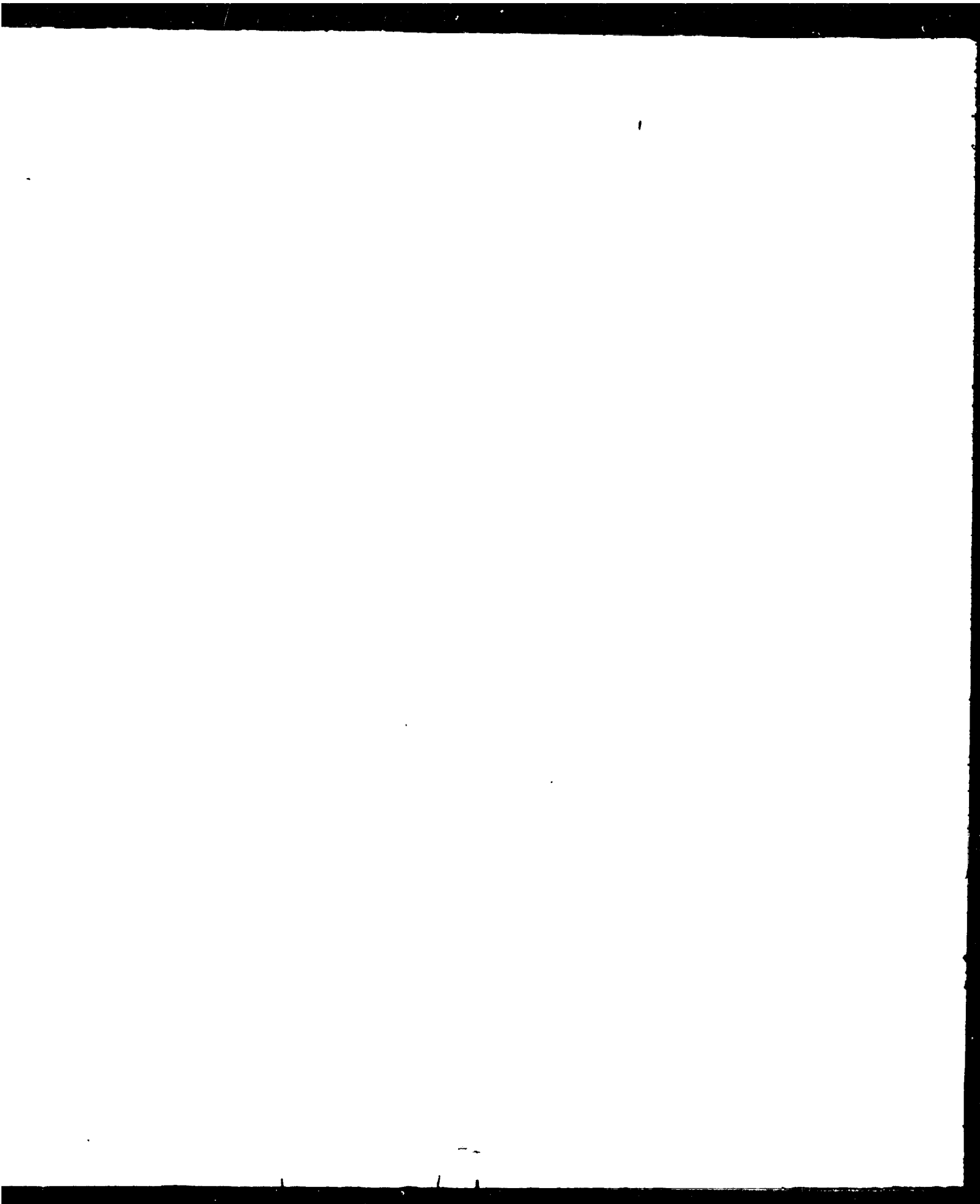
1) 37 XXIX and part of 47 V

2) 37 XXX and part of 47 VI



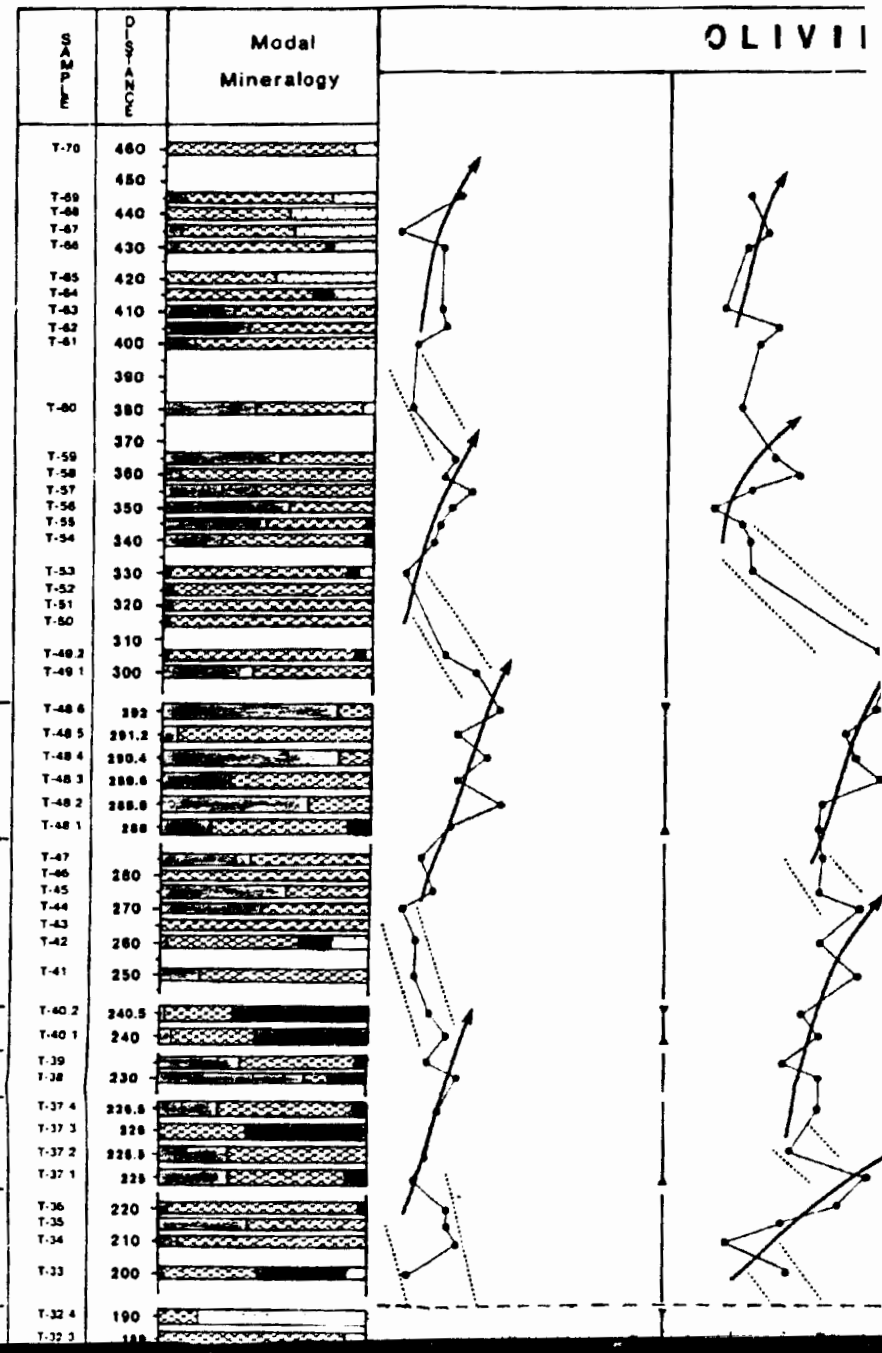
Complete range of the  
 primary fabrics are  
 shown  
 only cross out both  
 primary fabrics

Base maps used include: D.L.S. 1:5000 topographic  
 series maps generated from 1970 photography  
 1) 37 XUX and part of 47 V (western half)  
 2) 37 XUX and part of 47 VI (eastern half)



# LAYERED UL

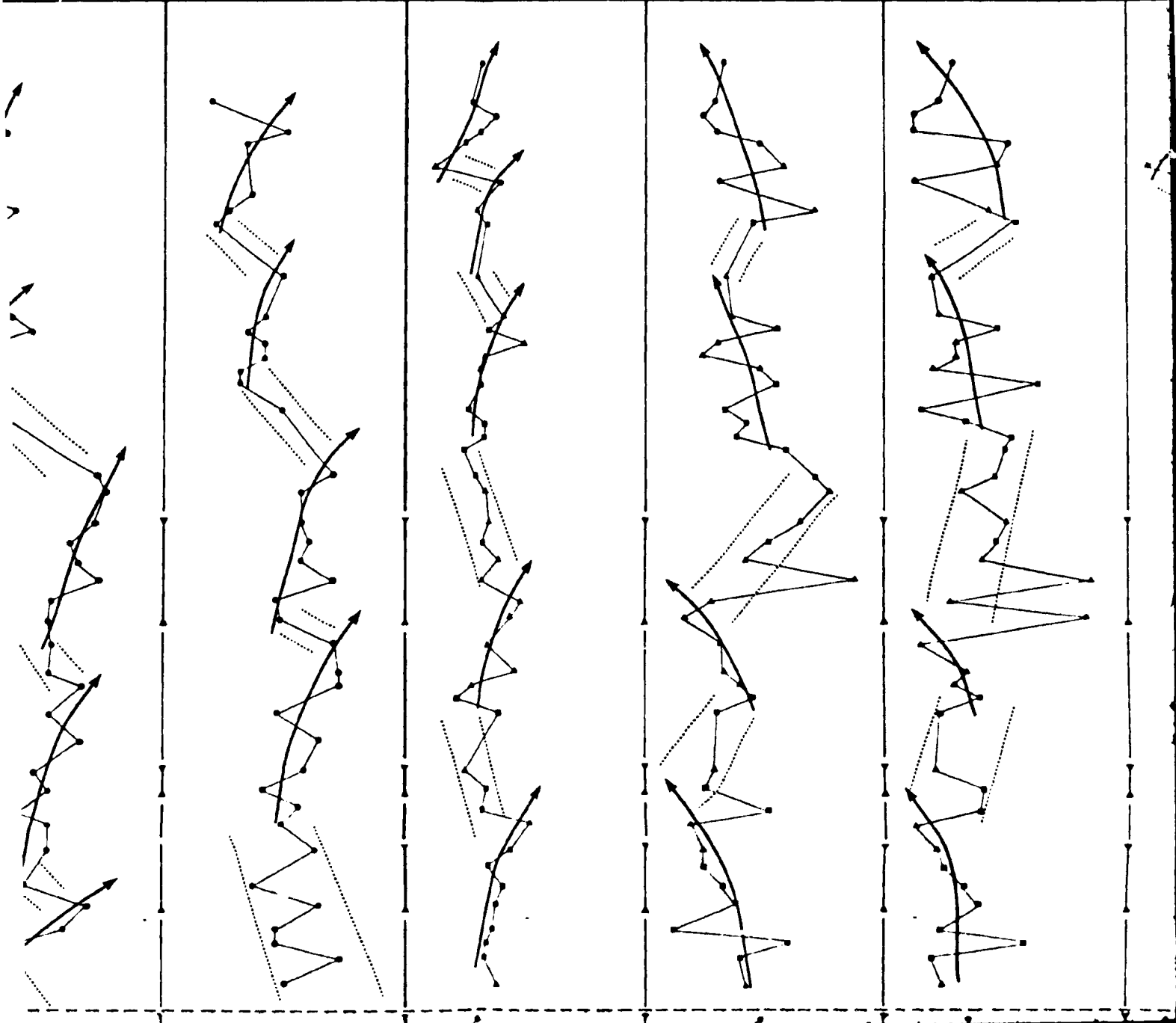
Figure 3.1



D ULTRAMAFIC CUMULATE SECTION WITHIN THE LAYERED TR  
MINERAL PHASE CHEMISTRY

IVINE

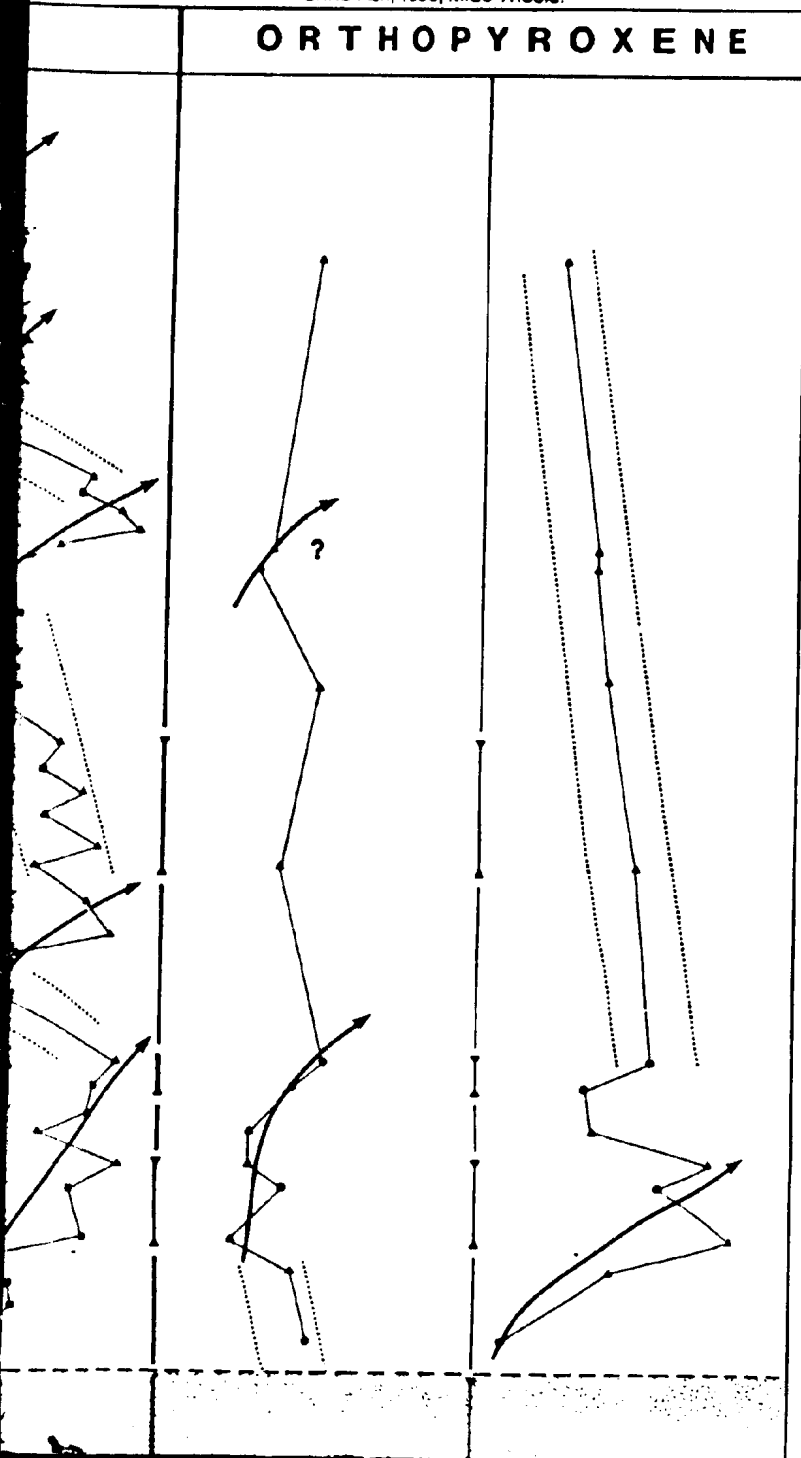
CLINOPYROXENE



ION ZONE, CYPRUS

Chris Ash, 1990, M.Sc Thesis.

ORTHO PYROXENE



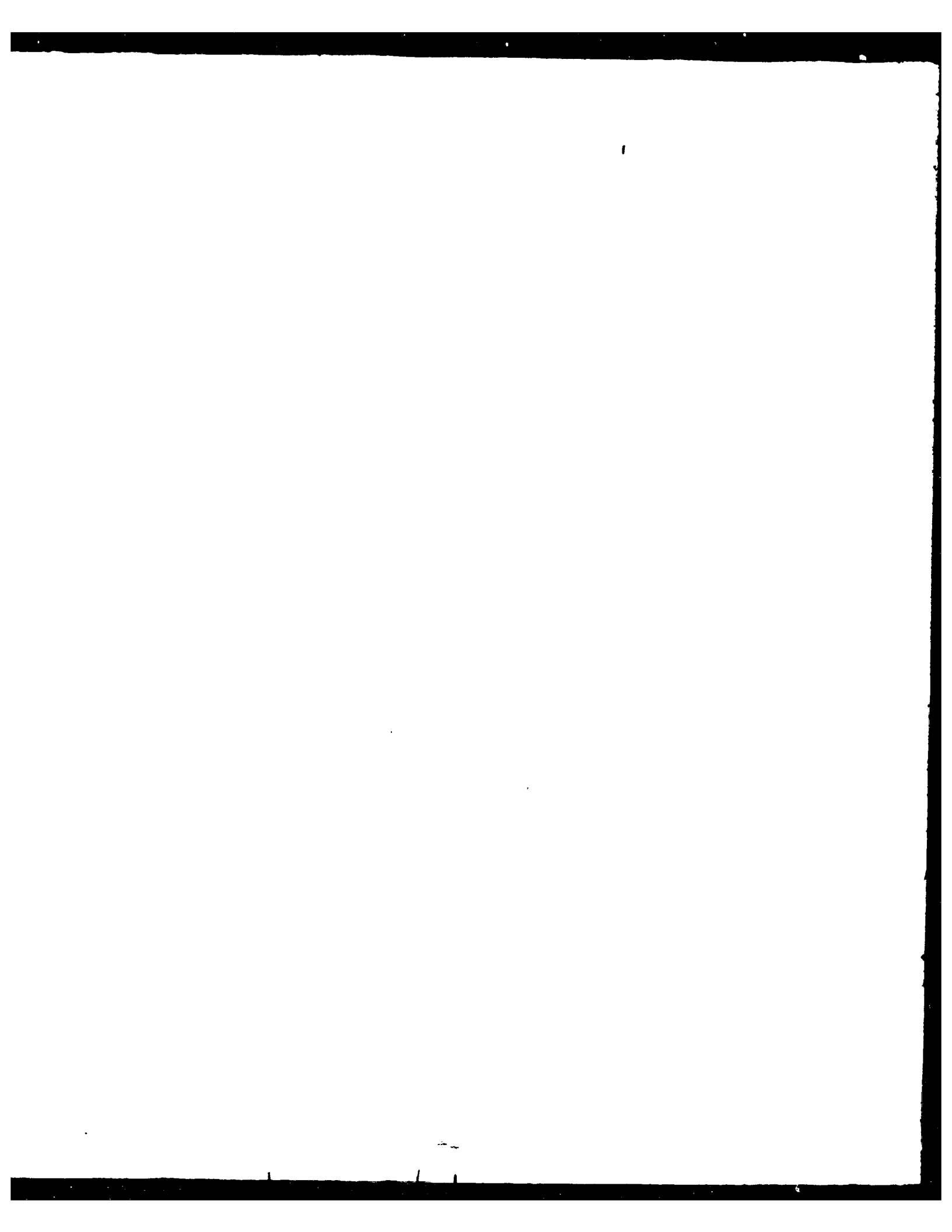
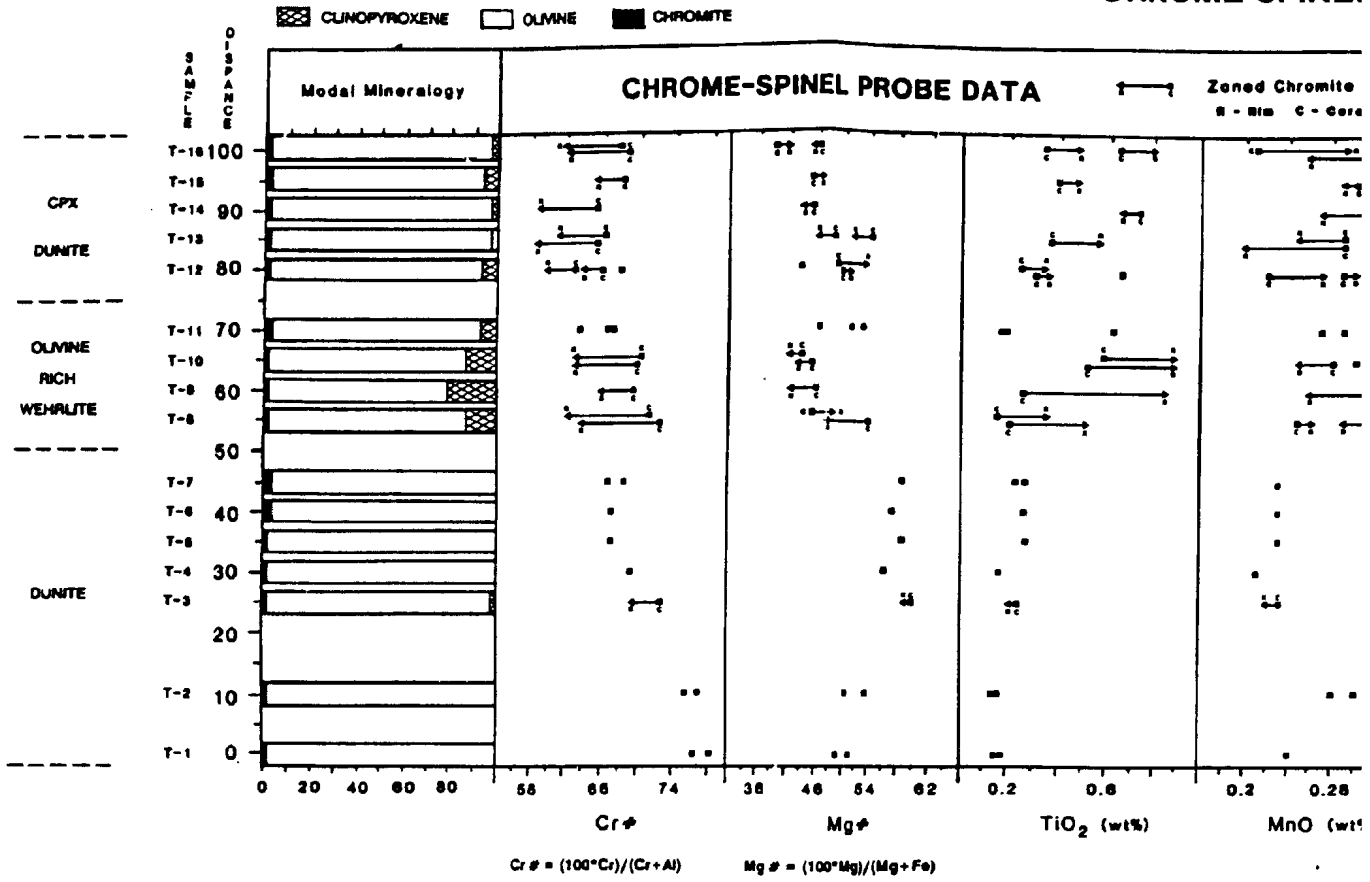


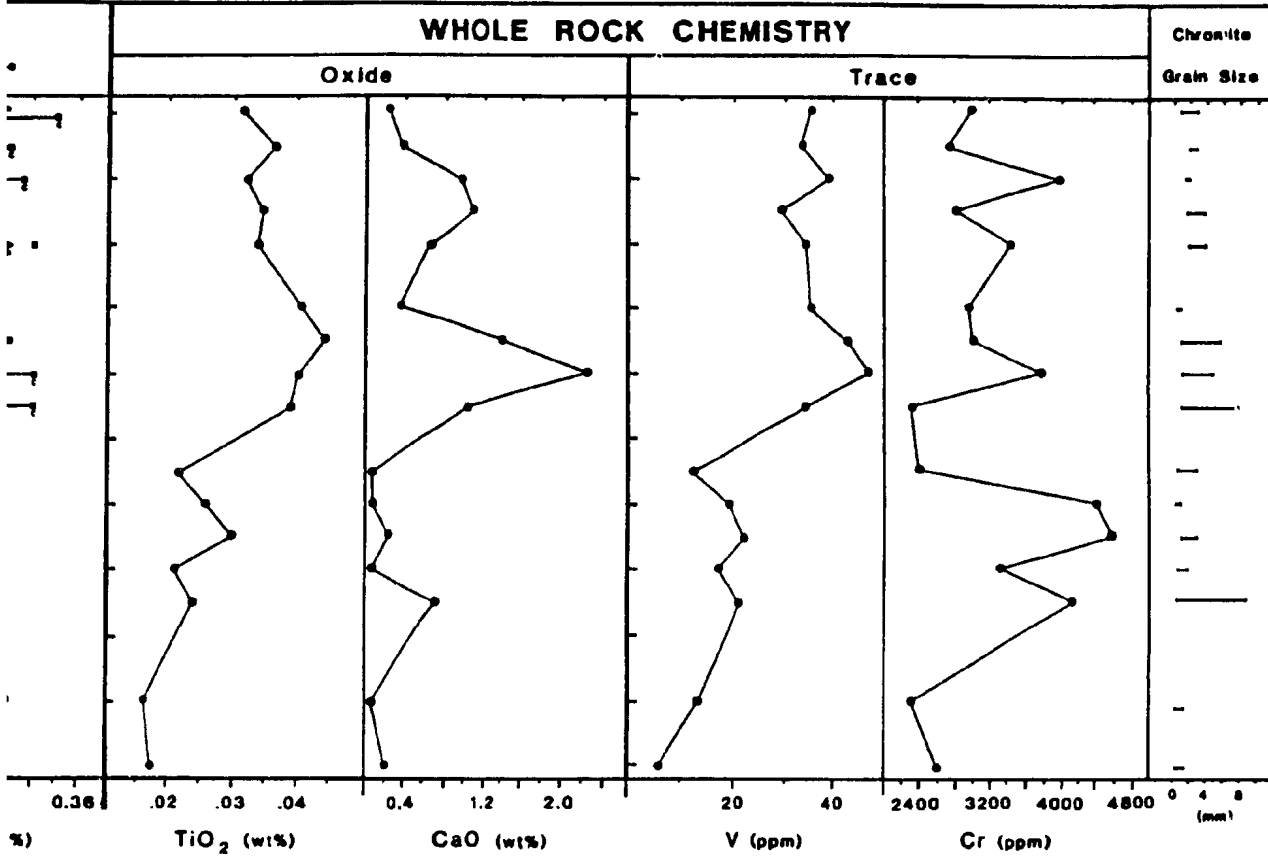
Figure 3.5

CHROME-SPINEL



# L CHEMISTRY

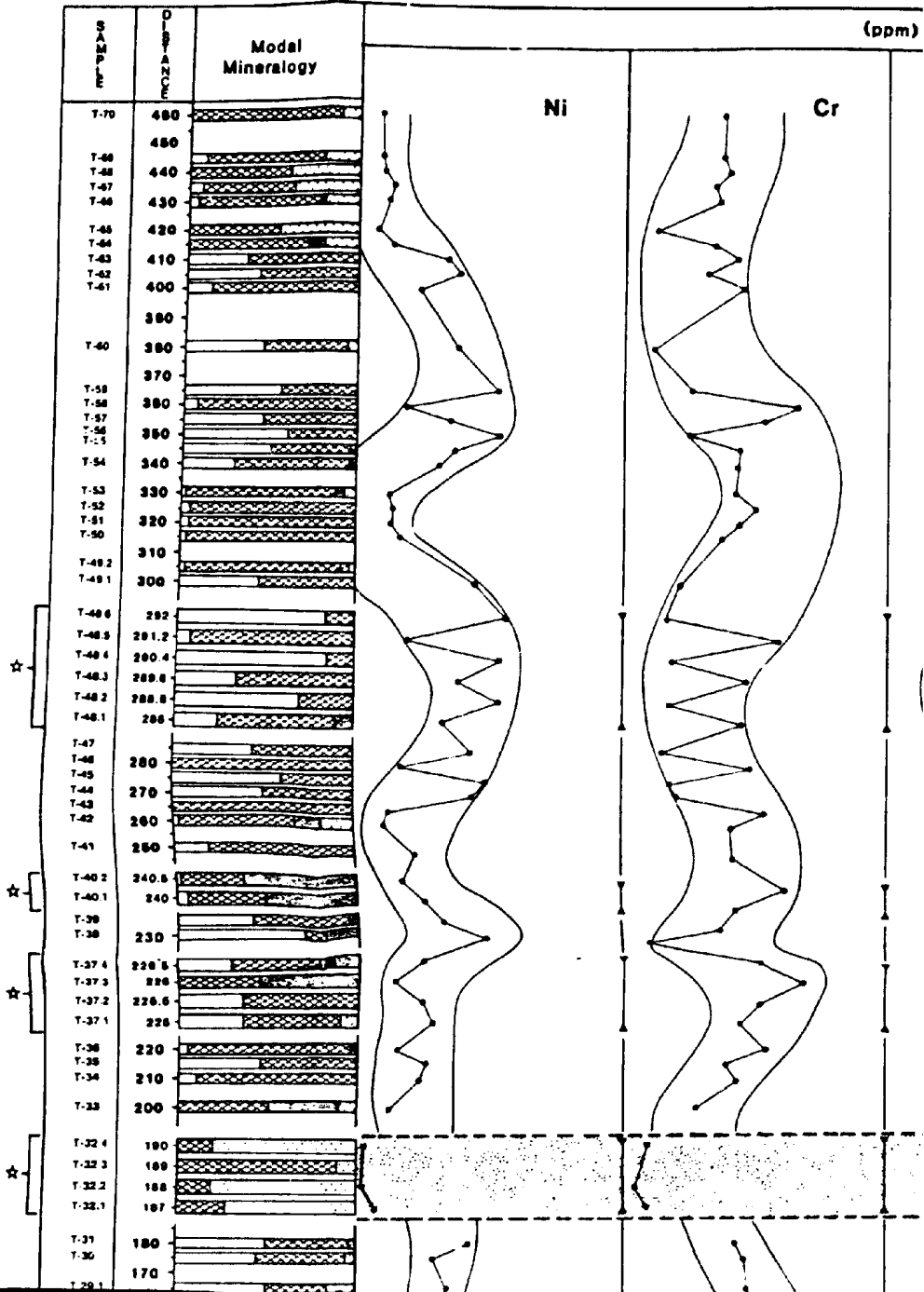
Chris Ash, 1990, M.Sc Thesis.



# LAYERED ULTRAMAFIC CUMULATES WHOLE ROCK

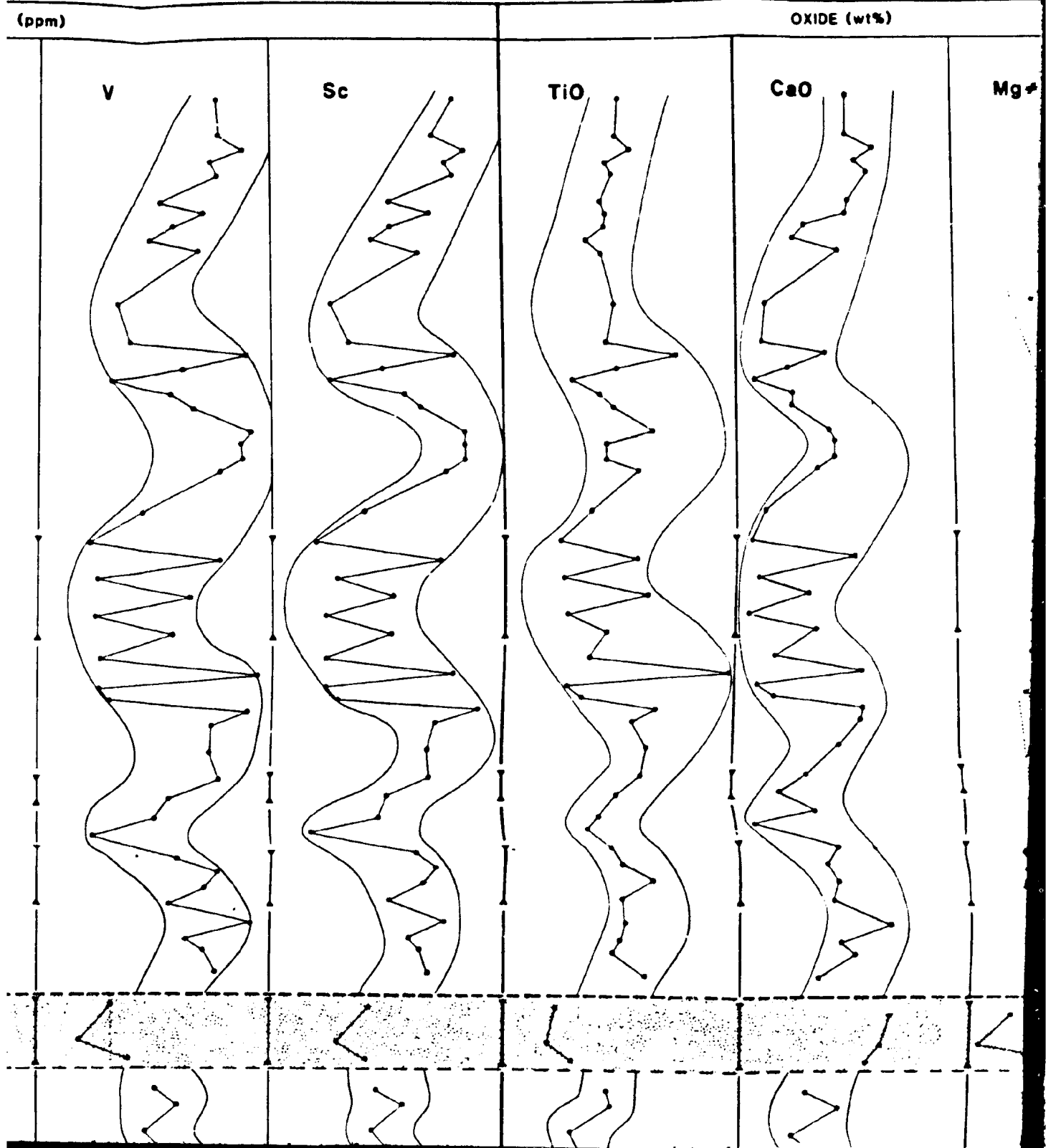
Figure 3.2

INTRUSIVE DIKES  
 Gabbro  
 Clinopyroxenite



# JLATE SECTION WITHIN THE OPHIOLITIC TRANSITION ZONE, CY ROCK TRACE AND MAJOR ELEMENT CHEMISTRY

Chris Ash, 1995



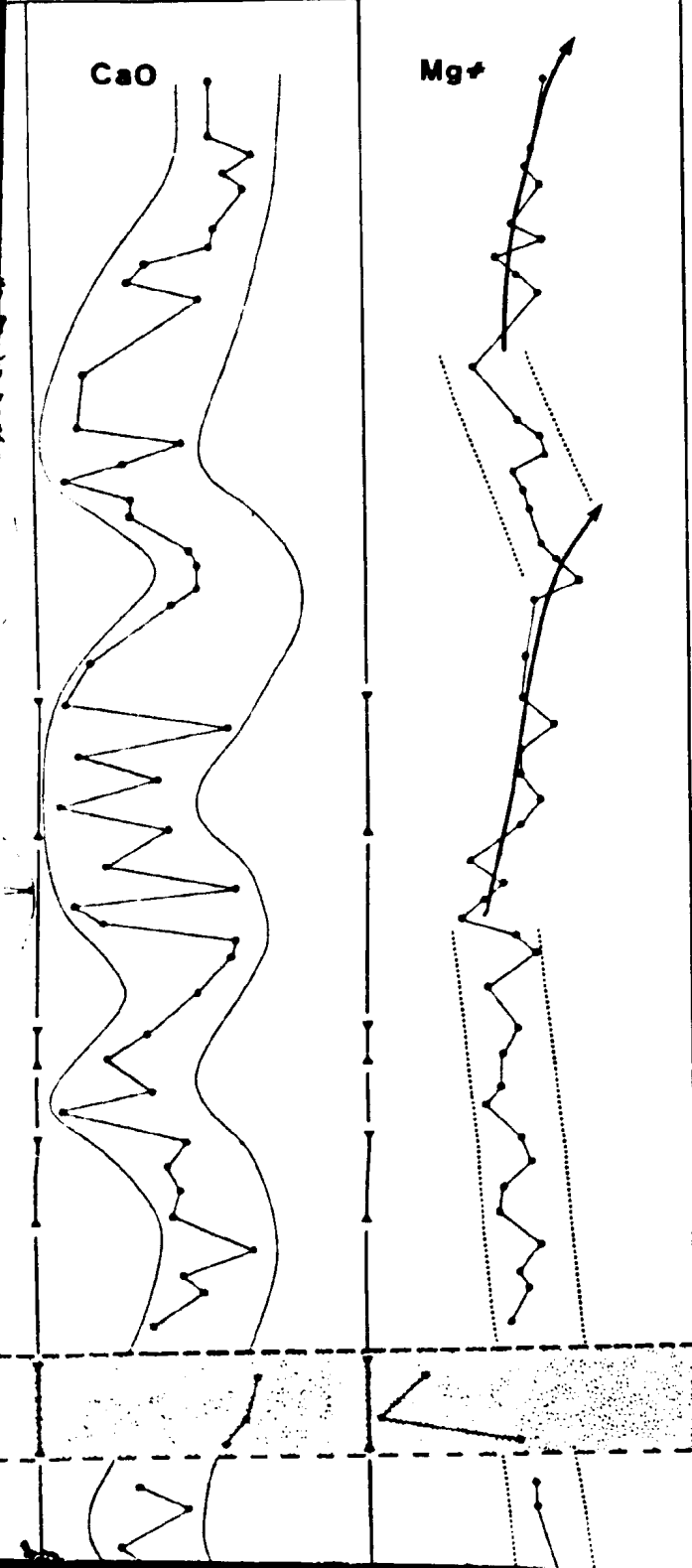
# TRANSITION ZONE, CYPRUS

Chris Ash, 1990, M.Sc Thesis.

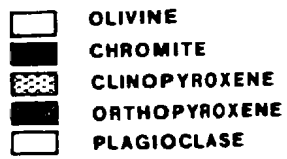
OXIDE (wt%)

CaO

Mg#

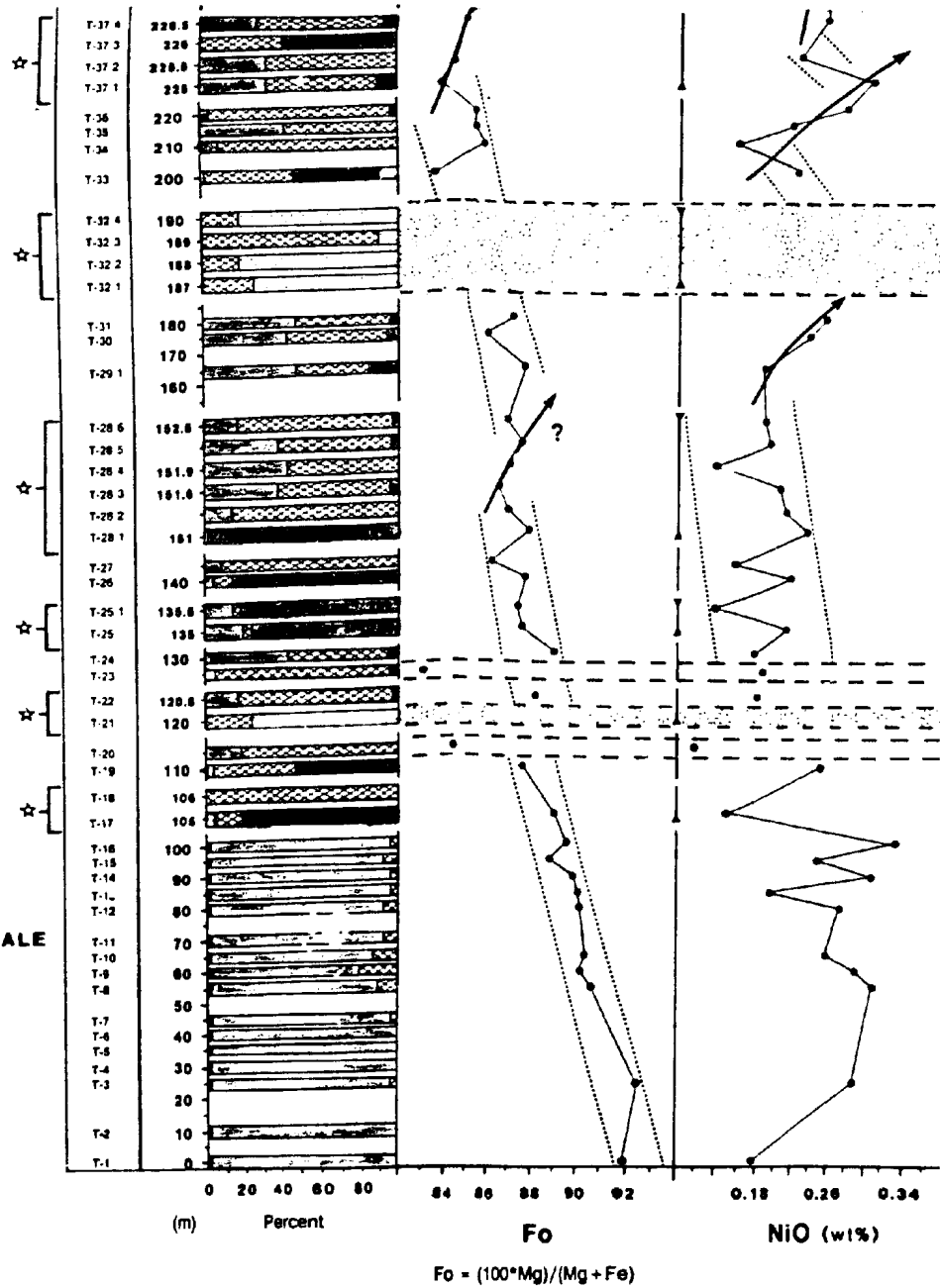


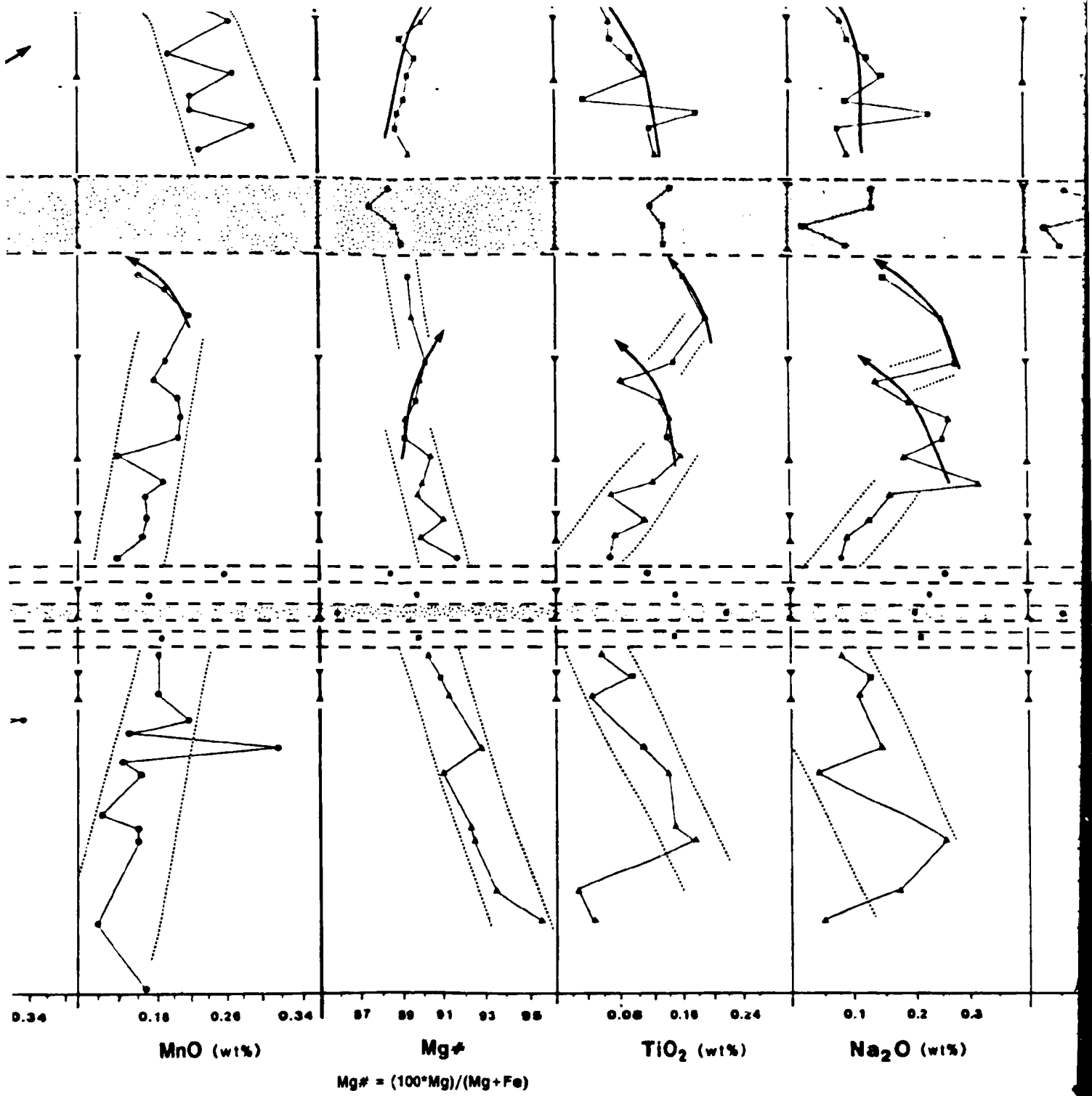


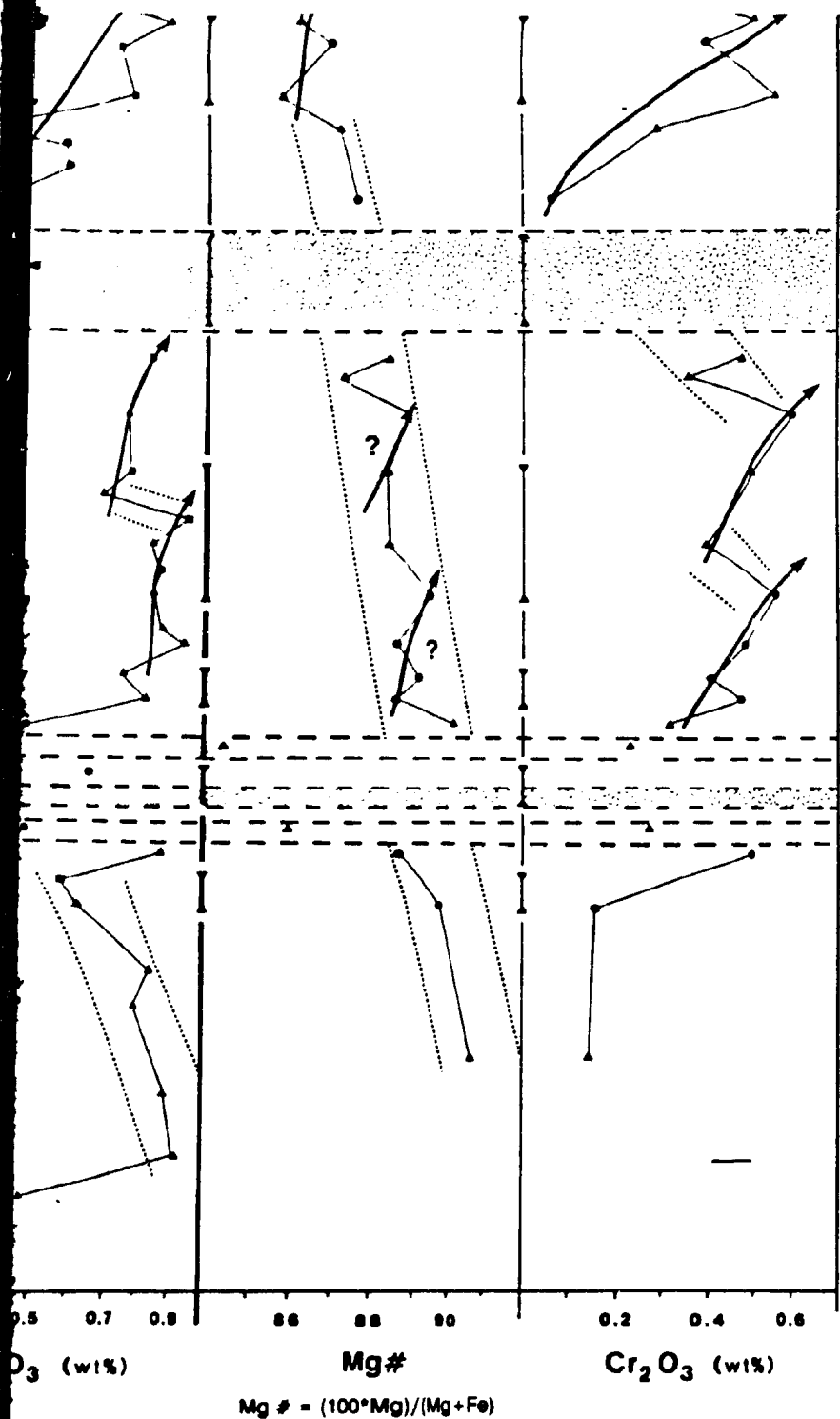


- CUMULATE
- ADCUMULATE
- ▲ INTERCUMULATE

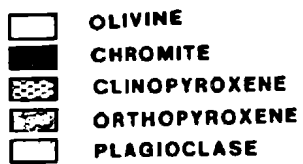
☆ INTERVAL NOT TO SCALE  
(Exaggerated)



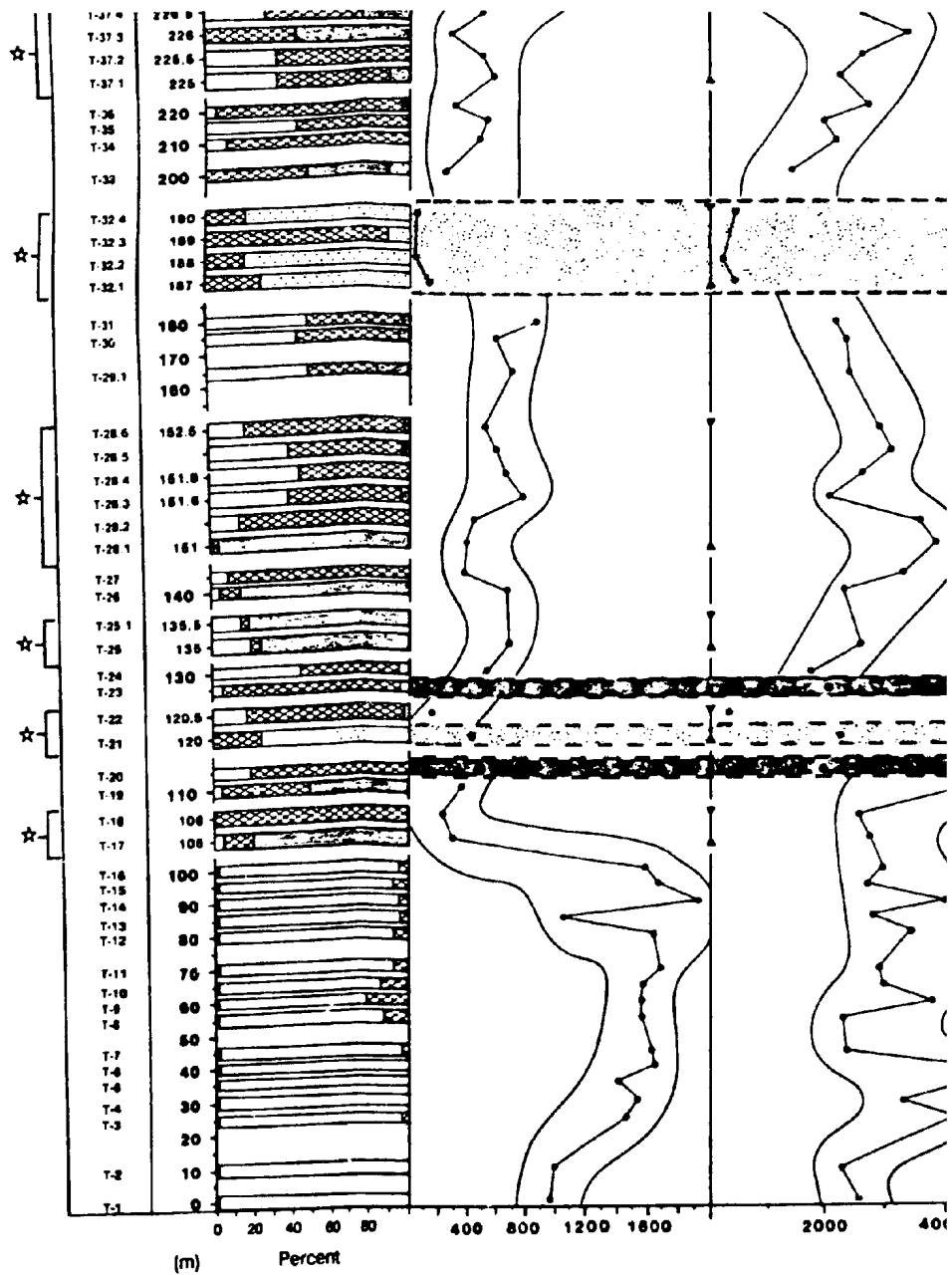


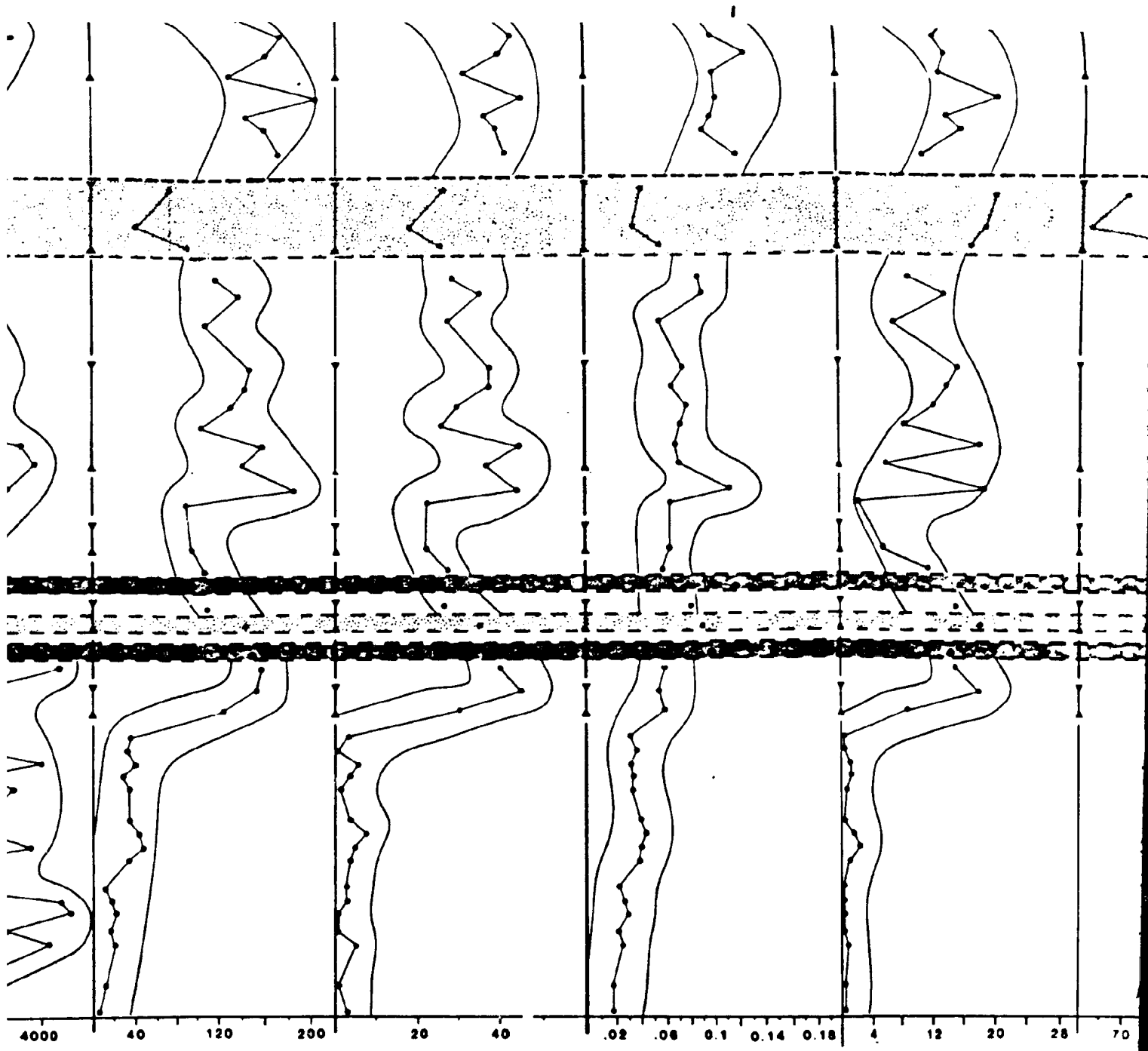




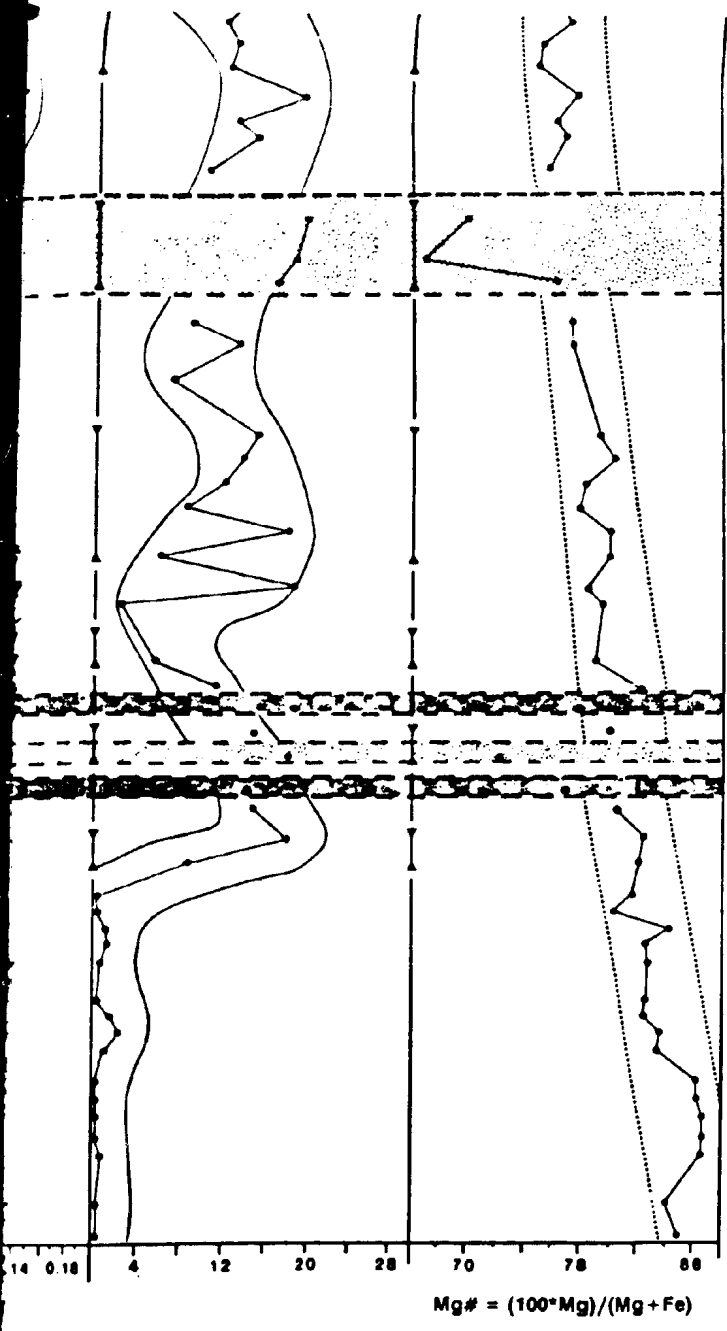


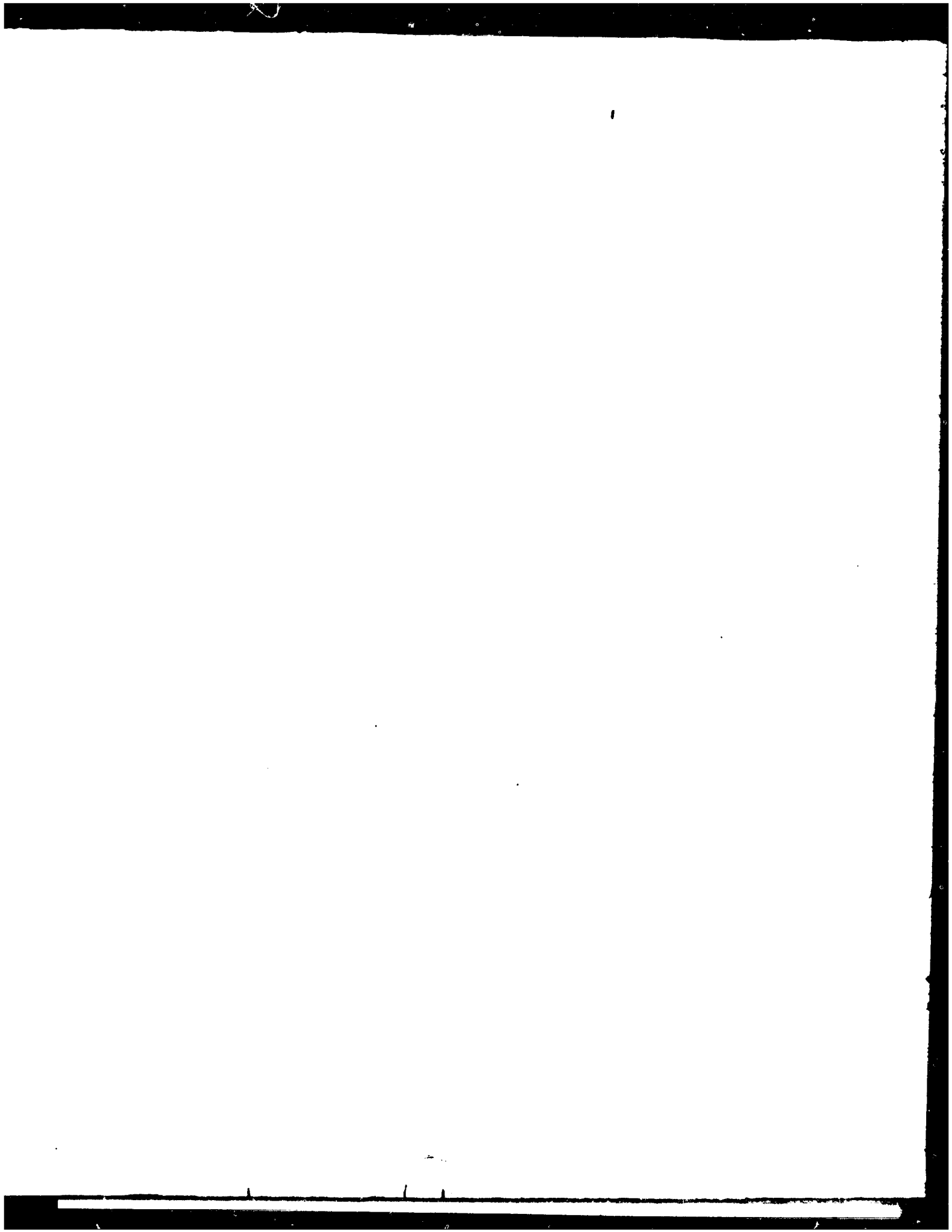
☆ INTERVAL NOT SCALE  
 (Exaggerated)



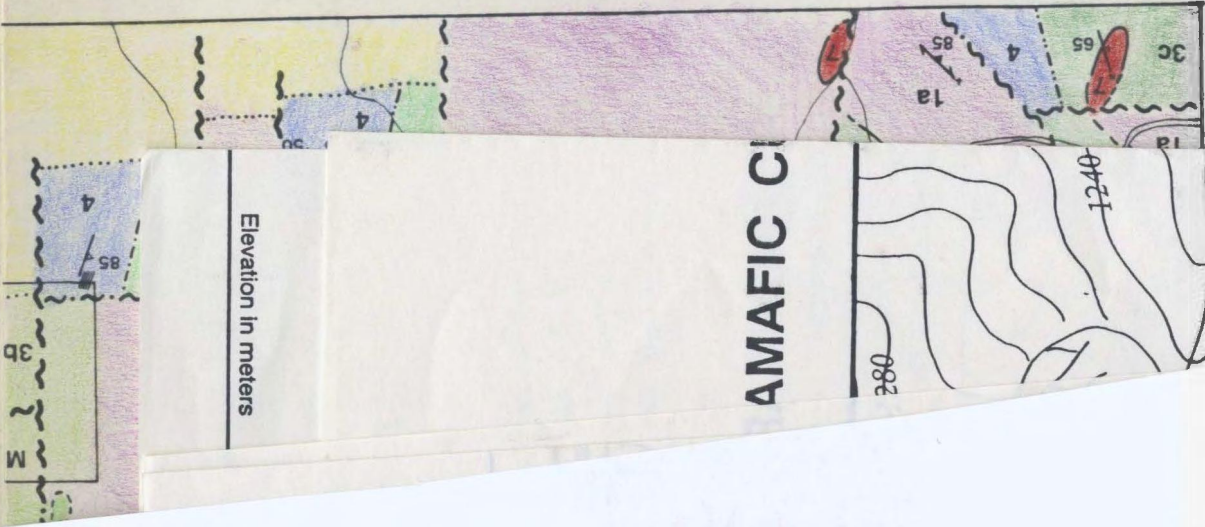


Mg#









Elevation in meters

AMAFIC C

082